

PALACKÝ UNIVERSITY OLMOUC

Dissertation

Olomouc 2019

Zdeněk Škrott

PALACKÝ UNIVERSITY OLOMOUC
FACULTY OF MEDICINE AND DENTISTRY



**Targeting the ubiquitin-proteasome system for cancer treatment:
the mechanism of action of drug disulfiram**

Mgr. Zdeněk Škrott

Study programme: Pediatrics

Department: Laboratory of Genome Integrity, Institute of Molecular and Translational medicine

Supervisor: Mgr. Martin Mistrík, Ph.D.

Olomouc 2019

Statement:

I hereby declare that this thesis entitled: „Targeting the ubiquitin-proteasome system for cancer treatment: the mechanism of action of drug disulfiram” was written by me, and all relevant resources are included in the reference part. The work was mostly carried out at the Laboratory of Genome Integrity, Institute of Molecular and Translational Medicine.

Acknowledgement:

First, I would like thank my supervisor Martin Mistrík, Ph.D. for his leadership, continuous support, trust, and great scientific discussions and contribution. My thanks also belong to prof. Jiří Bártek, Ph.D. for the opportunity to work on this exciting project. Second, I thank my colleagues, namely Dušana Majera, Ph.D. for help with cell toxicity assays and stable cell lines, Jan Gurský, Ph.D. for help with flow-cytometry, Tomáš Oždian Ph.D. for help with HPLC-MS, Jing Li, Ph.D. from California Institute of Technology for help with 26S proteasome assay, and MUDr. Andrea Miklovičová, MUDr. Petr Džubák, Ph.D., doc. MUDr. Marian Hajdúch, Ph.D. for providing tissue samples from patients and animals. Third, I would like to thank also to those who influenced my scientific thinking and career, namely to Boris Cvek, Ph.D. and prof. Raymond Deshaies, Ph.D.

Finally, I would like to thank my family for continuous support.

Research on the project was supported by: Palacky University (grants IGA_LF_2018_34; IGA_LF_2019_026), Czech Ministry of Health (AZV 16-32030), Czech National Program of Sustainability (LO1304).

Olomouc, June 2019.

.....

Mgr. Zdeněk Škrott

Bibliografická identifikace:

Jméno a příjmení autora: Zdeněk Škrott

Název práce: Cílení ubiquitin-proteazomového systému při léčbě nádorových onemocnění: mechanismus účinku léku disulfiram

Typ práce: Dizertační

Pracoviště: Laboratoř integrity genomu, Ústav molekulární a translační medicíny, Lékařská fakulta Univerzity Palackého v Olomouci

Vedoucí práce: Mgr. Martin Mistrík, Ph.D.

Rok obhajoby práce: 2019

Klíčová slova: ubiquitin-proteazomový systém, disulfiram, NPL4, p97, měď

Počet stran: 122

Jazyk: Anglický

Bibliographical identification:

Author's name and surname: Zdeněk Škrott

Title: Targeting the ubiquitin-proteasome system for cancer treatment: the mechanism of action of drug disulfiram

Type of thesis: Dissertation

Department: Laboratory of Genome Integrity, Institute of Molecular and Translational Medicine, Faculty of Medicine and Dentistry, Palacky University Olomouc

Supervisor: Mgr. Martin Mistrík, Ph.D.

The year of defence: 2019

Keywords: ubiquitin-proteasome system, disulfiram, NPL4, p97, copper

Number of pages: 122

Language: English

ABSTRACT

This thesis is focused on repurposing an old anti-alcohol drug disulfiram for cancer therapy. Disulfiram has been shown to be effective in various preclinical cancer models, but the unknown active metabolite, the unclear mechanism of action and unidentified molecular target, all obstruct repurposing disulfiram as an anti-cancer drug. This thesis describes

a new disulfiram metabolite found in humans, dithiocarbamate-copper complex, as the active metabolite toxic to cancer cells and accumulating in tumours. Moreover, it shows, that in the cells, dithiocarbamate-copper complex interferes with the NPL4 protein, an adaptor of p97 segregase, which is essential for the degradation of proteins involved in several regulatory and stress response pathways. After the treatment by dithiocarbamate-copper complex, NPL4 forms aggregates, which subsequently attract p97 and other stress proteins leading to induction of heat shock and unfolded protein responses, impairment of protein degradation, ubiquitin stress, and cell death as a consequence. Collectively, observations gathered in this thesis should encourage further clinical tests, help clinicians to monitor the treatment and identify suitable patients benefiting from the disulfiram, all together promoting eventual repurposing of this old, safe and cheap drug to save lives of patients with cancer worldwide.

ABSTRAKT

Tato disertační práce se týká znovuvyužití disulfiramu, starého léku používaného proti alkoholismu, pro léčbu rakoviny. Protinádorový účinek disulfiramu byl prokázán na několika preklinických modelech, ovšem nejasný mechanismus účinku, neznámý aktivní metabolit a také neznámý molekulární cíl, to vše brání nasazení disulfiramu pro léčbu nádorových onemocnění. Tato práce popisuje nový metabolit disulfiramu nalezený u pacientů léčených tímto lékem, a to komplex dithiokarbamátu s mědí. Jedná se o biologicky aktivní látku toxickou pro rakovinové buňky a hromadící se v nádorech. Tato práce dále ukazuje, že tento metabolit inhibuje protein NPL4, což je kofaktor proteinu p97, který je se podílí na degradaci celé řady proteinů zapojených v mnoha regulačních a signalizačních drahách. Komplex dithiokarbamátu s mědí vyvolává v buňkách agregaci NPL4. Tyto proteinové agregáty následně přitahují vedle proteinu p97 také další stresové proteiny a indukují v buňce specifickou stresovou odpověď. Navíc dochází k toxické akumulaci nezdegradovaných a

špatně poskládaných proteinů, ubiquitinovému stresu, a ve výsledku k buněčné smrti. Poznatky v této práci a také v příložených publikačních výstupech by měly podnítit další klinické testy disulfiramu, usnadnit práci lékařům při hodnocení účinku léčby a také identifikaci vhodných pacientů, pro něž by disulfiram mohl být přínosem. V důsledku by mohly vést k zavedení tohoto starého, bezpečného a levného léku do protinádorové terapie.

TABLE OF CONTENTS

1 INTRODUCTION.....	1
1.1 Overview of the Ubiquitin-proteasome system.....	1
1.2 The ubiquitin code.....	4
1.3 The structure and function of the proteasome.....	7
1.4 Protein quality control.....	10
1.5 The role of the p97 complex.....	15
1.6 The role of UPS in tumour development and treatment.....	22
1.7 Anti-cancer activity of disulfiram.....	30
2 AIMS.....	36
3 MATERIALS AND METHODS.....	37
3.1 HPLC/MS analysis of copper-dithiocarbamate complex (CuET).....	37
3.2 Sample preparation for HPLC/MS analysis.....	37
3.3 Blood collection from humans for HPLC/MS analysis of CuET.....	38
3.4 Cell lines.....	38
3.5 Stable cell lines construction, transfection, siRNA.....	39
3.6 Colony formation assay.....	40
3.7 XTT assay.....	40
3.8 Annexin V staining.....	40
3.9 Caspases 3/7 assay.....	40
3.10 Immunoblotting and antibodies.....	41
3.11 Immunofluorescence staining.....	41
3.12 Microscopy, FRAP and image analysis.....	42
3.13 Cell fractionation for Triton X insoluble pellets.....	42
3.14 Isolation of microsomal fraction.....	43
3.15 Ub ^(G76V) -GFP degradation.....	43
3.16 p97 ATPase activity assay.....	43
3.17 26S proteasome activity.....	43
3.18 Affinity precipitation.....	44
3.19 Protein expression and purification.....	44

3.20 Chemicals.....	45
3.21 Figures preparation, data analysis, used software.....	45
4 RESULTS.....	46
4.1 Ditiocarb-copper complex is a new metabolite of disulfiram.....	46
4.2 CuET complex is highly toxic to cancer cells.....	48
4.3 CuET complex induces both apoptotic and non-apoptotic cell death.....	49
4.4 CuET complex does not inhibit the proteasome directly.....	53
4.5 CuET complex inhibits the function of p97 segregase.....	55
4.6 Ubiquitinated proteins accumulated by CuET treatment are associated with insoluble structures.....	59
4.7 CuET complex impairs ER-associated degradation leading to the activation of Unfolded protein response.....	62
4.8 CuET complex immobilises p97 segregase.....	63
4.9 CuET complex targets NPL4 cofactor.....	65
4.10 NPL4 protein forms aggregates after the treatment by CuET.....	67
4.11 NPL4 protein mutated in putative zinc-finger domain resembles phenotypes induced by CuET.....	70
4.12 Aggregated NPL4 protein triggers heat shock response.....	73
4.13 Disulfiram is converted to CuET <i>in vitro</i>	75
5 DISCUSSION.....	78
6 CONCLUSION.....	88
7 ABBREVIATIONS.....	89
8 REFERENCES.....	93
9 BIBLIOGRAPHY.....	117
10 APPENDIX – FULL TEXT PUBLICATIONS RELATED TO THE THESIS.....	119

1 INTRODUCTION

Drugs often interact with more molecules than intended and such interaction with these off-targets could manifest not only as adverse side effects, but importantly also as the positive ones. In case the positive side effect is clinically relevant for any disease or medical condition, a drug could be repurposed for clinical use. As drug repositioning accelerates approval process and lower the financial cost, it is highly promising approach with growing importance and interest.

Disulfiram, a drug used to treat alcoholism, could be an example of drug repurposing. Disulfiram, also known as Antabuse, is used almost for seventy years as alcohol deterrent; however, as suggest case reports and preclinical studies, disulfiram has also interesting anti-cancer properties. While the active metabolite and the mechanism standing behind anti-alcoholism effect of disulfiram are well known, such information is largely missing regarding its impact on tumour cells. Nevertheless, it is generally accepted that anti-cancer activity of disulfiram is dependent on the presence of copper, and inhibition of the proteasome has been suggested as a plausible explanation for its toxicity towards malignant cells. The proteasome is the multi-subunit protease responsible for degradation of vast majority of cellular proteins, and is responsible not only for protein degradation, but also for cell signalling (Collins and Goldberg, 2017). The proteasome represents particularly interesting target for cancer therapy as demonstrated by three currently approved proteasome inhibitors, including bortezomib, a drug that has significantly changed the outcome of multiple myeloma patients (Manasanch and Orłowski, 2017).

To advance the repurposing of disulfiram for cancer, fresh insight to the role of copper potentiation, the active metabolite, and the mechanism of action of disulfiram in cancer cells is needed to be uncovered.

1.1 Overview of the Ubiquitin-proteasome system

Protein homeostasis within the cell is maintained by continuous cycle of protein synthesis and degradation. On the one side, a cell invests up to 75% of total energy to create billions of protein molecules using roughly 3 million of ribosomes, and on the other side, cells developed costly and highly sophisticated mechanisms of protein degradation (Wolff et al., 2014). While some proteins persist for months or even entire life of an individual, others,

somehow unreasonably, are degraded within minutes or even are designated to degradation already during the translation. Degradation of proteins is equally important as transcription and translation in regulation of protein functions, and in principle, it is crucial for all cellular processes, including cell cycle, differentiation, signalling and cell death (Wolff et al., 2014). Importantly, a considerable amount of proteins is unfolded, misfolded or damaged by radicals, heat or other factors. To survive and preserve its functions, a cell must recognise and either repair or eliminate all these proteins. As documented by a multitude of neurodegenerative disorders, a malfunction of protein quality control mechanisms has severe consequences for the entire organism (Hartl, 2017).

Cells evolved two complimentary systems responsible for the degradation of proteins. The majority of proteins are degraded by the ubiquitin-proteasome system (UPS), a highly specific system responsible for elimination of marked proteins. To be degraded, a designated protein is first covalently linked with a chain of small proteins - ubiquitin, which serves as a recognition signal for a large multi-subunit protease known as the proteasome (Finley, 2009). In contrast to UPS, autophagy-lysosomal pathway is generally viewed as nonselective mechanism for degradation of bulky molecules, aggregates, and even whole organelles. The process involves the formation of double-membrane vesicles engulfing objects intended for degradation, and the fusion of vesicles with lysosomes containing hydrolysing enzymes resulting in breakdown of the content (Bento et al., 2016). Despite the “bulky-autophagy” is more common, selective types of autophagy are also known, and plays important role in cellular homeostasis. Its specificity is based on ubiquitin-like proteins of so-called Atg family and ubiquitin, implying high degree of cross-talk between UPS and autophagy (Dikic, 2017).

In the light of the fascinating discoveries carried between 1950s and 1980s about how genetic code is transcribed and translated into proteins, the opposite – a protein degradation, remained largely neglected. In that time, scientists generally believed that proteins are long lived and degraded non-specifically. However, later discoveries demonstrated that protein degradation is rather selective and, paradoxically, energy-dependent process. With the discovery of lysosome, it was supposed for two decades that this organelle is responsible for hydrolysis of cellular proteins. Nevertheless, it became clear that besides the lysosome, other mechanisms must be involved in the degradation of the majority of proteins. A series of elegant experiments conducted by Aron Ciechanover and Avram Hershko in late 70s and early 80s led to a discovery of the protein ubiquitin, which could be covalently linked to a protein to serve as a signal for destruction (Ciechanover, 2009). A protease responsible for

degradation of ubiquitinated proteins was discovered later and named as the proteasome. For the discovery of the ubiquitination Ciechanover, Hersko and his colleague Irvin Rove were awarded by 2004 Nobel Prize in chemistry (Melino, 2005).

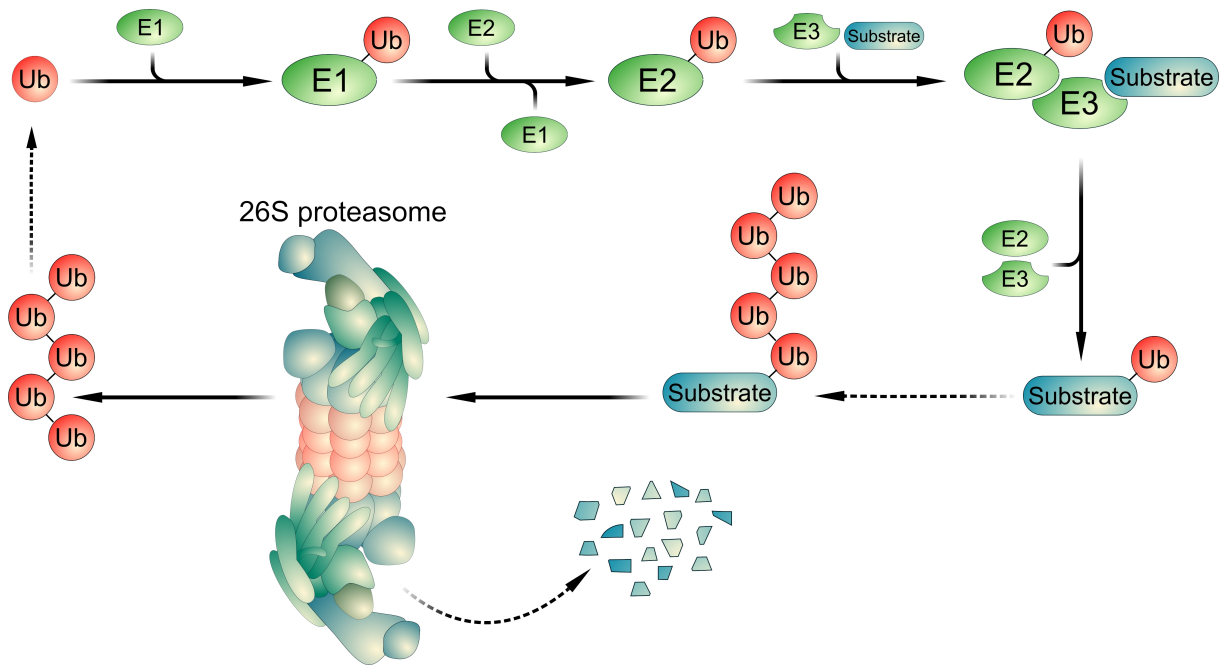


Figure 1 | The Ubiquitin-proteasome system. Prior their degradation by the proteasome, the majority of proteins must be ubiquitinated. First, ubiquitin is activated by E1 Ubiquitin-activating enzyme and transferred to E2 Ubiquitin-conjugating enzyme. E3 Ubiquitin-ligases than mediate the last step – the conjugation of ubiquitin from E2 to a substrate via isopeptide bond. By repeating this cycle (dotted arrow), the substrate became polyubiquitinated. The proteasome interacts with the substrate, removes the ubiquitin and translocates the substrate into proteolytic chamber of the proteasome, where the substrate is cleaved to small peptides.

It is estimated that up to 80% of cytosolic proteins is degraded by UPS (Lee and Goldberg, 1998). Remarkable selectivity and specificity of UPS is achieved mainly by ubiquitination, a coordinated process involving three layers of steps each dependent on different class of enzymes, collectively comprising more than 600 individual enzymes involved in ubiquitination (Grabbe et al., 2011). In ATP-dependent process, ubiquitin is first activated by E1 Ubiquitin-activating enzyme and transferred to E2 Ubiquitin-conjugating

enzyme. E3 Ubiquitin-ligases then mediate the last step – a conjugation of ubiquitin from E2 to target protein via iso-peptide bond. By repeating this cycle, a protein became polyubiquitinated which is usually prerequisite to be recognised by the proteasome, a barrel-like multi-subunit protease (Finley, 2009). The proteasome contains receptors for ubiquitin enabling the interaction with client protein, as well as deubiquitinating enzymes (DUB), which remove the ubiquitin chain from the protein. Deubiquitinated protein is then translocated in ATP-dependent manner inside the proteolytic chamber of the proteasome, where it is hydrolysed to small peptides (Collins and Goldberg, 2017) (Fig. 1).

1.2 The ubiquitin code

Ubiquitin is very stable, conserved 8,5 kDa protein containing 76 amino acids assembled into compact globular structure. At the first step of ubiquitination, ubiquitin is activated by E1 enzyme in ATP-dependent manner leading to attachment of ubiquitin to E1 by thioester bond between C-terminal glycine 76 and a cysteine in the active site of E1 (Pickart, 2004). While human genome contains at least two E1 enzymes able to activate ubiquitin, Ubiquitin activating enzyme E1 (UBE1) is known to be responsible for nearly all the biologically relevant ubiquitinations (Jin et al., 2007). Following activation, ubiquitin in its thioester form is moved to E2 conjugating enzyme by transthiolation reaction. In contrast to E1, tens of conjugating enzymes are known in humans and all interact with UBE1 and one or more E3 ligases (Stewart et al., 2016). The third step involves a linkage of C-terminal carboxyl group of ubiquitin via iso-peptide bond to ϵ -amino group of lysine residue of a substrate protein, which is catalysed by E3 ligase (Zheng and Shabek, 2017).

The efficiency and specificity of ubiquitination is facilitated by enormous diversity and regulation of E3 ligases. More than 600 different E3 enzymes are known in humans spanning to two main families. The vast majority belongs to RING (Really Interesting New Gene) family characteristic by their RING catalytic domain, cysteine rich sequence containing two zinc ions, which promotes direct transfer of ubiquitin from E2 to lysine of the substrate protein (Zheng and Shabek, 2017). RING E3 ligases operate in various states, as monomers, homodimers or heterodimers, which includes also well-known ligases such as MDM2/MDMX (Mouse double minute 2/X) regulating cancer-associated protein p53 or BRCA1/BARD1 (Breast cancer 1/BRCA-associated RING domain protein 1) which is acting on damaged DNA (Metzger et al., 2014). Alternatively, many RING ligases forms

multimeric complexes such as cullin-RING ubiquitin ligases (CRL) or Anaphase-promoting complex/cyclosome (APC/C) (Lipkowitz and Weissman, 2011). Due to their complexity, CRL shows huge variability and represents the largest subgroup of E3 ligases including SCF (Skp1 – cullin – F-box protein) ligases. SCF consist of cullin protein (usually cullin-1), which provides scaffold for other components such as Skp1 (S-phase kinase-associated protein 1), an adaptor protein mediating recruitment of F-box proteins that are responsible for specificity of substrate recognition. Cullins also mediate the interaction with RING proteins, namely Rbx1 (RING-box protein 1) possessing ubiquitin ligase activity (Deshaies and Joazeiro, 2009). Because of their complex mode of regulation, it is not surprising that many substrates of SCF ligases are stress responsive and signalling proteins, such as p27, I- κ B α (Inhibitor of nuclear factor kappa B alpha) or Cdc25A (Cell division cycle 25A) (Skaar et al., 2014).

The other, far less abundant family of E3 ligases, is known as HECT (Homologous to the E6AP Carboxyl Terminus). In contrast to RING-type E3 ligases, which mediates direct transfer of ubiquitin from E2 to substrate, HECT ligases first form an intermediate with ubiquitin, which is subsequently transferred to the substrate. Moreover, while linkage specificity of ubiquitin chains (e.g. K48 or K63 chains) is determined by E2 in case of RING ligases, HECT ligases govern the type of ubiquitin linkage on their own (Berndsen and Wolberger, 2014).

Despite being a quite simple polypeptide, the ubiquitin chains regulates myriads of processes in highly specific and context dependent manner. This is achieved mainly due to its ability to form multimeric chains of different lengths and types. The ubiquitin polypeptide contains seven lysine residues (K-6, K-11, K-27, K-29, K-33, K-48, and K-63) each of them serve as a possible site for linkage with other ubiquitin molecule forming polyubiquitin chain. Moreover, also N-terminal methionine can mediate the binding with another ubiquitin. The chains are usually homogenous, where only the same residue (e.g. K-48) is used during chain elongation forming e.g. K48-polyubiquitin chain. Each type of chain has different structure and topology defining the fate of modified substrate (Fig. 2). Such ubiquitin “code” is then read by specific proteins containing ubiquitin-binding domains recognizing different types of polyubiquitin chains. All possible polyubiquitin chains (seven different lysine linkages and N-terminal methionine) have been found in eukaryotic cells, but the far most common are K48, K63, and K11 chains (Komander and Rape, 2012). While K48 along with K11 chains are best known as the mediators of protein degradation by the proteasomes, K63 chains play a role in cell signalling such as NF- κ B (Nuclear factor-kappa B) (Iwai, 2012) or upon DNA damage

(Liu et al., 2018; Schwertman et al., 2016), and in endosomal transport system (Nathan et al., 2013). The role of others is far less known and it is difficult to make unifying conclusion as many functions have been reported (in DNA damage response and mitochondria-related functions for K6, in innate immunity for K27, in signalling for K29, in protein trafficking for K33) (Akutsu et al., 2016).

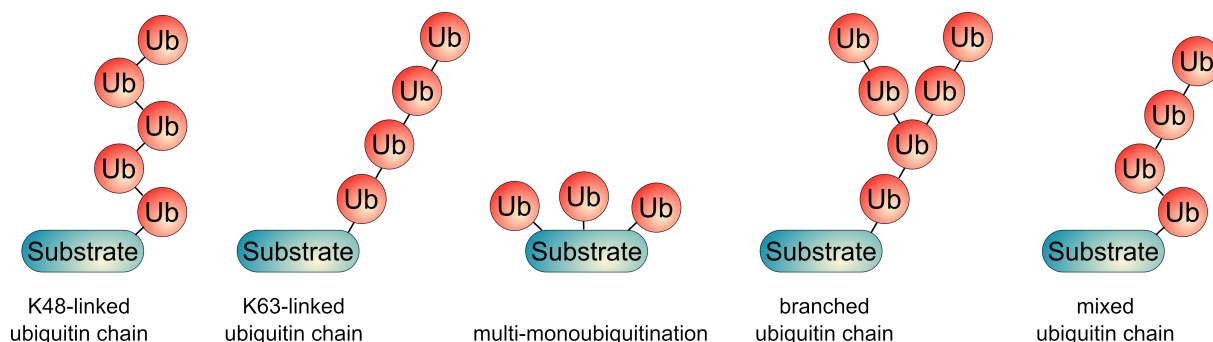


Figure 2 | The diversity of the ubiquitin code. Substrate proteins are modified by ubiquitin in many ways. Polyubiquitin chains are linked via different lysine residues (e.g. lysine(K)-48 or lysine(K)-63). Proteins are also modified by ubiquitin at multiple sites (multi-monoubiquitination) or by branched and mixed polyubiquitin chains.

The complexity of ubiquitination is even increased by multi-monoubiquitination of the substrate or by the formation of heterogeneous chains. In these mixed chains, ubiquitins are linked through different lysine residues, e.g. via K-48 and K-29. Additionally, more ubiquitins could be linked to single ubiquitin forming so called branched chains (Yau and Rape, 2016). The cellular functions of mixed and branched polyubiquitin chains still wait for deeper insight, but functions of mixed chains in protein degradation, signalling and endocytosis have been reported (Swatek and Komander, 2016). For branched chains, it has been discovered that significantly increase the interaction with proteasome and promotes protein degradation (Meyer and Rape, 2014).

Mixed chains are not limited only to ubiquitin, but also exist as heterotypic chains consisting of ubiquitin and some of ubiquitin-like proteins. For instance, chains made of ubiquitin and SUMO (Small ubiquitin-like modifier) or ubiquitin and NEDD8 have been

identified, but their physiological role remains largely unknown (Swatek and Komander, 2016).

On the basis of the above, it is clear that differentness and specificity of the “ubiquitin code” is far larger than previously thought making ubiquitination probably the most complex post-translational modification of proteins identified so far.

1.3 The structure and function of the proteasome

The ubiquitinated proteins dedicated for degradation are recognised by the proteasome. The eukaryotic proteasome is multi-subunit barrel-like complex of molecular weight ~2.5 MDa composed from two different components – a core particle (CP) called 20S proteasome where a protein degradation takes place, and a regulatory particle (RP) known as 19S proteasome responsible for recognition, unfolding and translocation of substrates prior their degradation. CP could interact with RP on one side (forming RP₁-CP) or both sides (forming RP₂-CP). The complex of CP with RP is known as the 26S proteasome (Budenholzer et al., 2017) (Fig. 3).

As stated above, the proteolysis of substrates is mediated by the 20S proteasome. CP is ~700 kDa barrel-like structure composed by 28 subunits that are arranged into four layered hetero-heptameric rings. Two outer rings consist of α -type closely related proteins and two inner rings consist of β -type subunits altogether forming α - β - β - α fitting cylinder, which contains three chambers. Subunits with proteolytic activity are located in the largest ~100 nm central cavity that is formed by β -rings. Three of the β -subunits (β 1, β 2, and β 5) are threonine proteases possessing caspase-like (C-like), trypsin-like (T-like), and chymotrypsin-like (CT-like) activities, respectively. Efficient protein cleavage by the proteasome is achieved by the combination of three different proteases with relatively low specificity enabling them to cleave almost any polypeptide. Proteasomal degradation of proteins is thus regulated solely by the entrance of substrates into proteolytic chamber. The gate is guarded by N-termini of α -type subunits, which close the pore under inactive state, so folded proteins cannot pass through the entrance. To activate the proteasome, α -subunits interact with RP leading to opening of the gate (Rousseau and Bertolotti, 2018; Tomko and Hochstrasser, 2013).

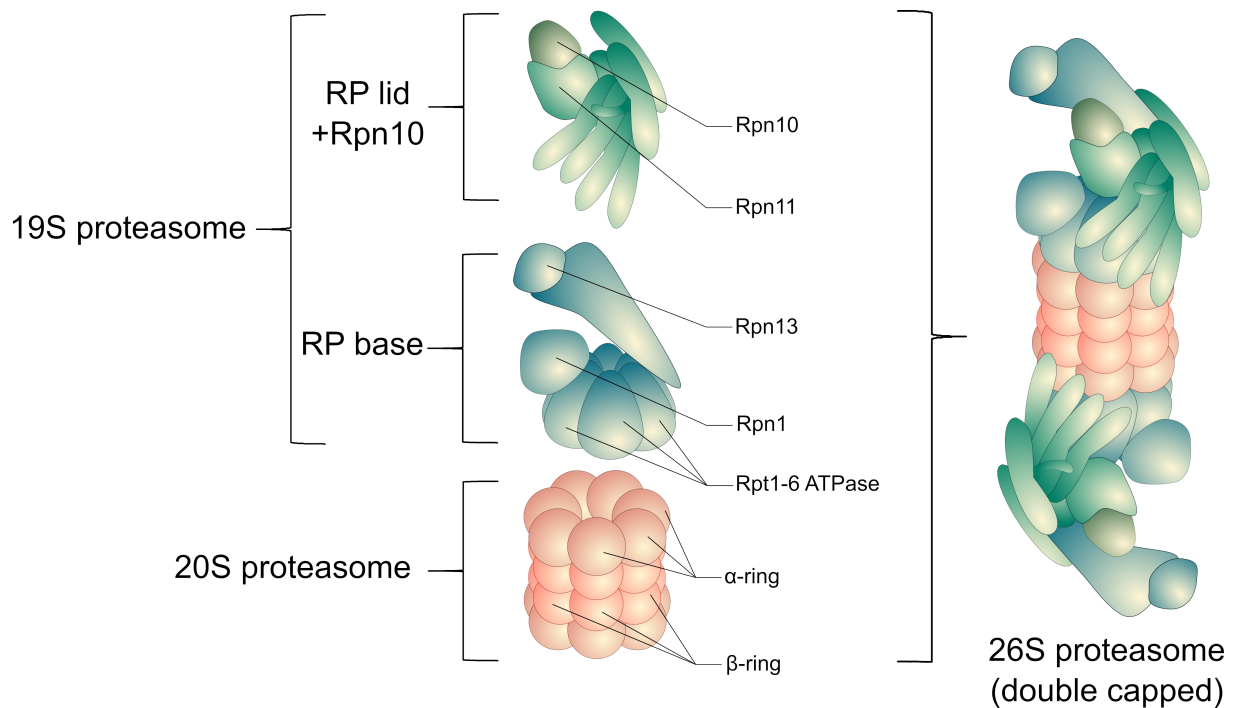


Figure 3 | The structure of the proteasome. The classical proteasome is composed from two components – 20S and 19S proteasome. 20S proteasome, where the protein degradation takes place, is composed of 28 subunits arranged as four layered hetero-heptameric α -type and β -type rings, which contain proteolytic subunits (not shown). 19S proteasome consists of the base and the lid particles. The base contains six related ATPases and ubiquitin recognising subunits Rpn1 and Rpn13. The lid contains Rpn11 deubiquitinase removing ubiquitin chain from the substrate. Rpn10 subunit serving as another ubiquitin receptor is not part of the base nor the lid. 20S particle interacts with one or two 19S particles forming 26S proteasome (single or double capped). (Note, for simplicity only selected subunits of the proteasome are named and marked).

As the 20S proteasome alone is largely inaccessible to substrates, the CP interacts with various activators to stimulate the degradation of proteins. In mammals, at least three different activators are known – proteasome activator PA200, 11S regulator complex (also known as REG) founded in alternative forms of the proteasome with unclear functions, and 19S RP that forms “canonical” 26S proteasomes (Finley, 2009).

The 19S RP, also known as PA700, is organised to two components – the base, and the lid. The base is composed of six related subunits with ATPase activity in yeast named as

Rpt1-6 (Regulatory particle triple-A protein) (in humans known as PSMC2,-1,-4,-6,-3,-5) that belongs to family of AAA (ATPases Associated with diverse cellular Activities) ATP-ases and form a ring directly interacting with outer ring of α -type subunits of the CP. The base also contains three non-ATPase proteins – Rpn1, Rpn2, Rpn13 (Regulatory particle non-ATPase) (in humans known as PSMD2, PSMD1 and ADRM1), that contains several binding sites for ubiquitin-binding proteins or ubiquitin. The lid is composed of six Rpn subunits (Rpn3,-5,-6,-7,-9,-12, in humans PSMD3,-12,-11,-6,-13,-8) with scaffolding function and two proteins (Rpn8 and Rpn11, in humans PDMD7 and PSMD14) that cooperate during deubiquitination of the substrate. Rpn10 (PSMD4) cofactor containing ubiquitin binding domain is not assigned to the base nor the lid and it is assumed to mediate the bridge between both sub-complexes (Bard et al., 2018; Lander et al., 2012). The proteasome contains three DUB – Rpn11 (PSMD14 or POH1) necessary for the function of the proteasome located in the lid (Yao and Cohen, 2002) and two other known as USP14 (Ubiquitin-specific protease 14) and UCH37 (Ubiquitin C-terminal hydrolase 37) stably associated with the base that have rather regulatory function (Lee et al., 2016).

It was previously thought that the ubiquitination solely determinates the fate and rate of substrate degradation, nevertheless recent discoveries demonstrated that proteasome is not just a passive machine for destruction, but rather highly organised and tightly regulated complex defining the fate of proteins, as the degradation of proteins by the proteasome involves several closely controlled steps (Collins and Goldberg, 2017).

First step involves recognition of ubiquitinated substrate. Initial binding of conjugates is mediated mainly by Rpn10 and Rpn13 via UIM (Ubiquitin-interactive domain) domain, and PRU (Pleckstrin-like receptor for ubiquitin) domain, respectively (Yu and Matouschek, 2017). Recently, new ubiquitin binding site was observed in Rpn1 explaining puzzling observations that proteasomes defective in both Rpn10 and Rpn13 still readily interact with ubiquitin conjugates (Shi et al., 2016). Ubiquitin conjugates bind proteasome with very high affinity, but potentially reversibly as the proteasomal DUBs USP14 and UCH37 remove ubiquitin from the substrate actually leading to its dissociation from the proteasome. On the other hand, the interaction of ubiquitinated protein with USP14 and UCH37 leads to a major conformational change enhancing substrate interaction with ATPases located in the base promoting substrate entry to the proteasome. The competition between these two opposite processes likely determines the fate of the substrates (Bard et al., 2018). Contrary to the early ideas, the proteasome is not so selective for the type and length of ubiquitin chains. *In vitro*,

even monoubiquitinated protein could be degraded, or K63 linked conjugates are degraded similarly like K48-marked proteins. In cells, the situation is likely more complicated as many competing factors determine the fate of ubiquitinated substrate. For example, K63 conjugates are efficiently captured by ESCORT system preventing its degradation by the proteasome (Nathan et al., 2013); monoubiquitinated substrates interact with the proteasome less tightly than substrates with long or branched chains, which are degraded very efficiently (Meyer and Rape, 2014).

The transition from initial binding to tight binding is dependent on ATP and partially unfolded or loosely folded region of the substrate, which activates ATPases and substrate transport into proteasome. The sequence of further steps is not fully clear, but involves deubiquitination of the substrate, unfolding and transport to proteolytic chamber (de la Peña et al., 2018). Rpn11 (PSMD14 or POH1) is deubiquitinase located near the entry to proteasome gate, which contains JAMM/MPN (Jab1/MPN/Mov34 metalloenzyme / Mpr1, Pad1 N-terminal) domain binding Zn^{+2} . This metalloprotease is essential for the degradation of substrates as it removes ubiquitin chain close to the substrate enabling its entry to the channel (Verma et al., 2002). Here, ATPase subunits Rpn1-Rpn6 unfold and transport the substrate to the proteolytic chamber through the gate, which is opened by Rpt2, Rpt3, and Rpt5 proteins. By the activity of β 1, β 2, and β 5 subunits, substrate is degraded into small peptides subsequently released to cytosol, where majority of them are digested by peptidases or used as precursors for antigen presentation by the MHC-class I (Major histocompatibility complex) molecules (Yu and Matouschek, 2017).

1.4 Protein quality control

Despite enormous quantity and rate of protein translation, the vast majority proteins do not contain errors in their amino acid sequence as only one in 10 000 amino acids is misincorporated. However, in the light of huge amount of proteome, millions of aberrant proteins are produced by the cell. Additionally, the proper folding and maintaining of correct structure of proteins is even far more challenging (Wolff et al., 2014). Proteins are constantly exposed to many environmental stressors including oxygen radicals, heat, or metal ions. As damaged, misfolded or aggregated proteins represent serious threat, documented by many diseases associated with their accumulation, the cells evolved sophisticated multi-layered system called protein quality control (PQC) for protection. PQC consists of systems for

identification of aberrant proteins, their refolding or, when necessary, for their destruction. Therefore, UPS is one of the central components of PQC in cytoplasm, ER, nucleus or mitochondria (Amm et al., 2014).

At least one third of all cellular proteins is translated on ER, which represents a key hub of PQC and a sensor of protein stress. Despite the existence of many protein-folding chaperones, it is estimated that more than one third of all proteins on ER does not fold properly and must be removed by ER-associated degradation (ERAD) pathway that employ the ubiquitination of unfolded proteins and their degradation by the proteasome (Christianson and Ye, 2014). In case the folding or degradative capacity of the cell is overwhelmed or impaired, accumulated defective proteins lead to ER-stress triggering so called Unfolded Protein Response (UPR) (Hetz, 2012).

Three main sensors of UPR have been identified - IRE1 α (Endoribonuclease inositol-requiring enzyme 1-alpha), PERK (Protein kinase RNA-like endoplasmic reticulum kinase), and ATF6 α (Activating transcription factor 6 alpha) (Hetz et al., 2015). The main ER chaperone, protein BIP (also known as GRP78 – glucose-regulated protein 78), plays important role in the activation of the sensors. Under normal conditions, it binds the sensors, but when unfolded proteins accumulate, BIP is sequestered and dissociates from the sensors leading to IRE1 α and PERK oligomerization and autophosphorylation, and to ATF6 α export to Golgi apparatus and nucleus, where it induces expression of target genes (Walter and Ron, 2011). Activated PERK phosphorylates translation initiation factor eIF2 α (eukaryotic translation initiation factor 2 alpha), which in turn disassembles polysomes and decreases total protein synthesis to reduce the load of new proteins, and concomitantly, to allow preferential translation of ATF4 (activating transcription factor 4), a transcription factor regulating genes involved in protein folding, autophagy and apoptosis. Additionally, activated IRE1 α induces alternative splicing of transcription factor Xbp1 (X-box binding protein 1), which controls mainly genes involved in protein folding (Fig. 4). Collectively, UPR activates proteins helping the cell to cope with aberrant proteins, attenuate global protein synthesis and thus promote the cell survival (Hetz, 2012). However, when unmitigated, the capacity of UPR is overwhelmed and terminal UPR is triggered, which involves for instance protein CHOP (CCAAT-enhancer-binding protein homologous protein), which serves as an activator of apoptosis (Lu et al., 2014).

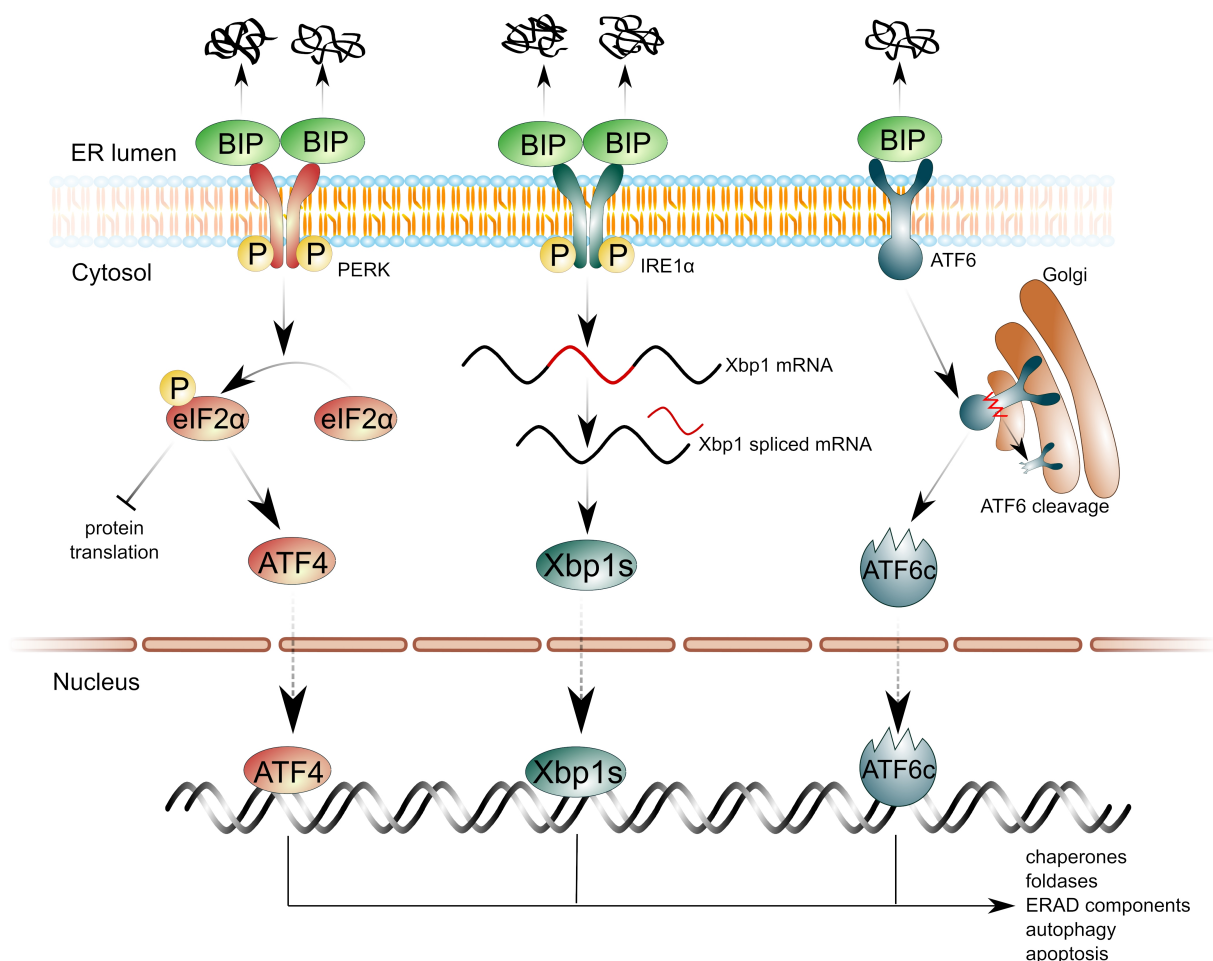


Figure 4 | The Unfolded protein response (UPR). Three main branches of the UPR are shown. Unfolded proteins in ER-lumen sequester BIP protein leading to activation of the UPR sensors – PERK, IRE α and ATF6. Autophosphorylated PERK phosphorylates eIF2 α , which in turn decreases total protein synthesis and activates ATF4 transcription factor regulating UPR target genes. Activated IRE1 α induces alternative splicing of Xbp1, resulting in production of Xbp1s form acting as a transcription factor. Activated ATF6 α is exported to Golgi apparatus, where it is cleaved to form the active transcription factor translocating into the nucleus to induce UPR-related genes.

To assist with folding of *de novo* synthesized proteins and to maintain proper structure of other proteins, cells evolved numerous chaperones that are vital part of PQC. Many of the chaperones belongs to the family of heat shock proteins (HSP), which have critical function in preventing protein unfolding and aggregation especially under various stress conditions (Sontag et al., 2017). Imbalance of protein homeostasis, accumulation of aberrant proteins or formation of protein aggregates trigger intense cellular response known as Heat shock response (HSR), as heat stress is common but not the only inductor of protein damage and unfolding (Åkerfelt et al., 2010). HSR is characterised by rapid activation of roughly 100 genes in human cells, majority of them belonging to chaperones or proteins involved in degradation, metabolism or DNA repair (Richter et al., 2010). HSR is regulated mainly by transcription factors, among them HSF1 (Heat shock factor 1) is assumed as the critical one. Under normal conditions, it is sequestered in the cytoplasm in inhibitory complex with HSP70 and HSP90 chaperones. Upon accumulation of aberrant proteins, HSP proteins dissociate and liberated HSF1 is activated leading to its oligomerization (formation of trimeric form), phosphorylation and translocation to nucleus, where it binds so called heat shock elements on DNA (after binding to DNA HSF1 can be detected as typical nuclear foci called as nuclear stress bodies) and triggers transcription of the target genes (Gomez-Pastor et al., 2017) (Fig. 5). Among them, genes of HSP70 family belong to the most important. Under physiological conditions involved mainly in folding of *de novo* translated proteins, stress-overexpressed HSP70 helps to prevent aggregation of unfolded proteins or even refold the aggregated one, and assist with sequestration or degradation of protein aggregates, occupying a critical role of cell response to stress conditions (Kim et al., 2013).

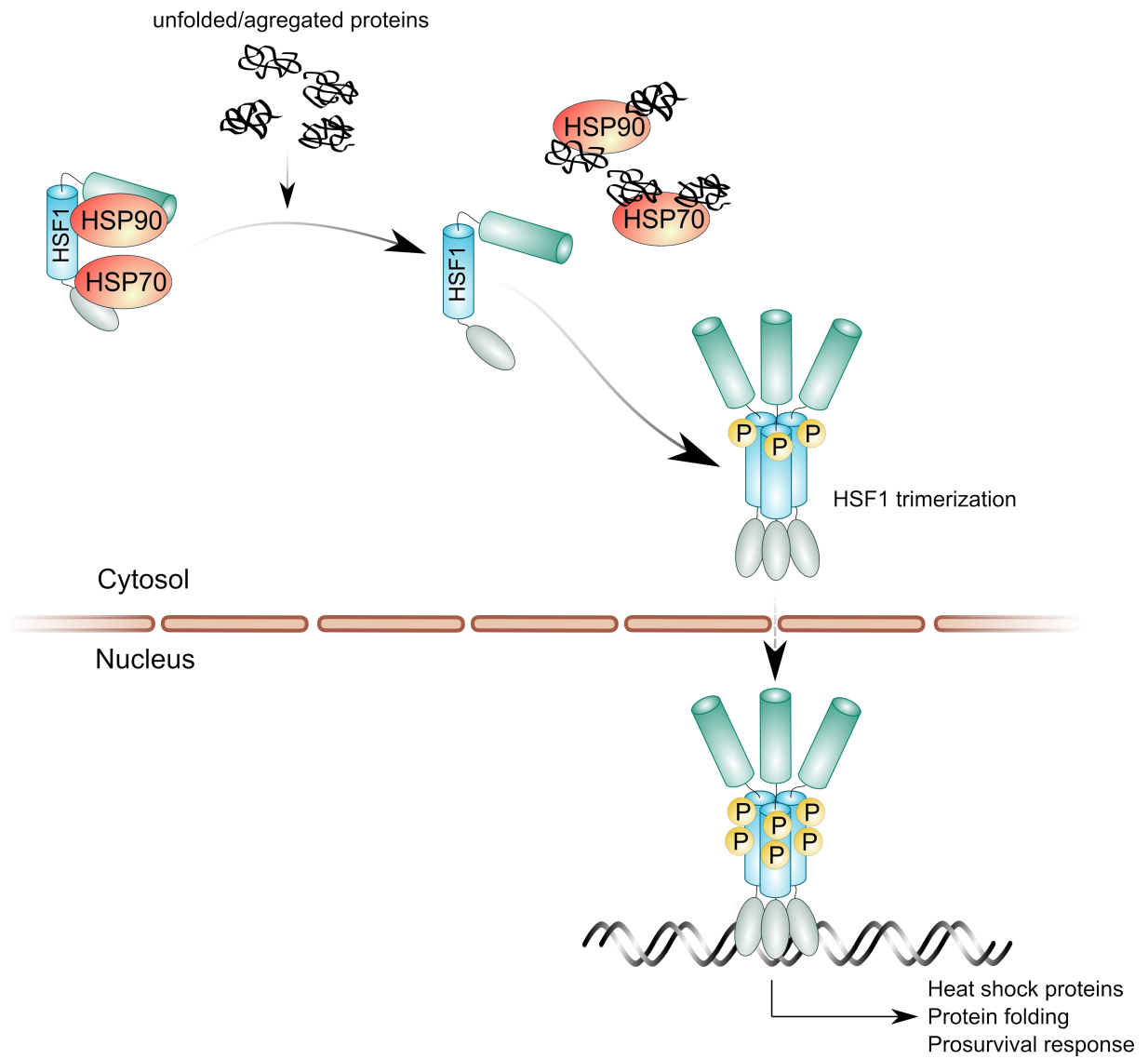


Figure 5 | The activation of Heat shock factor 1 (HSF1). In non-stressed cells, HSF1 is sequestered in the cytoplasm in inhibitory complex with Hsp70 and Hsp90 chaperones. Upon stress conditions, accumulated aberrant proteins unbind Hsp70/Hsp90 chaperones from HSF1, leading to liberation of HSF1, its phosphorylation, oligomerization and translocation to the nucleus to induce the expression of target genes.

1.5 The role of the p97 complex

Intensive research about how proteins are degraded revealed the existence of other layers of UPS except the ubiquitination and the proteasome, which are important or even indispensable for protein degradation. For instance, several shuttling factors have been discovered, which deliver ubiquitinated proteins to the proteasome or interact with the proteasome to assist with the recognition of substrates. These factors contain UBL-UBA (Ubiquitin-like and Ubiquitin-associated) domains enabling them to simultaneously interact with both ubiquitinated proteins via UBA domain and proteasome through UBL domain. In humans, the members of these factors include RAD23A/B, UBQLN1-4 (also known as ubiquilin family) or DDI1/2 (Saeki, 2017). While the importance and exact roles of these factors remained to be established, the physiological relevance is underlined by the fact that mutations in UBQLN2 are associated with severe neurodegenerative disorder known as amyotrophic-lateral sclerosis (Deng et al., 2011).

Another protein required for degradation of many substrates is p97, also known as VCP (Valosin-containing protein) or Cdc48 in yeast. This protein is far more than just shuttling factor, as growing evidence suggest p97 is involved in almost every aspect of cell biology connected to the ubiquitination. Similarly to the base of proteasome, p97 belongs to the family of hexameric AAA ATPases. It uses energy from ATP hydrolysis to perform many key steps required for degradation and processing of ubiquitinated proteins – unfolding and remodelling and segregase activity involving segregation of the ubiquitinated proteins from various complexes or chromatin, or their extraction from membranes before the actual transport to the proteasome (Meyer et al., 2012) (Fig. 6).

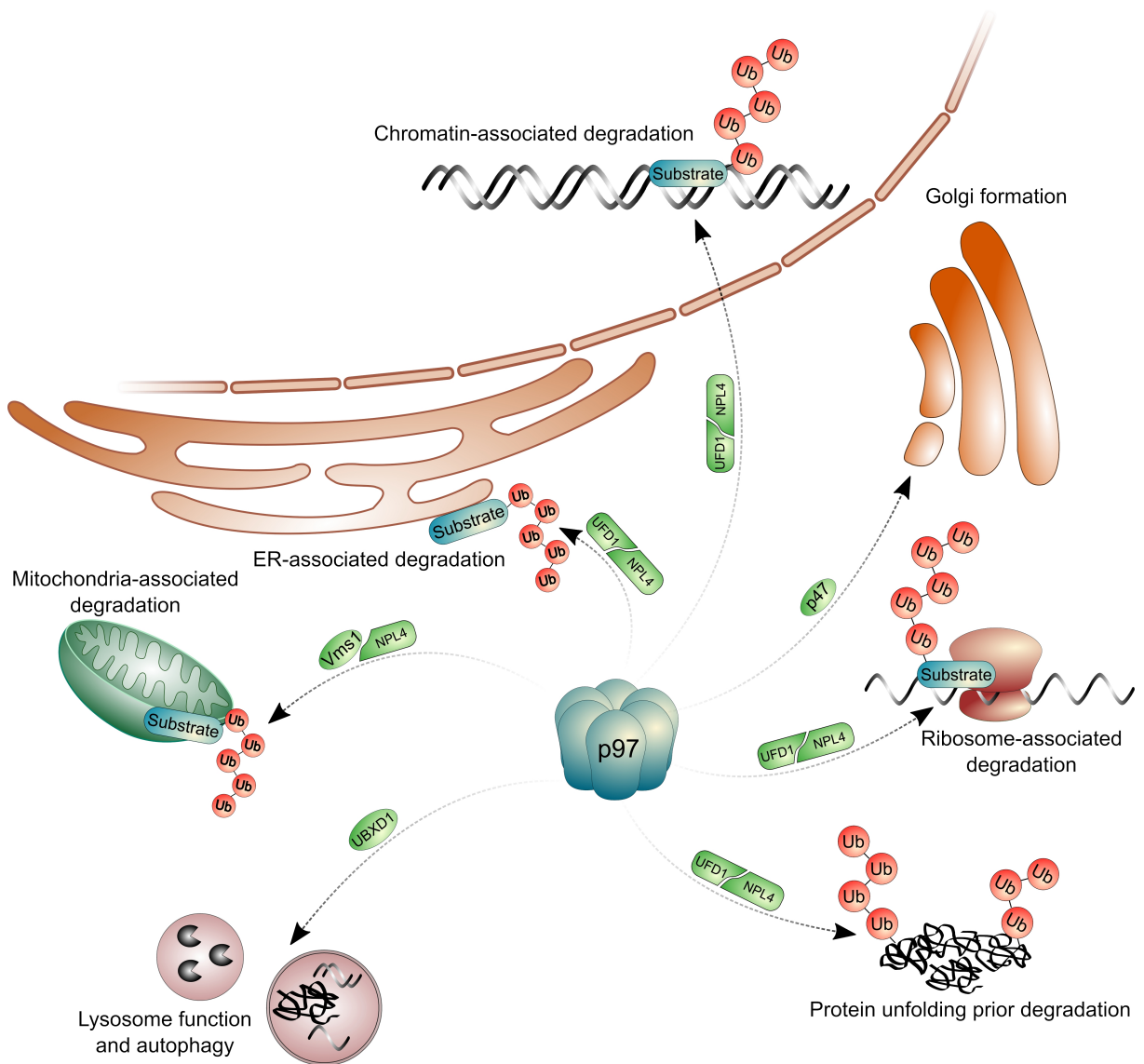


Figure 6 | The cellular functions of the p97 complex. p97 segregase in association with diverse cofactors operates in many essential processes. Together with NPL4-UFD1 heterodimer, p97 participates in ER-associated degradation, mitochondria-, chromatin-, ribosome-associated degradation, or in protein unfolding prior proteasomal degradation. In co-operation with p47 cofactor, p97 regulates also the biogenesis of Golgi apparatus, and with UBXD1 adaptor, p97 is involved in autophagy and lysosome function. (Note, only selected cellular activities of p97 are shown).

p97 contains N-terminal domain, two ATPase domains (D1 and D2) and flexible C-terminal tail. In the active hexameric form, ATPase domains form two stacked rings with the central pore. The exact functions of these domains is still not fully clear, but it seems that N-terminal domain is important for the interaction with client proteins and cofactors, while driving force is generated probably primarily by D2 (Bebeacua et al., 2012). Recently, a molecular mechanism of substrate processing by p97 was revealed (Bodnar and Rapoport, 2017). The model suggests that ubiquitinated substrate is transferred through central pore by the force produced by D2 domain. During the movement, the protein is unfolded, and with the assistance of D1 domain and associated DUB it is partially deubiquitinated and released.

p97 segregase plays an essential role in many aspects of cellular physiology and to perform a such variety of tasks, it interacts with a plethora of cofactors. Many of these cofactors contain binding site for ubiquitin and mediate the interaction of client proteins with p97, which itself has low affinity for ubiquitin; others are DUB enzymes or E3 ligases that rearrange ubiquitin chains attached to the substrates. About 30 different adaptors of p97 have been discovered according to a study published in 2016 (Xue et al., 2016).

The best studied cofactors are NPL4 (Nuclear protein localisation protein 4 homolog, also known as NPLOC4) and UFD1 (Ubiquitin fusion degradation 1), which participate in many functions of p97 including ERAD or chromatin associated degradation. NPL4 and UFD1 acts as heterodimer, which interacts with N-terminal domain of p97 hexamer, and recruits ubiquitinated client proteins (Meyer et al., 2002). The X-ray structure of NPL4 is unavailable until now, most likely because of high structural flexibility of the protein hampering the attempts to get it in crystal form and perform detailed X-ray analysis (Isaacson et al., 2007). Very recently, a high resolution cryo-EM structure of NPL4/p97 complex from thermophilic fungus *Chaetomium thermophilum*, which is presumably less sterically flexible, was published (Bodnar et al., 2018). It complements previous cryo-EM and biochemical studies (Bebeacua et al., 2012; Bruderer et al., 2004; Isaacson et al., 2007; Meyer et al., 2000; Pye et al., 2007) revealing that only one UFD1-NPL4 (UN) heterodimer interacts with p97 hexamer via UBX-L domain (Ubiquitin regulatory X-like) domain on NPL4 and via SHP (BS1, Binding segment 1) motive located on UFD1. Apart from UBX-L domain, NPL4 also contain putative zinc finger domain (put-ZF) followed by MPN domain similar to that found in POH1 (Rpn11) subunit of the proteasome. Last, C-terminal domain contain second zinc finger domain called NPL4 zinc-finger (NZF), which is most likely involved in recognition of the ubiquitinated proteins preferentially linked with K48 chains (Meyer et al., 2002). In

humans, NPL4 is expressed as two main isoforms, of which the “canonical” contains all domains, while the “alternative” lacks C-terminal NZF domain, which is substituted by another longer sequence making this variant little bit larger (visible on western blot as shifted second band) (Meyer et al., 2000). The physiological function of the alternative isoform is unknown. Besides SHP motive, UFD1 also contains UT3 domain recognising ubiquitin and C-terminal UT6 domain mediating the interaction with NPL4 partner (Bruderer et al., 2004). The exact site on NPL4, which UT6 interacts with, is not known, but according the study using *C. thermophilum* NPL4, it is probably located near putative zinc-finger and MPN domains (Bodnar et al., 2018); however, due to significant differences in sequence, it is questionable if these results are relevant also for human orthologues.

Apart from UN, p97 interacts with p47 protein, other core cofactor. p47 belongs to the family of UBA-UBX (Ubiquitin-associated; Ubiquitin regulatory X) domains containing proteins enabling p47 to simultaneously recognise ubiquitinated proteins via N-terminal UBA domain and p97 by C-terminal UBX domain. In contrast to UN, three p47 molecules bind p97 hexamer. p47 preferentially interacts with K63 linked ubiquitin chains enabling p97/p47 complex to regulate K63 chain dependent processes such as Golgi apparatus formation or membrane fusion (Bruderer et al., 2004; Kondo et al., 1997).

p97 interacts with UN or p47 in a mutually exclusive manner, so these cofactors are sometimes named as “core” adaptors. Apart of them, p97 binds plethora of other proteins, some of them, such as FAF1 or UBXD7, seems to have preference to bind p97/UN complex forming kind of secondary complex (Hänzelmann et al., 2011). On the other hands, Vms1 (VCP/Cdc48-associated mitochondrial stress-responsive 1) protein replaces UFD1 in UN dimer and forms stable p97/NPL4/Vms1 complex, which is required for mitochondria-associated degradation (Heo et al., 2010).

While the majority of p97 cofactors, represented mainly by UBA-UBX or UBX-L protein families, mediates the interaction with ubiquitinated client proteins, other p97-interacting proteins have different roles. For instance, p97 binds several E3-ubiquitin ligases and DUB enzymes that plays a role in many processes. Two main E3 ligases central for ERAD, HRD1 (HMG-CoA Reductase Degradation 1 Homolog) and gp78 (also known as AMFR-Autocrine Motility Factor Receptor), both interact with p97 (Stach and Freemont, 2017), as well as ligases of CRL family (Alexandru et al., 2008). Additionally, p97 is found in complex with several DUBs, including YOD1 (also known as OTU1), and ATX3 (Ataxin-3)

both involved in ERAD (Ernst et al., 2009; Wang et al., 2006), or VCIP135 (Valosin-containing protein/p47 complex-interacting protein, p135), a DUB essential for Golgi apparatus assembly (Uchiyama et al., 2002). Finally, there are also proteins with other activities that interact with C-terminal domain of p97, including PNGase (Peptide:N-glycanase) involved in ERAD (Stach and Freemont, 2017), or PLAA (Phospholipase A-2-activating protein) regulating clearance of damaged lysosomes (Papadopoulos et al., 2017). Such plurality, diversity, and versatility of cofactors makes p97 far more than just a shuttling factor upstream the proteasome, but rather another complex layer regulating the fate of growing number of proteins and cellular processes.

Among many processes in which p97 plays a role, ERAD is one of the most studied. Maturation-defective luminal and membrane proteins are dedicated to degradation in the proteasome, an action dependent on p97 activity. Defective proteins must be first translocated through ER-membrane, and once exposed to cytoplasm, they are ubiquitinated and recognised by p97 in complex with UN. p97 ATPase provides pulling force most likely required for final dislocation of ubiquitinated substrate and its release to cytoplasm where it is available to proteasomes (Stein et al., 2014). ERAD is multi-step process relying on coordinated action of proteins with different functions, thus p97 interacts with many proteins apart from core UN cofactors, including FAF1, UBXD8 recognising ubiquitin, with E3 ligases gp79 or HRD1, and also with DUBs YOD1 or ATX3 (Christianson and Ye, 2014).

Analogously to its role in ERAD, p97 is also critical for degradation of proteins located in outer mitochondrial membrane (OMM) during a process called mitochondria-associated degradation (MAD). Again, p97 mediates the extraction of ubiquitinated proteins out of OMM to facilitate their degradation by cytosolic proteasomes (Heo et al., 2010). The close relationship between ERAD and MAD was further demonstrated quite recently. It was shown that pro-apoptotic protein BOK (Bcl2 ovarian killer) regulating mitochondrial outer membrane permeabilisation, a critical event of intrinsic apoptosis, is degraded by classical ERAD components, including E3 ligase gp78 and p97 (Llambi et al., 2016).

p97 also act as a segregase using the pulling force to extract substrates from other complexes or structures such as chromatin. Growing body of evidence suggests an essential role of p97 in extraction and degradation of various proteins associated with chromatin (Dantuma and Hoppe, 2012). The first such identified substrate was Aurora B kinase, which is ubiquitinated and unloaded from the chromatin by p97-UN complex at the end of the mitosis

(Ramadan et al., 2007). p97-UN also mediates the degradation of Rpb1, the largest RNA polymerase II subunit, upon transcriptional stalling or UV damage (Verma et al., 2011). Additionally, according to published studies, p97 is recruited to the sites of DNA damage (Meerang et al., 2011) and regulates extraction of several key players acting on double strand breaks including L3MBTL1 (Acs et al., 2011), or presumably Ku70 and Ku80 (van den Boom et al., 2016). Moreover, several critical steps required for proper replication are dependent on p97-UN complex, comprising extraction of CDT1 replication origin licencing factor at the onset of S-phase (Raman et al., 2011), or removal of MCM7 helicase subunit, when the replication is completed (Moreno et al., 2014).

p97 complex is not linked only to the proteasomal degradation, but also to autophagy-lysosomal degradation, further extending its complex role in cellular physiology. It has been shown that p97 together with UBXD1 cofactor regulates endolysosomal sorting targeting the proteins to degradation in lysosomes (Ritz et al., 2011). p97 is also recruited to damaged lysosomes, where it removes K48 ubiquitin linked proteins to drive degradation of impaired lysosomes via a process called lysophagy (Papadopoulos et al., 2017). Similarly, p97 mediates a degradation of damaged mitochondria through mitophagy (Tanaka et al., 2010), degradation of cellular stress granules (Buchan et al., 2013), and processing of various cytoplasmic and nuclear aggregated proteins (Fujita et al., 2013; Gallagher et al., 2014; Kitami et al., 2006; Seguin et al., 2014).

Moreover, many proteins involved in regulation of cell cycle or signalling are substrates of p97. For instance, I κ B- α (Inhibitor of nuclear factor kappa B), a critical negative regulator of NF- κ B (Nuclear factor kappa B) transcription factor, is segregated from NF- κ B by p97-UN complex, which enables I κ B- α degradation by the proteasome and subsequent activation of NF- κ B (Li et al., 2014). Other protein, whose degradation is dependent on p97-UN complex, is Cdc25A (Cell division cycle 25 homolog A), a phosphatase regulating G2/M checkpoint, which must be efficiently degraded upon DNA damage to ensure the cell will not enter mitosis before the damage is repaired (Riemer et al., 2014). Further, the regulation of HIF1 α (Hypoxia inducible factor 1 alpha) transcription factor well illustrates the complexity of the p97 system. Together with UBXD7 cofactor, p97 interacts with ubiquitinated HIF1 α , and upon depletion of p97, HIF1 α accumulates as a high molecular mass species corresponding to ubiquitinated HIF1 α . However, the amount of accumulated HIF1 α is far lower than those observed after inhibition of the proteasome, suggesting that only a small subset of the HIF1 α is degraded in p97 dependent manner (Alexandru et al., 2008). This

indicates that perhaps p97 is involved only in degradation of protein molecules in some particular states, in case of HIF1 α presumably in complex with HIF1 β or DNA and transcription machinery (Alexandru et al., 2008; Bandau et al., 2012).

p97 complex does not need to be necessarily connected only to protein degradation, as exemplified by transcription factor NRF1 (also known as NFE2L1 - Nuclear factor erythroid derived 2-related factor 1, or TCF11 in humans). Cells evolved specialised response to proteasome stress or malfunction involving rapid induction on new proteasome subunits to compensate the insufficiency. This bounce-back response involves NRF1, a close relative of well-known NRF2 transcription factor, which is involved in the anti-oxidant response (Koch et al., 2011). The level of NRF1 is closely regulated mainly on the side of protein stability. Under normal conditions, NRF1 is synthesized as luminal protein on ER, which is, however, quickly translocated to cytosolic side of ER by p97 and presented for degradation to proteasomes. Thus, in non-stressed cells, the basal level of NRF1 is very low. Conversely, when the proteasome is inhibited or overloaded, translocated NRF1 cannot be degraded, but it is processed by a protease and the cleaved product translocates into the nucleus, where it induces expression of all proteasome subunits, and also p97/NPL4/UFD1 proteins (Radhakrishnan et al., 2010, 2014; Sha and Goldberg, 2014; Steffen et al., 2010). The identity of the protease responsible for the cleavage and release of NRF1 is still disputable, as some argue it is actually the proteasome itself (Sha and Goldberg, 2014), others suggest it is aspartyl protease DDI2 (DNA-damage inducible 1 homolog 2) (Koizumi et al., 2016; Lehrbach and Ruvkun, 2016). It is clear, however, that upon proteasome inhibition, NRF1 accumulates as two different species – the unprocessed form of molecular weight approximately 120 kDa (usually marked as p120), and the active cleaved form of 110 kDa (known as p110). As the translocation of NRF1 is dependent on p97, the inhibition of p97 results in accumulation of only uncleaved p120 form of NRF1 prohibiting induction of proteasome subunits (Le Moigne et al., 2017; Radhakrishnan et al., 2014). The physiological role of proteasome regulation by NRF1, and its potential role in resistance to proteasome inhibitors, is unclear so far, however, it has been shown that increased protein synthesis induced by growth factors or feeding elevated also degradative capacity via NRF1 (Zhang et al., 2014).

Taken together, p97 complex emerges as an important factor touching almost every aspect of cellular physiology, which has also numerous implications for tumour biology and therapeutic interventions.

1.6 The role of UPS in tumour development and treatment

Cancer cells harbour thousands of genetic alternations in their genomes including large rearrangements, amplifications, deletions, and translocations, as well as numerous point mutations. While a vast majority of these alternations is just accidental, some of them, such as mutations of certain receptors or kinases, drives cancer progression and cancer cells are highly dependent on their function, a phenomenon known as oncogene addiction (Weinstein, 2002). However, as the physiology of cancer cells is largely altered compared to their normal counterparts, malignant cells are also highly dependent on many stress-supporting pathways maintained by genes that are not classical oncogenes. Such dependency is called “non-oncogene addiction” (Solimini et al., 2007).

While many responses supporting cancer growth and survival are known, pathways regulating protein degradation and PQC systems are among the most important. Due to numerous genetic, epigenetic and transcriptional alternations, cancer cell rely more on mechanisms of proteostasis. These alternations likely challenge folding and degradative capacity of cells (Deshaies, 2014). To cope with such stress, cancer cells activate supporting pathways involving chaperones, UPS or autophagy. Many components of UPR response, including BIP, XBP1 or ATF6, are overexpressed in several solid and haematological malignancies; often correlate with progression and poor prognosis and have direct impact on tumour growth (Wang and Kaufman, 2014). Moreover, protein chaperones and HSF1, a master regulator of HSR, are upregulated in several cancers (Wu et al., 2017), and are required for their growth (Fok et al., 2018; Mendillo et al., 2012; Trepel et al., 2010). Similarly, the proteasome and p97, as critical components of UPS, are overexpressed in many cancers, including malignancies of breast, prostate, pancreas, liver, lung, or colon (Cui et al., 2015; Nakahara et al.; Petrocca et al., 2013; Tsujimoto et al., 2004; Valle et al., 2011; Yamamoto et al., 2004b, 2004c, 2004a, 2005), and usually correlates with invasiveness and poor prognosis.

The deregulation of UPS in cancer cells is not limited to their general demand to degrade multitude of damaged, unfolded or unwanted proteins, but includes also control of levels of specific proteins involved in signalling and cell-cycle regulation. Tumour suppressor protein p53 serves as an illustrating example. While mutated or lost in approximately half of all tumours, the second half of tumours still contains wild-type p53, which is relatively

frequently deregulated by increased degradation (Mandinova and Lee, 2011). For instance, in cervical carcinoma caused by HPV (Human papilloma virus) infection, E6 oncogenic viral protein induce rapid degradation of wt p53, as it triggers the interaction of p53 with E6AP (E6 associated protein) E3 ligase, which ubiquitinates p53 and commits it for degradation by the proteasome (Martinez-Zapien et al., 2016). The situation in cervical carcinoma is rather exception, as E6AP is not physiological regulator of p53, and the major E3 ligase regulating p53 is MDM2 (Hock and Vousden, 2014). Under normal conditions, p53 is constantly ubiquitinated by MDM2 and degraded by the proteasome, but various cellular stressors abolish the MDM2/p53 interaction leading to p53 stabilization and activation of downstream effects including cell-cycle arrest, senescence or cell death (Hock and Vousden, 2014). However, MDM2 ligase is overexpressed in significant percentage of tumours, leading to inactivation of wt p53 and inaccurate cellular response to stress (Wade et al., 2013). In sharp contrast to wt p53, various mutant forms of p53 are stable and frequently found in high levels in cancer tissues. While the explanation is not fully known, it is well accepted that MDM2 interacts with p53 mutant less tightly, and mut p53 is less efficiently ubiquitinated (Yue et al., 2017). Moreover, mut p53 is stabilised by interaction with HSPs or histone deacetylases, underwriting to high levels of mut p53, which probably promotes cancer growth, as gain-of functions of mut p53 are known to contributing to malignant progression (Muller and Vousden, 2014; Wiech et al., 2012).

Due to high dependency of cancer cells on protein degradation pathways, it is not surprising that targeting UPS represents promising approach for the treatment of cancer, especially for tumour types with secretory phenotype, such as neuroendocrine tumours, prostate cancer, but mainly certain hematologic malignancies, particularly multiple myeloma (Deshaies, 2014). Myeloma, as a malignancy originating from plasma cells producing immunoglobulins, is characteristic by the high levels of paraprotein, an immunoglobulin produced by a single cell clone in very high levels (Morgan et al., 2012). This secretory phenotype associated with extremely high levels of proteosynthesis and increased endogenous UPR stress is the likely explanation, why multiple myeloma is so far the most responsive cancer to inhibition of UPS, as illustrated by bortezomib, first-in-class proteasome inhibitor, which inhibits CT-like, and partially other proteolytic activities of the 20S proteasome (Moreau et al., 2012).

The development of bortezomib is an example of very effective, fast, and fruitful translational research based on collaboration of small group of scientist from academia and

private sector around Alfred L. Goldberg at Harvard Medical School. Originally, he intended to study proteasome inhibitors as a potential drug for muscle wasting, which occurs upon disease (e.g. cancer) or aging. For this purpose, he established biotech company MyoGenics, and in cooperation with chemist J. Adams, developed the most important inhibitors of proteasome such as MG-132 or bortezomib (MG-341) in less than one year solely based on knowledge of substrate specificity of the proteasome, without any screening efforts of random chemical libraries. In sharp contrast to usual practice, proteasome inhibitors were freely distributed to universities for academic research, yielding many discoveries about importance of the proteasome for cell cycle, apoptosis or cancer (Goldberg, 2011). For instance, the proteasome was shown to be essential regulator of NF- κ B, crucial transcription factor regulating inflammation or carcinogenesis (Palombella et al., 1994). These discoveries shifted the focus of company closer to cancer, however, as the proteasome was not accepted as a potential target for cancer treatment, the MyoGenics (later renamed as ProScript) lost financial support, and was sold for ridiculous price to company Millennium Pharmaceuticals as a rather not profitable project. Yet, encouraging results from various xenograft studies conducted by National Cancer Institute convinced Millennium Pharmaceuticals to invest to small clinical trial phase I involving all cancer types (Goldberg, 2012). By serendipity, one patient entering the trial had multiple myeloma, not so common cancer, and this patient showed a complete remission after bortezomib (Goldberg, 2012; Orłowski et al., 2002). Such promising result motivated to run phase II trial with multiple myeloma patients (Richardson et al., 2003). Bortezomib was very effective against this type of cancer, for which no adequate treatment was available at that time, leading to FDA approval of bortezomib (commercial name Velcade) based just on phase II clinical trials (Kane, 2003).

Currently, bortezomib is approved as first line therapy for multiple myeloma or mantle-cell lymphoma, and in clinical practice it is used to treat Waldenström's macroglobulinaemia, a disease characterised by high production of immunoglobulins (Manasanch and Orłowski, 2017). Despite extreme effort (bortezomib has been tested in more than 700 clinical trials) and promising preclinical results, its activity is limited only to few cancer types, challenging the theoretical concept that cancer cells in general are more dependent on UPS, and more broadly on PQC, and raising question what makes multiple myeloma so exceptionally sensitive to proteasome inhibition (Deshaies, 2014).

The original explanation based on the inhibition of NF- κ B transcription factor has been questioned by several contradictory observations (Hideshima et al., 2002, 2009), and

nowadays it is more accepted that the sensitivity to bortezomib is dominantly determined by proteotoxic stress, e.g. when the capacity of cells to handle and degrade unwanted proteins is overcome (Bianchi et al., 2009). In multiple myeloma, the level of endogenous stress is so high, that only partial and temporal inhibition of the proteasome, which is achieved in the clinic, is sufficient to activate strong UPR leading to cell death (Deshaies, 2014). This explanation is further supported by many observations that bortezomib is very effective as a treatment of several non-malignant conditions associated with plasma cells producing huge amount of antibodies. In pre-clinical models, and even in clinical practice, bortezomib was demonstrated as effective drug to combat some antibody-mediated autoimmune diseases, such as systemic lupus erythematosus, myasthenia gravis or autoimmune haemolytic anaemia, rheumatic arthritis or other non-cancerous monoclonal gammopathies (reviewed in Skrott and Cvek, 2014). In general, based on the efficacy of bortezomib against such diseases, which share the characteristic of a high-rate antibody production, it seems highly probable that the excessive production of proteins, and thus a strong need to efficiently degrade the damaged ones determines the sensitivity of certain cell types, including plasma and multiple myeloma cells, to proteasome inhibition (reviewed in Skrott and Cvek, 2014).

Despite significant improvement of prognosis of multiple myeloma patients after introduction of bortezomib into clinic, the acquired or intrinsic resistance considerably limits its benefit and durable response (McConkey and Zhu, 2008). There are many hypotheses to explain resistance to proteasome inhibition, including overexpression or mutation within the critical 20S subunit PSMB5, which is the main binding site for bortezomib, and possess CT-like proteolytic activity. Such mode of resistance is very common in cell culture models, where the resistance is induced artificially (Balsas et al., 2012; Franke et al., 2012; Oerlemans et al., 2008), however, all attempts to identify such mutations in multiple myeloma cells obtained from patients primarily or secondary resistant to bortezomib therapy failed, as no association between any variation within PSMB genes and response to bortezomib has been identified (Lichter et al., 2012; Politou et al., 2006). As an alternative scenario, it has been proposed that less differentiated myeloma cells secreting lower amount of immunoglobulins may stand behind the resistance. Using patient tumour samples, Xbp1s, a mediator of UPR and plasma cell maturation, has been shown to play a role in the resistance to bortezomib in patients. Xbp1s negative cells representing multiple myeloma B cells or pre-plasmablasts seem to survive therapeutic application of bortezomib and are enriched in samples obtained from patients refractory to bortezomib. These cells express lower amounts of

immunoglobulins and shows lower UPR stress, suggesting decreased dependency on the UPR pathway than Xbp1s positive plasma cells (Leung-Hagesteijn et al., 2013). However, only small fraction of patients not responding to bortezomib have non-secretory myeloma, suggesting that other mechanism of resistance must be employed (Manasanch and Orłowski, 2017). Recently, a case report of a multiple myeloma patient, which was followed over several years during the cycles of treatment with proteasome inhibitors, revealed that point mutations within PSMB5 may indeed be involved in resistance to bortezomib in a subset of patients (Barrio et al., 2019). During the cycles of therapy based on proteasome inhibitors, the status of genes coding for proteasome subunits was checked, and some cell clones harbouring different mutation within PSMB5 were detected. These mutations span to bortezomib binding pocket and makes cell resistant to proteasome inhibitors, confirming the clinical relevance of such mechanism of resistance (Barrio et al., 2019).

The unanswered question remains, however, what stands behind non-responsiveness of all solid tumours to bortezomib therapy. It is not clear if these tumours are intrinsically less sensitive to the inhibition of proteasome or the clinically achievable partial and transient inhibition by bortezomib is not strong enough to trigger cell death. Together with frequent acquired resistance in multiple myeloma, the lack of effectivity in solid tumours motivated the development of second generation of proteasome inhibitors with better pharmacokinetic properties and different mode of action (Deshaies, 2014).

Carfilzomib (Kyprolis), the first example of such drugs, is irreversible inhibitor of primarily CT-like activity of 20S. Early clinical trials revealed that carfilzomib is effective in relapsed and refractory multiple myeloma patients, leading to FDA approval for this group of patients (Kortuem and Stewart, 2013). Phase III study also demonstrated that carfilzomib combined with dexamethasone is at least equally efficient as bortezomib plus dexamethasone, and even it is superior in case of progression-free and overall survival (Dimopoulos et al., 2016, 2017). However, the potential activity of carfilzomib in solid tumour is unclear so far.

The last FDA approved proteasome inhibitor, ixazomib (Ninlaro), is first orally available inhibitor, again targeting CT-like activity of 20S, but reversibly. It is used in the clinic in pre-treated multiple myeloma patients. Due to better pharmacokinetic properties, and faster dissociation from the proteasome, it is hoped that ixazomib will show better penetration and activity in tissues outside circulation (Kupperman et al., 2010), which is supported by preclinical models revealing better activity in solid tumour compared to bortezomib

(Kupperman et al., 2010). The activity of ixazomib towards solid tumours is largely unknown until now, as trials are still running. However, the results from phase I involving patients with various solid tumours do not raise much expectations (Smith et al., 2015).

The proteasome and whole UPS provides several other potential targets appropriate for cancer treatment besides 20S proteolytic activities (Fig. 7). The relevance of these targets is so far based mostly on pre-clinical and experimental data, but yet first inhibitors entered clinical trials. Targeting DUBs associated with the proteasome represent one of such approaches. Molecule b-AP15 is supposed to inhibit DUBs UCHL5 and USP14 leading to impairment of proteasome activity, accumulation of non-degraded proteins, induction of apoptosis, and reduction of tumour growth (D'Arcy et al., 2011). POH1, a central DUB of 19S proteasome, represents also intriguing target, as revealed by recent series of papers describing various POH1 inhibitors (Li et al., 2017, 2018). Despite the activity *in vivo* needs to be established, these compounds potently inhibit the activity of the proteasome, activate UPR and apoptosis. The activity of 19S proteasome can be also compromised by molecules targeting ubiquitin receptors recognising substrates for degradation, as exemplified by compound RA190 that covalently binds to receptor Rpn13 (Anchoori et al., 2013). RA190 treatment leads to accumulation of ubiquitinated proteins, triggers apoptosis, and reduces tumour growth in several models (Anchoori et al., 2013; Song et al., 2016). At the opposite side of the whole UPS pathway lies E1 ubiquitin activating enzyme UBE1 necessary for ubiquitination of vast majority of proteins. As revealed quite recently, small molecule MLN7243 specifically targeting UBE1 has noteworthy anti-cancer activities in preclinical models (Hyer et al., 2018). UBE1 inhibition leads to depletion of ubiquitin conjugates, impairment of signalling cascades, and activation of proteotoxic stress, collectively leading to profound activity *in vivo* motivating first clinical trials (Hyer et al., 2018). However, preliminary results regarding anti-cancer activity from phase I are not so encouraging, yet further trials will be needed to reveal the potential of MLN7243 (Sarantopoulos et al., 2017).

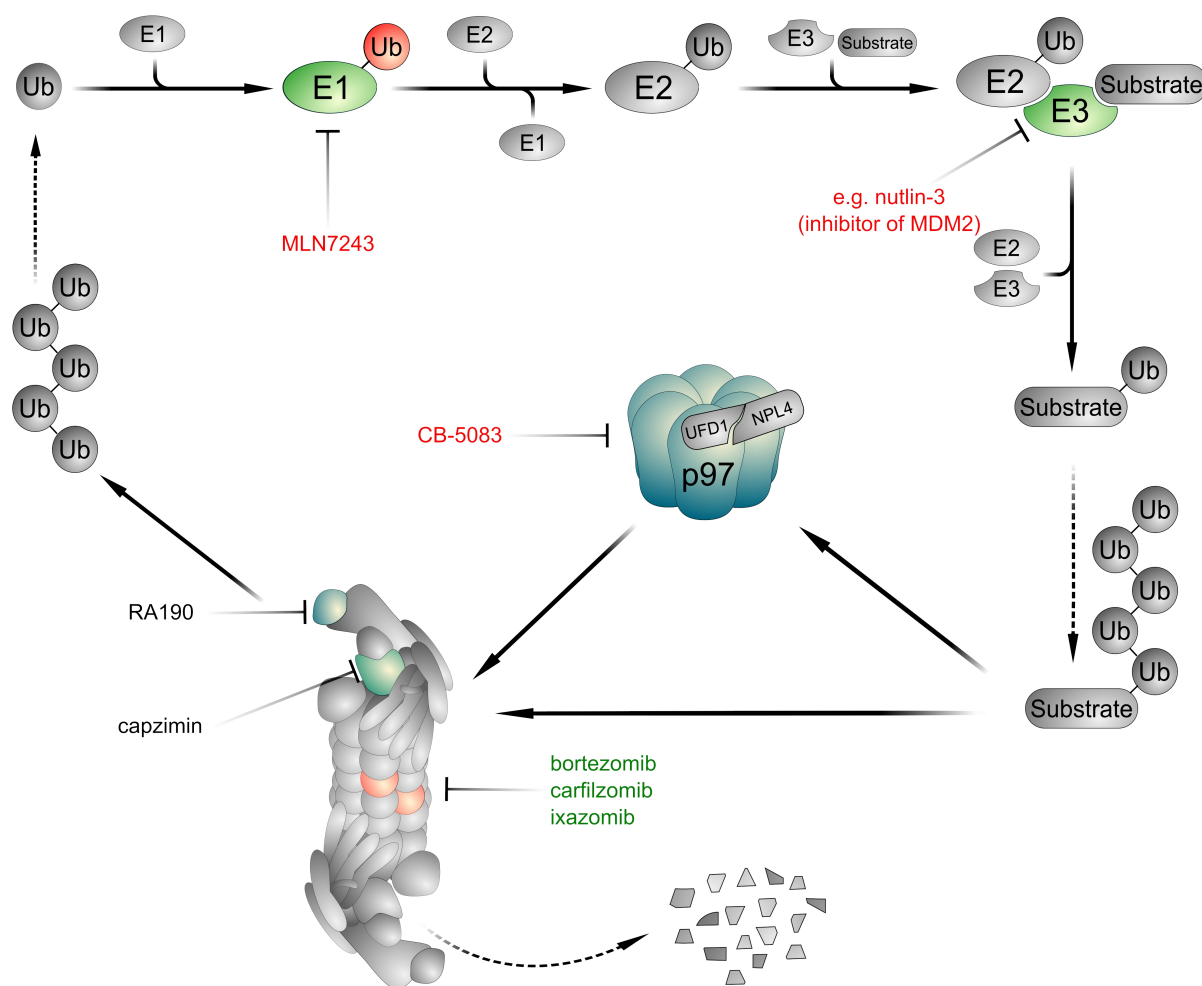


Figure 7 | The anti-cancer agents targeting components of UPS. UPS provides many attractive targets for small molecules intended to treat cancer. First of them are already in clinical use (in green), others entered clinical trials (in red), and the rest is in preclinical stage (in black). E1 ubiquitin activating enzyme (UBE1) is specifically inhibited by MLN7243. Enormous diversity of E3 ligases provides bottomless source of possible targets. Small molecule nutlin-3 targets MDM2 E3-ligase regulating p53 turnover. ATPase activity of p97 is targeted by first-in-class inhibitor CB-5083. Clinically used proteasome inhibitors bortezomib, carfilzomib and ixazomib target primarily $\beta 5$ subunit. 19S proteasome also provides promising targets. Rpn11 deubiquitinase is inhibited by experimental compound capzimin, and ubiquitin binding subunit Rpn13 by small molecule RA190.

Given the importance of p97 in many pathways associated with malignant transformation it is not surprising that recently emerged p97 inhibitors represent highly promising class of compounds. The first small molecule thought to interfering with p97 activity was Eeyarestatin I (EerI) identified ten years ago. EerI does not inhibit p97 directly, but rather it interferes with p97 associated DUB ATX3, leading to accumulation of ubiquitinated proteins, impaired degradation, and cell death in various cancer models including bortezomib-resistant multiple myeloma cells (Wang et al., 2008, 2009). However, as a ATPase, it might be more reasonable to target p97 via compounds inhibiting this domain. The first such compound, DBeQ, was identified by the screen involving the measurement of ATPase activity of p97, and cell-based degradation assay confirming the ability of compounds to specifically inhibit only degradation dependent on p97 (Chou and Deshaies, 2011; Chou et al., 2011). DBeQ impaired both ubiquitin-dependent and autophagy degradation pathways leading to death of cancer cells. More potent and specific derivatives of DBeQ, compounds ML240 and ML241 were further synthesized and characterised (Chou et al., 2013). In parallel, different group identified new more potent covalent and reversible p97 inhibitors NMS-859 and NMS-873 by high-throughput screen (Magnaghi et al., 2013). Particularly the later one, NMS-873, the first allosteric p97 inhibitor, was the best and the most thoroughly characterised inhibitor at that time, and became a common tool to study p97 function in cells. Similarly to DBeQ, NMS-873 impaired degradation of several proteins and activated UPR leading to death of dozens of cancer cell lines. Interestingly, no correlation between the toxicity of bortezomib and those of NMS-873 across the panel of cell lines was detected, and NMS-873 was not preferentially toxic to multiple myeloma cells indicating very different mode of action of p97 inhibitors compared to the inhibitors of the proteasome (Magnaghi et al., 2013).

To move p97 inhibitors to the clinics, pharmaceutical company Cleave Biosciences build on ML240 scaffold, and identified the lead p97 inhibitor, CB-5083, with suitable drug-like properties ensuring adequate pharmacokinetic properties and oral administration (Anderson et al., 2015). Highly selective and potent, CB-5083 specifically inhibits D2 ATPase domain of p97 leading to impairment of ERAD, accumulation of ubiquitinated proteins, and activation of UPR, autophagy, and finally apoptosis. CB-5083 shows activity in more than 300 cancer cell lines, and in several *in vivo* mouse models surpassing bortezomib, carfilzomib, and ixazomib in activity against solid tumours. Again, no correlation of cell responsiveness to bortezomib and CB-5083 was observed (Anderson et al., 2015). CB-5083

shows also remarkable activity against multiple myeloma models (Le Moigne et al., 2017) motivating currently running phase I clinical trial (NCT02223598). Another phase I trial involving patients with various solid and haematological malignancies is also ongoing (NCT02243917).

Interestingly, it has been observed that various ATPase inhibitors have diverse potency against p97 associated with different cofactors such as p47 or NPL4-UFD1 (Fang et al., 2015; Gui et al., 2016), raising question if p97 inhibitors specifically targeting p97 with certain cofactor could be developed in future. However, so far no such inhibitor exists nor a compound inhibiting the main p97 adaptors.

1.7 Anti-cancer activity of disulfiram

With the approval of bortezomib for clinical use and the proteasome as an established target for anti-cancer drugs, many compounds were tested for their effect on UPS, among them a number of drugs approved for different purposes. Such effort led to several interesting discoveries including repeated observations that a drug disulfiram impairs the function of UPS leading to death of cancer cells.

Disulfiram (commercial name Antabuse) is FDA-approved drug used to treat alcohol abuse for more than 60 years. Its metabolites irreversibly inhibit ALDH (Aldehyde dehydrogenase), mainly ALDH2, an enzyme critically involved in the metabolism of alcohol. ALDH mediates the conversion of toxic acetaldehyde, the main metabolite of ethanol, to acetic acid (Koppaka et al., 2012). When ALDH is inhibited by the metabolite of disulfiram, the level of acetaldehyde increase dramatically upon alcohol consumption leading to unpleasant reaction (in rare cases can be life threatening), which include sweating, flushing, respiratory difficulty, nausea, tachycardia, and hypotension, known as disulfiram-alcohol reaction. Consequently, such adverse effects preclude alcohol use under disulfiram therapy (Ehrenreich and Krampe, 2004).

Disulfiram, chemically tetraethylthiuram disulfide, belongs to the family of thiuram disulfides, organic compounds used frequently in industry as rubber accelerators or pesticides. The surprising anti-alcoholic properties of disulfiram were discovered through two independent accidental observations. First, in 1937, E. E. Williams, a plant physician working in a chemical company producing tetramethylthiuram disulfide, a compound closely related to

disulfiram, observed that workers were unable to drink any alcohol, since even one beer caused unpleasant reaction (Williams, 1937). Second, when searching for potential vermicide, two Danish scientists E. Jacobsen and J. Hald tried disulfiram, a compound with scabiescide properties. To evaluate potential side effect, Jacobsen first tested the drug on himself, revealing that the drug is safe, however, when combined with alcohol, it causes very unpleasant reaction (Hald and Jacobsen, 1948). Jacobsen and Hald as a researches connected to pharmaceutical company, immediately recognized the potential of disulfiram in the treatment of alcoholism. In 1949, just four years after the surprising initial observation, disulfiram was approved in Sweden followed by other countries. Nowadays, disulfiram is used by approximately 120 000 patients worldwide, of which significant number comes from Denmark (Kragh, 2008).

First indications about potential anti-cancer activity of disulfiram comes form 70's, when disulfiram was repeatedly shown to suppress chemically or UV induced tumours of various organs in mice (Black et al., 1978; Irving et al., 1983; Wattenberg, 1978). However, it was not clear if it did because of its direct effect on cancer or rather because it reacted chemically with carcinogens. More relevant signs of its anti-tumour activity were reported by a study conducted by National Cancer Institute aiming to identify potential chemical carcinogens, which involved also disulfiram, and its main metabolite diethyldithiocarbamate (ditiocarb, DTC), as the compounds frequently used in the industry. The study evaluated the occurrence of tumours after long term exposition of chemicals added to a diet of treated animals. Unexpectedly, the addition of disulfiram to diet significantly reduced the incidence of spontaneous tumours of breast, hypophysis, liver, pancreatic islets, thyroid and lymphomas in mice or rats (Program, 1979b, 1979a). The interest about disulfiram anti-cancer properties increased in late 90's, when a direct effect on cancer cells were reported (Liu et al., 1998) initiating the efforts to identify its mechanism of action in cancer cells resulting in hundreds of publications. In recent years, around 30 scientific papers a year are published about disulfiram connection to cancer.

From a clinical perspective, anti-cancer activity of disulfiram is also supported by the evidence from patients. First case report describes full regression of metastatic breast cancer in alcoholic women taking disulfiram (Lewison, 1977). Moreover, ditiocarb, the main disulfiram metabolite, was in late 80's and 90's very popular as a suspected modulator of immune response, and was successfully tested in HIV patients (Hersh et al., 1991), and produced under the commercial name Imuthiol. These positive results motivated to test

ditiocarb in cancer patients too. In randomised, double-blinded phase II trial involving high risk breast cancer patients, ditiocarb significantly prolonged both overall and disease-free survival as an adjuvant therapy (Dufour et al., 1993). Additionally, in a small phase II clinical trial assessing the addition of disulfiram to chemotherapy for the treatment of metastatic non-small cell lung cancer, disulfiram significantly prolonged overall survival, with two long term survivals in disulfiram group (Nechushtan et al., 2015). Disulfiram seems to be effective also in other types of cancers, including melanoma or glioblastoma, as suggest intriguing case reports (Brar et al., 2004; Karamanakos et al., 2017). Potential anti-cancer activity of disulfiram is also supported by epidemiological evidence, which indicates that it could have protective effect against breast, and prostate cancer (Askgaard et al., 2014). Currently, disulfiram is tested in several clinical trials involving different tumour types, including glioblastoma (NCT02678975, NCT01777919), breast (NCT03323346), and prostate (NCT02963051).

The anti-cancer activity of disulfiram is explained by several ways. Early studies demonstrated, that disulfiram interferes with several pathways important for tumour development, and spreading. These pathways include angiogenesis, which was reported to be suppressed by disulfiram via inhibition of superoxide dismutase (SOD-1), a zinc and copper containing protein important for vessel formation (Marikovsky et al., 2001). Moreover, it was reported that disulfiram blocks matrix metalloproteinases 2 and 9 (MMP) proteases playing a role in degradation of extracellular matrix, a process enabling spreading of cancer cells to surrounding tissues (Shian, 2003). Both proteins, SOD-1 and MMP, contain zinc, which is critical for their activity. It is well known that disulfiram rapidly decomposes *in vivo* to ditiocarb, a strong metal chelator, and the ejection of zinc from the active sites is believed to stand behind the inhibition of these enzymes. Additionally, it was suggested that disulfiram inhibits maturation of P-glycoprotein involved in resistance of cancer cells to conventional chemotherapy (Loo, 2000). Disulfiram and related dithiocarbamates were also shown to inhibit the activation of NF- κ B transcription factor participating in various processes promoting malignant transformation (Lövborg et al., 2006; Wang et al., 2003; Xu et al., 2017; Ziegler-Heitbrock et al., 1993).

Later, it became apparent that toxicity of disulfiram towards cancer cells is greatly potentiated by metal ions, namely zinc(II) and copper(II) (Allensworth et al., 2015; Brar et al., 2004; Cen et al., 2004; Chen et al., 2006). It was shown that disulfiram slowly reacts with copper(II) in distilled water forming high yields of bis-(diehtyldithiocarbamate)-copper

complex (CuET) in 24 hours. It was supposed that CuET facilitates intracellular uptake of copper ions leading to apoptotic cell death (Cen et al., 2004). Alternatively, it is also possible that in culture media disulfiram decomposes to ditiocarb, which is, in contrast to disulfiram, extremely strong metal chelator (Tawari et al., 2015). Consequently, it was suggested that not disulfiram or CuET itself is the active compound, but the toxicity is mediated solely by the copper(II) ions, which disturb cellular homeostasis and induce strong oxidative stress (Tardito et al., 2011). Alternative targets of disulfiram such phosphoinositide 3-kinase (Zhang et al., 2010a) or DNA demethylase (Lin et al., 2011) have been also suggested. Chemists even proposed that anti-cancer activity of disulfiram is likely just an artefact, since the toxic effect in cell cultures is not mediated by disulfiram or copper ions, but just by the reaction between these two compounds, which produce high amount of oxygen radicals toxic to cells in a petri dish (Lewis et al., 2014).

One of the most popular hypotheses in recent years explaining the activity of disulfiram in cancer cells relay on the first reported target of disulfiram – aldehyde dehydrogenase (ALDH). It is widely accepted that ALDH is overexpressed in various stem cells including cancer stem cells (CSC), and therefore, it is believed that ALDH is important for this population of cells despite the clear explanation is still lacking (Clark and Palle, 2016). Numerous studies claim that disulfiram (especially when combined with copper) inhibits various ALDH isoforms (mainly ALDH2 and ALDH1) in plenty of different cancer types leading to death of cancer cells (Liu et al., 2012, 2013, 2016; MacDonagh et al., 2017; Raha et al., 2014; Tacconi et al., 2017). Unfortunately, in these studies several logical gaps can be found. Most importantly, it is well established that disulfiram itself is not the active compound inhibiting ALDH *in vivo* (Koppaka et al., 2012). The metabolism of disulfiram was deeply studied, so it is well known that disulfiram decomposes rapidly to ditiocarb that is further metabolised to several intermediates including S-methyl-diethyldithiocarbamate sulfoxide, and S-methyl-diethylthiocarbamate sulfoxide, which are most likely responsible for ALDH inhibition as confirmed by *in vitro* and *in vivo* studies (Lipsky et al., 2001a, 2001b; Mays et al., 1995; Shen et al., 2001). Despite this clear fact, for unknown reason, no study so far used these direct and relevant metabolites to show if they are toxic to cancer cells. Moreover, according to many studies (Allensworth et al., 2015; Cong et al., 2017; Liu et al., 2012; MacDonagh et al., 2017), disulfiram must be combined with copper(II) to see the effect on cancer stem cells, which is puzzling if ALDH should be the relevant target. Moreover, it is not clear why disulfiram or disulfiram/copper(II) are toxic to all cells in the culture, if only a

few percent of them have detectable ALDH activity and are supposed to represent CSC (Liu et al., 2012, 2016). However, the physiological role of potential ALDH inhibition in tumour tissue by disulfiram metabolites remains completely unknown.

Probably the most accepted hypothesis explaining anti-cancer activity of disulfiram involves the inhibition of the proteasome. In 2006 two groups independently demonstrated that disulfiram or disulfiram/copper(II) combination efficiently inhibits protein degradation in cancer cells leading to cell death, and suggest the proteasome as the target (Chen et al., 2006; Lövborg et al., 2006). However, both studies disagree about the site of inhibition as the first study claims that not the proteolytic activities of 20S, but the whole 26S proteasome is impaired (Lövborg et al., 2006), while the second argues for CT-like activity of 20S as a primary target (Chen et al., 2006). Both studies demonstrated that disulfiram inhibits NF- κ B activation depending on the proteasome, and accumulates various endogenous proteasome substrates. As it was previously shown that dithiocarbamates inhibit proteasome function only in the presence of metal ions (Chen et al., 2005; Kim et al., 2004), it is not surprising that also disulfiram targets the proteasome in copper(II) dependent manner, as addition of copper(II) ions to the culture media greatly enhance both the proteasome inhibition and the toxicity (Chen et al., 2006). It was also shown that not only copper ions, but also other transition metals like cadmium or zinc significantly potentiates disulfiram activity towards the proteasome (Li et al., 2008). However, when tested synthetic CuET complex, as a suspected metabolite of disulfiram *in vivo* (Johansson and Stankiewicz, 1985), the complex did not inhibit 20S activity leading to a speculation that not 20S, but rather 19S particle is targeted by CuET complex (Cvek et al., 2008).

Such discrepancy is actually symptomatic for research about anti-cancer activity of disulfiram. The vast majority of publications relay on the combination of disulfiram (or dithiocarb) with copper(II) ions, both extremely reactive compounds, rather on synthetic complex of these two chemicals – CuET (Skrott and Cvek, 2012). This could lead easily to confusing or even misleading results, as currently it is not known how disulfiram reacts with copper(II) in the media, to which extent, and what is the identity of product(s). The use of disulfiram/copper(II) combination could be especially problematic in case of *in vitro* enzymatic assays, as both compound may non-specifically interact with the enzyme. For instance, in the landmark paper about disulfiram effect on the proteasome (Chen et al., 2006), disulfiram/copper(II) mixture is used to test the inhibition of the purified 20S proteasome, as the crucial initial experiment. The assay clearly demonstrated the inhibition by

disulfiram/copper mixture, however, importantly, copper(II) alone was equally efficient (Chen et al., 2006). How the contribution of disulfiram and copper(II) ions could be dissected? On the other hand, synthetic CuET complex was ineffective in the same assay (Cvek et al., 2008). From other point of view, the use of disulfiram could be also problematic to some extent. It is well known that disulfiram is extremely unstable, and rapidly decompose to other compounds, as minimal or zero levels of the drug could be detected in plasma from patients taking disulfiram (Johansson B, 1986; Masso and Kramer, 1981). Similarly, however, it is currently not known if CuET complex is indeed metabolite of disulfiram, as suggested 30 years ago (Johansson and Stankiewicz, 1985), but never confirmed. All these confusions about relevant targets or metabolites preclude straightforward research aiming to repurpose disulfiram for cancer, and urge for fresh insight and clarification.

2 AIMS

The aims of this thesis include:

1. To identify the active metabolite of disulfiram responsible for anti-cancer effect, and to find if this metabolite is also present in organisms undergoing disulfiram's therapy.
2. To uncover its mechanism of action in cancer cells especially in relation to protein degradation and ubiquitin-proteasome system.
3. To discover the potential molecular target of this anti-cancer metabolite.
4. To describe the phenotypes associated with the impairment of the targeted protein.

3 MATERIALS AND METHODS

3.1 HPLC/MS analysis of copper-dithiocarbamate complex (CuET)

The HR-MRM analysis was performed on HPLC-ESI-QTOF system consisting of HPLC chromatograph Thermo UltiMate 3000 with AB Sciex TripleTOF 5600+ mass spectrometer, using the DuoSpray ESI source operated at ion source voltage 5500 V, ion source gas flow rates 40 units, curtain gas flow rate 30 units, declustering potential 100 V and temperature 400°C. Data were acquired in Product ion mode with two parent masses 358.9 and 360.9 for analysis of CuET. Chromatographic separation was done by PTFE column especially designed for analysis of strong metal chelators filled by C18 sorbent (IntellMed, cat.no.IM_301). Analysis was performed at room temperature and flow rate 1500 µL/min with isocratic chromatography. Mobile phase consisted of HPLC grade acetone (Lachner) 99.9%, HPLC water (Merck Millipore) 0.1% and 0.03% HPLC formic acid (Sigma). Acquired mass spectra were evaluated in software PeakView 1.2, where extracted ion chromatograms of transitions 88.0 and 116.0 (common for both parent masses) with 0.1 mass tolerance was Gaussian smoothed with width of 2 points. Peak area was then recorded and recalculated to ng/ml according to calibration curve.

3.2 Sample preparation for HPLC/MS analysis

For HPLC/MS analysis MDA-MB-231 xenografted mice were used. MDA-MB-231 was injected (5×10^6 cells were transplanted s.c.) to grow tumours in SCID mice (ENVIGO, NL). After the tumours were palpable, mice were treated by DSF (50 mg/kg/day) and DSF (50 mg/kg/day; orally) plus copper gluconate (0,15 mg/kg/day; orally) regime for 5 days, and sacrificed. All aspects of the animal study met the accepted criteria for the care and experimental use of laboratory animals, and protocols were approved by the Ethical Committee of Faculty of Medicine and Dentistry, Palacky University in Olomouc. Liquid nitrogen-frozen biological samples were cut into small pieces by scalpel. Sample (30-100 mg) was immediately processed by homogenization in 100% acetone in ratio 1:10 sample vs. acetone (for plasma or serum the ratio was 1:4). Homogenization was done in a table homogenizer (Retsch MM301) placed in a cold room (4°C) in 2 ml Eppendorf tube with 2 glass balls (5mm) for 1min, 30Hz. Next, tube was immediately centrifuged at 4°C, 20.000G, 2min. Supernatant was decanted into a new 1,5 ml Eppendorf tube and immediately centrifuged for 30min using small table centrifuge (BioSan FVL-2400N) placed inside a -80°C freezer. Supernatant was quickly decanted into glass HPLC vial and kept at -80°C not

longer than 6 hours. Just before the HPLC analysis the vial was placed into the pre-cooled (4°C) LC-sample rack and immediately analysed. To enable approximate quantification of analyzed CuET, calibration curve was prepared. Various amounts of CuET were spiked to plasma, frozen in liquid nitrogen, and placed at -80°C to exactly mimic sample processing. Standards were then processed similarly as the samples described above. To measure circulating CuET concentrations, mice were dosed with single per oral DSF (50 mg/kg) and sacrificed at different time points. Serum was collected and frozen for analysis.

3.3 Blood collection from humans for HPLC/MS analysis of CuET

Blood samples were collected before and 3 hours after per oral application of the DSF (Antabuse 400 mg) dissolved in water. Used needles were of special type for metal analysis - Sarstedt Safety Kanule 21G x 1½'' REF 85.1162.600. Collection tubes were of special type for metal analysis - Sarstedt – S-Monovette 7,5 ml LH, REF 01.1604.400. Immediately after the blood collection the samples were centrifuged in a pre-cooled centrifuge (4°C at 1300G for 10min). After the spinning, tubes were placed on ice and the plasma fraction was immediately aliquoted into the 1,5-ml Eppendorf tubes with approx. 500ul per tube. The tubes with plasma were immediately frozen on dry ice and later stored in -80°C. Blood samples were collected from volunteers who signed the informed consent for undergoing Antabuse therapy due to alcohol abuse. Human participants were 4 males (ages 34, 38, 41, 60 years) and 5 females (ages 37, 56, 46, 59, 63 years). All individuals were freshly diagnosed for alcohol use disorder and were scheduled for Antabuse therapy. Blood samples were collected before and after the first application of Antabuse. The study was approved by the Ethical Committee of Faculty of Medicine and Dentistry, Palacky University in Olomouc.

3.4 Cell lines

Cell lines were cultured in appropriate growth media supplemented with 10% fetal bovine serum and penicillin/streptomycin; and maintained at humidified, 5% CO₂ atmosphere at 37°C. Lines cultured in DMEM medium were: HCT116 (ATCC), DU145 (ECACC), PC3 (ECACC), T47D (NCI60), HS578T (NCI60), MCF7 (ECACC), MDA-MB-231 (ATCC), U-2-OS (ECACC), HeLa (ATCC), NIH-3T3 (ATCC), CAPAN-1 (ATCC), A253 (ATCC), FaDu (ATCC), , h-TERT-RPE1 (ATCC), HeLa-Ub(G76V)-GFP-ODD-Luc (kindly provided by prof. R.J. Deshaies, Pasadena, California). Cell lines cultured in RPMI1640 medium were: AMO-1 (WT and adapted to bortezomib kindly provided by prof. C. Driessen, St. Gallen, Switzerland), MM-1S (kindly provided by prof. C. Driessen, St. Gallen, Switzerland), Cell

line A549 (ATCC) was cultured in F12K medium, RWPE-1 (ATCC) cells were cultured in a keratinocyte serum-free medium supplemented with the bovine pituitary extract and human recombinant epidermal growth factor (Thermo Scientific). DU145-RS (radio-surviving) cell line was previously characterised (Kyjacova et al., 2015). Cell lines were tested for mycoplasma contamination.

3.5 Stable cell lines construction, transfection, siRNA

For construction of all stably transfected cell lines U-2OS cell line (ECACC) was used. For U-2OS-Ub-GFP the commercial Ub-GFP EGFP-C1 vector (Addgene) was used, for U-2OS-NPL4-GFP the commercial NPLOC4-GFP pCMV6-AC-GFP vector (Origene), was used, for U-2OS-p97-GFP the commercial VCP-GFP pCMV6-AC-GFP vector (Origene) was used and for U-2OS-UFD1-GFP the commercial UFD1L-GFP pCMV6-AC-GFP vector (Origene) was used. MDA-MB-231 cell line expressing POH1-myc was established using the commercial PSMD14 vector (Origene). Cells were transfected using Promega FugeneHD according to manufacturers' instructions. Cells were further cultivated in the appropriate antibiotics (geneticin, 400 µg/ml). Medium with geneticin was replaced every 2-3 days until the population of resistant cells was fully established. Cells were further refined by sorting for cells expressing GFP signal (BD FACS Aria). For preparation of inducible MUT-NPL4-GFP cells, U-2OS cells were transfected with pcDNA6/TR plasmid (Invitrogen, V1025-20) using FugeneHD transfection reagent (Promega, E2311) according to manufacturer's protocol. To generate a cell line that stably expresses the Tet repressor, U-2OS cells were cultured in selective medium with blasticidin (10 µg/ml) for 10 days. Blasticidin-resistant colonies were picked, expanded and screened for clones that exhibit the lowest basal levels and highest inducible levels of expression. Next, the most suitable clones were transfected with the PCDNA4/TO expression vector encoding the mutated NPL4-GFP protein using the Fugene transfection reagent. Cells were cultured in medium with Zeocin (500 µg/ml) to select clones that contain pcDNA 4/TO-mutated NPL4-GFP. The MUT-NPL4-GFP-encoding plasmid were obtained from GenериBiotech. To induce expression of protein, cells were incubated with doxycycline (Sigma) 1 µg/ml for 16-48 hours. For siRNA-mediated knock-down, U-2OS cells were transfected with anti-TDP43 siRNA (Dharmacon; L-012394-00) or non-targeting siRNA (Eurofins Genomics-UAA UGU AUU GGA ACG CAU A) using Lipofectamine RNAiMAX transfection reagent (Invitrogen) according to manufacturer's protocol. After 48 hours, the knock-down efficiency was evaluated by immunofluorescence analysis.

3.6 Colony formation assay

Cells were seeded into 6-well plates at 100-300 cells per well (depending on the cell line). Next day the cells were treated with compounds as indicated in the specific experiments and kept in culture for 7-14 days. Colonies were visualized by crystal violet and counted.

3.7 XTT assay

10.000 cells were seeded into a 96-well plate. Next day, the cells were treated as indicated. After 24 or 48 hours (as indicated in legends of individual figures) an XTT assay was performed according to manufacturer's instructions (Applichem). XTT solution was added to media and incubated for 30-60 minutes, and then dye intensity was measured at the 475nm wavelength using spectrometer (TECAN, Infinite M200PRO). Results are shown as mean values and standard deviations from 3 independent experiments, each performed in 3 replicates. IC50s are calculated using Graphpad Prism software based on survival curves from at least two independent experiments.

3.8 Annexin V staining

Cell cultures were treated as indicated and harvested by trypsinization. Initial culture medium and washing buffer were collected to include detached cells. Cells were centrifuged (250G, 5min) and re-suspended in a staining buffer (140 mM NaCl, 4 mM KCl, 0.75 mM MgCl₂, 10 mM HEPES) containing 2.5 mM CaCl₂, Annexin V-APC (1:20, BD Biosciences) and 2.5 µg/ml 7-AAD (BD Biosciences) for 15 minutes on ice in the dark. Samples were analysed by flow cytometry using BD FACSVerser (BD Biosciences), at least 10.000 events were acquired per sample. Collected data were processed by BD FACSSuite (BD Biosciences) and exported into Microsoft Excel.

3.9 Caspases 3/7 assay

Activity of caspase-3 and -7 was quantified by cleavage of fluorogenic substrate CellEvent™ Caspase-3/7 Green Detection Reagent (ThermoFisher Scientific). Briefly, samples prepared in the same staining buffer as described for Annexin V staining above were supplemented with 2% FBS, 0.5 µM CellEvent™ Caspase-3/7 Green Detection Reagent and incubated for 45 minutes at room temperature in the dark. Subsequently, 0.5 µg/mL DAPI was added and samples were analysed by flow cytometry using BD FACSVerser (BD

Biosciences), at least 10.000 events were acquired per sample. Collected data were processed by BD FACSSuite (BD Biosciences) and exported into Microsoft Excel.

3.10 Immunoblotting and antibodies

Equal amounts of cell lysates were separated by SDS-PAGE on hand-cast or precast tris-glycine gradient (4-20%) gels (Life Technologies), and then transferred onto nitrocellulose membrane. The membrane was blocked with 5% milk in Tris-buffered saline containing 0.1% Tween 20 for 1 hour at room temperature, and then incubated overnight at 4°C or 1hour at room temperature, with one of the following primary antibodies (all antibodies were used in the system under study (assay and species) according to the profile of manufacturer): anti-ubiquitin (1:1000; Cell Signaling, cat.n.:3933), anti-HIF1 α (1:1000; BD Biosciences, cat. n.: 610958), anti-Cdc25A (1:500; Santa Cruz Biotechnology, clone DCS-120), anti-NRF1 (1:1000, Cell Signaling, clone D5B10), anti-VCP (1:2000; Abcam, cat. n.: ab11433), anti-VCP (1:1000; Novus Bio, cat. n.: NBP100-1557), anti-NPLOC4 (1:1000; Novus Bio, cat. n.: NBP1-82166), anti-ubiquitin lys48-specific (1:1000; Merck Millipore, clone Apu2), anti- β -actin (1:500, Santa Cruz Biotechnology, cat. n. sc-87778), anti-GAPDH (1:1000, GeneTex, clone 1D4), anti-Lamin B (1:1000; Santa Cruz Biotechnology, cat. n.: sc-6217), anti-calnexin (1:500; Santa Cruz Biotechnology, cat. n.: sc-11397), anti- α -Tubulin (1:500; Santa Cruz Biotechnology, cat. n.: sc-5286), anti-Xbp1 (1:500; Santa Cruz Biotechnology, cat. n.: sc-7160), Ufd1 (1:500; Abcam, cat. n.: ab155003), cleaved PARP1 (1:500; Cell Signaling, cat. n.: 9544), p-eIF2a (1:500; Cell Signaling, cat. n.: 3597), ATF4 (1:500; Merck Millipore, cat. n.: ABE387), HSP90 (1.500; Enzo, cat. n.: ADI-SPA-810), HSP70 (1:500; Enzo, cat. n.: ADI-SPA-830), HSF1(1:500; Cell Signaling, cat. n.: 4356), pHSP27 (1:1000; Abcam, cat. n.: 155987), HSP27 (1:1000; Abcam, cat. n.: 109376) CHOP (1:500; cat. n.:2895, Cell Signaling) followed by detection by secondary antibodies: goat-anti mouse IgG-HRP (GE Healthcare), goat-anti rabbit (GE Healthcare), donkey-anti goat IgG-HRP (Santa Cruz Biotechnology, sc-2020). Bounded secondary antibodies were visualized by ELC detection reagent (Thermo Scientific) and images were recorded by imaging system equipped with CCD camera (ChemiDoc, Bio-Rad) operated by Image Lab software or developed on film (Amersham).

3.11 Immunofluorescence staining

Cells were grown in 24-well plates with 0.170mm glass bottom (In Vitro Scientific). Where indicated, the cells were pre-extracted before fixation with pre-extraction buffer (10

mM PIPES, pH 6.8, 100 mM NaCl, 1.5 mM MgCl₂, 300 mM sucrose, 0.5% Triton-X 100, 1mM DTT, 5 µg/ml leupeptin, 2 µg/ml aprotinin, 0.1 mM PMSF) for 20 minutes at 4°C, washed by PBS and then immediately fixed with 4% formaldehyde for 15 minutes at room temperature. Cells were stained with primary antibodies: anti-ubiquitylated conjugated mouse FK2 antibody (1:500; Enzo, cat. n.: BML-PW8810), anti-VCP (1:500; Abcam; cat. n.: ab11433), anti-NPL4 (1:500; Novus Bio, cat. n.: NBP1-82166), HSP70 (1:100; Enzo, cat. n.: ADI-SPA-830), HSF1 (1:500; Cell Signaling, cat. n.: 4356) anti-ubiquitin lys48-specific (1:500; Merck Millipore, clone Apu2), SC-35 (1:500; Abcam, cat. n.: ab11826), Sumo2/3 (1:500; Abcam, cat. n.: ab3742), TDP-43 (1:300; Proteintech, cat. n.: 10782-2-AP), PML (1:300, Santa Cruz) and appropriate Alexa Fluor 488 and 568 secondary antibodies (Invitrogen, 1:1000). Cytochrome c was stained by Alexa Fluor 555 conjugated mouse anti-cytochrome c antibody according manufacture protocol (BD Pharmingen, cat. n.: 558700).

3.12 Microscopy, FRAP and image analysis

Samples were examined in a Zeiss Axioimager Z.1 platform equipped with the Elyra PS.1 super-resolution module for structured illumination (SIM) and the LSM780 module for CLSM. High resolution images were acquired in super-resolution mode using Zeiss Pln Apo100x/1.46 oil objective (tot. mag. 1600x) with appropriate oil (Immersion 518F). SR-SIM setup involved 5 rotations and 5 phases for each image layer and up to 7 Z-stacks (101nm) were acquired per image. CLSM setup for FRAP and live cells acquisition involved c-Apo 40x/1.2W water immersion objective. Bleaching of regions of interest (ROI) was performed using Argon 488nm laser. Lower resolution images of fixed samples were acquired using Plan Apo 63x/1.4 Oil objective (tot. mag. 1008x). FRAP and image acquisitions were performed in Zeiss Zen 11 software. For FRAP internal Zen's "Bleach" and "Regions" modules were used. Data from FRAP analysis involving multiple bleached ROI's were exported into MS-Excel and charted. Basic processing of acquired images such as contrast and brightness setting was done in Adobe Photoshop on images exported as tiff. Quantitative microscopy-based cytometry of the IF stained samples was performed using an automatic inverted fluorescence microscope BX71 (Olympus) in the ScanR Acquisition software (Olympus), analyzed with ScanR Analysis software (Olympus).

3.13 Cell fractionation for Triton X insoluble pellets

Cells were treated as indicated, washed in cold PBS and lysed in lysis buffer (50 mM HEPES, pH 7.4, 150 mM NaCl, 2 mM MgCl₂, 10% glycerol, 0.5% Triton-X100, protease

inhibitor cocktail by Roche) for 10 minutes gently agitating at 4°C. Then, cells were scraped to Eppendorf tubes and kept for another 10 minutes on ice with intermittent vortexing. After that, the lysate was centrifuged at 20.000G for 10 minutes at 4°C. Insoluble fraction and supernatant, respectively, were re-suspended in 1x LSB buffer.

3.14 Isolation of microsomal fraction

After the desired treatment in cell culture, cells were washed with cold PBS and lysed (250 mM sucrose, 20 mM HEPES pH 7.4, 10 mM KCl, 1.5 mM MgCl₂, 1 mM EDTA, 1 mM DTT, protease inhibitor cocktail). Lysates were homogenised by Potter-Elvehjem PTFE homogeniser and kept on ice for 20 minutes. The homogenates were subjected to serial centrifugation steps (720G and 10000G for 5 minutes both, and 100 000G for 1 hour). Pellets and supernatants from the last ultracentrifugation step were re-suspended in the 1x LSB buffer and used for WB analysis.

3.15 Ub^(G76V)-GFP degradation

HeLa-Ub(G76V)-GFP-ODD-Luc cells expressing Ub^(G76V)-GFP were treated with 5 µM MG-132 for 4 hours. After that, the medium was discarded and cells were twice washed with PBS and then incubated with tested compound in the presence of 50 µg/ml cycloheximide for another 2 hours. GFP intensity was acquired using flow cytometry (BD FACSVerser-BD Biosciences). The median of GFP intensity for each condition was used in calculation. The percent of remaining Ub^(G76V)-GFP for each compound was calculated using the following formula: (Test compound/MG-132 treatment for 4 hours) * 100.

3.16 p97 ATPase activity assay

P97 ATPase assay was performed as described previously (Chou et al., 2011). 250 nM of p97 protein was diluted in assay buffer (50 mM Tris-HCl pH 7.4, 20 mM MgCl₂, 0.5 mM DTT). Test compounds were added in DMSO (final concentration of DMSO was 5%). After 10 minutes of incubation, the reaction was started with ATP (100 µM final concentration) followed by 1-hour incubation at room temperature. The reaction was stopped by adding Biomol green solution (Enzo) and free phosphate was measured according to manufacturer instructions. Results are expressed as a percent activity of the control (well containing only DMSO).

3.17 26S proteasome activity

The Rpn11 assay was done as described previously (Li et al., 2018). Briefly, a synthetic fluorescent labeled substrate, Ub4pepOG was used to measure Rpn11 activity. Fluorescence polarization assay was performed in a low-volume 384-well solid black plate in the presence of 1) 5 μ l compound (difference concentration of 1, 10 phenanthroline or CuEt) in 3% DMSO or 3% DMSO control 2) 5 μ l of BioMol 26S proteasome and 3) 5 μ l of substrate (15 nM Ub4-pepOG). Fluorescence polarization is measured using a plate reader with excitation of 480 nm and emission of 520 nm filter set. The activity was normalized to DMSO control and fitted using dose-response equation.

3.18 Affinity precipitation

For GFP immunoprecipitation, NPL4-GFP expressing U2-OS cells were lysed (50 mM HEPES, pH 7.4, 150 mM NaCl, 2 mM MgCl₂, 10% glycerol, 0.5% Triton-X100, protease inhibitor cocktail by Roche) and centrifuged (20,000G for 10 minutes at 4°C). Supernatant was incubated with anti-GFP agarose beads (Origene) overnight at 4°C. Beads were then 3 times washed by lysis buffer and bound proteins eluted by Laemmli buffer for WB analysis. For GST-precipitation, purified WT-NPL4-GST or MUT-NPL4-GST proteins were incubated with glutathione sepharose 4B beads (Life Technologies) for 1 h at room temperature. Unbound proteins were washed (50 mM Tris-HCl, pH 7.4, 150 mM NaCl, 2 mM MgCl₂, 10% glycerol, 0.5% Triton-X100) and beads were incubated with purified p97-His or MDA-MB-231 cell lysate (as a source of ubiquitinated proteins) for 1 h at room temperature. Beads were then 3 times washed by buffer and bound proteins eluted by Laemmli buffer for WB analysis. For His-tag precipitation, purified UFD1-His protein was incubated with Ni-NTA agarose beads (Qiagen) for 1 h at room temperature. Unbound proteins were washed (50 mM Tris-HCl pH 7.5, 150 mM NaCl, 2.5 mM MgCl₂, 20 mM imidazole, 5% glycerol) and incubated with purified WT-NPL4-GST or MUT-NPL4-GST proteins for 1 h at room temperature. Beads were then 3 times washed by buffer and bound proteins eluted by Laemmli buffer for WB analysis.

3.19 Protein expression and purification

All proteins were expressed in *E. coli* BL21 (DE3) cells (Novagen). p97-His (pET28a vector) and Ufd1-His (pET28a vector) expression were induced by 1 mM IPTG (Life Technologies) at an OD₆₀₀ of 0.6 for 10 hours at 22°C. NPL4 WT and MUT (pGEX-2TK) were induced by 0.4 mM IPTG at an OD₆₀₀ of 0.8 overnight at 16°C. In case of p97 and

UFD1, bacterial pellet was suspended in buffer (50 mM Tris-HCl pH 8.0, 300 mM NaCl, 2.5 mM MgCl₂, 20 mM imidazole, 5% glycerol) and lysed by sonication and centrifuged (14000xg for 20 minutes). Proteins were purified by Ni-NTA chromatography (Qiagen) according to manufacturer instructions. In case of p97, the protein was further purified by gel filtration (Superdex 200, GE Healthcare). In case of WT and MUT GST-NPL4, bacterial pellet was suspended in phosphate buffer (PBS, 0.1% Triton-X100, 300 mM NaCl) and lysed by sonication and centrifuged (14000xg for 10 min). Proteins were purified by glutathione sepharose 4B (Life Technologies) according manufacturer's protocol. The proteins were further purified by gel filtration (Superdex 200, GE Healthcare).

3.20 Chemicals

CuET was synthesized as described previously (Cvek et al., 2008). The following chemicals were purchased from commercial vendors: tetraethylthiuram disulfide (disulfiram, DSF) (Sigma), sodium diethyldithiocarbamate trihydrate (Sigma), copper chloride (Sigma), copper gluconate (Sigma), bortezomib (Velcade, Janssen-Cilag International N.V.), MG-132 (Sigma), DBeQ (Sigma), NMS-873 (Abmole), cycloheximide (Sigma), 1,10-phenanthroline (Sigma), MLN7243 (Active Biochem).

3.21 Figures preparation, data analysis, used software

All figures and drawings were prepared using Inkscape 0.17 and MS Office 2016 software. The data was analysed by MS Office 2016, STATISTICA 12, Graphpad Prism 4, PeakView 1.2, Image Lab 4.1, Carl Zeiss Zen 2011 SP6 (black), Nano Analyze Software 2.3.6, Olympus ScanR Analysis 1.3.0.3 software.

4 RESULTS

4.1 Ditiocarb-copper complex is a new metabolite of disulfiram

The mechanism of the anti-cancer activity of disulfiram (DSF) is still controversial and poorly defined, but many studies agreed on the essential role of copper ions for the toxicity of disulfiram. Indeed, we confirmed and extended previous *in vitro* (Cen et al., 2004; Chen et al., 2006) and *in vivo* (Allensworth et al., 2015) studies, and demonstrated that copper supplementation in the form of copper gluconate significantly enhanced ability of disulfiram to reduce the growth of mammary MDA-MB-231 xenografts in mice (Skrott et al., 2017). However, it is not clear what mechanism is behind such property of copper. The metabolic fate of disulfiram upon digestion was deeply studied, so it is well known that disulfiram is quickly reduced to give two molecules of ditiocarb (diethyldithiocarbamate, DTC). Ditiocarb is further processed to several metabolites finally to give S-methyl diethyldithiocarbamate sulfoxide and S-methyl diethylthiocarbamate sulfoxide, proposed inhibitors of aldehyde dehydrogenase (Johansson, 1992). Importantly, ditiocarb, as well as other members of dithiocarbamate family, is a very strong metal chelator and its complex with copper is in fact the most stable among biogenic metals (Hogarth, 2012). Ditiocarb readily reacts with copper ions *in vitro* to form ditiocarb-copper complex (bis-(diethyldithiocarbamate)-copper, CuET). However, the presence of CuET in the body after disulfiram intake was never clearly showed, despite attempts dated back 30 years ago (Johansson and Stankiewicz, 1985).

To test if CuET really forms in the body and if it may represent a candidate metabolite responsible for anti-cancer activity of disulfiram (Fig. 8a), I first developed method employing High-pressure liquid chromatography coupled to mass spectrometry (HPLC-MS). Optimised method was specific and sensitive enough to detect even low CuET concentrations in tissue samples as documented by detection of spiked synthetic CuET to mouse serum (Fig. 8b). In following experiments, I confirmed that CuET metabolite was indeed present in mouse serum after a single oral dose of disulfiram (50 mg/kg) even without copper supplementation (Fig. 8b). The highest concentration of CuET was detected soon after disulfiram intake and then dropped gradually (Fig. 8c). To further investigate if CuET penetrates to tissues and more importantly to tumours, I analysed the extracts from plasma, liver, brain, and tumours of mouse undergoing disulfiram therapy (50 mg/kg/day) with and without copper gluconate supplementation (0,15 mg/kg/day) for 5 days. CuET was readily detected in livers or brains and, importantly, in tumours as well (Fig. 8d). As hypothesised, copper addition led to clearly elevated CuET levels compared to disulfiram alone. Intriguingly, CuET

concentrations in tumours were obviously higher compared to other organs, a phenomenon even pronounced by copper supplementation. Finally, to prove CuET as a new metabolite of disulfiram in humans, I analysed also plasma obtained from alcoholics undergoing disulfiram therapy. Indeed, CuET was present in all samples albeit with diverse concentration (Fig. 8e).

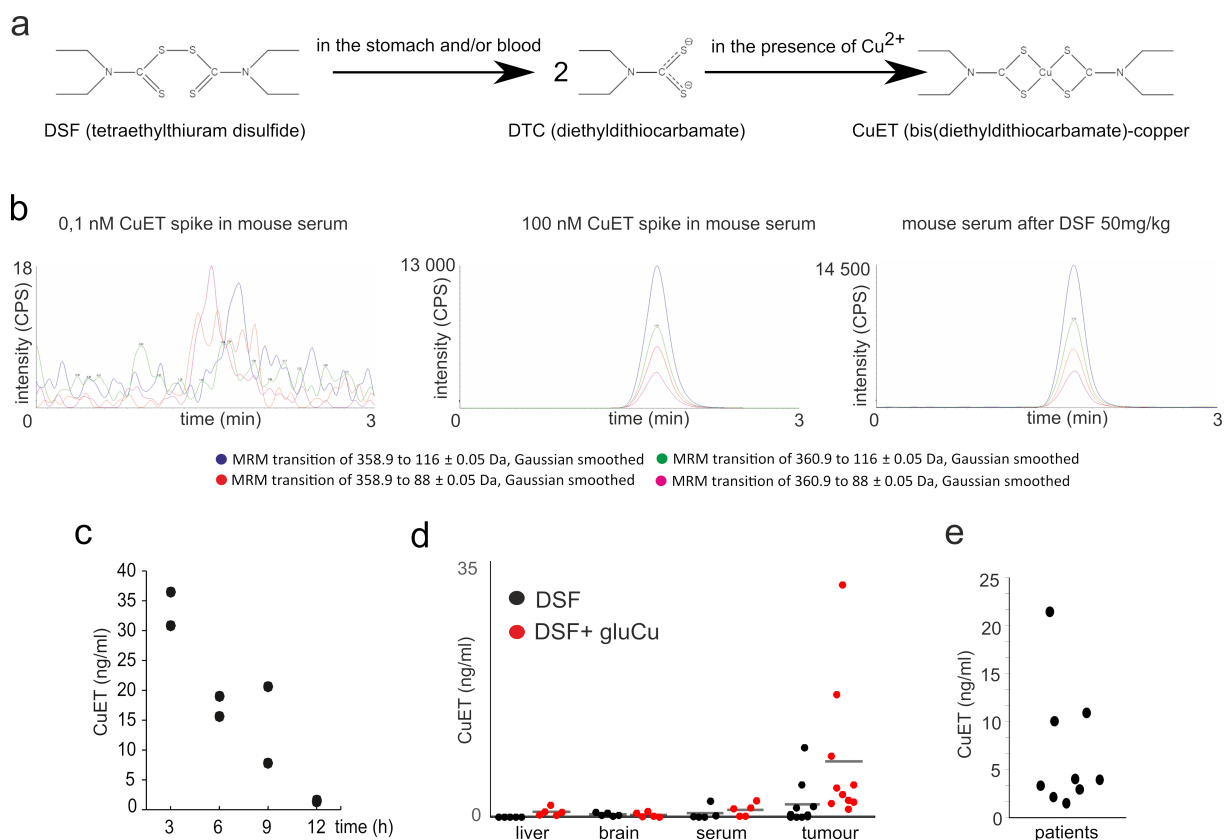


Figure 8 | CuET complex is new metabolite of disulfiram. a) A model of CuET formation in the human body after orally administered disulfiram. b) Examples of mass-spectrometry spectra of CuET visualised as peaks of 4 MRM transitions in murine serum after CuET spikes, compared to orally applied disulfiram (single dose, 50 mg/kg). c) Pharmacokinetic analysis of CuET levels in murine serum after orally applied disulfiram (50 mg/kg) (n=2 animals for each time point). d) CuET levels in murine tumours and tissues (mean; n=5 tissues; n=10 tumours). e) CuET levels in human plasma after disulfiram dose (400 mg) (n=9 patients).

Taken together, these results strongly argue that CuET is the ultimate metabolite responsible for anti-cancer activity of disulfiram because CuET is the only known metabolite of disulfiram containing copper, a metal that enhances the anti-tumour effects of disulfiram *in vitro* and *in vivo*. As addition of copper further promotes CuET formation at the expense of other DSF's metabolites, the increased (rather than decreased) toxicity to cancer cells correlates with elevated CuET and with likely lower levels of other metabolites.

4.2 CuET complex is highly toxic to cancer cells

To get further insight into the effect of CuET to cancer cells, I performed series of experiments employing cancer cell lines. First, I compared the toxicity of disulfiram (DSF) and its main primary metabolite ditiocarb (DTC) with CuET in short-term XTT-base assay using mammary MDA-MB-231 cancer cell line (Fig. 9a). In sharp contrast to CuET, both DSF and DTC were negligibly toxic, which was further corroborated by long-term colony-forming assay (CFA) again verifying higher toxicity of CuET compared to DTC (Fig. 9b). CFA assay revealed that CuET was also similarly potent ($IC_{50} < 100$ nM) to other three breast cancer cell lines (Fig. 9c). To cover wider spectrum of human malignancies, CuET toxicity was also tested by XTT assay on a panel of cell lines comprising 11 different cell lines (Fig. 9d). While CuET was toxic to all of them, IC_{50} values varied considerably (from ~80 nM to ~700 nM). Interestingly, among the most sensitive were identified multiple myeloma cell lines (AMO1, MM1S) or BRCA2 deficient prostate adenocarcinoma line Capan-1. On the other hand, non-cancerous prostate cell line RWPE1 was virtually insensitive with IC_{50} far above 1 μ M.

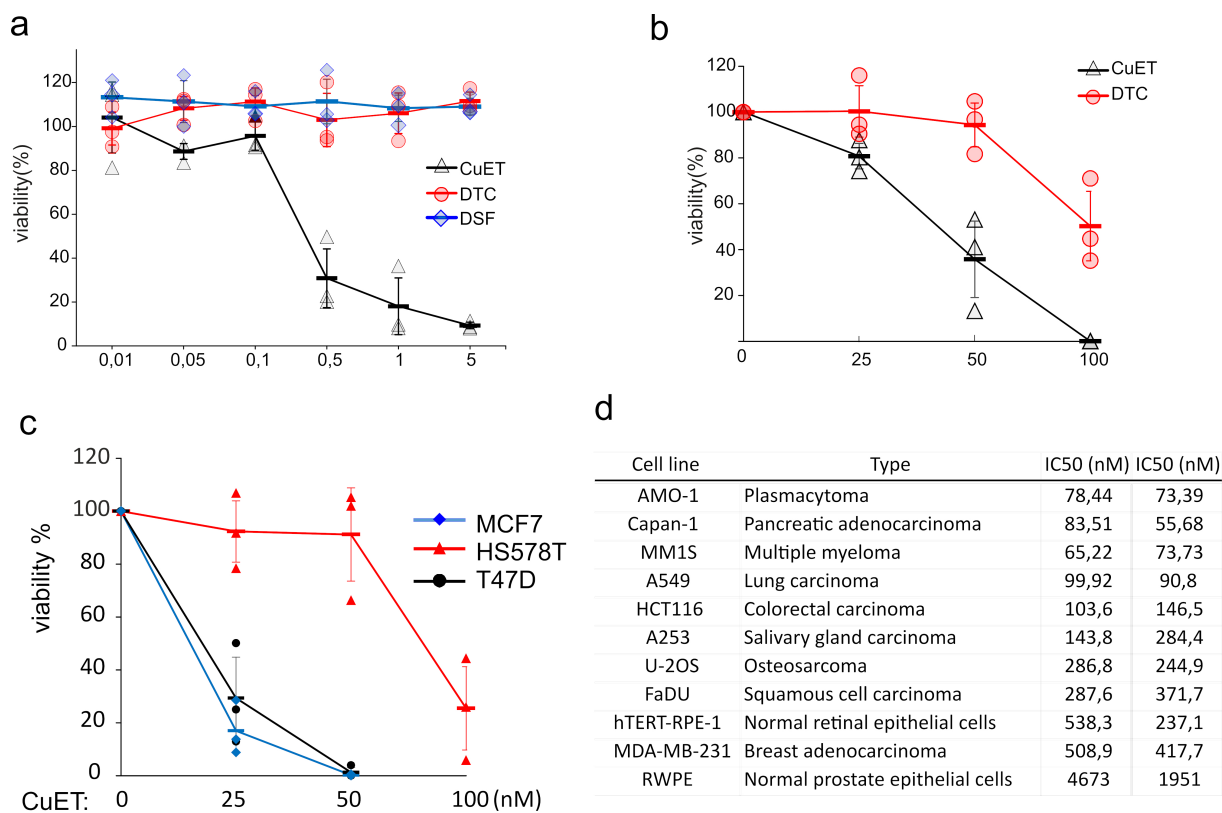


Figure 9 | Cytotoxicity of CuET complex. **a)** Toxicity of DSF, DTC and CuET in MDA-MB-231 cells (24 h, mean, SD, and individual data from 3 experiments). **b)** Effect of DTC and CuET on MDA-MB-231 cells analysed by colony formation assay (CFA) (mean, SD and individual data from 3 experiments). **c)** CuET cytotoxicity measured by CFA in human breast cancer cell lines (mean, SD and individual data from 3 experiments). **d)** Table summarising IC50 values documenting cytotoxicity of CuET across a panel of cancer and non-cancer cell lines (48 h treatment, 2 independent biological experiments).

4.3 CuET complex induces both apoptotic and non-apoptotic cell death

To get further insight into toxicity of CuET complex, I analysed in detail the mode of cell death it triggers in cancer cells. Since several published studies (Allensworth et al., 2015; Cen et al., 2004; Chen et al., 2006) state that disulfiram combined with copper induce apoptosis, I first checked for this type of programmed cell death. The main hallmark of apoptosis is the activation of cysteine proteases responsible for cell death execution – caspases, and especially the activity of effector caspase-3 or caspase-7 is measured frequently (Kepp et al., 2011). To measure caspase-3/7 activity, cells were incubated with substrate that becomes fluorescent after specific caspase-mediated cleavage, and fluorescence in cells was

analysed by flow cytometry. Unexpectedly, while a small molecule NMS-873, known inductor of apoptosis (Magnaghi et al., 2013) here used as a positive control, clearly increased caspase-3/7 activity in U-2OS or MDA-MB-231 cells, no such elevation was observed in CuET treated samples despite massive death documented by increased number of permeabilised cells (Fig. 10a, upper-right – e.g. positive for DNA stain).

To further corroborate these surprising results, caspase-3/7 activity was analysed by other independent assays. First, Annexin V staining coupled with flow cytometry was employed. During the apoptosis, activated caspases cleave handful of targets, among them membrane associated flippase that maintain cytosolic orientation of a phospholipid phosphatidylserine. Upon flippase cleavage, phosphatidylserine flips to extracellular surface of the cell, where it can be recognized by macrophages to enable engulfing of the dying cell (Fadok et al., 1992). Phosphatidylserine is also specifically bounded by a protein Annexin V, which is used as a probe to detect apoptotic cells. Early apoptotic cells are positive for Annexin V while negative for non-permeable DNA dyes such as propidium iodide or 7-AAD confirming that the plasma membrane is still intact and Annexin V positivity is not due to membrane rupture as typical for necrosis. Indeed, such population (Annexin V⁺/7-AAD⁻) was clearly identified in NMS-873 treated samples, but again not in cells exposed to CuET (Fig. 10b) confirming results obtained from direct measurement of caspase-3/7 activity. As a second assay, I performed WB analysis of direct and well known caspase-3/7 substrate PARP-1 protein. In apoptotic cells, activated caspase-3/7 cleave PARP-1 and cleaved product of lower molecular weight can be easily detected (Chaitanya et al., 2010). In line with previous results, PARP-1 cleavage was readily detected in NMS-873 treated sample, but not in case of CuET (Fig. 10c). These data were further confirmed with specific antibody recognizing only cleaved product of PARP-1 (Fig. 10c).

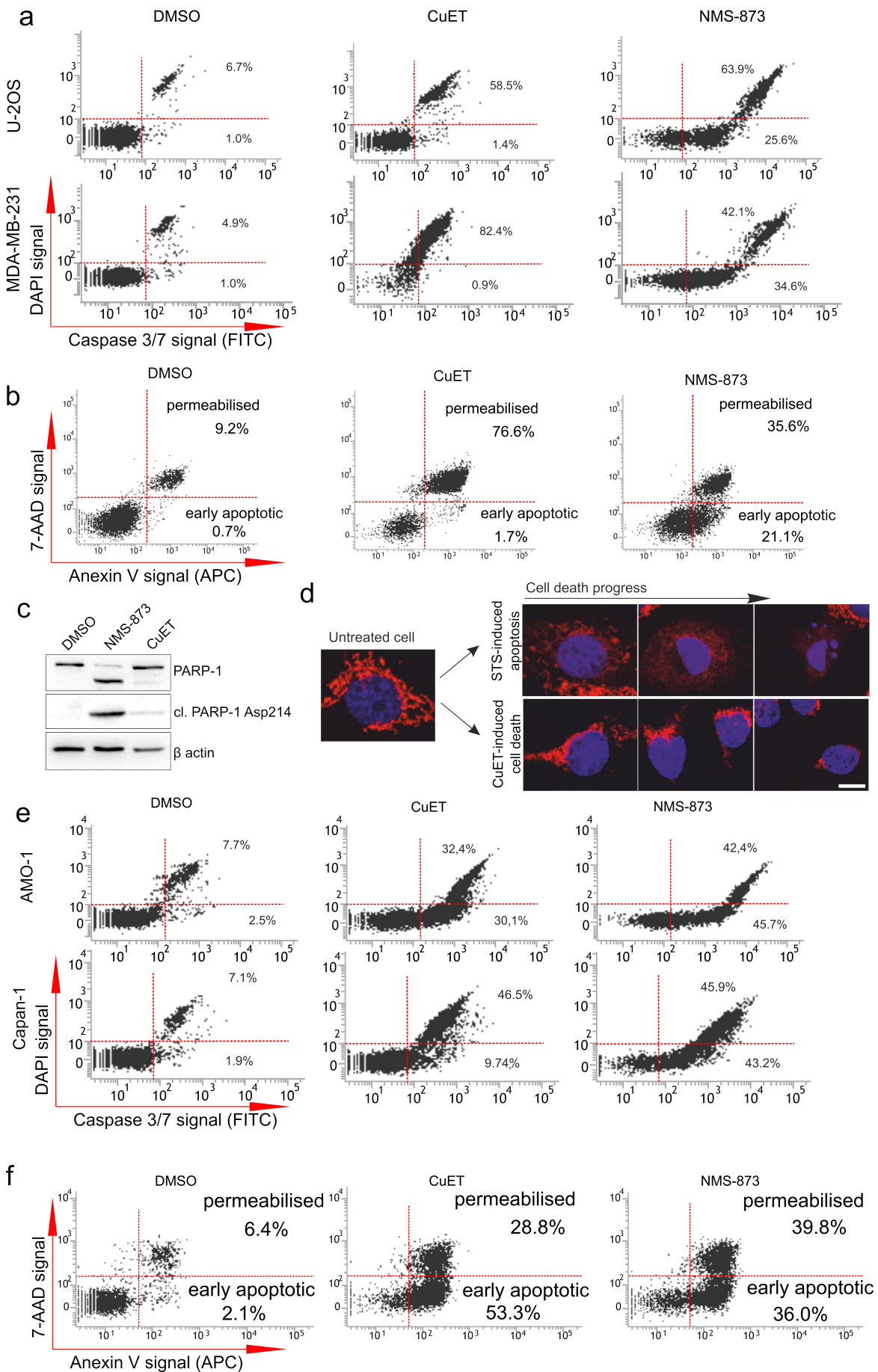


Figure 10| CuET complex induces both apoptotic and non-apoptotic cell death. **a)** Analysis of Caspase 3/7 activity in U-2OS and MDA-MB-231 cell lines after the treatment by NMS-873 (10 μ M; U-2OS: 16 h, MDA-MB-231: 24 h,) or CuET (1 μ M; U-2OS: 16 h, MDA-MB-231: 24 h). **b)** Analysis of Annexin V signal in U-2OS cell exposed to NMS-873 or CuET (treatment the same as in (a). **c)** Cleaved PARP-1 analysis after NMS-873 (10 μ M) and CuET (250 nM) in U-2OS cells (16 h). **d)** Analysis of cytochrome c (in red) release from mitochondria in U-2OS cells during cell death induced either by the positive control staurosporin (STS, 1 μ M) compared to cell death induced by CuET (1 μ M) (blue=DAPI signal). **e)** Analysis of Caspase 3/7 activity in AMO-1 and Capan-1 cell lines after the treatment by NMS-873 (16 h; AMO-1: 5 μ M; Capan-1: 10 μ M) or CuET (16 h; AMO-1: 100 nM, Capan-1: 250 nM). **f)** Analysis of Annexin V signal in AMO-1 cells exposed to NMS-873 or CuET (treatment the same as in (e)).

These results clearly exclude fully activated apoptosis as a mode of CuET-induced cell death. However, there is still a possibility that apoptosis is actually initiated but for some reason did not progress into late state with fully activated caspases, as reported previously (Cande et al., 2002). Since the activation of effector caspases is one of the later events during apoptosis, I want to check also some initial process, such as cytochrome-c release. Cytochrome-c translocation out of outer mitochondrial membrane is critical step and hallmark of intrinsic apoptosis and can be analysed by immunofluorescent staining (Kepp et al., 2011). In non-treated cells, cytochrome-c was clearly localised in intact mitochondria, but during treatment with staurosporine, a known apoptosis inducer, cytochrome-c released out of mitochondria and diffused throughout cytoplasm. Conversely, cytochrome-c remained in mitochondria in CuET treatment despite ongoing death manifested by visibly altered cell morphology (Fig. 10d).

Taken together, these results practically exclude apoptosis as a type of cell death triggered by CuET, which is in sharp contrast to several published reports (Allensworth et al., 2015; Cen et al., 2004; Chen et al., 2006). Surprisingly, further experiments revealed that the mode of cell death induced by CuET is cell line-specific. In multiple myeloma line AMO-1 and pancreatic adenocarcinoma line Capan-1, CuET clearly activated caspase-3/7 to the level comparable with positive control (NMS-873) as measured by direct activity assay (Fig. 10e). Apoptotic cells were further confirmed by Annexin V assay (subpopulation of Annexin V⁺/7-ADD⁻ cells) (Fig. 10f).

The type of non-apoptotic cell death induced by CuET in cell lines such as MDA-MB-231 or U-2OS is highly interesting and needs further investigation, as well as to find a factor causing apoptosis in others cell lines. It is worth of mention that cell lines dying by apoptosis are also the most CuET-sensitive (Fig. 9d).

4.4 CuET complex does not inhibit the proteasome directly

The toxicity of disulfiram to cancer cell has been explained by a plenty of hypothesis (Cvek, 2011; Skrott and Cvek, 2012). The most likely explanation for so much heterogeneous theories is the chemical nature of disulfiram itself. It contains two very reactive thiol groups readily reacting with cysteine residues of various proteins, as reported for ALDH (Vallari and Pietruszko, 1982) or MDR (Loo, 2000). Despite not listed as a typical example, disulfiram shares several characteristics with pan-assay interfering compounds (PAINS) such as curcumin or quinones (Baell and Walters, 2014). These compounds, as the name suggest, score in various screening assays as positive hits, however such activity is often just an artefact. PAINS, similarly to disulfiram, are usually very reactive compounds, metal chelators or redox-cycling compounds. Due to their pleiotropic effect, it is extremely challenging to validate the hit appropriately in cells and consequently such compounds are described as having promising activity against a wide variety of targets (Baell and Walters, 2014). Such scenario could be valid also for disulfiram.

It is also important to stress out, that disulfiram has very complex and rapid metabolism, and very low or even undetectable plasma levels of circulating disulfiram (Johansson, 1992) raise a question if it is even appropriate to test disulfiram in cancer cell cultures, as it is not known if disulfiram reaches tumours *in vivo*. Conversely, majority of studies agrees on the strong potentiation of disulfiram effect by copper. Therefore, to find the mechanism standing behind disulfiram toxicity, it should be searched within the theories involving the copper and CuET.

Notably, the only one hypothesis relies on the presence of copper consistently – the inhibition of protein degradation by the interference with the activity of the proteasome (Cvek, 2011). First reported in 2006 (Lövborg et al., 2006) and further confirmed (Chen et al., 2006) by the group of prof. Q.P. Dou, this theory explaining the disulfiram's mechanism of action became the most accepted by the scientific community. However, further analysis raised a direct inhibition of the proteasome questionable (Cvek et al., 2008). During my

research stay in prof. Dou's lab, I have found that CuET complex did not directly inhibit any of three proteolytic activities of the core proteasome particle (20S proteasome), but still, CuET clearly inhibited degradation of proteins such as I κ B or p53. These data are summarised in my master thesis (Skrott, 2014). Such conflicting results urged for further investigation and final answer.

In my previous results, I have confirmed that CuET induces accumulation of poly-ubiquitinated proteins. However, the type of ubiquitin chain which determines the fate of the substrate, was not known. Not all types of linkage commit the protein for the degradation in proteasome, as ubiquitin has also many different roles. Lysine 48 (K-48) linkage is first and foremost associated with proteasomal degradation (Komander and Rape, 2012), so I performed WB analysis with an antibody specifically recognising K48-ubiquitin chains. CuET treatment induced clear accumulation of this linkage type with similar potency and kinetics like 20S proteasome inhibitor bortezomib used as positive control (Fig. 11a). As the core particle of proteasome was excluded as a suspected target, the regulatory 19S part of the proteasome was an obvious option. POH1 deubiquitinase (DUB) was especially interesting (Cvek et al., 2008; Skrott and Cvek, 2012). This enzyme deubiquitinates proteins before their translocation into the proteasome and its activity is crucial for proper proteasome function (Verma et al., 2002). Since POH1 belongs to the family of JAMM domain DUBs, it contains zinc in the catalytic site, and the reaction between the zinc and CuET was particularly attractive (Cvek et al., 2008).

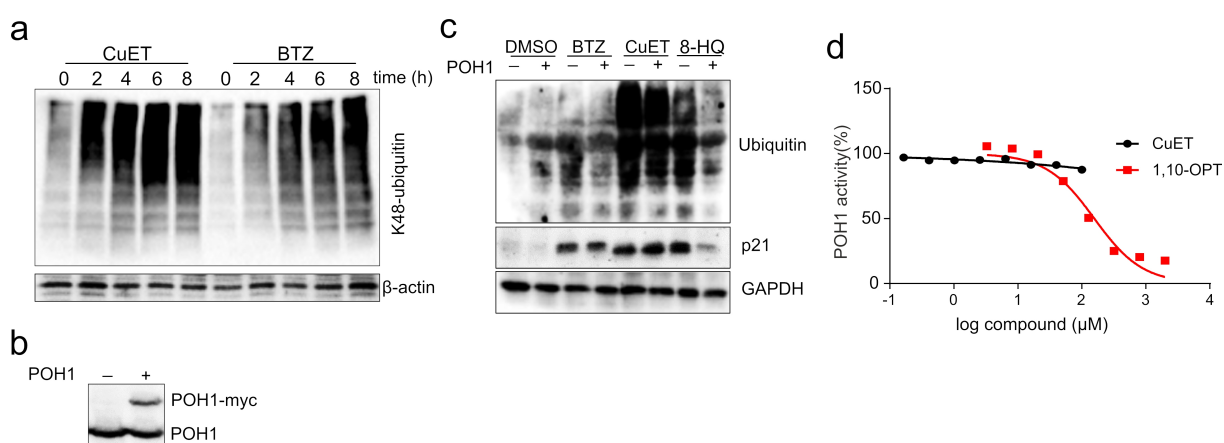


Figure 11 | The proteasome is not directly inhibited by CuET complex. **a**) Time-course WB analysis of K48-ubiquitin in U-2OS cells treated by CuET or BTZ (both 1 μ M). **b**) The level of POH1 in WT and POH1-myc expressing MDA-MB-2231 cells. **c**) POH1 overexpression alleviates the effect of POH1 inhibitor 8-HQ (10 μ M) in contrast to BTZ

(1 μ M) or CuET (1 μ M) as measured by ubiquitin and p21 protein levels in MDA-MB-231 cells treated for 6 h. **d)** CuET does not inhibit POH1 activity *in vitro* (1,10-OPT used as a positive control).

It is well known that overexpression of the protein targeted by its specific inhibitor can elicit partial resistance to the inhibitor and such mechanism is frequently involved in the acquired resistance to the chemotherapy (Morganti et al., 2000; Oerlemans et al., 2008). Such approach was chosen to test a potential link between CuET and POH1 enzyme. Firstly, POH1 was overexpressed in MDA-MB-231 cell line by stable introduction of ectopic POH1. The amount of POH1 was further analysed by WB confirming satisfactory overexpression (Fig. 11b). Control and POH1 cell lines were further compared in their response to CuET. Specific POH1 inhibitor 8-HQ (8-quinolinethiol hydrochloride) was used as a positive control (Li et al., 2017) while bortezomib as a negative. While 8-HQ was apparently less active in POH1 overexpressed cell line as measured by accumulation of polyubiquitinated proteins or proteasome substrate protein p21, CuET behaved similarly to bortezomib, i.e. with similar potency in both cell lines (Fig. 11c). Such results obviously argue against the hypothesis that CuET targets POH1 deubiquitinase.

To get final answer, I visited the laboratory of professor R. J. Deshaies, the world-leading expert in the family of JAMM domain deubiquitinases. In his lab, I employed biochemical assay with artificial POH1 substrate measuring not only POH1 activity but indirectly the whole 26S proteasome altogether (Li et al., 2017). Consistently with the data obtained from cells, CuET failed to inhibit the deubiquitinase (Fig. 11d), in contrast to positive control 1,10-phenantroline (Verma et al., 2002), finally excluding POH1 as well as the whole proteasome as the direct target of CuET complex.

4.5 CuET complex inhibits the function of p97 segregase

Data gathered so far were quite confusing – while CuET complex induced the accumulation of polyubiquitinated proteins and stabilisation of several proteins rapidly degraded by proteasome, the proteasome seemed untouched. To find an explanation for such puzzling discrepancy, I looked to the UPS more deeply. Proteasomal substrates could be stabilised by impairment of its ubiquitination, as documented for ubiquitin-activating E1 enzyme inhibitors (Hyer et al., 2018). However, a such mechanism presumes a decrease of polyubiquitinated proteins, and not an increase as observed in the case of CuET. Mammalian

cells also contain more than one hundred of deubiquitinases associated with several functions including deubiquitination and thus stabilisation of proteins dedicated to degradation in the proteasome (Harrigan et al., 2017). If CuET complex acts as a kind of pan-deubiquitinase inhibitor, one would expect gross accumulation of polyubiquitinated proteins, however on the other hand, in theory, the degradation of proteins should not be blocked, but should remained the same or should be even promoted (Harrigan et al., 2017). Such speculations suggest that suspected target of CuET should be somewhere between the polyubiquitinated substrate and the proteasome.

It is well known that some substrates use adaptor proteins, such as RAD23 or DSK2, that shuttle them to the proteasome (Saeki, 2017). However, it is not very likely that inhibition of any of these factors could induce such global accumulation of polyubiquitinated proteins and inhibit the degradation of several different substrates. Importantly, accumulating evidence emphasises another crucial factor implicated in the multitude of processes associated with ubiquitin – Valosin-containing protein (VCP or p97). p97 acts as a segregase pulling out ubiquitinated proteins out of membranes, protein complexes or chromatin, and thus enables their degradation by the proteasome (Meyer et al., 2012). Recent reports show that inhibitors of p97 induce several phenotypes similar to the inhibition of the proteasome, including accumulation and stabilisation of polyubiquitinated substrates dedicated to degradation (Anderson et al., 2015; Chou et al., 2011).

Interestingly not all proteasome substrates are dependent on p97 activity, providing a possible way how to distinguish between proteasome versus p97 inhibitors (Chou and Deshaies, 2011). Importantly, all substrates reported so far to be stabilised by CuET, i.e. I- κ B, Ub(G76V)-GFP, p53 (Skrott, 2014) are all dependent on the activity of p97 segregase (Chou et al., 2011; Li et al., 2014; Valle et al., 2011). To investigate if CuET specifically inhibits only the degradation of proteins dependent on p97 activity, I analysed the behaviour of Hypoxia-inducible factor 1 (HIF-1 α). This transcription factor is continuously degraded by the proteasome under normal conditions, and its degradation is largely independent on the p97, as only transcriptionally active form of HIF-1 α , representing just a small subset of the protein, is degraded with the assistance of p97 (Alexandru et al., 2008). First, I treated the cells with CuET or proteasome inhibitor MG-132 and analysed the level of HIF-1 α . Intriguingly, in contrast with MG-132, which significantly accumulated HIF-1 α , CuET induced only marginal elevation of the protein compared to non-treated cells (Fig. 12a). Such results were consistent with the scenario presuming that CuET inhibits degradation of only

p97-dependent proteins and not all proteasome substrates as in case of MG-132. However, the previous experiment is not strong enough for such statement – fail to accumulate the protein is not the same as fail to inhibit its degradation, and can be interpreted by several ways. To get more convincing data, I chose pulse-chase experiment, as a more appropriate. In such experiment, the cells are first pre-treated with reversible proteasome inhibitor such as MG-132 to completely block the degradation and to induce accumulation of looked-for proteins. After desired time, MG-132 inhibitor is washed-out to restore the activity of the proteasome. At the same time, cells are exposed to tested compounds and cycloheximide, an inhibitor of ribosome, to stop protein synthesis. Under normal conditions, the level of accumulated protein should decrease with time – the proteasome is again functional and *de novo* synthesis is blocked. If the degradation of desired protein is inhibited by tested compound, the level of the protein should remain the same or at least the decline should be significantly slowed down. Such approach enables more direct assessment of the compound's effect on protein degradation with shorter exposure times lowering the possibility of unspecific cellular effects. Employing for HIF-1 α protein, results clearly shows that CuET, in contrast to bortezomib, failed to stabilise HIF-1 α similarly to DBeQ, a specific p97 inhibitor (Chou et al., 2011) (Fig. 12b). On the other hand, with the same conditions, all three compounds, CuET, bortezomib, and DBeQ, prevented the degradation of a protein Cdc25A, a phosphatase involved in cell-cycle regulation, which is degraded by p97-dependent manner (Riemer et al., 2014) (Fig. 12b). These result clearly shows that CuET blocs only the degradation of proteins dependent on p97 activity.

p97 segregase is involved not only in protein degradation, but it plays a role also in other processes such as activation of transcription factors, such as Nuclear respiratory factor 1 (NRF1) (Radhakrishnan et al., 2014). Closely related to the well-known NRF2 involved in antioxidant response, NRF1 is a major regulator of protein degradation. It activates expression of all proteasome units and p97 as well upon proteasome impairment or overload (Sha and Goldberg, 2014). NRF1 is tethered on endoplasmic reticulum (ER) in the inactive form and it is constitutively degraded by the proteasome (Steffen et al., 2010). After insufficient activity of the proteasome, NRF1 accumulates at the ER membrane as inactive 120 kDa precursor. This form is first pulled out of ER membrane by the translocase activity of p97 and then cleaved to active 110 kDa form that translocates to the nucleus to start expression of proteasome subunits (Radhakrishnan et al., 2014). Proteasome inhibitors induce accumulation of both pre-processed 120 kDa and cleaved 110 kDa form of NRF1. On the other hand,

inhibitors of p97 blocks NRF1 translocation prior the cleavage, so only full-length 120 kDa form accumulates (Le Moigne et al., 2017; Radhakrishnan et al., 2014; Sha and Goldberg, 2014). Therefore, NRF1 behaviour could be used as an elegant model substrate to monitor p97 translocase activity to and distinguish p97 versus proteasome inhibition. As human cells contain several isoforms of NRF1, which complicates the analysis, mouse cells expressing only one variant are frequently used (Radhakrishnan et al., 2010, 2014). In NIH-3T3 mouse fibroblast treated with bortezomib, both 120 kDa and 110 kDa species accumulated in contrast to CuET treated cells, where only full-length form was present (Fig. 12c). When combined with bortezomib, both CuET and NMS-873 (a specific p97 inhibitor) effectively blocked the formation of cleaved 110 kDa form (Fig. 12d) further confirming that CuET impairs p97 activity. The effect of CuET on NRF1 was also further corroborated in human cancer cell lines (Fig. 12e). Collectively, such results confirmed that CuET impairs p97 segregase activity in cells but not the proteasome.

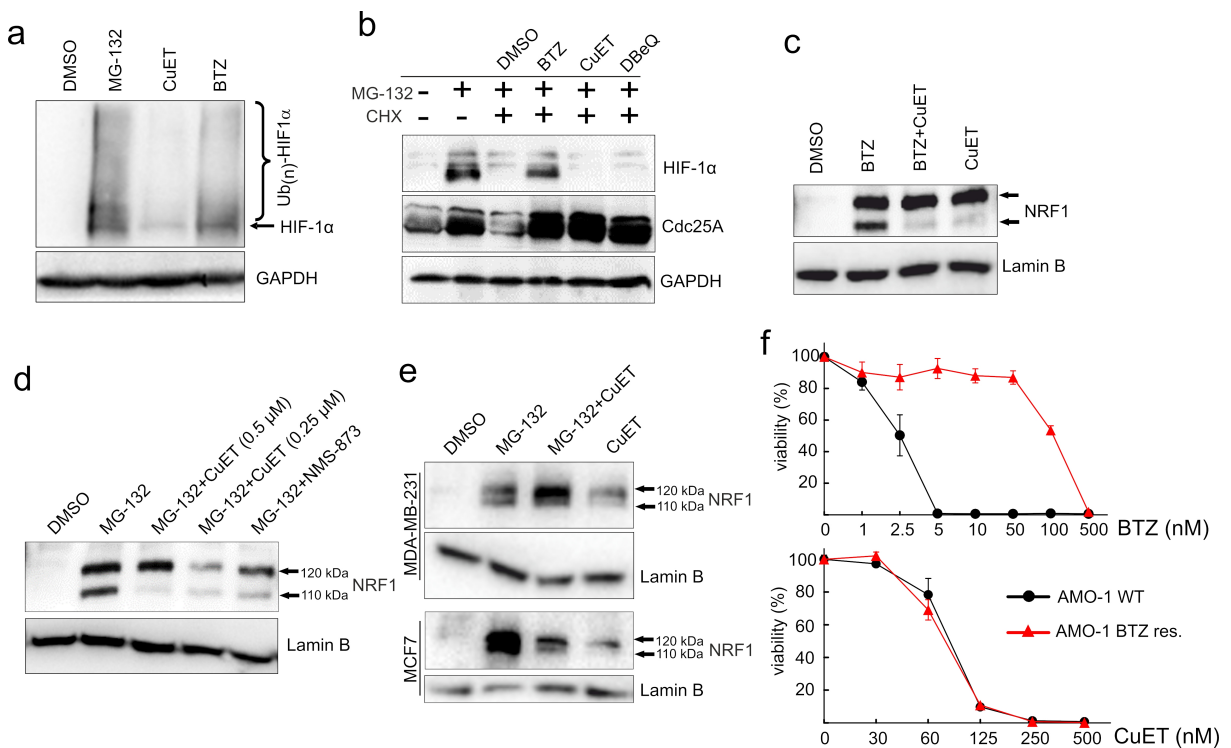


Figure 12 | CuET inhibits p97-dependent degradation and translocation. a CuET (1 μ M) induces only minor accumulation of HIF-1 α in contrast to MG-132 (5 μ M) or BTZ (1 μ M) in HeLa cells treated for 2 h. **b** Differential impact of BTZ (1 μ M), CuET (1 μ M) and DBeQ (10 μ M) on Cdc25A vs HIF-1 α . HeLa cells were first pre-treated by MG-132 (4 h, 5 μ M), then MG-132 was washed-out and cells were exposed to cycloheximide (50 μ g/ml) combined with DMSO, BTZ, CuET or DBeQ for 1 h. **c** BTZ (1 μ M) induces NRF1 120 kDa (upper arrow)

and 110 kDa (lower arrow) forms; while CuET (0.5 μ M) only the non-cleaved 120 kDa form (NIH-3T3 cells treated for 8 h). **d**) Inhibition of the NRF1 cleavage process (appearance of the lower band) by CuET and NMS-873 (5 μ M) in NIH-3T3 cells co-treated with the proteasome inhibitor MG-132 (5 μ M for 6 h). **e**) Cells treated by MG-132 (5 μ M, 6h) accumulate both forms of NRF1 while CuET-treated cells (1 μ M) accumulate only the non-cleaved 120-KDa form in MDA-MB-231 and MCF7 cells. **f**) AMO-1 cells resistant to BTZ (AMO-1 BTZ res.) are similarly sensitive to CuET as AMO-1 WT cells (48 h, representative results, mean, SD from technical triplicate).

Such findings could be potentially of clinical relevance for the management of multiple myeloma. Intrinsic or acquired resistance to bortezomib is a very frequent obstacle limiting the applicability of proteasome inhibitors and the benefit of the treatment (Manasanch and Orłowski, 2017). The inhibition of p97 segregase is one of the suggested ways how to cope with the resistance (Le Moigne et al., 2017; Wang et al., 2009). To analyse if CuET, a metabolite of readily available drug disulfiram, could be used to treat such refractory disease, I tested its toxicity to AMO-1 cells adapted to bortezomib (Soriano et al., 2016). Importantly, the potency of CuET was the same to WT cells and cells surviving extremely high bortezomib concentrations (Fig. 12f), opening a new intriguing possibility for the use of disulfiram with copper supplementation in patients not responding to proteasome inhibitors.

4.6 Ubiquitinated proteins accumulated by CuET treatment are associated with insoluble structures

Given that the most important function of p97 is to translocate or segregate ubiquitinated proteins out of cellular structures including membranes, chromatin, organelles and protein complexes for subsequent proteasomal degradation (Meyer et al., 2012), I wondered if ubiquitinated proteins accumulated upon CuET treatment can be detected as a part of such structures. First, I fractionated cell lysate to soluble and insoluble parts and analysed for K48-ubiquitin. Interestingly, ubiquitinated proteins were highly enriched in the insoluble fraction in CuET treated cells (Fig. 13a). To compare it with the inhibition of proteasome or p97, I treated the cells with CuET, bortezomib or NMS-873. After the treatment, I briefly pre-extracted the cells with Triton X-100 containing solution to wash out

all freely soluble proteins followed by fixation and staining for K48-ubiquitin. As shown in Figure 13b, compared to bortezomib or untreated cells, stronger signal corresponding to extraction-resistant insoluble ubiquitinated proteins was observed in both NMS-873 and CuET treated cells, as further confirmed by image quantitative analysis (Fig. 13c).

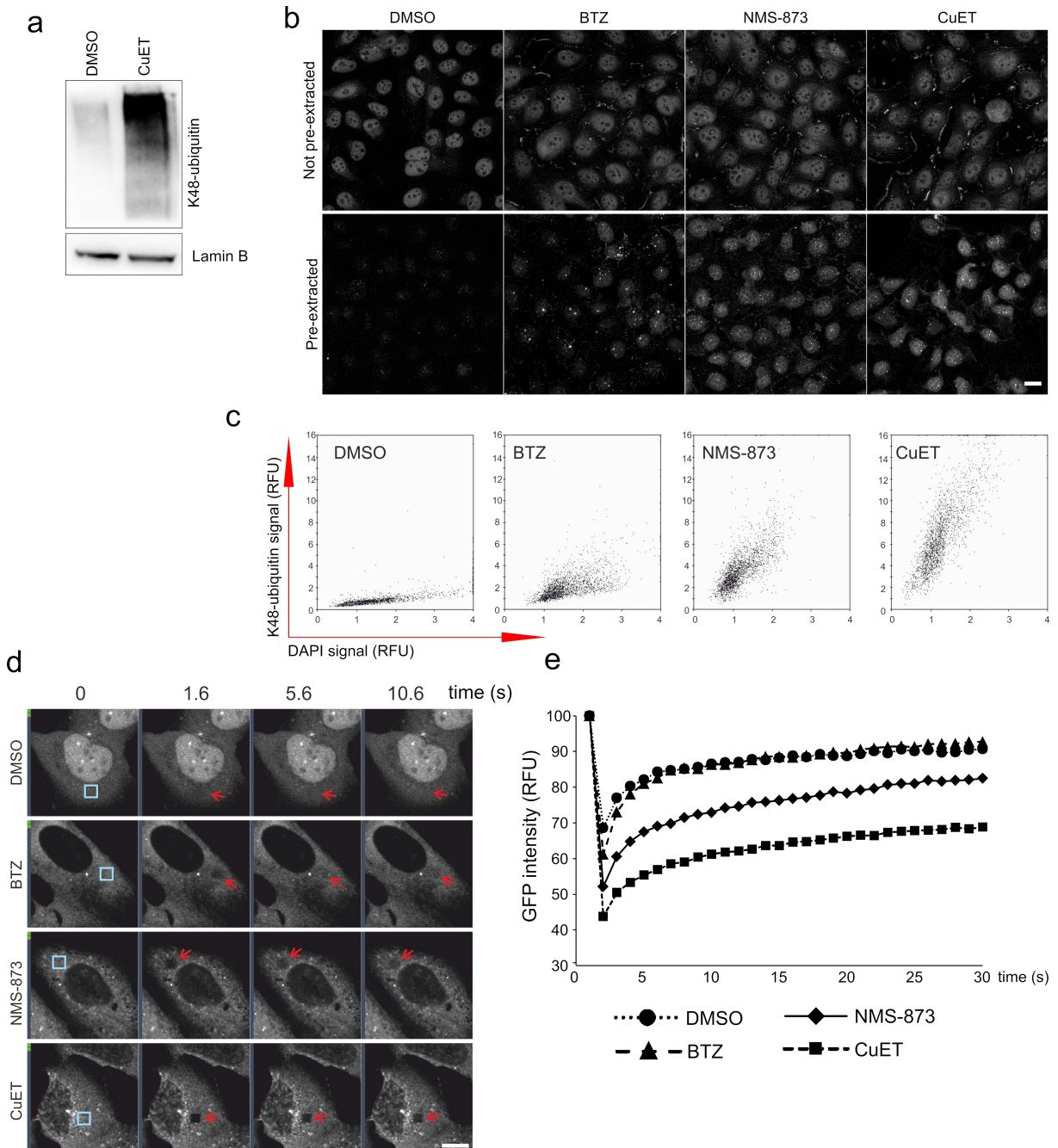


Figure 13 | CuET induces accumulation of immobile ubiquitinated proteins. a) Ubiquitinated proteins are part of TritonX-100 insoluble cellular fraction after CuET treatment (1 μ M, 3 h, U-2OS cells). **b)** IF analysis of K48-ubiquitin conjugates in not pre-extracted and

Triton X-100 pre-extracted U-2OS cells treated with DMSO, BTZ (1 μ M), NMS873 (10 μ M) and CuET (1 μ M) (Scale bar = 20 μ m). **c)** Microscopic quantitative analysis of Triton X-100 pre-extracted U-2OS cells treated as in (b). **d)** Time-course images from a FRAP experiment. U-2OS cells expressing GFP-ubiquitin were treated with NMS-873 (10 μ M), CuET (1 μ M) or BTZ (1 μ M) for 2 h (blue boxes mark areas before bleaching, arrows after bleaching), (Scale bar = 10 μ m). **e)** Quantification of FRAP experiment (relative mean signal of the bleached region from 10 cells).

To analyse the mobility of ubiquitinated proteins after CuET by another independent approach, I used fluorescence recovery after photobleaching (FRAP) microscopic method. This method relies on the quantification of recovered fluorescent signal in specific area after the photobleaching, and it is frequently used to measure protein mobility or transport (Ishikawa-Ankerhold et al., 2012). A protein of interest must be fluorescent, thus it is usually tagged with fluorescent protein such as green fluorescent protein (GFP). In this experiment, I used GFP-tagged ubiquitin, that behaves as normal ubiquitin and it is attached to proteins dedicated to degradation, as previously confirmed (Qian et al., 2002). In untreated cells, GFP-ubiquitin was so mobile that it was even hard to bleach the signal completely as new GFP-ubiquitin molecules diffused into bleached area extremely quickly (Fig. 13d, bleached area is marked by blue box). The signal in the bleached area also recovered already within a few seconds as quantified in Figure 13e. Bortezomib treated cells behaved the same, indicating that polyubiquitinated proteins accumulated upon proteasome inhibition are fully mobile (Fig. 13d,e). Conversely, in NMS-873 or CuET treated samples, GFP-ubiquitin was visibly bleached and low signal intensity persisted for a longer time in bleached areas indicating slowed diffusion (Fig. 13d), as confirmed by quantitative analysis (Fig. 13e). Consistently with previous experiments, these results indicate that after inhibition of p97 function at least a subset of the accumulated polyubiquitinated proteins remains immobile and tightly associated with cellular structures.

Collectively, these experiments demonstrated that significant fraction of polyubiquitinated proteins accumulated after CuET treatment are largely immobile, consistent with impairment of p97 segregase. They also suggest that experiments analysing the mobility of ubiquitinated proteins could be used in future studies to dissect p97 and proteasome inhibitors.

4.7 CuET complex impairs ER-associated degradation leading to the activation of Unfolded protein response

While p97 plays a role in many cellular processes, probably the most important and best understood is its function in endoplasmic reticulum-associated degradation (ERAD) (Meyer et al., 2012). Prior degradation in proteasome, polyubiquitinated proteins associated with ER must be first extracted from the membrane, a process dependent on p97 segregase activity. As shown previously (Chou et al., 2011; Wang et al., 2009), several p97 inhibitors inhibited a degradation of specific ERAD substrates and induced the accumulation of polyubiquitinated proteins on ER-membrane (Locke et al., 2014). To investigate, if CuET blocs also this p97-dependent process, I isolated microsomal fraction that contains mainly ER membranes by ultracentrifugation and analysed it for K48-ubiquitin by WB. While microsomes from untreated cells were only slightly positive for K48-ubiquitinated proteins, CuET and NMS-873 treatments induced marked accumulation of non-degraded proteins associated with ER-membrane in both tested cell lines (Fig. 14a). The same was observed also for bortezomib, which is consistent with previous report (Locke et al., 2014) showing that proteasome inhibition could to some extent also impair upstream steps including extraction of proteins from ER-membrane by p97.

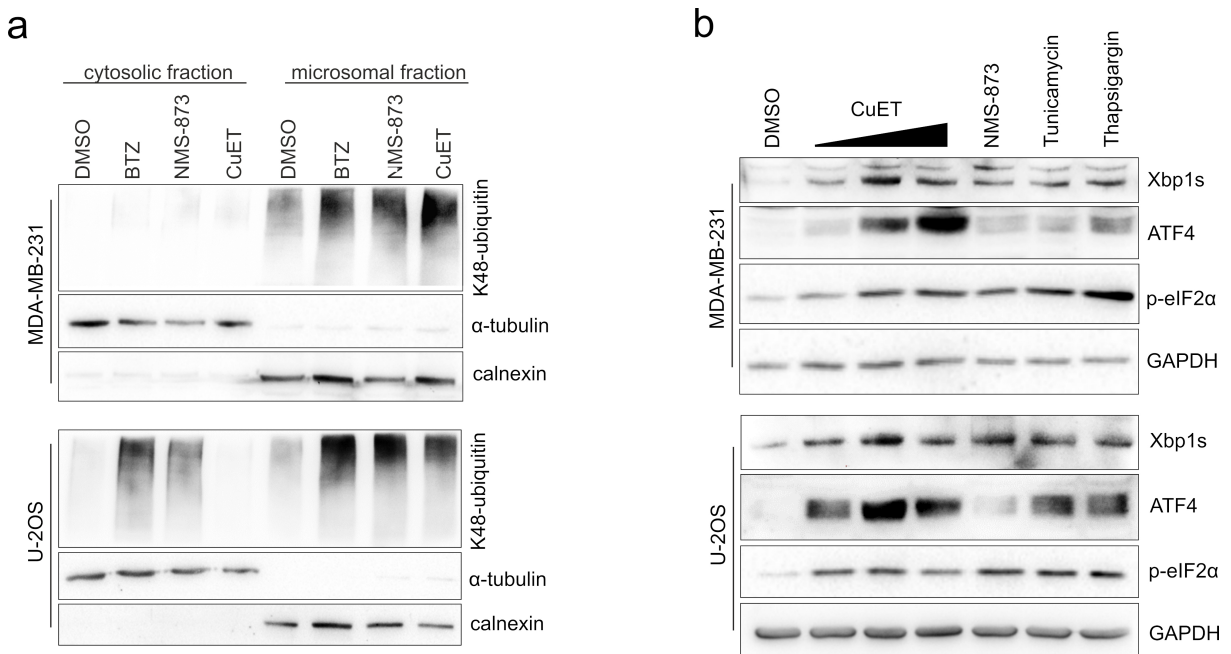


Figure 14 | CuET impairs ERAD and activates UPR. a) Western blot analysis of accumulated K48-ubiquitin conjugates in microsomal fraction from U-2OS and MDA-MB-231 cells treated by DMSO, CuET (1 μM), NMS-873 (10 μM) or BTZ (1 μM) for 3 h. **b)** UPR in U-2OS and MDA-MB-231 cell lines induced by 6 h treatment with CuET (125 nM, 250 nM),

500 nM) or positive controls (NMS-873 5 μ M, tunicamycin 2 μ g/ml, thapsigargin 1 μ M) manifested by increased levels of Xbp1s, ATF4 and p-eIF2 α .

The efficacy and accuracy of protein synthesis, maturation and degradation in the ER is tightly controlled. In case of increased protein load or accumulation of unfolded and non-degraded proteins, compensatory program called unfolded protein response (UPR) is triggered (Wang and Kaufman, 2014). UPR activates several pro-survival and adaptation processes to deal with damaged proteins, however, in case a severe stress condition persists, it stimulates cell death as well (Hetz, 2012). To examine if CuET triggers UPR, I compared its effect with p97 inhibition by NMS-873 and with two commonly used activators of UPR, tunicamycin and thapsigargin, inhibiting protein glycosylation and calcium ion pumping into ER, respectively (Samali et al., 2010). Treated cells were then analysed for several effectors of UPR, including phosphorylated eukaryotic initiation factor 2 α (p-eIF2 α) that negatively regulates polysome formation, and two transcription factors ATF4 and Xbp1s that control UPR target genes (Hetz et al., 2015). CuET treatment obviously activated all three markers in dose-dependent manner to similar extent as positive controls, clearly indicating that it activated robust UPR in both tested cell lines (Fig. 14b).

Taken together, these results suggest that CuET impairs p97-dependent translocation of substrates during ERAD, causing an accumulation of damaged polyubiquitinated proteins associated with ER-membrane ultimately triggering ER-stress and UPR activation. As ERAD is indispensable process and UPR is tightly connected to cell death pathways, the induction of UPR could contribute significantly to the toxicity of CuET complex.

4.8 CuET complex immobilises p97 segregase

The data gathered so far apparently demonstrates that CuET inhibits several processes dependent on p97 function, but the mechanism involved is unclear. To possess its activities, p97 hydrolyses ATP as a source of energy, so the inhibition of its ATP-ase activity was the most likely hypothesis as illustrated for other p97 inhibitors (Anderson et al., 2015; Chou et al., 2011; Magnaghi et al., 2013). Unexpectedly, in contrast to NMS-873, CuET failed to inhibit p97-mediated ATP hydrolysis *in vitro* (Fig. 15a). As an alternative scenario, I checked the protein levels of p97, as CuET treatment could potentially downregulate the amount of the protein leading to malfunction of the system in cells. However, no effect was observed (Fig. 15b). p97 segregase does not operate alone, but it associates with plethora of cofactors.

Among the most important is a heterodimer consisting of NPL4 and UFD1 proteins that is thought to mediate the interaction with client ubiquitinated proteins (Meyer et al., 2012). As NPL4 and UFD1 are necessary for multitude of p97 activities, I checked also the level of these proteins, however, again, no effect was observed (Fig. 15b).

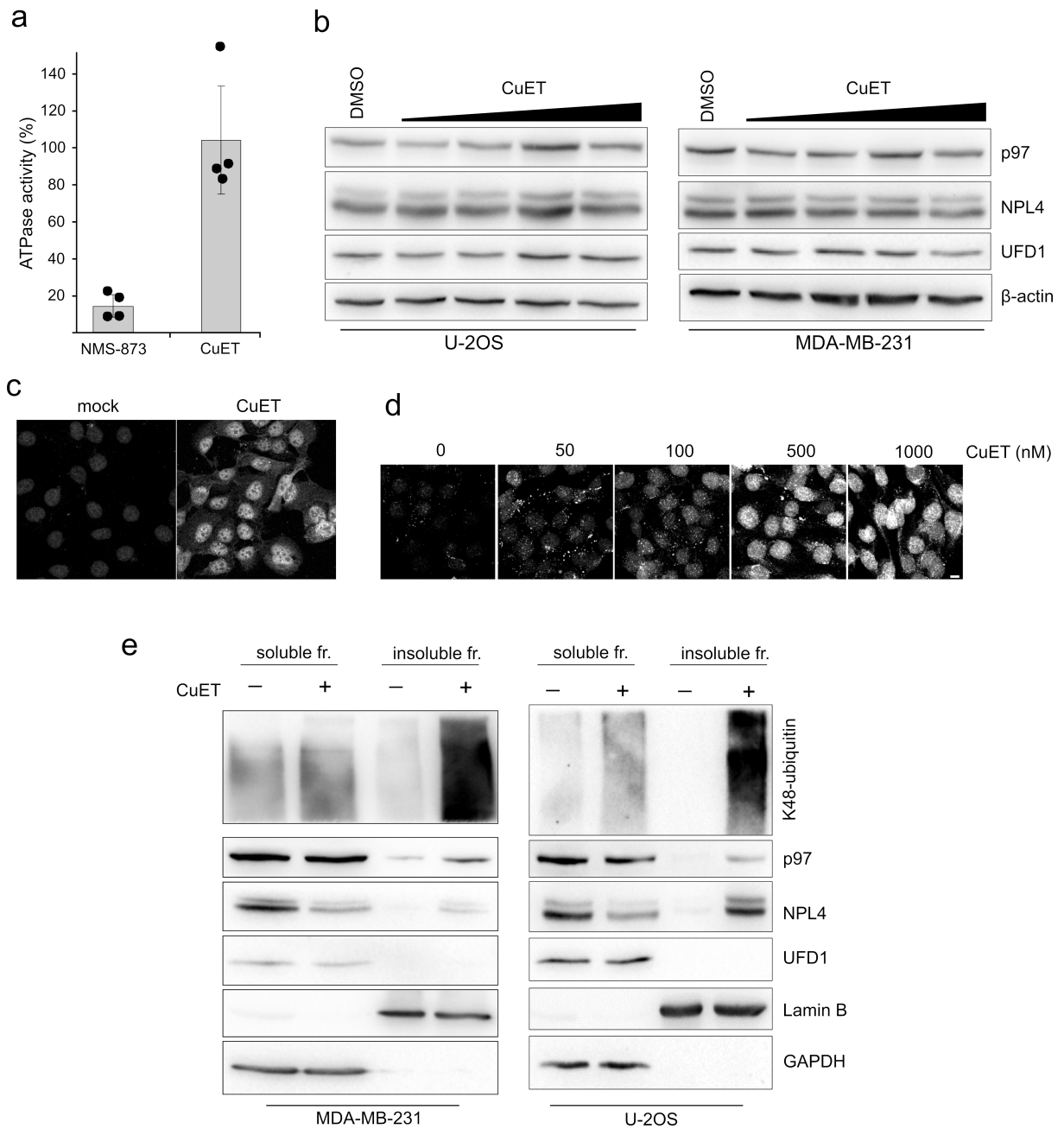


Figure 15 | CuET complex immobilises p97 segregase. **a**) CuET (1 μ M) does not inhibit ATPase activity of p97, NMS-873 (5 μ M) was used as a positive control (mean, SD and individual data from 4 independent experiments). **b**) WB analysis of levels of p97, NPL4 and UFD1 proteins in CuET-treated (8 h; 125 nM, 250 nM, 500 nM, 1000 nM) U-2OS and MDA-

MB-231 cells. **c)** IF analysis of p97 in pre-extracted U-2OS cells (CuET 1 μ M for 3 h). **d)** Dose-dependent immobilization of p97 in pre-extracted MDA-MB-231 cells treated by CuET for 3 h. (Scale bar = 10 μ m). **e)** Immobilization of p97, NPL4 and K48-ubiquitin conjugates in Triton X-100 insoluble fraction in U-2OS and MDA-MB-231 cells treated by CuET (1 μ M) for 3 h.

To get further insight into p97 behaviour after CuET treatment, I stained p97 segregase by immunofluorescence (IF) for analysis by confocal microscope. Interestingly, when the cells were first pre-extracted before fixation and IF staining, that is the same approach used for K48-ubiquitinated proteins, obvious effect of CuET on p97 was observed. While in non-treated cells the signal disappears almost completely, consistent with p97 being very mobile protein (Song et al., 2015), CuET induced very prominent immobilisation of p97 on insoluble cellular structures (Fig. 15c). Such effect was so intensive that extraction-resistant pool of p97 was clearly visible also after the treatment with very low concentrations of CuET (50 nM) (Fig. 15d). To assess if the immobilization effect of CuET complex is valid also for NPL4 and UFD1 proteins, the most important cofactors of p97, I fractionated cell lysate to soluble and insoluble pellet fraction and analysed by WB. As expected from previous results, K48-ubiquitinated proteins and p97 were clearly detected in pellet fraction in CuET treated cells (Fig. 15e). Interestingly, NPL4 cofactor was also visibly enriched in insoluble fraction, while the second partner of heterodimer UFD1 seemed not (Fig. 15e).

These results suggest that CuET impairs p97 pathway by considerably unusual way. It seems that CuET induce immobilisation of p97 itself and at least one of its essential cofactor, NPL4, leading to a malfunction of the pathway.

4.9 CuET complex targets NPL4 cofactor

According to results shown in Fig. 15e, NPL4 enrichment in pellet fraction is very pronounced, even leading to a visible decrease of total soluble pool of NPL4, which is not the case for p97. To explore this interesting observation in more detail, I followed NPL4 transition from soluble into pellet fraction in time. Remarkably, CuET treatment induced almost complete switch of NPL4 protein into insoluble fraction within 5 hours in both cell lines (Fig. 16a), suggesting very prominent impact of CuET on this protein. NPL4, as the essential cofactor of p97 necessary for its proper function and cell physiology (Meyer et al.,

2012), represents intriguing possible target of CuET complex. Since the resistance to the drugs is frequently associated with amplification or overexpression of target protein, as seen in case of bortezomib or methotrexate (Morganti et al., 2000; Oerlemans et al., 2008) for instance, similar approach was employed to resolve the relevance of NPL4 protein as a target of CuET complex. Stable cell lines overexpressing NPL4-GFP, p97-GFP, UFD1-GFP proteins and cells transfected only with empty vector were generated (Fig. 16b), and the effect of the overexpression of individual proteins on CuET toxicity was evaluated. Importantly, NPL4 overexpression caused the cells more resistant to CuET treatment compared to p97, UFD1 or control cells (Fig. 16c). To investigate the impact of NPL4 overexpression on phenotypes induced by CuET, I also analysed the level of ubiquitinated proteins, a general marker of protein degradation. Similarly, CuET-treated cells overexpressing NPL4-GFP had visibly lower amount of accumulated K48-ubiquitinated proteins compared to controls (Fig. 16d).

To look in more detail to the behaviour of NPL4, cells expressing NPL4-GFP were treated by CuET and followed in time by fluorescent microscopy. Interestingly, within 2-3 hours, NPL4-GFP formed clearly visible clusters in the nucleus and granular pattern in the cytoplasm (Fig. 16f). Such effect was not observed in case of p97-GFP or UFD1-GFP (Fig. 16e). Subsequent FRAP analysis confirmed that NPL4-GFP is strongly immobilised in both the nucleus and cytoplasm in CuET-treated cells (Fig. 16f). Similar nuclear clusters induced by CuET were also detected by IF staining of endogenous NPL4 (Fig. 16g).

These findings indicate that NPL4 cofactor is prominently affected by CuET complex, leading to its complete immobilization and formation of nuclear and cytoplasmic clusters, explaining well the effect of CuET on p97 segregase and protein degradation. Importantly, these data should be also viewed in the light of the biochemical experiments confirming the direct interaction of CuET with purified NPL4 protein *in vitro* (Skrott et al., 2017).

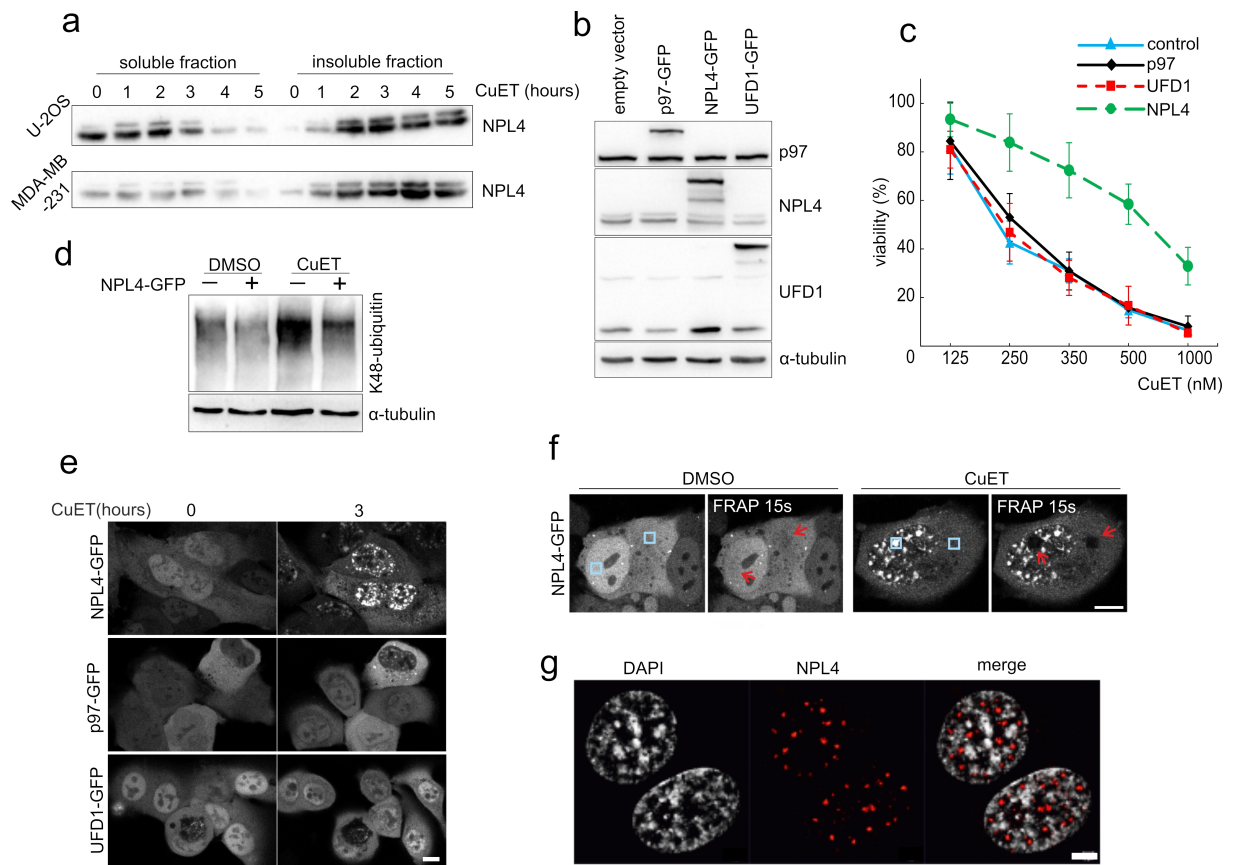


Figure 16 | CuET complex targets NPL4 cofactor. **a)** WB analysis showing NPL4 enrichment in Triton X-100-insoluble fractions after CuET (1 μ M) treatment. **b)** WB analysis documenting levels of ectopic p97-GFP, NPL4-GFP and UFD1-GFP in stable U-2OS cell lines used for the CuET-treatment rescue and cluster-formation experiments. **c)** Ectopic NPL4-GFP, but not p97-GFP or UFD1-GFP rescues CuET toxicity (mean, SD, from 3 experiments, 24 h, U-2OS). **d)** Ectopic expression of NPL4-GFP alleviates CuET-induced (125 nM, 4 h) accumulation of K48-ubiquitinated proteins in U-2OS cells. **e)** CuET (1 μ M) induces intra-nuclear clustering of NPL4-GFP, but not p97-GFP or UFD1-GFP. **f)** CuET (1 μ M, 2 h)-induced immobilization of NPL4-GFP (FRAP, blue boxes: areas before bleaching, arrows: after bleaching). **g)** Distribution of endogenous NPL4 nuclear clusters relative to chromatin in cells treated by CuET (1 μ M, 2 h). Scale bars = 10 μ m, in (g) = 2 μ m).

4.10 NPL4 protein forms aggregates after the treatment by CuET

Detailed picture of NPL4 nuclear clusters revealed that the clusters occupy areas poorly labelled with DAPI and are not part of nucleoli (Fig. 16g). To explore their nature

more closely, several nuclear structures were stained and analysed by IF for a possible co-localization. Unexpectedly, no overlap was observed with diverse nuclear structures including nuclear speckles or PML bodies as revealed by staining for their markers (SC-35, PML) (Fig. 17a). In late-G2 cells, NPL4 was obviously segregated from the partially condensed chromatin (Fig. 17b), suggesting NPL4 is not recruited into specific nuclear sites but rather excluded, which is typical for aggregated proteins (Enam et al., 2018; Sontag et al., 2017). Further experiments revealed that the immobilized cytoplasmic and nuclear signals of NPL4-GFP co-localize with polyubiquitylated proteins (stained with anti-K48-ubiquitin antibody) (Fig. 17c). The nuclear clusters are also positive for small ubiquitin-like modifier (SUMO2/3) protein (Fig. 17d), which plays an important role in the recognition of aggregated nuclear proteins (Guo et al., 2014). Interestingly, immobilised NPL4-GFP co-localised in addition with TAR DNA binding protein 43 (TDP-43) (Fig. 17d), a protein involved in RNA maturation that is found as a part of protein aggregates in several neurodegenerative diseases (Becker et al., 2017; Buratti and Baralle, 2012; Guo et al., 2014; Vogler et al., 2018).

Such results suggest NPL4 is part of protein aggregates after CuET treatment, which could be explained by two alternative scenarios. First, CuET could induce aggregation of another unknown cellular protein(s) (such as TDP-43 for instance) and NPL4 is recruited into such aggregates consequently to promote their degradation. Alternatively, NPL4 could be the primary target of CuET, which aggregates and secondary attracts other proteins. To test these hypotheses, I performed a couple of experiments. NPL4 protein, as a part of p97 complex with UFD1 cofactor, is believed to recognise its client proteins via polyubiquitin chain (Meyer et al., 2012, 2002). To investigate if NPL4 is recruited to the protein aggregates via ubiquitin, I pre-treated the cells with ubiquitin-activating enzyme 1 inhibitor (MLN7243), which should in principle block all ubiquitination in the cell (Hyer et al., 2018). Importantly, while all ubiquitination was indeed completely stopped as revealed by immunofluorescent staining for all ubiquitin conjugates by FK2 antibody, NPL4-GFP still formed clusters in cells pre-treated by MLN7243 (Fig. 17e). Moreover, siRNA mediated knock-down of TDP-43 did not prevent immobilization of NPL4-GFP (Fig. 17f), indicating that this protein is dispensable for NPL4 clusters formation. These results strongly support the hypothesis that NPL4 is aggregated first and independently on other factors like ubiquitinated proteins or TDP-43 are rather recruited secondarily.

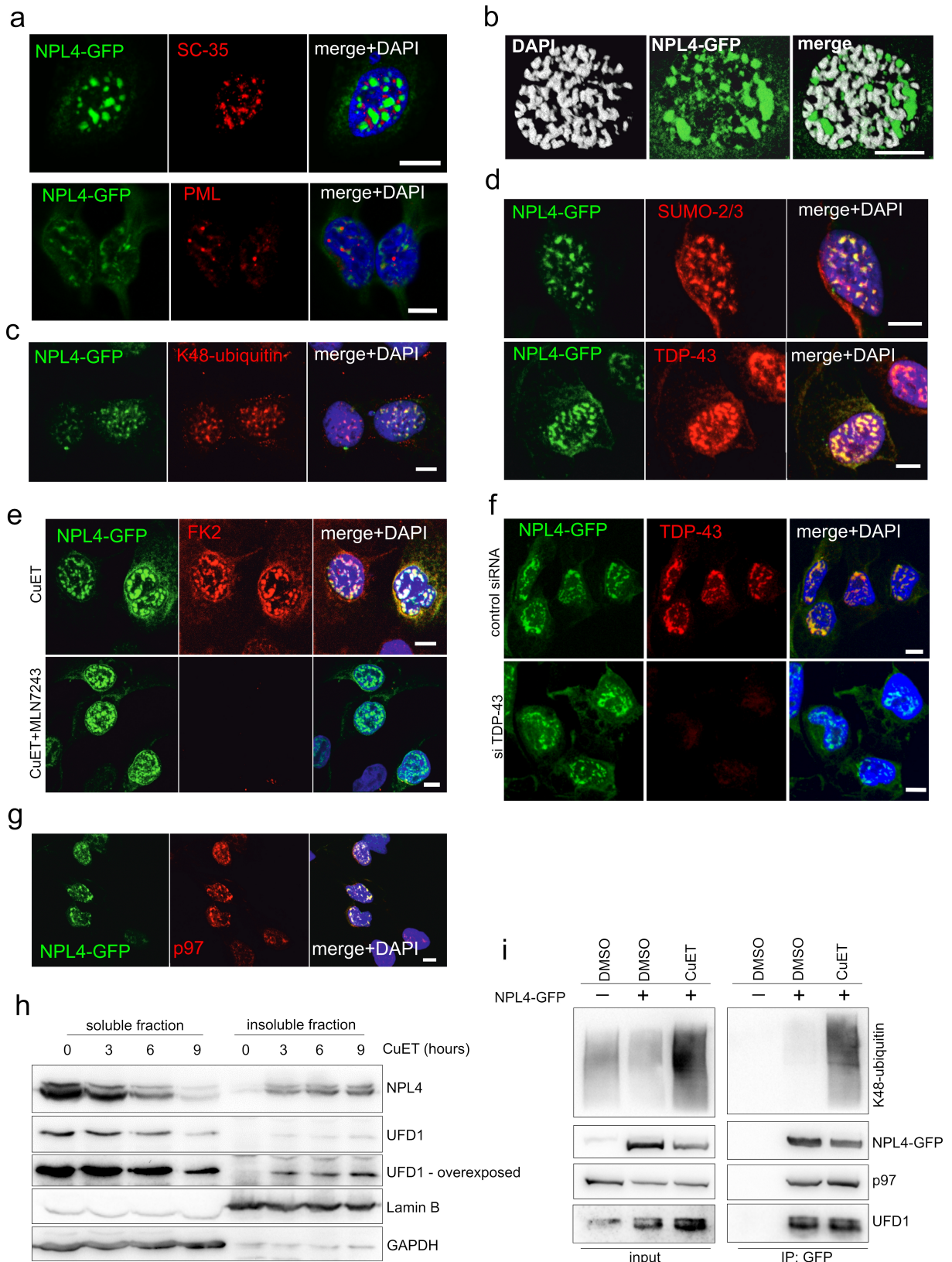


Figure 17 | NPL4 protein forms aggregates after CuET treatment. a) NPL4-GFP clusters induced by CuET treatment (1 μ M for 3h) do not co-localize with nuclear speckles (stained by SC-35 antibody) or PML bodies. b) NPL4-GFP nuclear aggregates induced by CuET (1 μ M,

3 h) are excluded from chromatin in early prometaphase U-2OS cells. **c)** NPL4-GFP co-localizes with K48-ubiquitinated conjugates in cells treated by CuET (1 μ M, 3 h; pre-extracted). **d)** NPL4-GFP co-localizes with SUMO-2/3 and TDP-43 in cells treated by CuET (1 μ M, 3 h; pre-extracted). **e)** NPL4-GFP aggregates are formed independently of ubiquitylations, as documented on CuET (1 μ M, 3h) treated cells pre-treated with a chemical UBE1 inhibitor (MLN7243, 10 μ M for 1 h); The lack of the cellular FK2 staining for ubiquitylated proteins validates the efficacy of the MLN7243 inhibitor. **f)** NPL4-GFP aggregates are formed independently of TDP-43, as documented on CuET (1 μ M, 3 h) treated cells, in which TDP-43 was downregulated by siRNA. **g)** The amount of immobilised p97 in CuET-treated cells (1 μ M for 3 h) correlates with the intensity of NPL4-GFP aggregates (pre-extracted). **h)** Detailed WB analysis of UFD1 behaviour in CuET-treated (1 μ M) U-2OS cells revealing limited UFD1 immobilization compared to NPL4. **i)** Immunoprecipitated soluble NPL4-GFP protein from cells treated by CuET (1 μ M for 3h) still interacts with p97, UFD1 binding partners and K48-ubiquitin conjugates. Scale bars = 10 μ m.

Consistent with previous results (Fig. 15c,d,e), p97 also co-localise with NPL4-GFP, indicating that subset of p97 is attracted to aggregates (Fig. 17g). The amount of p97 within the NPL4-GFP clusters correlated with the GFP intensity suggesting that p97 is immobilized via its interaction with NPL4. On the other hand, the virtual absence of UFD1 in pellet fraction (Fig. 15e) suggests disruption of NPL4-UFD1 complex. Detailed analysis confirmed very limited presence of UFD1 in insoluble fraction in contrast to NPL4 (Fig. 17h) raising a question if CuET directly break the complex or if NPL4 aggregates interact with UFD1 less tightly. To dissect between these hypotheses, I performed immunoprecipitation (IP) against NPL4-GFP in soluble fraction. No difference in the levels of UFD1 and p97 associated with NPL4 was observed after CuET treatment (Fig. 17i), indicating that CuET does not disrupt soluble heterodimer directly, but rather aggregated NPL4 lost its affinity for UFD1 partner.

4.11 NPL4 protein mutated in putative zinc-finger domain resembles phenotypes induced by CuET

NPL4 protein is a particularly interesting as a target for CuET because it contains two zinc-finger domains termed as NZF (NPL4-zinc-finger) located at C-terminus and putative zf-NPL4 (Lass et al., 2008). Importantly, zinc-finger domains are known to bind bi-valent metal ions or complexes that might chemically resemble CuET (Voráčková et al., 2011).

Interestingly, NPL4 protein is expressed as two isoforms in human cells, one of them lacks C-terminal NZF. In this isoform, NZF domain is completely substituted with different amino acid sequence making this isoform larger, which is visible as an upper band as it migrates more slowly in SDS-PAGE. Lacking NZF, yet this isoform responds to CuET treatment normally by immobilization in the insoluble pellet fraction (Fig. 16a), suggesting c-terminal NZF domain does not play a role in the response to CuET.

Putative zinc-finger domain is located closer to the N-terminus and its zinc-binding pocket consist of two histidine and two cysteine residues (Lass et al., 2008). To test a potential role of this domain, all four critical amino acids within the zinc-finger pocket were mutated to alanine (Fig. 18a) and doxycycline (DOX) inducible cell line expressing mutated form of NPL4 (MUT-NPL4-GFP) was established. Surprisingly, upon the induction, MUT-NPL4-GFP spontaneously formed nuclear and cytoplasmic immobile aggregates (Fig. 18b), reminiscent of those observed in cells ectopically expressing WT-NPL4-GFP and treated with CuET. Moreover, in contrast to ectopic WT-NPL4-GFP (Fig. 16c), the ectopic MUT-NPL4-GFP did not render the cells resistant towards CuET, and in fact it was rather toxic to the acceptor cells and made them more susceptible to CuET (Fig. 18c). By further examination I found that multiple CuET-induced phenotypes were shared with MUT-NPL4-GFP overexpression. First, it induced accumulation of K48-ubiquitinated proteins and activation of UPR (Fig. 18d). Second, similarly to CuET treatment, MUT-NPL4-GFP expression caused immobilisation of polyubiquitinated proteins and p97, but not UFD1, as revealed by WB analysis of soluble and pellet fractions (Fig. 18e). Third, MUT-NPL4-GFP aggregates were also positive for several proteins found also in WT-NPL4-GFP aggregates induced by CuET, such as ubiquitinated proteins, p97, SUMO or TDP-43 (Fig. 18f). Moreover, just like in the case of CuET treatment, soluble MUT-NPL4 maintained its ability to bind ubiquitinated proteins, p97 and UFD1 partners, as efficiently as WT-NPL4 protein, which was confirmed *in vitro* by pull-down assay involving purified proteins (Fig. 18g). These results suggest that it is not simply a gross misfolding that occurs in the MUT-NPL4, but rather a more restricted folding alteration, with phenotypic consequences that are reminiscent of the scenario triggered by CuET in the WT-NPL4.

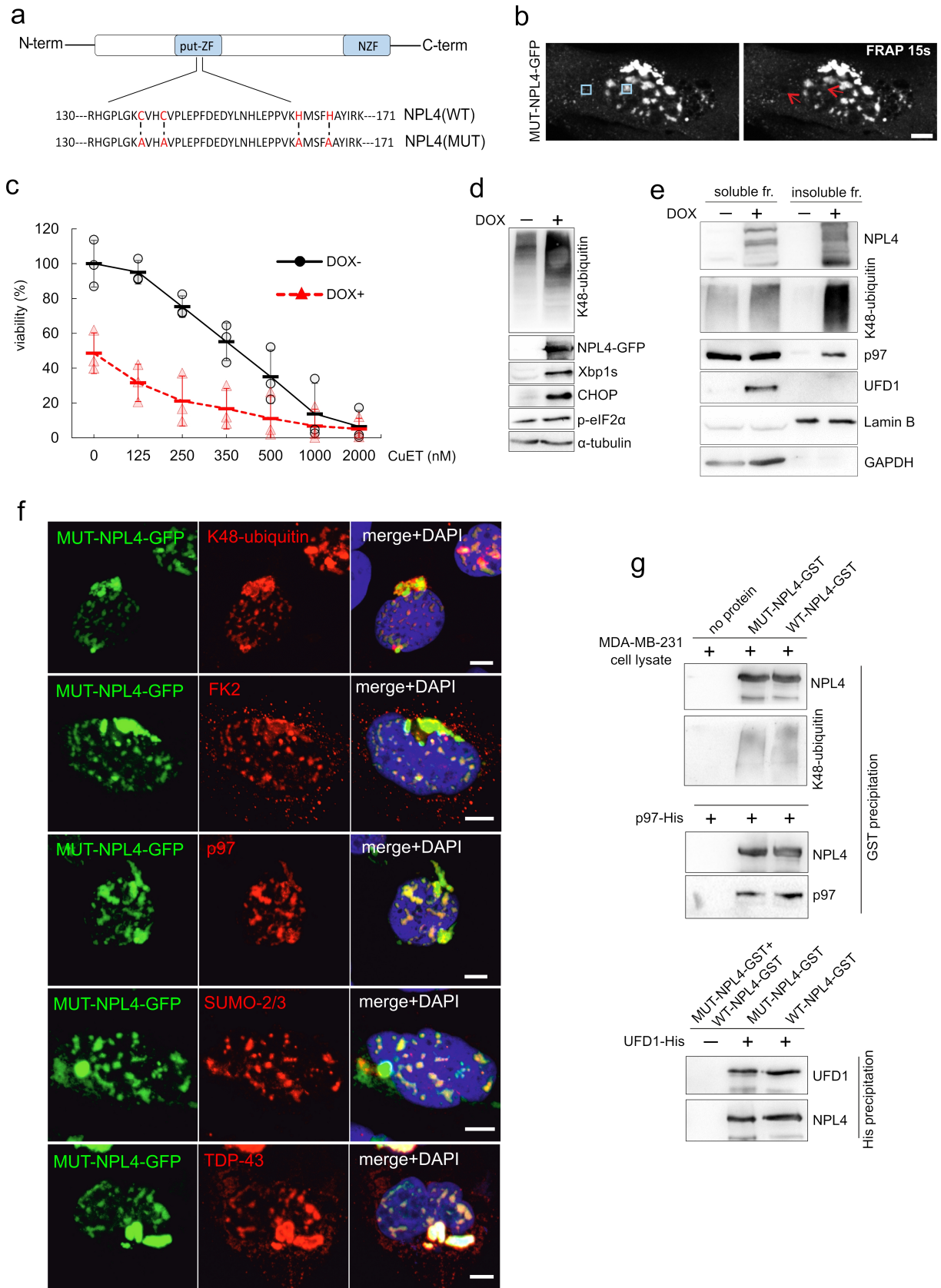


Figure 18 | NPL4 mutated in putative zinc-finger domain resembles phenotypes induced by CuET. a) Schematic representation of site-directed mutagenesis within the amino acid sequence of the putative zinc finger domain of NPL4. **b)** Spontaneous intra-

nuclear clustering and immobilization of MUT-NPL4-GFP (FRAP, U-2OS cells, blue boxes: areas before bleaching, arrows: after bleaching). **c)** Viability of cells expressing a doxycycline-inducible MUT-NPL4-GFP, treated with CuET for 48 h (mean and SD, individual points from 3 independent experiments are shown). **d)** Accumulation of K48-ubiquitinated proteins and activation of UPR in cells expressing the doxycycline-inducible MUT-NPL4-GFP. **e)** Immobilization of selected proteins in TritonX-100 insoluble pellet fractions from U-2OS cells expressing doxycycline-inducible MUT-NPL4-GFP (48 h after induction). **f)** Co-localization of spontaneous MUT-NPL4-GFP aggregates with ubiquitin conjugates (detected by FK2 and anti-K48-ubiquitin antibodies), p97, SUMO-2/3 and TDP43 (pre-extracted). **g)** Purified MUT-NPL4-GST retains ability to interact *in vitro* with ubiquitin conjugates (MDA-MB-231 whole cell lysate was used as a source of ubiquitin conjugates), purified p97-His and purified UFD1-His similarly like WT-NPL4-GST as revealed by GST or His precipitations. Scale bars = 10 μ m.

Collectively, it seems that CuET targets putative zinc-finger domain of NPL4. This domain is important for proper conformational stability of NPL4 and its disruption causes the aggregation of NPL4 protein resulting to several phenotypes induced by CuET treatment. As MUT-NPL4-GFP is itself sufficient to induce all these phenotypes, it also strengthens NPL4 protein as a critical, and possibly dominant, target of CuET in human cells whose alteration is likely sufficient to cause the observed toxic cellular effects.

4.12 Aggregated NPL4 protein triggers heat shock response

It is well known that aggregation of unfolded or damaged proteins triggers cellular heat shock response (HSR), a mainly protective mechanism allowing the cells to handle aggregates (Richter et al., 2010). Transcription factor HSF1 that regulates the expression of several heat shock proteins (HSP) belongs to the most important proteins involved in HSR (Gomez-Pastor et al., 2017). To induce the expression of HSP, phosphorylated HSF1 trimerises and binds to specific sequences of the genome known as heat shock elements forming specific foci called nuclear stress bodies (Gomez-Pastor et al., 2017). Interestingly, such stress bodies were clearly visible by IF after CuET treatment (Fig. 19a) as well as HSF1 shift in molecular weight detected by WB corresponding to phosphorylated form of HSF1 (Fig. 19b). HSP70 protein, the main effector managing aggregated proteins, was also markedly induced by CuET treatment (Fig. 19b), and, as revealed by IF analysis after pre-

extraction of cells, HSP70 was actually directly associated with immobilised NPL4 aggregates (Fig. 19c). Importantly, robust HSR activation was also induced by expression of MUT-NPL4-GFP protein, accompanied by formation of HSF1 stress bodies, co-localisation of HSP70 with MUT-NPL4-GFP aggregates (Fig. 19d) and induction of HSF1 and HSP70 as revealed by WB analysis (Fig. 19e). These results indicate that NPL4 aggregates induced either by CuET or mutation are strong activators of HSR and HSP70 chaperone is involved in their processing.

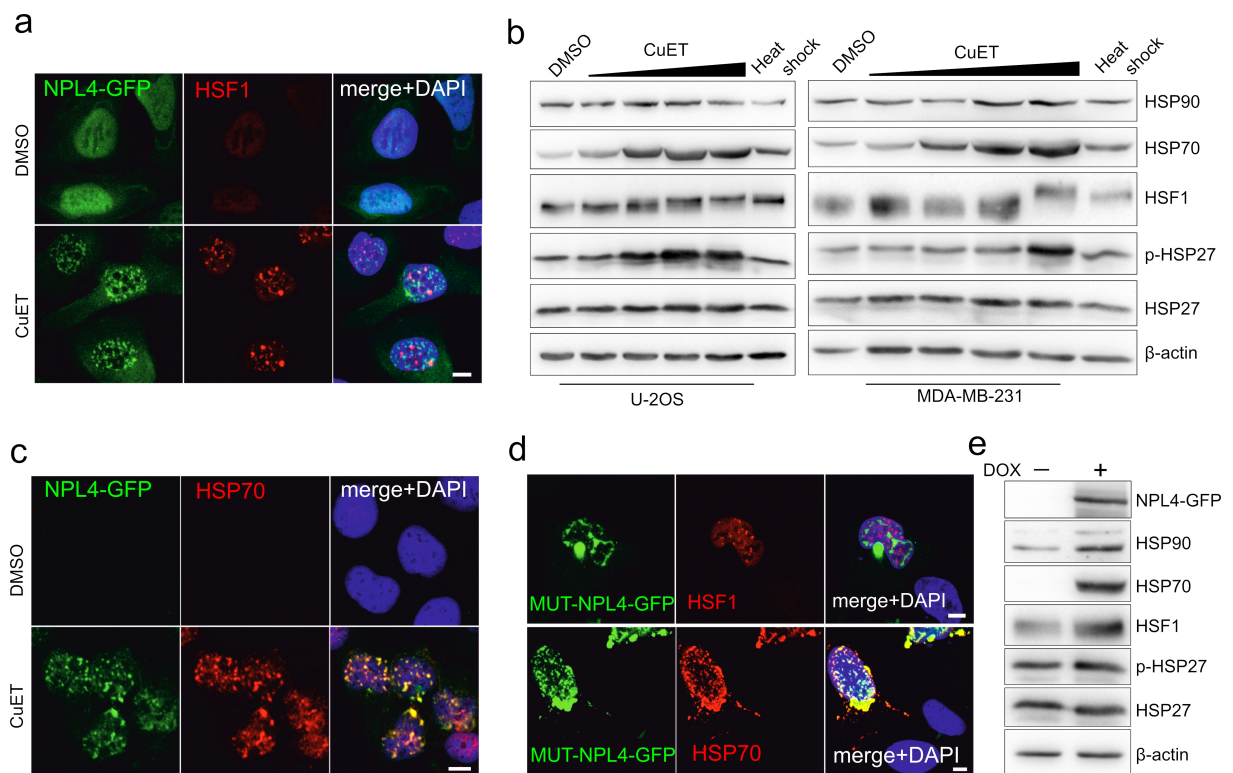


Figure 19 | Aggregated NPL4 triggers heat shock response (HSR). **a**) CuET treatment (1 μ M, 3 h) induces HSF1 stress bodies. **b**) CuET treatment (125 nM, 250 nM, 500 nM, 1000 nM for 8 h) triggers HSR as manifested by various markers: HSF1, HSP70 and p-HSP27 detected by WB in U-2OS and MDA-MB-231 cells. **c**) NPL4-GFP co-localizes with HSP70 in CuET-treated U-2OS cells (1 μ M, 3 h, pre-extracted). **d**) HSF1 stress bodies and HSP70 in U-2OS cells expressing MUT-NPL4-GFP. **e**) Activation of HSR markers in U-2OS cells expressing doxycycline-inducible MUT-NPL4-GFP (24 h after induction). Scale bars = 10 μ m.

4.13 Disulfiram is converted to CuET *in vitro*

The vast majority of research publications aiming to elucidate anti-cancer activity of disulfiram and its potentiation by copper are based on combined treatment by disulfiram and copper ions (Allensworth et al., 2015; Chen et al., 2006; Liu et al., 2013, 2016; Xu et al., 2017). This approach has certain limitations (Skrott and Cvek, 2012), as for now it is completely unknown what is happening in culture media and if disulfiram reacts with copper *in vitro*. It has been even suggested that not disulfiram itself or disulfiram-copper complex is responsible for toxic effect, but rather the reaction between disulfiram and copper yielding high amount of oxygen radicals (Lewis et al., 2014). To bring more light into this poorly explored area, I performed a series of experiments.

First, I incubated disulfiram or disulfiram with copper(ii) chloride (CuCl_2) with complete culture medium (DMEM with 10% FBS) and found that, in the presence of equimolar CuCl_2 , a majority of disulfiram is quickly converted to CuET. Interestingly, even without addition of extra copper ions, certain amount of CuET is also formed, as medium contain traces of copper ions (Fig. 20a). According to these results, disulfiram combination with copper should behave similarly like direct CuET treatment, and disulfiram alone should have only negligible activity. To test this hypothesis, I compared the toxicity of disulfiram and copper treatments with CuET. As expected, disulfiram combination with CuCl_2 was comparable toxic to CuET, in contrast to disulfiram or CuCl_2 alone in different cell lines (Fig. 20b). Similarly, only CuET and disulfiram/ Cu^{+2} combination markedly blocked a degradation of Ub(G76V)-GFP, a reporter protein, which degradation is dependent on p97 activity (Fig. 20c). To follow other phenotypes associated with mechanism of action of CuET complex in cells, I also confirmed that the combination of disulfiram with Cu^{+2} induced the aggregation of NPL4 (Fig. 20d), immobilisation of NPL4, p97 and K48-ubiquitinated proteins (Fig. 20e) and activation UPR as documented by elevated levels of several UPR markers (ATF4, eIF2 α , and CHOP) in various cancer cell lines (Fig. 20f). Finally, similarly to CuET, disulfiram/ Cu^{+2} treatment activated HSR confirmed by the presence of HSF1 stress bodies (Fig. 20g,h) and concomitant upregulation of HSP70 chaperone (Fig. 20i).

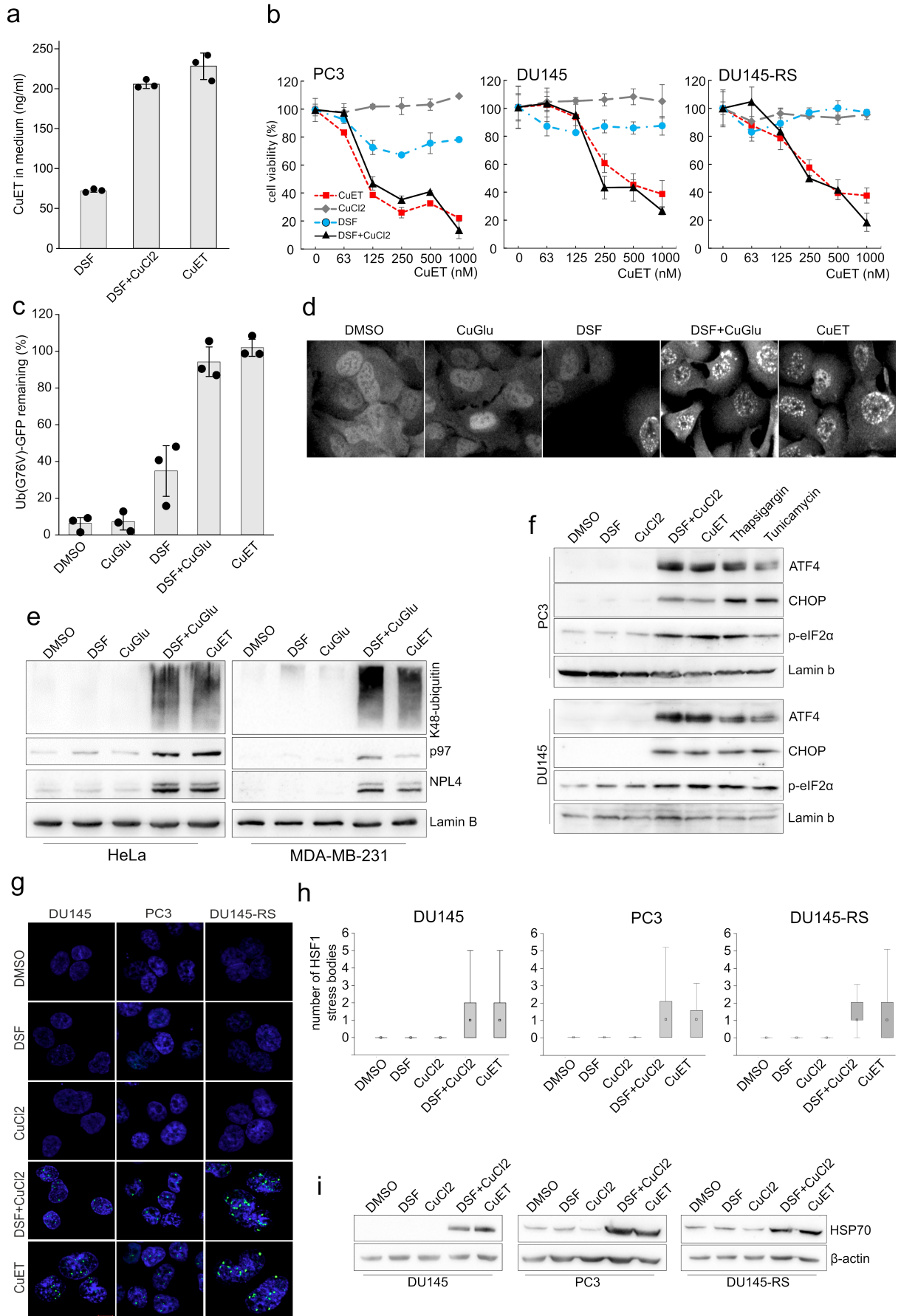


Figure 20 | Disulfiram is converted to CuET *in vitro*. **a)** The amount of CuET complex in the media with added CuET, DSF or DSF combination with CuCl₂ (each 1 μM). **b)** Toxicity of CuET, DSF, CuCl₂ and DSF combination with CuCl₂ in various cell lines (48 h treatment, mean, SD from technical triplicate, representative results). **c)** Stabilization of Ub(G76V)-GFP reporter in Hela cell line. Reporter was pre-accumulated with MG-132 (5 μM for 6 h), followed by MG-132 wash out and incubation of cells with cycloheximide (50 μg/ml) and tested compounds for 2 h. Each compound was used at 1 μM (mean, SD and individual points from 3 independent experiments) **d)** Analysis of NPL4-GFP cluster formation after treatment with indicated compounds (3 h treatment, 1 μM). **e)** WB analysis of K48-ubiquitinated proteins, p97 and NPL4 in Triton X-100 insoluble cell fraction. Cells were treated with 1 μM concentration of indicated compounds for 3 hours. **f)** UPR analysis in cell lines induced by 8 h treatment with CuET (0,5 μM) or DSF combination with CuCl₂ (both 0,5 μM) or positive controls (tunicamycin 5 μg/ml, thapsigargin 5 μM) manifested by increased levels of CHOP, ATF4 and p-eIF2α. **g)** IF analysis of HSF1 stress bodies in various cell lines treated with CuET (0,5 μM) or DSF combination with CuCl₂ (both 0,5 μM) for 3 h. **h)** Microscopic quantitative analysis of HSF1 stress bodies in various cell lines treated as in (g) (mean, lower/upper quartile, n>300 cells). **i)** WB analysis of HSP70 induction in various cell lines treated with CuET (0,5 μM) or DSF combination with CuCl₂ (both 0,5 μM) for 6 h.

Collectively, these results suggest that disulfiram is converted to CuET in the media containing copper ions, and thus such treatment induces phenotypes related to treatment with synthetic CuET complex. If extrapolated, also other published observations based on disulfiram/copper combination should be attributed to CuET complex itself. However, such experiments should be interpreted with a caution, as the extent of contribution of CuET could vary greatly and as disulfiram and copper ions are extremely reactive compounds, likely with pleiotropic effects.

5 DISCUSSION

The repurposing of existing approved drugs for a treatment of other diseases is currently relevant topic for academia, drug developers and regulatory officials (Collins, 2011). Owing to their considerable promiscuity, drugs have many “off-targets” that can be relevant for widely unrelated diseases. Drug repurposing is especially applicable for rare diseases or for diseases urgently needing new therapies. Drug thalidomide could serve as nice example of such repositioning. Being infamous for its teratogenicity when used to treat nausea in pregnant women, nowadays thalidomide found its place in the treatment of multiple myeloma and even gave rise to new drug class, known as immunomodulatory drugs, with new successors, lenalidomide and pomalidomide (Holstein and McCarthy, 2017).

Some upcoming years will show if drug disulfiram, also known as Antabuse, will join thalidomide and others as an additional example of repurposing. Originally investigated as a potential vermicide (disulfiram is used to suppress scabies parasite until now), disulfiram was accidentally found to be a potent anti-alcoholic drug, and it is approved to manage alcoholism for more than 60 years (Kragh, 2008). Increasing body of evidence gathered during last 20 years now argues for its repurposing for cancer. Numerous preclinical studies, case reports and small clinical trials are now extended by epidemiological evidence (Skrott et al., 2017). Our analysis revealed that alcoholics continuing on disulfiram had lower cancer-related mortality compared to alcoholics who ceased disulfiram at the time of their cancer diagnosis (Skrott et al., 2017). Although it is not possible to draw conclusions about causality, such findings support the hypothesis that disulfiram has anti-cancer activity in patients suffering from common cancers, prompting to perform more preclinical analyses and detailed mechanical insight.

Despite intensive research, disulfiram metabolite responsible for observed anti-cancer effects and its mechanism of action was largely unknown. In this thesis, I gather evidence describing its mechanism of action. I propose a new model of disulfiram toxicity to cancer cells, featuring rapid conversion of disulfiram into CuET, which accumulates in tumours. After entering cells, CuET interacts with NPL4 protein and induces its aggregation, consequently compromising the essential p97–NPL4–UFD1 pathway and inducing a complex cellular phenotype finally leading to cell death (Fig. 21).

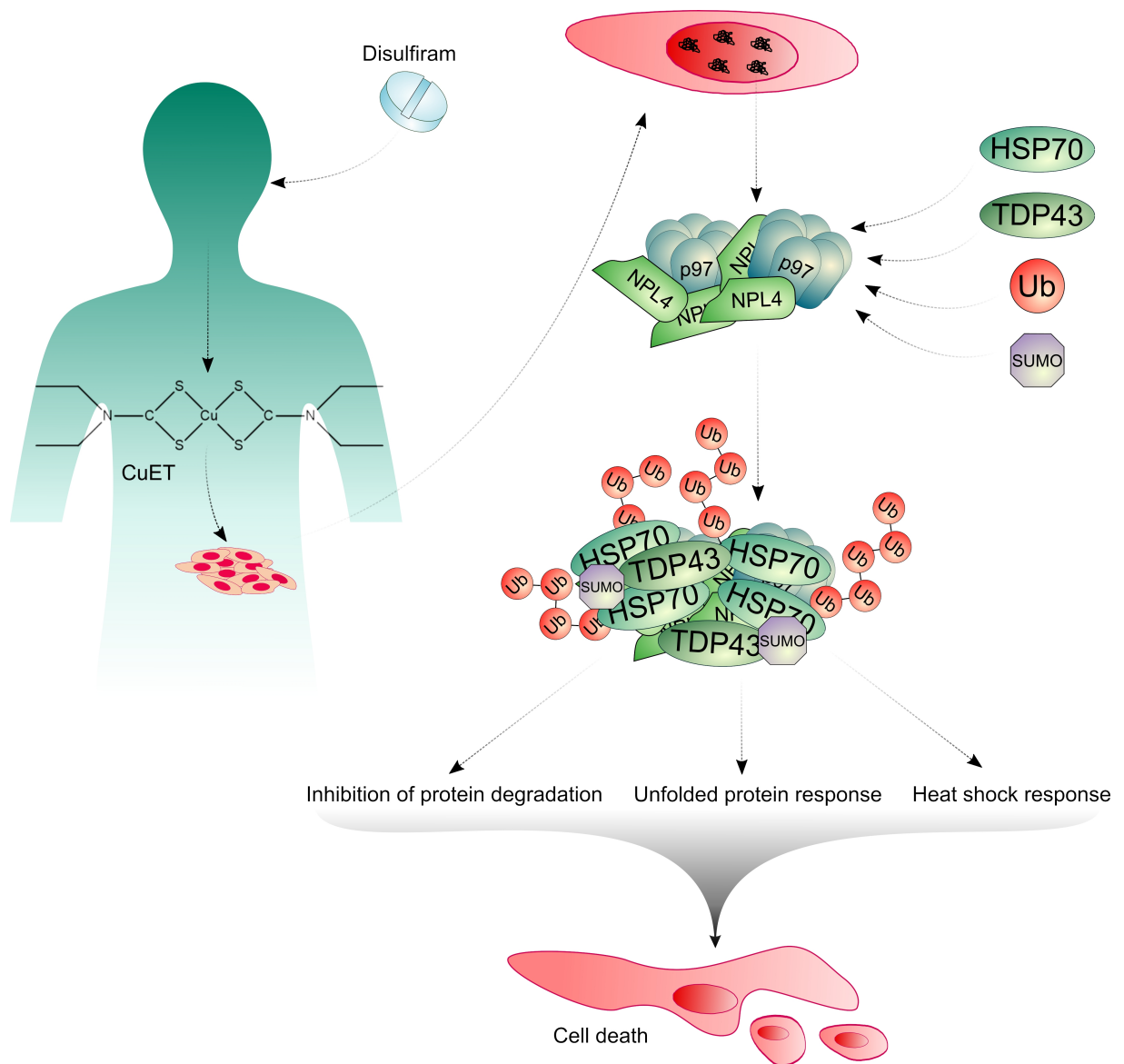


Figure 21 | The mechanism of disulfiram's action. Upon ingestion, disulfiram is rapidly metabolised to disulfiram-copper complex (CuET), which is the active anti-cancer agent toxic to transformed cells and accumulating in tumours. In cells, CuET interacts with NPL4 protein, an adaptor of p97 segregase, leading to NPL4 aggregation. The aggregates subsequently attract p97 and other stress proteins, including HSP70, TDP-43, ubiquitin or SUMO, and induce heat shock and unfolded protein responses, impairs protein degradation, and trigger cell death as a consequence.

Research community agrees that anti-cancer activity of disulfiram is strongly dependent on the presence of copper ions, however, the reason for such phenomenon was largely unclear. Here, I confirmed that CuET is new disulfiram's metabolite *in vivo* and represents the active compound responsible for toxicity to cancer cells (Fig. 8e). As additional argument for this statement is a fact that CuET is the only known metabolite of DSF containing copper ions, a metal that enhances the anti-tumour effects of disulfiram *in vivo*; and it is unlikely that another disulfiram's metabolite could represent the major anti-cancer agent as levels of other metabolites besides CuET should be always lowered by copper addition. Moreover, compared to disulfiram itself or its main metabolite, diethyldithiocarbamate, CuET is far more potent anti-cancer agent *in vitro* (Fig. 9a) and even the toxicity of disulfiram *in vitro* can be in fact attributed to CuET, which is formed rapidly when disulfiram is added to culture media form available copper ions (Fig. 20a). Moreover, strong toxicity to cancer cells and good tolerability of CuET was confirmed *in vivo* on mouse models. Direct application of CuET formulated in albumin solution significantly reduced growth of mammary MDA-MB-231 xenograft or prolonged survival of mice bearing multiple myeloma AMO-1 xenograft (Skrott et al., 2017), finally proving CuET as the active anti-cancer metabolite *in vivo*.

Interestingly, CuET levels were markedly higher in tumour tissue compared to liver, brain or serum of disulfiram or disulfiram/copper treated animals (Fig. 8d). The reason for such phenomenon is unknown so far. Disulfiram has been previously suggested (Chen et al., 2006) to be specifically toxic to cancer cells, as tumour tissue contains elevated levels of heavy metals including copper (Wang et al., 2010). Following such logic, the highest concentrations of CuET should be, however, found rather in the liver, where copper is very abundant (Linder and Hazegh-Azam, 1996). Specific transport or accumulation of CuET in tumours represents more likely explanation. However, it is entirely unknown how CuET enters cells. Cancer cells of different origins overexpress the main copper transporter Ctr1 to meet high demand for copper, thus Ctr1-mediated transport of copper complex was suggested as plausible way (Allensworth et al., 2015; Cai et al., 2014). Nevertheless, Ctr1 knock-down failed to protect the cells from disulfiram/copper treatment or block the increase of intracellular copper after disulfiram/copper treatment (Allensworth et al., 2015; Fujie et al., 2016). As a highly lipophilic compound, CuET likely binds to plasma proteins in blood stream, in that case a co-transport with such protein(s) consequently preferentially taken by

cancer cells may represent another intriguing explanation for higher CuET concentrations in tumour tissue. It is of great importance, to explore the fate and behaviour of CuET *in vivo* and its transport into tumours, as it may help to modulate the treatment or identify patients who will more likely benefit from disulfiram medication.

Higher levels of CuET complex in tumour tissue compared to other organs may provide clue to another puzzling issue: how disulfiram, as a drug with anti-cancer activity, could be so well tolerated. It is known that disulfiram usage is associated with several side effects and a subset of patients does not tolerate the treatment at all, however, the adverse effects are usually rather marginal compared to the cytotoxic drugs used for cancer treatment. If the level of CuET in normal tissues does not reach a critical value to induce toxicity, disulfiram could be used safely, but still with significant anti-cancer effect. On the other hand, it is well accepted that in fraction of patient disulfiram could be neurotoxic and induces neuropathy (Huang et al., 2018; Kulkarni et al., 2013; Tran et al., 2016), for a reason unknown so far. The mechanism of action of CuET uncovered in this thesis, involving formation of protein aggregates and activation of HSR and UPR, may shed some light also on this problem. It is well acknowledged that neurons are particularly susceptible to protein aggregates, which are associated with several neurodegenerative diseases (Hartl, 2017). It cannot be ruled out that not disulfiram itself or other metabolites, but rather CuET is responsible for observed neurotoxicity. It would be very interesting to measure if affected patients have higher levels of CuET complex and available copper (e.g. due to a diet) than patients without neurological troubles. If CuET is accountable for neurotoxicity, this adverse effect should be frequently observed in clinical trials (Huang et al., 2018) testing efficacy and safety of disulfiram/copper combination, as circulating concentration of CuET should be significantly higher than in case of disulfiram alone, as animal experiments suggest (Fig. 8d).

Peripheral neuropathy is also fundamental dose-limiting factor of therapy with bortezomib, a proteasome inhibitor used to treat multiple myeloma (Argyriou et al., 2008). Interestingly, the proteasome was also widely accepted as a target of disulfiram. Some 13 years ago, disulfiram was reported to block the degradation of several proteins and inhibition of the proteasome was suggested as an explanation (Lövborg et al., 2006). Alongside, disulfiram/copper combination was shown to directly inhibit chymotrypsin-like proteolytic activity of the proteasome (Chen et al., 2006). However, me in this work, and others failed to observe 20S proteasome inhibition by CuET complex (Cvek et al., 2008; Skrott, 2014; Skrott et al., 2017). I further excluded also the whole 26S proteasome as a possible target of CuET

(Fig. 11d). There are some possible explanations for such discrepant results. First, and most importantly, I used synthetic CuET complex and not mixture of disulfiram and copper, both very reactive compounds, which react with many proteins *in vitro* (Skrott and Cvek, 2012), making the interpretation of experiments more difficult. Indeed, it was observed that copper(ii) chloride inhibits purified 20S proteasome itself, irrespectively of disulfiram (Chen et al., 2006; Xiao et al., 2010). Second, it is not clear if observed decrease of 20S proteasome activity in disulfiram/copper treated cells was a result of direct inhibition or rather just a consequence of complex cellular phenotype and toxicity induced by CuET. It should be stressed out that disulfiram/copper markedly inhibited chymotrypsin-like activity of 20S proteasome only after prolonged incubation, but not within first few hours (Chen et al., 2006). Actually, very nice correlation between cell death and proteasome inhibition was observed, further supporting the hypothesis that proteasome malfunction is rather consequence of ongoing cell stress and death. In a sharp contrast, bortezomib, as a prototypical compound targeting 20S proteasome, inhibits the proteasome almost fully after one hour and cell death occurs much later (Skrott, 2014). While a relationship between proteasome inhibition and consequent cell death is well established, the effect of ongoing cell death on proteasome function is far less clear. In a pioneering work (Sun et al., 2004), authors observed that several subunits of the proteasome are efficiently cleaved by caspases, resulting in proteasome malfunction, stabilisation of otherwise degraded pro-apoptotic proteins, and accumulation of ubiquitinated proteins. These processes took place promptly after apoptosis induction; thus, ongoing cell death cannot be ruled out as a possible explanation for a decrease of proteasome activity observed in cells treated by disulfiram and copper.

As an alternative scenario, CuET was suggested (Cvek et al., 2008) to inhibit JAMM domain of POH1 deubiquitinase of 19S regulatory particle, essential for proper function of the proteasome (Verma et al., 2002). However, in this thesis, I present both *in vitro* and *in cellulo* data (Fig. 11c,d) clearly excluding POH1 as a possible target of CuET. Together with previous work (Skrott, 2014), this study confronts preceding publications (Chen et al., 2006; Lövborg et al., 2006; Lun et al., 2016) that suggest the proteasome as the main target of disulfiram.

Despite the lack of direct activity towards proteasome, CuET still targets UPS, as previously suggested. Through the series of experiments, I have identified that CuET inhibits segregase function of p97-Npl4-Ufd1 complex involved in processing of variety substrates to proteasome for degradation (Meyer et al., 2012). After CuET treatment, large portion of

ubiquitinated proteins and p97 as well become immobilized on various cellular structures, in a sharp contrast to proteasome inhibition (Fig. 13b, 15c). Moreover, CuET also blocked another p97 dependent process such as translocation and processing of NRF1 to become an active transcription factor triggering expression of proteasome subunits (Radhakrishnan et al., 2010; Steffen et al., 2010). This observation can be of clinical relevance as proteasome inhibitors (e.g. bortezomib) strongly activate NRF1, which in turn induce expression of new proteasomes to compensate the inhibition. Although the role of NRF1 in resistance to bortezomib in patients remains to be established, data from cell lines clearly demonstrated that functional NRF1 is important for a tolerance to proteasome inhibition (Radhakrishnan et al., 2010). Consistently, inhibition of p97 combines well with proteasome inhibitors in multiple myeloma, which is likely owing to inhibition of NRF1 activation (Le Moigne et al., 2017). A potential of p97 inhibitors for the treatment of multiple myeloma has been explored with investigational inhibitors Eeyarestatin I and DBeQ. Both inhibitors were toxic to primary myeloma cells as well as bortezomib-resistant cells, and, when combined with bortezomib, the toxicity was further augmented suggesting non-redundant roles of p97 and the proteasome (Wang et al., 2009). Similarly to these p97 inhibitors, CuET is effective in multiple myeloma cells resistant to proteasome inhibitors with comparable potency to wild type cells (Fig.12f). More importantly, CuET kills also myeloma cells obtained from a patient not responding to bortezomib-based therapy (Skrott et al., 2017). In line with considerable effect of CuET complex on multiple myeloma xenograft (Skrott et al., 2017), disulfiram combined with copper should be promptly tested on patients with relapsed, bortezomib-resistant multiple myeloma, as therapeutic options for this particular group of patients are limited.

From a broader perspective, targeting of p97 emerged as promising treatment strategy for cancer. Due altered metabolism, genetic and proteomic changes, cancer cells experience constant proteotoxic stress, which makes them highly dependent on protein-quality control system including p97 segregase, as a vital part of UPS (Deshaies, 2014). Therefore, it is not surprising, that overexpression of p97 has been observed in plethora of tumour types, including cancers of breast (Cui et al., 2015), lung (Valle et al., 2011), colon (Yamamoto et al., 2004c), prostate (Tsujiimoto et al., 2004), liver (Yamamoto et al., 2003), and others (Yamamoto et al., 2004b, 2004a, 2005), and its upregulation is associated with progression, invasion, metastasis and poor prognosis in many of these cancers. As observed in pioneering studies employing EerI and DBeQ, (Chou et al., 2011; Wang et al., 2008) the potency of p97 inhibitors is not limited to multiple myeloma, since they are toxic to wide range of cancer cell

lines *in vitro*. The phenotypes they induce are largely similar to those elicited by CuET, and include accumulation of polyubiquitinated proteins, inhibition of degradation of several proteins, activation of UPR leading to cell death; however, in contrast to CuET, only apoptosis has been reported for p97 inhibitors. This difference is most likely due to different mode of action, as CuET does not target p97 itself (Fig. 15a), but it causes NPL4 aggregation (Fig. 16a,e). CB-5083 inhibitor, a derivative of DBeQ currently entering clinical trials (NCT02243917, NCT02223598), and NMS-873, another well characterised inhibitor (both are targeting ATP-ase domain of p97) (Anderson et al., 2015; Magnaghi et al., 2013) showed very good potency across different cancer types, and particularly CB-5083 seems to be very promising drug candidate. In preclinical models, it suppresses growth of wide range of solid tumours and shows spectacular potency against multiple myeloma model, as only single application of the drug induced complete regression of the tumours (Anderson et al., 2015; Le Moigne et al., 2017).

However, as nicely illustrated by kinase or other ATP-ase inhibitors, resistance to such specifically targeted compounds is often inevitable usually due to single amino acid mutations within the binding region. Indeed, cells resistant to either CB-5083 or NMS-873 have been promptly identified harbouring point mutation spanning to ATP-ase domain of p97 (Anderson et al., 2015; Magnaghi et al., 2013), raising a caution for further clinical use as acquired resistance may severely limit the potential of these drugs. In a sharp contrast, CuET does not inhibit a function of p97 enzyme, but it targets essential adaptor protein NPL4 by quite unconventional mechanism, causing its aggregation. So far, it is not known if such mechanism of toxicity could be easily overcome by cancer cells, or not. To my knowledge, no observation reporting acquired resistance to disulfiram/copper treatment has been published until now. Consistently, my attempts to establish cell lines resistant to CuET by conventional methods involving long term dose escalation (McDermott et al., 2014) all failed (data not shown). The only exception is data presented here showing moderate rescue of cells overexpressing ectopically NPL4 (Fig. 16c).

The unique mode of action of CuET possibly explains the difficulty to generate resistant cells. The integrity of putative zinc-finger domain, which is most likely targeted by CuET, is necessary for proper NPL4 conformational stability and function. Mutation within this domain causing loss of zinc abolished CuET interaction as assessed by isothermal calorimetry and drug affinity responsive target stability methods (Skrott et al., 2017). Nevertheless, NPL4 mutated in this domain (MUT-NPL4) aggregates spontaneously and fully

mimicks CuET-induced phenotypes including toxicity to cells (Fig. 18c). Thus, the mutation precluding CuET binding is lethal *per se*. It remains to be explored, however, if a subtler mutation not affecting zinc binding could simultaneously prevent CuET interaction, presumably leading to resistance to CuET.

Observations gathered in this study support a hypothesis that NPL4 is directly targeted by CuET complex, which induces aggregation of NPL4 concomitantly causing immobilisation of its partner p97, and subsequent recruitment of several stress proteins including ubiquitin, SUMO and HSP70. However, also alternative model proposing that CuET treatment leads to aggregation of other protein(s) and NPL4, as a part of p97 complex, is just one of many recruited stress proteins should be taken in consideration. While this opposite scenario is not easy to unambiguously disprove, yet there are several arguments suggesting that the first model is highly likely.

First, higher concentration of CuET (e.g. 1 μ M) always induces complete aggregation/immobilization of NPL4, no matter how strong the ectopic expression is. The alternative model suggesting recruitment of NPL4 to aggregates of another cellular protein(s), the putative primary target(s) of CuET, predicts that binding of NPL4 should be rate-limiting and hence a subset of highly overexpressed NPL4 should remain unaffected and fully soluble upon saturation of the primary target. Moreover, in the NPL4–GFP cells, the amount of p97 within NPL4 clusters is markedly higher than in non/low-expressing cells and correlates with the GFP signal intensity (Fig. 17g), suggesting that p97 is immobilized via its interaction with NPL4.

Second, TDP-43, another protein which is typically associated with protein aggregates (Becker et al., 2017) and which can be detected within NPL4 clusters after CuET treatment (Fig. 17f) could represent an imaginable candidate for putative CuET target. However, it turned out to be fully dispensable for NPL4 aggregation as revealed by TDP-43 knock-down experiment (Fig. 17f), rather suggesting TDP-43 being attracted to NPL4 aggregates consequently.

Third, importantly, endogenous isoform of NPL4 lacking C-term NZF, which is responsible for substrate recognition, is also aggregated/immobilised by CuET (Fig. 16a). Consistently, inhibition of UBA1 enzyme which is indispensable for any ubiquitination within the cell, does not affect NPL4 aggregation (Fig. 17e). According to current understanding,

NPL4 recognises only ubiquitinated proteins, thus its binding to hypothetical CuET target would imply so-far unknown recognition mechanism.

Fourth, UFD1 partner of NPL4 is not markedly enriched in the insoluble fraction after CuET suggesting a dissociation of the UFD1 from the complex (Fig. 15e). This would be unreasonable if the p97-NPL4-UFD1 complex should be recruited to handle a protein aggregate.

Finally, and most notably, the MUT-NPL4-GFP expression induces nearly identical phenotypic responses as CuET treatment. These similarities include also the same pattern of protein aggregates (Fig. 18b) and the same spectrum of attracted proteins, strongly suggesting that NPL4 is the primary target of CuET and NPL4 itself is sufficient to induce almost indistinguishable phenotype like the treatment by CuET.

These arguments are also well supported by the experimental data confirming the direct interaction of CuET with purified NPL4 *in vitro* (Skrott et al., 2017).

While NPL4 protein, as a critical and possibly dominant target of CuET responsible for the majority of observed phenotypes, seems reliable, additional potential targets of CuET cannot be excluded. Actually, the mechanism of interaction with NPL4 is not known at all and a binding of CuET to other zinc-finger containing proteins sounds plausible. Future studies will be needed to uncover the specificity of CuET and to identify its other possible targets, some of which might be relevant for certain medical conditions.

From a broader perspective, this study illustrates a feasibility of targeting NPL4 protein as a novel way to treat cancer. A potential clinical relevance of this approach was underlined by a mouse model revealing that orally administrated disulfiram or disulfiram combination with copper gluconate induced immobilisation of NPL4 and p97 leading to suppression of tumour growth (Skrott et al., 2017). The unorthodox mechanism of the inhibition of NPL4 function by CuET, which is based on the induction of NPL4 immobilization and aggregation, opens new possibilities for targeting relevant proteins not possessing enzymatic activity yet containing structural elements sensitive to conformational change, such as zinc-fingers. To my knowledge, similar mechanism of action of a small molecule is extremely rare. To some extent, the mode of action of arsenic trioxide towards acute promyelocytic leukaemia (APL) resembles the mechanism of CuET activity. In most cases, a proliferation of APL cells is eminently dependent on the fusion oncogene PML-RAR

and its targeting by all-*trans* retinoic acid (ATRA) leads often to complete and durable remissions (Wang and Chen, 2008). Besides ATRA, arsenic trioxide has remarkable activity too, and it is FDA approved for APL treatment. It has been reported that arsenic binds directly PML-RAR oncogene and induce its degradation leading to cell death. More specifically, arsenic binds to zinc-finger within PML, causing a conformational change leading to oligomerization of PML-RAR, subsequent SUMOylation and ubiquitination followed by degradation by the proteasome (Zhang et al., 2010b). It would be very interesting to see if there is any overlap in activity between CuET and arsenic trioxide, and whether disulfiram could represent potential treatment option also for APL.

Finally, results presented in this thesis could be interesting also from a point of view of medicinal chemistry. After great activity of cisplatin, and its platinum-based successors, enormous effort has been spent to find new metal complexes with anti-cancer activity. Thousands of complexes have been synthesized, characterised and evaluated, but with negligible impact on cancer treatment. CuET, a metabolite of disulfiram, indicates that metal complexes still have a place as a potential anti-cancer drugs. Somehow ironically, it is possible that one of the most promising metal complexes, CuET, does not have to be synthesized in chemical laboratory, but it is formed spontaneously in a body of a patient taking disulfiram.

6 CONCLUSION

Collectively, this thesis, as a part of broader project, helps to explain anti-cancer effect of alcohol-abuse drug disulfiram. It should encourage copper supplementation with disulfiram in upcoming clinical trials. Validation of CuET as the active metabolite and development of method for its detection in human samples should help clinical oncologist to set proper dose, monitor impact of the treatment and explain potential variability of outcomes. Identification of NPL4 protein as a molecular target of CuET is surprising given the NPL4 has never been mentioned as a potential anti-cancer target in scientific literature. This study should promote further research on NPL4 potentially leading to development of better inhibitors and identification of subset of sensitive tumour types to NPL4 inhibition. Finally, with respect to disulfiram safety, very good long-term tolerability and established clinical practice, these results should motivate series of clinical trials to specifically identify cancer types responding to disulfiram. Repurposing of disulfiram as anti-cancer drug could be especially important for developing countries. Due to the financial demands of new drugs, they are inaccessible for countries with poor health-care systems. The cost of a few US dollars for one-month therapy makes disulfiram an ideal candidate for such countries to combat cancer.

7 ABBREVIATIONS

1,10-OPT	–	1,10 orthophenanthroline
8-HQ	–	8-quinolinethiol hydrochloride
AAA ATPase	–	ATPases associated with diverse cellular activities
ALDH	–	Aldehyde dehydrogenase
AMFR	–	Autocrine Motility Factor Receptor
APC/C	–	Anaphase-promoting complex/cyclosome
APL	–	Acute promyelocytic leukaemia
ATF4	–	Activating transcription factor 4
ATF6 α	–	Activating transcription factor 6 alpha
ATP	–	Adenosine tri phosphate
ATRA	–	All- <i>trans</i> retinoic acid
ATX3	–	Ataxin-3
BARD1	–	BRCA-associated RING domain protein 1
BOK	–	Bcl2 ovarian killer
BRCA1	–	Breast cancer 1
C-like	–	Caspase-like
Cdc25A	–	Cell division cycle 25A
CHOP	–	CCAAT-enhancer-binding protein homologous protein
CP	–	Core particle of the proteasome
CRL	–	Cullin-RING ubiquitin ligases
CSC	–	Cancer stem cells
CT-like	–	Chymotrypsin-like
CuET	–	Bis(diethyldithiocarbamate)-copper complex
CuGlu	–	Copper gluconate
DDI2	–	DNA-damage inducible 1 homolog 2
DNA	–	Deoxyribonucleic acid

DOX	–	Doxycycline
DSF	–	Disulfiram
DTC	–	Diethylthiocarbamate, ditiocarb
DUB	–	Deubiquitinating enzyme
eIF2 α	–	Eukaryotic translation initiation factor 2 alpha
ER	–	Endoplasmic reticulum
ERAD	–	ER-associated degradation
FRAP	–	Fluorescence recovery after photobleaching
GFP	–	Green fluorescent protein
GRP78	–	Glucose-regulated protein 78
HECT	–	Homologous to the E6AP carboxyl terminus
HIF1 α	–	Hypoxia inducible factor 1 alpha
HIV	–	Human Immunodeficiency virus
HPLC-MS	–	High-pressure liquid chromatography - mass spectrometry
HRD1	–	HMG-CoA Reductase Degradation 1 Homolog
HSF1	–	Heat shock factor 1
HSP	–	Heat shock protein
HSR	–	Heat shock response
I- κ B α	–	Inhibitor of nuclear factor kappa B alpha
IP	–	Immunoprecipitation
IRE1 α	–	Endoribonuclease inositol-requiring enzyme 1-alpha
JAMM	–	JAB1/MPN/Mov34 metalloenzyme
kDa	–	kilo Dalton
MAD	–	Mitochondria-associated degradation
MDa	–	mega Dalton
MDM2/MDMX	–	Mouse double minute 2/X
MDR	–	Multidrug resistant

MPN	–	Mpr1, Pad1 N-terminal
NF-κB	–	Nuclear factor-kappa B
NPL4	–	Nuclear protein localisation protein 4 homolog
NRF1 TCF11)	–	Nuclear factor erythroid derived 2-related factor 1 (NFE2L1, or
NZF	–	NPL4 zinc finger
OMM	–	Outer mitochondrial membrane
PAINS	–	Pan-assay interfering compounds
PERK	–	Protein kinase RNA-like endoplasmic reticulum kinase
PLAA	–	Phospholipase A-2-activating protein
PNGase	–	Peptide:N glycanase
PQC	–	Protein quality control
PRU	–	Pleckstrin-like receptor for ubiquitin
put-ZF	–	Putative zinc finger of NPL4
Rbx1	–	RING-box protein 1
RING	–	Really interesting new gene
RP	–	Regulatory particle of the proteasome
Rpn	–	Regulatory particle non-ATPase
Rpt	–	Regulatory particle triple-A protein
SCF	–	Skp1-cullin-F-box protein ligases
siRNA	–	small interfering RNA
Skp1	–	S-phase kinase-associated protein 1
SUMO	–	Small ubiquitin-like modifier
T-like	–	Trypsin-like
UBE1	–	Ubiquitin activating enzyme E1
UCH37	–	Ubiquitin C-terminal hydrolase 37
UBA	–	Ubiquitin-associated domain

UBA-UBX	–	Ubiquitin-associated; Ubiquitin regulatory X
UBL	–	Ubiquitin-like domain
UBX-L	–	Ubiquitin regulatory X-like
UFD1	–	Ubiquitin fusion degradation 1
UIM	–	Ubiquitin-interactive domain
UPR	–	Unfolded protein response
UPS	–	Ubiquitin-proteasome system
USP14	–	Ubiquitin-specific protease 14
VCIP135	–	Valosin-containing protein/p47 complex-interacting protein, p135
VCP	–	Valosin-containing protein
Vms1	–	VCP/Cdc48-associated mitochondrial stress-responsive 1
Xbp1	–	X-box binding protein 1

8 REFERENCES

- Acs, K., Luijsterburg, M.S., Ackermann, L., Salomons, F.A., Hoppe, T., and Dantuma, N.P. (2011). The AAA-ATPase VCP/p97 promotes 53BP1 recruitment by removing L3MBTL1 from DNA double-strand breaks. *Nat. Struct. Mol. Biol.* *18*, 1345.
- Åkerfelt, M., Morimoto, R.I., and Sistonen, L. (2010). Heat shock factors: integrators of cell stress, development and lifespan. *Nat. Rev. Mol. Cell Biol.* *11*, 545–555.
- Akutsu, M., Dikic, I., and Bremm, A. (2016). Ubiquitin chain diversity at a glance. *J. Cell Sci.* *129*, 875–880.
- Alexandru, G., Graumann, J., Smith, G.T., Kolawa, N.J., Fang, R., and Deshaies, R.J. (2008). UBXD7 Binds Multiple Ubiquitin Ligases and Implicates p97 in HIF1 α Turnover. *Cell* *134*, 804–816.
- Allensworth, J.L., Evans, M.K., Bertucci, F., Aldrich, A.J., Festa, R.A., Finetti, P., Ueno, N.T., Safi, R., McDonnell, D.P., Thiele, D.J., et al. (2015). Disulfiram (DSF) acts as a copper ionophore to induce copper-dependent oxidative stress and mediate anti-tumor efficacy in inflammatory breast cancer. *Mol. Oncol.* *9*, 1155–1168.
- Amm, I., Sommer, T., and Wolf, D.H. (2014). Protein quality control and elimination of protein waste: The role of the ubiquitin–proteasome system. *Biochim. Biophys. Acta - Mol. Cell Res.* *1843*, 182–196.
- Anchoori, R.K., Karanam, B., Peng, S., Wang, J.W., Jiang, R., Tanno, T., Orłowski, R.Z., Matsui, W., Zhao, M., Rudek, M.A., et al. (2013). A bis-Benzylidene Piperidone Targeting Proteasome Ubiquitin Receptor RPN13/ADRM1 as a Therapy for Cancer. *Cancer Cell* *24*, 791–805.
- Anderson, D.J., Le Moigne, R., Djakovic, S., Kumar, B., Rice, J., Wong, S., Wang, J., Yao, B., Valle, E., Kiss von Soly, S., et al. (2015). Targeting the AAA ATPase p97 as an Approach to Treat Cancer through Disruption of Protein Homeostasis. *Cancer Cell* *28*, 653–665.
- Argyriou, A.A., Iconomou, G., and Kalofonos, H.P. (2008). Bortezomib-induced peripheral neuropathy in multiple myeloma: a comprehensive review of the literature. *Blood* *112*, 1593–1599.
- Askgaard, G., Friis, S., Hallas, J., Thygesen, L.C., and Pottegard, A. (2014). Use of disulfiram and risk of cancer: a population-based case-control study. *Eur. J. Cancer Prev.* *23*, 225–232.
- Baell, J., and Walters, M.A. (2014). Chemistry: Chemical con artists foil drug discovery.

Nature *513*, 481–483.

Balsas, P., Galán-Malo, P., Marzo, I., and Naval, J. (2012). Bortezomib resistance in a myeloma cell line is associated to PSM β 5 overexpression and polyploidy. *Leuk. Res.* *36*, 212–218.

Bandau, S., Knebel, A., Gage, Z.O., Wood, N.T., and Alexandru, G. (2012). UBXN7 docks on neddylated cullin complexes using its UIM motif and causes HIF1 α accumulation. *BMC Biol.* *10*, 36.

Bard, J.A.M., Goodall, E.A., Greene, E.R., Jonsson, E., Dong, K.C., and Martin, A. (2018). Structure and Function of the 26S Proteasome. *Annu. Rev. Biochem.* *87*, 697–724.

Barrio, S., Stühmer, T., Da-Viá, M., Barrio-Garcia, C., Lehnert, N., Besse, A., Cuenca, I., Garitano-Trojaola, A., Fink, S., Leich, E., et al. (2019). Spectrum and functional validation of PSMB5 mutations in multiple myeloma. *Leukemia* *33*, 447–456.

Bebeacua, C., Forster, A., McKeown, C., Meyer, H.H., Zhang, X., and Freemont, P.S. (2012). Distinct conformations of the protein complex p97-Ufd1-Npl4 revealed by electron cryomicroscopy. *Proc. Natl. Acad. Sci.* *109*, 1098–1103.

Becker, L.A., Huang, B., Bieri, G., Ma, R., Knowles, D.A., Jafar-Nejad, P., Messing, J., Kim, H.J., Soriano, A., Auburger, G., et al. (2017). Therapeutic reduction of ataxin-2 extends lifespan and reduces pathology in TDP-43 mice. *Nature* *544*, 367–371.

Bento, C.F., Renna, M., Ghislat, G., Puri, C., Ashkenazi, A., Vicinanza, M., Menzies, F.M., and Rubinsztein, D.C. (2016). Mammalian Autophagy: How Does It Work? *Annu. Rev. Biochem.* *85*, 685–713.

Berndsen, C.E., and Wolberger, C. (2014). New insights into ubiquitin E3 ligase mechanism. *Nat. Struct. Mol. Biol.* *21*, 301–307.

Bianchi, G., Oliva, L., Cascio, P., Pengo, N., Fontana, F., Cerruti, F., Orsi, A., Pasqualetto, E., Mezghrani, A., Calbi, V., et al. (2009). The proteasome load versus capacity balance determines apoptotic sensitivity of multiple myeloma cells to proteasome inhibition. *Blood* *113*, 3040–3049.

Black, H.S., Chan, J.T., and Brown, G.E. (1978). Effects of dietary constituents on ultraviolet light-mediated carcinogenesis. *Cancer Res.* *38*, 1384–1387.

Bodnar, N.O., and Rapoport, T.A. (2017). Molecular Mechanism of Substrate Processing by

the Cdc48 ATPase Complex. *Cell* 169, 722-735.e9.

Bodnar, N.O., Kim, K.H., Ji, Z., Wales, T.E., Svetlov, V., Nudler, E., Engen, J.R., Walz, T., and Rapoport, T.A. (2018). Structure of the Cdc48 ATPase with its ubiquitin-binding cofactor Ufd1–Npl4. *Nat. Struct. Mol. Biol.* 25, 616–622.

van den Boom, J., Wolf, M., Weimann, L., Schulze, N., Li, F., Kaschani, F., Riemer, A., Zierhut, C., Kaiser, M., Iliakis, G., et al. (2016). VCP/p97 Extracts Sterically Trapped Ku70/80 Rings from DNA in Double-Strand Break Repair. *Mol. Cell* 64, 189–198.

Brar, S.S., Grigg, C., Wilson, K.S., Holder, W.D.J., Dreau, D., Austin, C., Foster, M., Ghio, A.J., Whorton, A.R., Stowell, G.W., et al. (2004). Disulfiram inhibits activating transcription factor/cyclic AMP-responsive element binding protein and human melanoma growth in a metal-dependent manner in vitro, in mice and in a patient with metastatic disease. *Mol. Cancer Ther.* 1049–1060.

Bruderer, R.M., Brasseur, C., and Meyer, H.H. (2004). The AAA ATPase p97/VCP interacts with its alternative co-factors, Ufd1-Np14 and p47, through a common bipartite binding mechanism. *J. Biol. Chem.* 279, 49609–49616.

Buchan, J.R., Kolaitis, R.-M., Taylor, J.P., and Parker, R. (2013). Eukaryotic stress granules are cleared by autophagy and Cdc48/VCP function. *Cell* 153, 1461–1474.

Budenholzer, L., Cheng, C.L., Li, Y., and Hochstrasser, M. (2017). Proteasome Structure and Assembly. *J. Mol. Biol.* 429, 3500–3524.

Buratti, E., and Baralle, F.E. (2012). TDP-43: gumming up neurons through protein–protein and protein–RNA interactions. *Trends Biochem. Sci.* 37, 237–247.

Cai, H., Wu, J. -s., Muzik, O., Hsieh, J.-T., Lee, R.J., and Peng, F. (2014). Reduced ⁶⁴Cu Uptake and Tumor Growth Inhibition by Knockdown of Human Copper Transporter 1 in Xenograft Mouse Model of Prostate Cancer. *J. Nucl. Med.* 55, 622–628.

Cande, C., Cecconi, F., Dessen, P., and Kroemer, G. (2002). Apoptosis-inducing factor (AIF): key to the conserved caspase-independent pathways of cell death? *J. Cell Sci.* 115, 4727–4734.

Cen, D., Brayton, D., Shahandeh, B., Meyskens, F.L., and Farmer, P.J. (2004). Disulfiram Facilitates Intracellular Cu Uptake and Induces Apoptosis in Human Melanoma Cells. *J. Med. Chem.* 47, 6914–6920.

- Chaitanya, G., Alexander, J.S., and Babu, P. (2010). PARP-1 cleavage fragments: signatures of cell-death proteases in neurodegeneration. *Cell Commun. Signal.* 8, 31.
- Chen, D., Peng, F., Cui, Q.C., Daniel, K.G., Orlu, S., Liu, J., and Dou, Q.P. (2005). Inhibition of prostate cancer cellular proteasome activity by a pyrrolidine dithiocarbamate-copper complex is associated with suppression of proliferation and induction of apoptosis. *Front. Biosci.* 10, 2932–2939.
- Chen, D., Cui, Q.C., Yang, H., and Dou, Q.P. (2006). Disulfiram, a Clinically Used Anti-Alcoholism Drug and Copper-Binding Agent, Induces Apoptotic Cell Death in Breast Cancer Cultures and Xenografts via Inhibition of the Proteasome Activity. *Cancer Res.* 66, 10425–10433.
- Chou, T.-F., and Deshaies, R.J. (2011). Quantitative Cell-based Protein Degradation Assays to Identify and Classify Drugs That Target the Ubiquitin-Proteasome System. *J. Biol. Chem.* 286, 16546–16554.
- Chou, T.-F., Brown, S.J., Minond, D., Nordin, B.E., Li, K., Jones, A.C., Chase, P., Porubsky, P.R., Stoltz, B.M., Schoenen, F.J., et al. (2011). Reversible inhibitor of p97, DBeQ, impairs both ubiquitin-dependent and autophagic protein clearance pathways. *Proc. Natl. Acad. Sci.* 108, 4834–4839.
- Chou, T.-F., Li, K., Frankowski, K.J., Schoenen, F.J., and Deshaies, R.J. (2013). Structure-Activity Relationship Study Reveals ML240 and ML241 as Potent and Selective Inhibitors of p97 ATPase. *ChemMedChem* 8, 297–312.
- Christianson, J.C., and Ye, Y. (2014). Cleaning up in the endoplasmic reticulum: ubiquitin in charge. *Nat. Struct. Mol. Biol.* 21, 325–335.
- Ciechanover, A. (2009). Tracing the history of the ubiquitin proteolytic system: The pioneering article. *Biochem. Biophys. Res. Commun.* 387, 1–10.
- Clark, D.W., and Palle, K. (2016). Aldehyde dehydrogenases in cancer stem cells: potential as therapeutic targets. *Ann. Transl. Med.* 4, 518–518.
- Collins, F.S. (2011). Mining for therapeutic gold. *Nat. Rev. Drug Discov.* 10, 397–397.
- Collins, G.A., and Goldberg, A.L. (2017). The Logic of the 26S Proteasome. *Cell* 169, 792–806.
- Cong, J., Wang, Y., Zhang, X., Zhang, N., Liu, L., Soukup, K., Michelakos, T., Hong, T.,

- DeLeo, A., Cai, L., et al. (2017). A novel chemoradiation targeting stem and nonstem pancreatic cancer cells by repurposing disulfiram. *Cancer Lett.* *409*, 9–19.
- Cui, Y., Niu, M., Zhang, X., Zhong, Z., Wang, J., and Pang, D. (2015). High expression of valosin-containing protein predicts poor prognosis in patients with breast carcinoma. *Tumor Biol.* *36*, 9919–9927.
- Cvek, B. (2011). Targeting Malignancies with Disulfiram (Antabuse): Multidrug Resistance, Angiogenesis, and Proteasome. *Curr. Cancer Drug Targets* *11*, 332–337.
- Cvek, B., Milacic, V., Taraba, J., and Dou, Q.P. (2008). Ni(II), Cu(II), and Zn(II) Diethyldithiocarbamate Complexes Show Various Activities Against the Proteasome in Breast Cancer Cells. *J. Med. Chem.* *51*, 6256–6258.
- D'Arcy, P., Brnjic, S., Olofsson, M.H., Fryknäs, M., Lindsten, K., De Cesare, M., Perego, P., Sadeghi, B., Hassan, M., Larsson, R., et al. (2011). Inhibition of proteasome deubiquitinating activity as a new cancer therapy. *Nat. Med.* *17*, 1636–1640.
- Dantuma, N.P., and Hoppe, T. (2012). Growing sphere of influence: Cdc48/p97 orchestrates ubiquitin-dependent extraction from chromatin. *Trends Cell Biol.* *22*, 483–491.
- Deng, H.-X., Chen, W., Hong, S.-T., Boycott, K.M., Gorrie, G.H., Siddique, N., Yang, Y., Fecto, F., Shi, Y., Zhai, H., et al. (2011). Mutations in UBQLN2 cause dominant X-linked juvenile and adult-onset ALS and ALS/dementia. *Nature* *477*, 211–215.
- Deshaies, R.J. (2014). Proteotoxic crisis, the ubiquitin-proteasome system, and cancer therapy. *BMC Biol.* *12*, 94.
- Deshaies, R.J., and Joazeiro, C.A.P. (2009). RING Domain E3 Ubiquitin Ligases. *Annu. Rev. Biochem.* *78*, 399–434.
- Dikic, I. (2017). Proteasomal and Autophagic Degradation Systems. *Annu. Rev. Biochem.* *86*, 193–224.
- Dimopoulos, M.A., Moreau, P., Palumbo, A., Joshua, D., Pour, L., Hájek, R., Facon, T., Ludwig, H., Oriol, A., Goldschmidt, H., et al. (2016). Carfilzomib and dexamethasone versus bortezomib and dexamethasone for patients with relapsed or refractory multiple myeloma (ENDEAVOR): a randomised, phase 3, open-label, multicentre study. *Lancet Oncol.* *17*, 27–38.
- Dimopoulos, M.A., Goldschmidt, H., Niesvizky, R., Joshua, D., Chng, W.-J., Oriol, A.,

- Orlowski, R.Z., Ludwig, H., Facon, T., Hajek, R., et al. (2017). Carfilzomib or bortezomib in relapsed or refractory multiple myeloma (ENDEAVOR): an interim overall survival analysis of an open-label, randomised, phase 3 trial. *Lancet Oncol.* *18*, 1327–1337.
- Dufour, P., Lang, J.M., Giron, C., Duclos, B., Haehnel, P., Jaeck, D., Jung, J.M., and Oberling, F. (1993). Sodium ditiocarb as adjuvant immunotherapy for high risk breast cancer: A randomized study. *Biotherapy* *6*, 9–12.
- Ehrenreich, H., and Krampe, H. (2004). Does disulfiram have a role in alcoholism treatment today? not to forget about disulfiram's psychological effects. *Addiction* *99*, 26–27.
- Enam, C., Geffen, Y., Ravid, T., and Gardner, R.G. (2018). Protein Quality Control Degradation in the Nucleus. *Annu. Rev. Biochem.* *87*, 725–749.
- Ernst, R., Mueller, B., Ploegh, H.L., and Schlieker, C. (2009). The Otubain YOD1 Is a Deubiquitinating Enzyme that Associates with p97 to Facilitate Protein Dislocation from the ER. *Mol. Cell* *36*, 28–38.
- Fadok, V.A., Voelker, D.R., Campbell, P.A., Cohen, J.J., Bratton, D.L., and Henson, P.M. (1992). Exposure of phosphatidylserine on the surface of apoptotic lymphocytes triggers specific recognition and removal by macrophages. *J. Immunol.* *148*, 2207–2216.
- Fang, C.-J., Gui, L., Zhang, X., Moen, D.R., Li, K., Frankowski, K.J., Lin, H.J., Schoenen, F.J., and Chou, T.-F. (2015). Evaluating p97 Inhibitor Analogues for Their Domain Selectivity and Potency against the p97-p47 Complex. *ChemMedChem* *10*, 52–56.
- Finley, D. (2009). Recognition and Processing of Ubiquitin-Protein Conjugates by the Proteasome. *Annu. Rev. Biochem.* *78*, 477–513.
- Fok, J.H.L., Hedayat, S., Zhang, L., Aronson, L.I., Mirabella, F., Pawlyn, C., Bright, M.D., Wardell, C.P., Keats, J.J., De Billy, E., et al. (2018). HSF1 Is Essential for Myeloma Cell Survival and A Promising Therapeutic Target. *Clin. Cancer Res.* *24*, 2395–2407.
- Franke, N.E., Niewerth, D., Assaraf, Y.G., van Meerloo, J., Vojtekova, K., van Zantwijk, C.H., Zweegman, S., Chan, E.T., Kirk, C.J., Geerke, D.P., et al. (2012). Impaired bortezomib binding to mutant $\beta 5$ subunit of the proteasome is the underlying basis for bortezomib resistance in leukemia cells. *Leukemia* *26*, 757–768.
- Fujie, T., Murakami, M., Yoshida, E., Tachinami, T., Shinkai, Y., Fujiwara, Y., Yamamoto, C., Kumagai, Y., Naka, H., and Kaji, T. (2016). Copper diethyldithiocarbamate as an activator of Nrf2 in cultured vascular endothelial cells. *JBIC J. Biol. Inorg. Chem.* *21*, 263–273.

- Fujita, K., Nakamura, Y., Oka, T., Ito, H., Tamura, T., Tagawa, K., Sasabe, T., Katsuta, A., Motoki, K., Shiwaku, H., et al. (2013). A functional deficiency of TERA/VCP/p97 contributes to impaired DNA repair in multiple polyglutamine diseases. *Nat. Commun.* *4*, 1816.
- Gallagher, P.S., Clowes Candadai, S. V, and Gardner, R.G. (2014). The requirement for Cdc48/p97 in nuclear protein quality control degradation depends on the substrate and correlates with substrate insolubility. *J. Cell Sci.* *127*, 1980–1991.
- Goldberg, A.L. (2011). Bortezomib's Scientific Origins and Its Tortuous Path to the Clinic. In *Bortezomib in the Treatment of Multiple Myeloma*, (Basel: Springer Basel), pp. 1–27.
- Goldberg, A.L. (2012). Development of proteasome inhibitors as research tools and cancer drugs. *J. Cell Biol.* *199*, 583–588.
- Gomez-Pastor, R., Burchfiel, E.T., and Thiele, D.J. (2017). Regulation of heat shock transcription factors and their roles in physiology and disease. *Nat. Rev. Mol. Cell Biol.* *19*, 4–19.
- Grabbe, C., Husnjak, K., and Dikic, I. (2011). The spatial and temporal organization of ubiquitin networks. *Nat. Rev. Mol. Cell Biol.* *12*, 295.
- Gui, L., Zhang, X., Li, K., Frankowski, K.J., Li, S., Wong, D.E., Moen, D.R., Porubsky, P.R., Lin, H.J., Schoenen, F.J., et al. (2016). Evaluating p97 Inhibitor Analogues for Potency against p97-p37 and p97-Npl4-Ufd1 Complexes. *ChemMedChem* *11*, 953–957.
- Guo, L., Giasson, B.I., Glavis-Bloom, A., Brewer, M.D., Shorter, J., Gitler, A.D., and Yang, X. (2014). A Cellular System that Degrades Misfolded Proteins and Protects against Neurodegeneration. *Mol. Cell* *55*, 15–30.
- Hald, J., and Jacobsen, E. (1948). A DRUG SENSITISING THE ORGANISM TO ETHYL ALCOHOL. *Lancet* *252*, 1001–1004.
- Hänzelmann, P., Buchberger, A., and Schindelin, H. (2011). Hierarchical Binding of Cofactors to the AAA ATPase p97. *Structure* *19*, 833–843.
- Harrigan, J.A., Jacq, X., Martin, N.M., and Jackson, S.P. (2017). Deubiquitylating enzymes and drug discovery: emerging opportunities. *Nat. Rev. Drug Discov.* *17*, 57–78.
- Hartl, F.U. (2017). Protein Misfolding Diseases. *Annu. Rev. Biochem.* *86*, 21–26.
- Heo, J.-M., Livnat-Levanon, N., Taylor, E.B., Jones, K.T., Dephoure, N., Ring, J., Xie, J.,

- Brodsky, J.L., Madeo, F., Gygi, S.P., et al. (2010). A Stress-Responsive System for Mitochondrial Protein Degradation. *Mol. Cell* *40*, 465–480.
- Hersh, E.M., Brewton, G., Abrams, D., Bartlett, J., Galpin, J., Gill, P., Gorter, R., Gottlieb, M., Jonikas, J.J., and Landesman, S. (1991). Ditiocarb sodium (diethyldithiocarbamate) therapy in patients with symptomatic HIV infection and AIDS. A randomized, double-blind, placebo-controlled, multicenter study. *JAMA* *265*, 1538–1544.
- Hetz, C. (2012). The unfolded protein response: controlling cell fate decisions under ER stress and beyond. *Nat. Rev. Mol. Cell Biol.* *13*, 89–102.
- Hetz, C., Chevet, E., and Oakes, S.A. (2015). Proteostasis control by the unfolded protein response. *Nat. Cell Biol.* *17*, 829–838.
- Hideshima, T., Chauhan, D., Richardson, P., Mitsiades, C., Mitsiades, N., Hayashi, T., Munshi, N., Dang, L., Castro, A., Palombella, V., et al. (2002). NF- κ B as a Therapeutic Target in Multiple Myeloma. *J. Biol. Chem.* *277*, 16639–16647.
- Hideshima, T., Ikeda, H., Chauhan, D., Okawa, Y., Raje, N., Podar, K., Mitsiades, C., Munshi, N.C., Richardson, P.G., Carrasco, R.D., et al. (2009). Bortezomib induces canonical nuclear factor- κ B activation in multiple myeloma cells. *Blood* *114*, 1046–1052.
- Hock, A.K., and Vousden, K.H. (2014). The role of ubiquitin modification in the regulation of p53. *Biochim. Biophys. Acta* *1843*, 137–149.
- Hogarth, G. (2012). Metal-dithiocarbamate complexes: chemistry and biological activity. *Mini Rev. Med. Chem.* *12*, 1202–1215.
- Holstein, S.A., and McCarthy, P.L. (2017). Immunomodulatory Drugs in Multiple Myeloma: Mechanisms of Action and Clinical Experience. *Drugs* *77*, 505–520.
- Huang, J., Campian, J.L., Gujar, A.D., Tsien, C., Ansstas, G., Tran, D.D., DeWees, T.A., Lockhart, A.C., and Kim, A.H. (2018). Final results of a phase I dose-escalation, dose-expansion study of adding disulfiram with or without copper to adjuvant temozolomide for newly diagnosed glioblastoma. *J. Neurooncol.* *138*, 105–111.
- Hyer, M.L., Milhollen, M.A., Ciavarrri, J., Fleming, P., Traore, T., Sappal, D., Huck, J., Shi, J., Gavin, J., Brownell, J., et al. (2018). A small-molecule inhibitor of the ubiquitin activating enzyme for cancer treatment. *Nat. Med.* *24*, 186–193.
- Irving, C.C., Daniel, D.S., and Murphy, W.M. (1983). The effect of disulfiram on the

carcinogenicity of N-butyl-N-(3-carboxypropyl)nitrosamine in the rat. *Carcinogenesis* 4, 617–620.

Isaacson, R.L., Pye, V.E., Simpson, P., Meyer, H.H., Zhang, X., Freemont, P.S., and Matthews, S. (2007). Detailed structural insights into the p97-Npl4-Ufd1 interface. *J. Biol. Chem.* 282, 21361–21369.

Ishikawa-Ankerhold, H.C., Ankerhold, R., and Drummen, G.P.C. (2012). Advanced fluorescence microscopy techniques--FRAP, FLIP, FLAP, FRET and FLIM. *Molecules* 17, 4047–4132.

Iwai, K. (2012). Diverse ubiquitin signaling in NF- κ B activation. *Trends Cell Biol.* 22, 355–364.

Jin, J., Li, X., Gygi, S.P., and Harper, J.W. (2007). Dual E1 activation systems for ubiquitin differentially regulate E2 enzyme charging. *Nature* 447, 1135–1138.

Johansson, B. (1992). A review of the pharmacokinetics and pharmacodynamics of disulfiram and its metabolites. *Acta Psychiatr. Scand.* 86, 15–26.

Johansson, B., and Stankiewicz, Z. (1985). Bis-(diethyldithiocarbamate) copper complex: a new metabolite of disulfiram? *Biochem. Pharmacol.* 34, 2989–2991.

Johansson B (1986). Rapid and sensitive on-line precolumn purification and high-performance liquid chromatographic assay for disulfiram and its metabolites. *J Chromatogr* 419–426.

Kane, R.C. (2003). Velcade(R): U.S. FDA Approval for the Treatment of Multiple Myeloma Progressing on Prior Therapy. *Oncologist* 8, 508–513.

Karamanakos, P.N., Trafalis, D.T., Papachristou, D.J., Panteli, E.S., Papavasiliopoulou, M., Karatzas, A., Kardamakis, D., Nasioulas, G., and Marselos, M. (2017). Evidence for the efficacy of disulfiram and copper combination in glioblastoma multiforme - A propos of a case. *J. BUON.* 22, 1227–1232.

Kepp, O., Galluzzi, L., Lipinski, M., Yuan, J., and Kroemer, G. (2011). Cell death assays for drug discovery. *Nat. Rev. Drug Discov.* 10, 221–237.

Kim, I., Kim, C.H., Kim, J.H., Lee, J., Choi, J.J., Chen, Z.A., Lee, M.G., Chung, K.C., Hsu, C.Y., and Ahn, Y.S. (2004). Pyrrolidine dithiocarbamate and zinc inhibit proteasome-dependent proteolysis. *Exp. Cell Res.* 298, 229–238.

- Kim, Y.E., Hipp, M.S., Bracher, A., Hayer-Hartl, M., and Ulrich Hartl, F. (2013). Molecular Chaperone Functions in Protein Folding and Proteostasis. *Annu. Rev. Biochem.* 82, 323–355.
- Kitami, M.-I., Kitami, T., Nagahama, M., Tagaya, M., Hori, S., Kakizuka, A., Mizuno, Y., and Hattori, N. (2006). Dominant-negative effect of mutant valosin-containing protein in aggresome formation. *FEBS Lett.* 580, 474–478.
- Koch, A., Steffen, J., and Krüger, E. (2011). TCF11 at the crossroads of oxidative stress and the ubiquitin proteasome system. *Cell Cycle* 10, 1200–1207.
- Koizumi, S., Irie, T., Hirayama, S., Sakurai, Y., Yashiroda, H., Naguro, I., Ichijo, H., Hamazaki, J., and Murata, S. (2016). The aspartyl protease DDI2 activates Nrf1 to compensate for proteasome dysfunction. *Elife* 5, e18357.
- Komander, D., and Rape, M. (2012). The ubiquitin code. *Annu. Rev. Biochem.* 81, 203–229.
- Kondo, H., Rabouille, C., Newman, R., Levine, T.P., Pappin, D., Freemont, P., and Warren, G. (1997). p47 is a cofactor for p97-mediated membrane fusion. *Nature* 388, 75–78.
- Koppaka, V., Thompson, D.C., Chen, Y., Ellermann, M., Nicolaou, K.C., Juvonen, R.O., Petersen, D., Deitrich, R.A., Hurley, T.D., and Vasiliou, V. (2012). Aldehyde Dehydrogenase Inhibitors: a Comprehensive Review of the Pharmacology, Mechanism of Action, Substrate Specificity, and Clinical Application. *Pharmacol. Rev.* 64, 520–539.
- Kortuem, K.M., and Stewart, A.K. (2013). Carfilzomib. *Blood* 121, 893–897.
- Kragh, H. (2008). From Disulfiram to Antabuse: The Invention of a Drug. *Bull Hist Chem* 33, 82–88.
- Kulkarni, R.R., Pradeep, A. V., and Bairy, B.K. (2013). Disulfiram-Induced Combined Irreversible Anterior Ischemic Optic Neuropathy and Reversible Peripheral Neuropathy: A Prospective Case Report and Review of the Literature. *J. Neuropsychiatry Clin. Neurosci.* 25, 339–342.
- Kupperman, E., Lee, E.C., Cao, Y., Bannerman, B., Fitzgerald, M., Berger, A., Yu, J., Yang, Y., Hales, P., Bruzzese, F., et al. (2010). Evaluation of the proteasome inhibitor MLN9708 in preclinical models of human cancer. *Cancer Res.* 70, 1970–1980.
- Kyjacova, L., Hubackova, S., Krejcikova, K., Strauss, R., Hanzlikova, H., Dzijak, R., Imrichova, T., Simova, J., Reinis, M., Bartek, J., et al. (2015). Radiotherapy-induced plasticity of prostate cancer mobilizes stem-like non-adherent, Erk signaling-dependent cells.

Cell Death Differ. 22, 898–911.

de la Peña, A.H., Goodall, E.A., Gates, S.N., Lander, G.C., and Martin, A. (2018). Substrate-engaged 26S proteasome structures reveal mechanisms for ATP-hydrolysis-driven translocation. *Science* 362.

Lander, G.C., Estrin, E., Matyskiela, M.E., Bashore, C., Nogales, E., and Martin, A. (2012). Complete subunit architecture of the proteasome regulatory particle. *Nature* 482, 186.

Lang, J.M., Touraine, J.L., Trepo, C., Choutet, P., Kirstetter, M., Falkenrodt, A. H., Livrozet, J.M., Retornaz, G., Touraine, F., et al. (1988). randomised, double-blind, placebo-controlled trial of ditiocarb sodium (imuthiol) in human immunodeficiency virus infection. *Lancet* 332, 702–706.

Lass, A., McConnell, E., Fleck, K., Palamarchuk, A., and Wójcik, C. (2008). Analysis of Npl4 deletion mutants in mammalian cells unravels new Ufd1-interacting motifs and suggests a regulatory role of Npl4 in ERAD. *Exp. Cell Res.* 314, 2715–2723.

Lee, D.H., and Goldberg, A.L. (1998). Proteasome inhibitors: valuable new tools for cell biologists. *Trends Cell Biol.* 8, 397–403.

Lee, B.-H., Lu, Y., Prado, M.A., Shi, Y., Tian, G., Sun, S., Elsasser, S., Gygi, S.P., King, R.W., and Finley, D. (2016). USP14 deubiquitinates proteasome-bound substrates that are ubiquitinated at multiple sites. *Nature* 532, 398–401.

Lehrbach, N.J., and Ruvkun, G. (2016). Proteasome dysfunction triggers activation of SKN-1A/Nrf1 by the aspartic protease DDI-1. *Elife* 5, e17721.

Leung-Hagesteijn, C., Erdmann, N., Cheung, G., Keats, J.J., Stewart, A.K., Reece, D.E., Chung, K.C., and Tiedemann, R.E. (2013). Xbp1s-Negative Tumor B Cells and Pre-Plasmablasts Mediate Therapeutic Proteasome Inhibitor Resistance in Multiple Myeloma. *Cancer Cell* 24, 289–304.

Lewis, D.J., Deshmukh, P., Tedstone, A.A., Tuna, F., and O'Brien, P. (2014). On the interaction of copper(*II*) with disulfiram. *Chem. Commun.* 50, 13334–13337.

Lewis, E.F. (1977). Spontaneous regression of breast cancer. *Prog. Clin. Biol. Res.* 12, 47–53.

Li, J.-M., Wu, H., Zhang, W., Blackburn, M.R., and Jin, J. (2014). The p97-UFD1L-NPL4 Protein Complex Mediates Cytokine-Induced I B Proteolysis. *Mol. Cell. Biol.* 34, 335–347.

- Li, J., Yakushi, T., Parlati, F., Mackinnon, A.L., Perez, C., Ma, Y., Carter, K.P., Colayco, S., Magnuson, G., Brown, B., et al. (2017). Capzimin is a potent and specific inhibitor of proteasome isopeptidase Rpn11. *Nat. Chem. Biol.* *13*, 486–493.
- Li, J., Zhang, Y., Da Silva Sil Dos Santos, B., Wang, F., Ma, Y., Perez, C., Yang, Y., Peng, J., Cohen, S.M., Chou, T.-F., et al. (2018). Epidithiodiketopiperazines Inhibit Protein Degradation by Targeting Proteasome Deubiquitinase Rpn11. *Cell Chem. Biol.* *25*, 1350-1358.e9.
- Li, L., Yang, H., Chen, D., Cui, C., and Ping Dou, Q. (2008). Disulfiram promotes the conversion of carcinogenic cadmium to a proteasome inhibitor with pro-apoptotic activity in human cancer cells. *Toxicol. Appl. Pharmacol.* *229*, 206–214.
- Lichter, D.I., Danaee, H., Pickard, M.D., Tayber, O., Sintchak, M., Shi, H., Richardson, P.G., Cavenagh, J., Blade, J., Facon, T., et al. (2012). Sequence analysis of β -subunit genes of the 20S proteasome in patients with relapsed multiple myeloma treated with bortezomib or dexamethasone. *Blood* *120*, 4513–4516.
- Lin, J., Haffner, M.C., Zhang, Y., Lee, B.H., Brennen, W.N., Britton, J., Kachhap, S.K., Shim, J.S., Liu, J.O., Nelson, W.G., et al. (2011). Disulfiram is a DNA demethylating agent and inhibits prostate cancer cell growth. *Prostate* *71*, 333–343.
- Linder, M.C., and Hazegh-Azam, M. (1996). Copper biochemistry and molecular biology. *Am. J. Clin. Nutr.* *63*, 797S-811S.
- Lipkowitz, S., and Weissman, A.M. (2011). RINGs of good and evil: RING finger ubiquitin ligases at the crossroads of tumour suppression and oncogenesis. *Nat. Rev. Cancer* *11*, 629–643.
- Lipsky, J.J., Shen, M.L., and Naylor, S. (2001a). In vivo inhibition of aldehyde dehydrogenase by disulfiram. *Chem. Biol. Interact.* *130–132*, 93–102.
- Lipsky, J.J., Shen, M.L., and Naylor, S. (2001b). Overview — In vitro inhibition of aldehyde dehydrogenase by disulfiram and metabolites. *Chem. Biol. Interact.* *130–132*, 81–91.
- Liu, G.Y., Frank, N., Bartsch, H., and Lin, J.K. (1998). Induction of apoptosis by thiuramdisulfides, the reactive metabolites of dithiocarbamates, through coordinative modulation of NFkappaB, c-fos/c-jun, and p53 proteins. *Mol. Carcinog.* *22*, 235–246.
- Liu, P., Brown, S., Goktug, T., Channathodiyil, P., Kannappan, V., Hugnot, J.-P., Guichet, P.-O., Bian, X., Armesilla, A.L., Darling, J.L., et al. (2012). Cytotoxic effect of

disulfiram/copper on human glioblastoma cell lines and ALDH-positive cancer-stem-like cells. *Br. J. Cancer* *107*, 1488–1497.

Liu, P., Kumar, I.S., Brown, S., Kannappan, V., Tawari, P.E., Tang, J.Z., Jiang, W., Armesilla, A.L., Darling, J.L., and Wang, W. (2013). Disulfiram targets cancer stem-like cells and reverses resistance and cross-resistance in acquired paclitaxel-resistant triple-negative breast cancer cells. *Br. J. Cancer* *109*, 1876–1885.

Liu, P., Gan, W., Su, S., Hauenstein, A. V., Fu, T., Brasher, B., Schwerdtfeger, C., Liang, A.C., Xu, M., and Wei, W. (2018). K63-linked polyubiquitin chains bind to DNA to facilitate DNA damage repair. *Sci. Signal.* *11*, eaar8133.

Liu, X., Wang, L., Cui, W., Yuan, X., Lin, L., Cao, Q., Wang, N., Li, Y., Guo, W., Zhang, X., et al. (2016). Targeting ALDH1A1 by disulfiram/copper complex inhibits non-small cell lung cancer recurrence driven by ALDH-positive cancer stem cells. *Oncotarget* *7*, 58516–58530.

Llambi, F., Wang, Y.-M., Victor, B., Yang, M., Schneider, D.M., Gingras, S., Parsons, M.J., Zheng, J.H., Brown, S.A., Pelletier, S., et al. (2016). BOK Is a Non-canonical BCL-2 Family Effector of Apoptosis Regulated by ER-Associated Degradation. *Cell* *165*, 421–433.

Locke, M., Toth, J.I., and Petroski, M.D. (2014). Lys 11 - and Lys 48 -linked ubiquitin chains interact with p97 during endoplasmic-reticulum-associated degradation. *Biochem. J.* *459*, 205–216.

Loo, T.W. (2000). Blockage of Drug Resistance In Vitro by Disulfiram, a Drug Used to Treat Alcoholism. *J. Natl. Cancer Inst.* *92*, 898–902.

Lövborg, H., Öberg, F., Rickardson, L., Gullbo, J., Nygren, P., and Larsson, R. (2006). Inhibition of proteasome activity, nuclear factor-KB translocation and cell survival by the antialcoholism drug disulfiram. *Int. J. Cancer* *118*, 1577–1580.

Lu, M., Lawrence, D.A., Marsters, S., Acosta-Alvear, D., Kimmig, P., Mendez, A.S., Paton, A.W., Paton, J.C., Walter, P., and Ashkenazi, A. (2014). Opposing unfolded-protein-response signals converge on death receptor 5 to control apoptosis. *Science* *345*, 98–101.

Lun, X., Wells, J.C., Grinshtein, N., King, J.C., Hao, X., Dang, N.-H., Wang, X., Aman, A., Uehling, D., Datti, A., et al. (2016). Disulfiram when Combined with Copper Enhances the Therapeutic Effects of Temozolomide for the Treatment of Glioblastoma. *Clin. Cancer Res.* *22*, 3860–3875.

MacDonagh, L., Gallagher, M.F., Ffrench, B., Gasch, C., Breen, E., Gray, S.G., Nicholson,

- S., Leonard, N., Ryan, R., Young, V., et al. (2017). Targeting the cancer stem cell marker, aldehyde dehydrogenase 1, to circumvent cisplatin resistance in NSCLC. *Oncotarget* 8, 72544–72563.
- Magnaghi, P., D'Alessio, R., Valsasina, B., Avanzi, N., Rizzi, S., Asa, D., Gasparri, F., Cozzi, L., Cucchi, U., Orrenius, C., et al. (2013). Covalent and allosteric inhibitors of the ATPase VCP/p97 induce cancer cell death. *Nat. Chem. Biol.* 9, 548.
- Manasanch, E.E., and Orłowski, R.Z. (2017). Proteasome inhibitors in cancer therapy. *Nat. Rev. Clin. Oncol.* 14, 417–433.
- Mandinova, A., and Lee, S.W. (2011). The p53 Pathway as a Target in Cancer Therapeutics: Obstacles and Promise. *Sci. Transl. Med.* 3, 64rv1-64rv1.
- Marikovsky, M., Nevo, N., Vadai, E., and Harris-Cerruti, C. (2001). Cu/Zn superoxide dismutase plays a role in angiogenesis. *Int. J. Cancer* 97, 34–41.
- Martinez-Zapien, D., Ruiz, F.X., Poirson, J., Mitschler, A., Ramirez, J., Forster, A., Cousido-Siah, A., Masson, M., Vande Pol, S., Podjarny, A., et al. (2016). Structure of the E6/E6AP/p53 complex required for HPV-mediated degradation of p53. *Nature* 529, 541–545.
- Masso, P.D., and Kramer, P.A. (1981). Simultaneous determination of disulfiram and two of its dithiocarbamate metabolites in human plasma by reversed-phase liquid chromatography. *J. Chromatogr. B Biomed. Sci. Appl.* 224, 457–464.
- Mays, D.C., Nelson, A.N., Fauq, A.H., Shriver, Z.H., Veverka, K.A., Naylor, S., and Lipsky, J.J. (1995). S-Methyl N,N-diethylthiocarbamate sulfone, a potential metabolite of disulfiram and potent inhibitor of low Km mitochondrial aldehyde dehydrogenase. *Biochem. Pharmacol.* 49, 693–700.
- McConkey, D.J., and Zhu, K. (2008). Mechanisms of proteasome inhibitor action and resistance in cancer. *Drug Resist. Updat.* 11, 164–179.
- McDermott, M., Eustace, A.J., Busschots, S., Breen, L., Crown, J., Clynes, M., O'Donovan, N., and Stordal, B. (2014). In vitro Development of Chemotherapy and Targeted Therapy Drug-Resistant Cancer Cell Lines: A Practical Guide with Case Studies. *Front. Oncol.* 4, 40.
- Meerang, M., Ritz, D., Paliwal, S., Garajova, Z., Bosshard, M., Mailand, N., Janscak, P., Hübscher, U., Meyer, H., and Ramadan, K. (2011). The ubiquitin-selective segregase VCP/p97 orchestrates the response to DNA double-strand breaks. *Nat. Cell Biol.* 13, 1376.

- Melino, G. (2005). Discovery of the ubiquitin proteasome system and its involvement in apoptosis. *Cell Death Differ.* *12*, 1155–1157.
- Mendillo, M.L., Santagata, S., Koeva, M., Bell, G.W., Hu, R., Tamimi, R.M., Fraenkel, E., Ince, T.A., Whitesell, L., and Lindquist, S. (2012). HSF1 drives a transcriptional program distinct from heat shock to support highly malignant human cancers. *Cell* *150*, 549–562.
- Metzger, M.B., Pruneda, J.N., Klevit, R.E., and Weissman, A.M. (2014). RING-type E3 ligases: Master manipulators of E2 ubiquitin-conjugating enzymes and ubiquitination. *Biochim. Biophys. Acta - Mol. Cell Res.* *1843*, 47–60.
- Meyer, H.-J., and Rape, M. (2014). Enhanced Protein Degradation by Branched Ubiquitin Chains. *Cell* *157*, 910–921.
- Meyer, H., Bug, M., and Bremer, S. (2012). Emerging functions of the VCP/p97 AAA-ATPase in the ubiquitin system. *Nat. Cell Biol.* *14*, 117–123.
- Meyer, H.H., Shorter, J.G., Seemann, J., Pappin, D., and Warren, G. (2000). A complex of mammalian ufd1 and npl4 links the AAA-ATPase, p97, to ubiquitin and nuclear transport pathways. *EMBO J.* *19*, 2181–2192.
- Meyer, H.H., Wang, Y., and Warren, G. (2002). Direct binding of ubiquitin conjugates by the mammalian p97 adaptor complexes, p47 and Ufd1-Npl4. *EMBO J.* *21*, 5645–5652.
- Le Moigne, R., Aftab, B.T., Djakovic, S., Dhimolea, E., Valle, E., Murnane, M., King, E.M., Soriano, F., Menon, M.-K., Wu, Z.Y., et al. (2017). The p97 Inhibitor CB-5083 Is a Unique Disrupter of Protein Homeostasis in Models of Multiple Myeloma. *Mol. Cancer Ther.* *16*, 2375–2386.
- Moreau, P., Richardson, P.G., Cavo, M., Orłowski, R.Z., San Miguel, J.F., Palumbo, A., and Housseau, J.-L. (2012). Proteasome inhibitors in multiple myeloma: 10 years later. *Blood* *120*, 947–959.
- Moreno, S.P., Bailey, R., Campion, N., Herron, S., and Gambus, A. (2014). Polyubiquitylation drives replisome disassembly at the termination of DNA replication. *Science* *346*, 477–481.
- Morgan, G.J., Walker, B.A., and Davies, F.E. (2012). The genetic architecture of multiple myeloma. *Nat. Rev. Cancer* *12*, 335–348.
- Morganti, M., Coronello, M., Caciagli, B., Biondi, C., Quattrone, A., Capaccioli, S., Mazzei,

- T., and Mini, E. (2000). Modulation of dihydrofolate reductase gene expression in methotrexate-resistant human leukemia CCRF-CEM/E cells by antisense oligonucleotides. *Anticancer. Drugs* 11, 285–294.
- Muller, P.A.J., and Vousden, K.H. (2014). Mutant p53 in Cancer: New Functions and Therapeutic Opportunities. *Cancer Cell* 25, 304–317.
- Nakahara, T., Takeuchi, M., Kinoyama, I., Minematsu, T., Shirasuna, K., Matsuhisa, A., Kita, A., Tominaga, F., Yamanaka, K., Kudoh, M., et al. YM155, a Novel Small-Molecule Survivin Suppressant, Induces Regression of Established Human Hormone-Refractory Prostate Tumor Xenografts. *Cancer Res.* 67, 8014–8021.
- Nathan, J.A., Kim, H.T., Ting, L., Gygi, S.P., and Goldberg, A.L. (2013). Why do cellular proteins linked to K63-polyubiquitin chains not associate with proteasomes? *EMBO J.* 32, 552–565.
- Nechushtan, H., Hamamreh, Y., Nidal, S., Gotfried, M., Baron, A., Shalev, Y.I., Nisman, B., Peretz, T., and Peylan-Ramu, N. (2015). A Phase IIb Trial Assessing the Addition of Disulfiram to Chemotherapy for the Treatment of Metastatic Non-Small Cell Lung Cancer. *Oncologist* 20, 366–367.
- Oerlemans, R., Franke, N.E., Assaraf, Y.G., Cloos, J., van Zantwijk, I., Berkers, C.R., Scheffer, G.L., Debipersad, K., Vojtekova, K., Lemos, C., et al. (2008). Molecular basis of bortezomib resistance: proteasome subunit 5 (PSMB5) gene mutation and overexpression of PSMB5 protein. *Blood* 112, 2489–2499.
- Orlowski, R.Z., Stinchcombe, T.E., Mitchell, B.S., Shea, T.C., Baldwin, A.S., Stahl, S., Adams, J., Esseltine, D.-L., Elliott, P.J., Pien, C.S., et al. (2002). Phase I trial of the proteasome inhibitor PS-341 in patients with refractory hematologic malignancies. *J. Clin. Oncol.* 20, 4420–4427.
- Palombella, V.J., Rando, O.J., Goldberg, A.L., and Maniatis, T. (1994). The ubiquitin-proteasome pathway is required for processing the NF- κ B1 precursor protein and the activation of NF- κ B. *Cell* 78, 773–785.
- Papadopoulos, C., Kirchner, P., Bug, M., Grum, D., Koerver, L., Schulze, N., Poehler, R., Dressler, A., Fengler, S., Arhzaouy, K., et al. (2017). VCP/p97 cooperates with YOD1, UBXD1 and PLAA to drive clearance of ruptured lysosomes by autophagy. *EMBO J.* 36, 135 LP – 150.

- Petrocca, F., Altschuler, G., Tan, S.M., Mendillo, M.L., Yan, H., Jerry, D.J., Kung, A.L., Hide, W., Ince, T.A., and Lieberman, J. (2013). A Genome-wide siRNA Screen Identifies Proteasome Addiction as a Vulnerability of Basal-like Triple-Negative Breast Cancer Cells. *Cancer Cell* 24, 182–196.
- Pickart, C.M. (2004). Back to the Future with Ubiquitin. *Cell* 116, 181–190.
- Politou, M., Karadimitris, A., Terpos, E., Kotsianidis, I., Apperley, J.F., and Rahemtulla, A. (2006). No evidence of mutations of the PSMB5 (beta-5 subunit of proteasome) in a case of myeloma with clinical resistance to Bortezomib. *Leuk. Res.* 30, 240–241.
- Program, N.T. (1979a). Bioassay of tetraethylthiuram disulfide for possible carcinogenicity. *Natl. Cancer Inst. Carcinog. Tech. Rep. Ser.* 166, 1–115.
- Program, N.T. (1979b). Bioassay of sodium diethyldithiocarbamate for possible carcinogenicity. *Natl. Cancer Inst. Carcinog. Tech. Rep. Ser.* 172, 1–115.
- Pye, V.E., Beuron, F., Keetch, C.A., McKeown, C., Robinson, C. V., Meyer, H.H., Zhang, X., and Freemont, P.S. (2007). Structural insights into the p97-Ufd1-Npl4 complex. *Proc. Natl. Acad. Sci. U. S. A.* 104, 467–472.
- Qian, S.-B., Ott, D.E., Schubert, U., Bennink, J.R., and Yewdell, J.W. (2002). Fusion Proteins with COOH-terminal Ubiquitin Are Stable and Maintain Dual Functionality in Vivo. *J. Biol. Chem.* 277, 38818–38826.
- Radhakrishnan, S.K., Lee, C.S., Young, P., Beskow, A., Chan, J.Y., and Deshaies, R.J. (2010). Transcription Factor Nrf1 Mediates the Proteasome Recovery Pathway after Proteasome Inhibition in Mammalian Cells. *Mol. Cell* 38, 17–28.
- Radhakrishnan, S.K., den Besten, W., and Deshaies, R.J. (2014). p97-dependent retrotranslocation and proteolytic processing govern formation of active Nrf1 upon proteasome inhibition. *Elife* 3, e01856.
- Raha, D., Wilson, T.R., Peng, J., Peterson, D., Yue, P., Evangelista, M., Wilson, C., Merchant, M., and Settleman, J. (2014). The Cancer Stem Cell Marker Aldehyde Dehydrogenase Is Required to Maintain a Drug-Tolerant Tumor Cell Subpopulation. *Cancer Res.* 74, 3579–3590.
- Ramadan, K., Bruderer, R., Spiga, F.M., Popp, O., Baur, T., Gotta, M., and Meyer, H.H. (2007). Cdc48/p97 promotes reformation of the nucleus by extracting the kinase Aurora B from chromatin. *Nature* 450, 1258–1262.

- Raman, M., Havens, C.G., Walter, J.C., and Harper, J.W. (2011). A Genome-wide Screen Identifies p97 as an Essential Regulator of DNA Damage-Dependent CDT1 Destruction. *Mol. Cell* *44*, 72–84.
- Richardson, P.G., Barlogie, B., Berenson, J., Singhal, S., Jagannath, S., Irwin, D., Rajkumar, S.V., Srkalovic, G., Alsina, M., Alexanian, R., et al. (2003). A phase 2 study of bortezomib in relapsed, refractory myeloma. *N. Engl. J. Med.* *348*, 2609–2617.
- Richter, K., Haslbeck, M., and Buchner, J. (2010). The Heat Shock Response: Life on the Verge of Death. *Mol. Cell* *40*, 253–266.
- Riemer, A., Dobrynin, G., Dressler, A., Bremer, S., Soni, A., Iliakis, G., and Meyer, H. (2014). The p97-Ufd1-Npl4 ATPase complex ensures robustness of the G2/M checkpoint by facilitating CDC25A degradation. *Cell Cycle* *13*, 919–927.
- Ritz, D., Vuk, M., Kirchner, P., Bug, M., Schütz, S., Hayer, A., Bremer, S., Lusk, C., Baloh, R.H., Lee, H., et al. (2011). Endolysosomal sorting of ubiquitylated caveolin-1 is regulated by VCP and UBXD1 and impaired by VCP disease mutations. *Nat. Cell Biol.* *13*, 1116–1123.
- Rousseau, A., and Bertolotti, A. (2018). Regulation of proteasome assembly and activity in health and disease. *Nat. Rev. Mol. Cell Biol.* *19*, 697–712.
- Saeki, Y. (2017). Ubiquitin recognition by the proteasome. *J. Biochem.* *161*, 113–124.
- Samali, A., FitzGerald, U., Deegan, S., and Gupta, S. (2010). Methods for Monitoring Endoplasmic Reticulum Stress and the Unfolded Protein Response. *Int. J. Cell Biol.* *2010*, 1–11.
- Sarantopoulos J, Infante J, Cohen R, Haeseong P, Lockhart AC, Gourdin T, et al. (2017). No Title. In First-in-Human (FIH) Phase 1, Open-Label, Multicenter, Dose-Escalation Study to Assess the Safety and Tolerability of TAK-243, a First-in-Class Investigational Inhibitor of Ubiquitin (Ub)-Activating Enzyme (UAE), in Adult Patients (Pts) with Advanced Solid, (Cavtat-Dubrovnik, Croatia: EMBO Conference Ubiquitin and SUMO: From molecular mechanisms to system-wide responses).
- Schwertman, P., Bekker-Jensen, S., and Mailand, N. (2016). Regulation of DNA double-strand break repair by ubiquitin and ubiquitin-like modifiers. *Nat. Rev. Mol. Cell Biol.* *17*, 379–394.
- Seguin, S.J., Morelli, F.F., Vinet, J., Amore, D., De Biasi, S., Poletti, A., Rubinsztein, D.C., and Carra, S. (2014). Inhibition of autophagy, lysosome and VCP function impairs stress

granule assembly. *Cell Death Differ.* *21*, 1838–1851.

Sha, Z., and Goldberg, A.L. (2014). Proteasome-mediated processing of Nrf1 is essential for coordinate induction of all proteasome subunits and p97. *Curr. Biol.* *24*, 1573–1583.

Shen, M.L., Johnson, K.L., Mays, D.C., Lipsky, J.J., and Naylor, S. (2001). Determination of in vivo adducts of disulfiram with mitochondrial aldehyde dehydrogenase. *Biochem. Pharmacol.* *61*, 537–545.

Shi, Y., Chen, X., Elsasser, S., Stocks, B.B., Tian, G., Lee, B.-H., Shi, Y., Zhang, N., de Poot, S.A.H., Tuebing, F., et al. (2016). Rpn1 provides adjacent receptor sites for substrate binding and deubiquitination by the proteasome. *Science*. *351*, aad9421–aad9421.

Shian, S.-G. (2003). Inhibition of Invasion and Angiogenesis by Zinc-Chelating Agent Disulfiram. *Mol. Pharmacol.* *64*, 1076–1084.

Skaar, J.R., Pagan, J.K., and Pagano, M. (2014). SCF ubiquitin ligase-targeted therapies. *Nat. Rev. Drug Discov.* *13*, 889–903.

Skrott, Z. (2014). Vliv komplexu disulfiramu s mědí na proteazom v buněčných liniích rakoviny prsu. Univerzita Palackého v Olomouci, Přírodovědecká fakulta, Olomouc.

Skrott, Z., and Cvek, B. (2012). Diethyldithiocarbamate complex with copper: the mechanism of action in cancer cells. *Mini-Reviews Med. Chem.* *12*, 1184–1192.

Skrott, Z., and Cvek, B. (2014). Linking the activity of bortezomib in multiple myeloma and autoimmune diseases. *Crit. Rev. Oncol. Hematol.* *92*, 61–70.

Skrott, Z., Mistrik, M., Andersen, K.K., Friis, S., Majera, D., Gursky, J., Ozdian, T., Bartkova, J., Turi, Z., Moudry, P., et al. (2017). Alcohol-abuse drug disulfiram targets cancer via p97 segregase adaptor NPL4. *Nature* *552*, 194–199.

Smith, D.C., Kalebic, T., Infante, J.R., Siu, L.L., Sullivan, D., Vlahovic, G., Kauh, J.S., Gao, F., Berger, A.J., Tirrell, S., et al. (2015). Phase 1 study of ixazomib, an investigational proteasome inhibitor, in advanced non-hematologic malignancies. *Invest. New Drugs* *33*, 652–663.

Solimini, N.L., Luo, J., and Elledge, S.J. (2007). Non-Oncogene Addiction and the Stress Phenotype of Cancer Cells. *Cell* *130*, 986–988.

Song, C., Wang, Q., Song, C., Lockett, S.J., Colburn, N.H., Li, C.-C.H., Wang, J.M., and Rogers, T.J. (2015). Nucleocytoplasmic shuttling of valosin-containing protein (VCP/p97)

- regulated by its N domain and C-terminal region. *Biochim. Biophys. Acta* 1853, 222–232.
- Song, Y., Ray, A., Li, S., Das, D.S., Tai, Y.T., Carrasco, R.D., Chauhan, D., and Anderson, K.C. (2016). Targeting proteasome ubiquitin receptor Rpn13 in multiple myeloma. *Leukemia* 30, 1877–1886.
- Sontag, E.M., Samant, R.S., and Frydman, J. (2017). Mechanisms and Functions of Spatial Protein Quality Control. *Annu. Rev. Biochem.* 86, 97–122.
- Soriano, G.P., Besse, L., Li, N., Kraus, M., Besse, A., Meeuwenoord, N., Bader, J., Everts, B., den Dulk, H., Overkleeft, H.S., et al. (2016). Proteasome inhibitor-adapted myeloma cells are largely independent from proteasome activity and show complex proteomic changes, in particular in redox and energy metabolism. *Leukemia* 30, 2198–2207.
- Stach, L., and Freemont, P.S. (2017). The AAA+ ATPase p97, a cellular multitool. *Biochem. J.* 474, 2953–2976.
- Steffen, J., Seeger, M., Koch, A., and Krüger, E. (2010). Proteasomal degradation is transcriptionally controlled by TCF11 via an ERAD-dependent feedback loop. *Mol. Cell* 40, 147–158.
- Stein, A., Ruggiano, A., Carvalho, P., and Rapoport, T.A. (2014). Key Steps in ERAD of Luminal ER Proteins Reconstituted with Purified Components. *Cell* 158, 1375–1388.
- Stewart, M.D., Ritterhoff, T., Klevit, R.E., and Brzovic, P.S. (2016). E2 enzymes: more than just middle men. *Cell Res.* 26, 423–440.
- Sun, X.-M., Butterworth, M., MacFarlane, M., Dubiel, W., Ciechanover, A., and Cohen, G.M. (2004). Caspase Activation Inhibits Proteasome Function during Apoptosis. *Mol. Cell* 14, 81–93.
- Swatek, K.N., and Komander, D. (2016). Ubiquitin modifications. *Cell Res.* 26, 399–422.
- Tacconi, E.M., Lai, X., Folio, C., Porru, M., Zonderland, G., Badie, S., Michl, J., Sechi, I., Rogier, M., Matía García, V., et al. (2017). BRCA1 and BRCA2 tumor suppressors protect against endogenous acetaldehyde toxicity. *EMBO Mol. Med.* 9, 1398–1414.
- Tanaka, A., Cleland, M.M., Xu, S., Narendra, D.P., Suen, D.-F., Karbowski, M., and Youle, R.J. (2010). Proteasome and p97 mediate mitophagy and degradation of mitofusins induced by Parkin. *J. Cell Biol.* 191, 1367–1380.
- Tardito, S., Bassanetti, I., Bignardi, C., Elviri, L., Tegoni, M., Mucchino, C., Bussolati, O.,

- Franchi-Gazzola, R., and Marchiò, L. (2011). Copper Binding Agents Acting as Copper Ionophores Lead to Caspase Inhibition and Paraptotic Cell Death in Human Cancer Cells. *J. Am. Chem. Soc.* *133*, 6235–6242.
- Tawari, P.E., Wang, Z., Najlah, M., Tsang, C.W., Kannappan, V., Liu, P., McConville, C., He, B., Armesilla, A.L., and Wang, W. (2015). The cytotoxic mechanisms of disulfiram and copper(ii) in cancer cells. *Toxicol. Res. (Camb)*. *4*, 1439–1442.
- Tomko, R.J., and Hochstrasser, M. (2013). Molecular Architecture and Assembly of the Eukaryotic Proteasome. *Annu. Rev. Biochem.* *82*, 415–445.
- Tran, A.T., Rison, R.A., and Beydoun, S.R. (2016). Disulfiram neuropathy: two case reports. *J. Med. Case Rep.* *10*, 72.
- Trepel, J., Mollapour, M., Giaccone, G., and Neckers, L. (2010). Targeting the dynamic HSP90 complex in cancer. *Nat. Rev. Cancer* *10*, 537–549.
- Tsujimoto, Y., Tomita, Y., Hoshida, Y., Kono, T., Oka, T., Yamamoto, S., Nonomura, N., Okuyama, A., and Aozasa, K. (2004). Elevated expression of valosin-containing protein (p97) is associated with poor prognosis of prostate cancer. *Clin. Cancer Res.* *10*, 3007–3012.
- Uchiyama, K., Jokitalo, E., Kano, F., Murata, M., Zhang, X., Canas, B., Newman, R., Rabouille, C., Pappin, D., Freemont, P., et al. (2002). VCI135, a novel essential factor for p97/p47-mediated membrane fusion, is required for Golgi and ER assembly in vivo. *J. Cell Biol.* *159*, 855 LP – 866.
- Vallari, R.C., and Pietruszko, R. (1982). Human aldehyde dehydrogenase: mechanism of inhibition of disulfiram. *Science* *216*, 637–639.
- Valle, C.W., Min, T., Bodas, M., Mazur, S., Begum, S., Tang, D., and Vij, N. (2011). Critical Role of VCP/p97 in the Pathogenesis and Progression of Non-Small Cell Lung Carcinoma. *PLoS One* *6*, e29073.
- Verma, R., Aravind, L., Oania, R., McDonald, W.H., Yates, J.R., Koonin, E. V, and Deshaies, R.J. (2002). Role of Rpn11 metalloprotease in deubiquitination and degradation by the 26S proteasome. *Science* *298*, 611–615.
- Verma, R., Oania, R., Fang, R., Smith, G.T., and Deshaies, R.J. (2011). Cdc48/p97 mediates UV-dependent turnover of RNA Pol II. *Mol. Cell* *41*, 82–92.
- Vogler, T.O., Wheeler, J.R., Nguyen, E.D., Hughes, M.P., Britson, K.A., Lester, E., Rao, B.,

- Betta, N.D., Whitney, O.N., Ewachiw, T.E., et al. (2018). TDP-43 and RNA form amyloid-like myo-granules in regenerating muscle. *Nature* *563*, 508–513.
- Voráčková, I., Suchanová, Š., Ulbrich, P., Diehl, W.E., and Ruml, T. (2011). Purification of proteins containing zinc finger domains using immobilized metal ion affinity chromatography. *Protein Expr. Purif.* *79*, 88–95.
- Wade, M., Li, Y.-C., and Wahl, G.M. (2013). MDM2, MDMX and p53 in oncogenesis and cancer therapy. *Nat. Rev. Cancer* *13*, 83–96.
- Walter, P., and Ron, D. (2011). The unfolded protein response: from stress pathway to homeostatic regulation. *Science* *334*, 1081–1086.
- Wang, M., and Kaufman, R.J. (2014). The impact of the endoplasmic reticulum protein-folding environment on cancer development. *Nat. Rev. Cancer* *14*, 581–597.
- Wang, Z.-Y., and Chen, Z. (2008). Acute promyelocytic leukemia: from highly fatal to highly curable. *Blood* *111*, 2505–2515.
- Wang, F., Jiao, P., Qi, M., Frezza, M., Dou, Q.P., and Yan, B. (2010). Turning Tumor-Promoting Copper into an Anti-Cancer Weapon via High-Throughput Chemistry. *Curr. Med. Chem.* *17*, 2685–2698.
- Wang, Q., Li, L., and Ye, Y. (2006). Regulation of retrotranslocation by p97-associated deubiquitinating enzyme ataxin-3. *J. Cell Biol.* *174*, 963–971.
- Wang, Q., Li, L., and Ye, Y. (2008). Inhibition of p97-dependent protein degradation by Eeyarestatin I. *J. Biol. Chem.* *283*, 7445–7454.
- Wang, Q., Mora-Jensen, H., Weniger, M.A., Perez-Galan, P., Wolford, C., Hai, T., Ron, D., Chen, W., Trenkle, W., Wiestner, A., et al. (2009). ERAD inhibitors integrate ER stress with an epigenetic mechanism to activate BH3-only protein NOXA in cancer cells. *Proc. Natl. Acad. Sci.* *106*, 2200–2205.
- Wang, W., McLeod, H.L., and Cassidy, J. (2003). Disulfiram-mediated inhibition of NF- κ B activity enhances cytotoxicity of 5-fluorouracil in human colorectal cancer cell lines. *Int. J. Cancer* *104*, 504–511.
- Wattenberg, L.W. (1978). Inhibition of chemical carcinogenesis. *J. Natl. Cancer Inst.* *60*, 11–18.
- Weinstein, I.B. (2002). Cancer. Addiction to oncogenes--the Achilles heel of cancer. *Science*

297, 63–64.

Wiech, M., Olszewski, M.B., Tracz-Gaszewska, Z., Wawrzynow, B., Zylicz, M., and Zylicz, A. (2012). Molecular mechanism of mutant p53 stabilization: the role of HSP70 and MDM2. *PLoS One* 7, e51426.

Williams, E.E. (1937). Effects of alcohol on workers with carbon disulfide. *JAMA J. Am. Med. Assoc.* 109, 1472–1473.

Wolff, S., Weissman, J.S., and Dillin, A. (2014). Differential Scales of Protein Quality Control. *Cell* 157, 52–64.

Wu, J., Liu, T., Rios, Z., Mei, Q., Lin, X., and Cao, S. (2017). Heat Shock Proteins and Cancer. *Trends Pharmacol. Sci.* 38, 226–256.

Xiao, Y., Chen, D.I., Zhang, X., Cui, Q., Fan, Y., Bi, C., and Dou, Q.P. (2010). Molecular study on copper-mediated tumor proteasome inhibition and cell death. *Int. J. Oncol.* 37, 81–87.

Xu, B., Wang, S., Li, R., Chen, K., He, L., Deng, M., Kannappan, V., Zha, J., Dong, H., and Wang, W. (2017). Disulfiram/copper selectively eradicates AML leukemia stem cells in vitro and in vivo by simultaneous induction of ROS-JNK and inhibition of NF- κ B and Nrf2. *Cell Death Dis.* 8, e2797.

Xue, L., Blythe, E.E., Freiburger, E.C., Mamrosh, J.L., Hebert, A.S., Reitsma, J.M., Hess, S., Coon, J.J., and Deshaies, R.J. (2016). Valosin-containing protein (VCP)-Adaptor Interactions are Exceptionally Dynamic and Subject to Differential Modulation by a VCP Inhibitor. *Mol. Cell. Proteomics* 15, 2970–2986.

Yamamoto, S., Tomita, Y., Nakamori, S., Hoshida, Y., Nagano, H., Dono, K., Umeshita, K., Sakon, M., Monden, M., and Aozasa, K. (2003). Elevated Expression of Valosin-Containing Protein (p97) in Hepatocellular Carcinoma Is Correlated With Increased Incidence of Tumor Recurrence. *J. Clin. Oncol.* 21, 447–452.

Yamamoto, S., Tomita, Y., Hoshida, Y., Nagano, H., Dono, K., Umeshita, K., Sakon, M., Ishikawa, O., Ohigashi, H., Nakamori, S., et al. (2004a). Increased Expression of Valosin-Containing Protein (p97) is Associated With Lymph Node Metastasis and Prognosis of Pancreatic Ductal Adenocarcinoma. *Ann. Surg. Oncol.* 11, 165–172.

Yamamoto, S., Tomita, Y., Hoshida, Y., Iizuka, N., Kidogami, S., Miyata, H., Takiguchi, S., Fujiwara, Y., Yasuda, T., Yano, M., et al. (2004b). Expression level of valosin-containing protein (p97) is associated with prognosis of esophageal carcinoma. *Clin. Cancer Res.* 10,

5558–5565.

Yamamoto, S., Tomita, Y., Hoshida, Y., Sakon, M., Kameyama, M., Imaoka, S., Sekimoto, M., Nakamori, S., Monden, M., and Aozasa, K. (2004c). Expression of valosin-containing protein in colorectal carcinomas as a predictor for disease recurrence and prognosis. *Clin. Cancer Res.* *10*, 651–657.

Yamamoto, S., Tomita, Y., Uruno, T., Hoshida, Y., Qiu, Y., Iizuka, N., Nakamichi, I., Miyauchi, A., and Aozasa, K. (2005). Increased expression of valosin-containing protein (p97) is correlated with disease recurrence in follicular thyroid cancer. *Ann. Surg. Oncol.* *12*, 925–934.

Yao, T., and Cohen, R.E. (2002). A cryptic protease couples deubiquitination and degradation by the proteasome. *Nature* *419*, 403–407.

Yau, R., and Rape, M. (2016). The increasing complexity of the ubiquitin code. *Nat. Cell Biol.* *18*, 579–586.

Yu, H., and Matouschek, A. (2017). Recognition of Client Proteins by the Proteasome. *Annu. Rev. Biophys.* *46*, 149–173.

Yue, X., Zhao, Y., Xu, Y., Zheng, M., Feng, Z., and Hu, W. (2017). Mutant p53 in Cancer: Accumulation, Gain-of-Function, and Therapy. *J. Mol. Biol.* *429*, 1595–1606.

Zhang, H., Chen, D., Ringler, J., Chen, W., Cui, Q.C., Ethier, S.P., Dou, Q.P., and Wu, G. (2010a). Disulfiram treatment facilitates phosphoinositide 3-kinase inhibition in human breast cancer cells in vitro and in vivo. *Cancer Res.* *70*, 3996–4004.

Zhang, X.-W., Yan, X.-J., Zhou, Z.-R., Yang, F.-F., Wu, Z.-Y., Sun, H.-B., Liang, W.-X., Song, A.-X., Lallemand-Breitenbach, V., Jeanne, M., et al. (2010b). Arsenic trioxide controls the fate of the PML-RAR α oncoprotein by directly binding PML. *Science* *328*, 240–243.

Zhang, Y., Nicholatos, J., Dreier, J.R., Ricoult, S.J.H., Widenmaier, S.B., Hotamisligil, G.S., Kwiatkowski, D.J., and Manning, B.D. (2014). Coordinated regulation of protein synthesis and degradation by mTORC1. *Nature* *513*, 440–443.

Zheng, N., and Shabek, N. (2017). Ubiquitin Ligases: Structure, Function, and Regulation. *Annu. Rev. Biochem.* *86*, 129–157.

Ziegler-Heitbrock, H.W., Sternsdorf, T., Liese, J., Belohradsky, B., Weber, C., Wedel, A., Schreck, R., Bäuerle, P., and Ströbel, M. (1993). Pyrrolidine dithiocarbamate inhibits NF- κ B mobilization and TNF production in human monocytes. *J. Immunol.* *151*, 6986–6993.

9 BIBLIOGRAPHY

ORIGINAL ARTICLES AND REVIEWS

Skrott Z, Mistrik M, Andersen KK, Friis S, Majera D, Gursky J, Ozdian T, Bartkova J, Turi Z, Moudry P, Kraus M, Michalova M, Vaclavkova J, Dzubak P, Vrobel I, Pouckova P, Sedlacek J, Miklovcova A, Kutt A, Li J, Mattova J, Driessen C, Dou QP, Olsen J, Hajduch M, Cvek B, Deshaies RJ, Bartek J. Alcohol-abuse drug disulfiram targets cancer via p97 segregase adaptor NPL4. *Nature*. 2017 Dec 14;552(7684):194-199. IF₍₂₀₁₇₎: 41.577

Skrott Z, Majera D, Gursky J, Buchtova T, Hajduch M, Mistrik M, Bartek J. Disulfiram's anti-cancer activity reflects targeting NPL4, not inhibition of aldehyde dehydrogenase. *Oncogene*. 2019 Aug 7. *In press*. IF₍₂₀₁₈₎: 6.634

Skrott Z, Cvek B. Linking the activity of bortezomib in multiple myeloma and autoimmune diseases. *Crit Rev Oncol Hematol*. 2014 Nov;92(2):61-70. IF₍₂₀₁₄₎: 4.027

Majera D, **Skrott Z**, Bouchal J, Bartkova J, Simkova D, Gachechiladze M, Steigerova J, Kurfurstova D, Gursky J, Korinkova G, Cwierka K, Hodny Z, Mistrik M, Bartek J. Targeting genotoxic and proteotoxic stress-response pathways in human prostate cancer by clinically available PARP inhibitors, vorinostat and disulfiram. *Prostate*. 2019 Mar;79(4):352-362. IF₍₂₀₁₇₎: 3.347

Chroma K, Mistrik M, Moudry P, Gursky J, Liptay M, Strauss R, **Skrott Z**, Vrtel R, Bartkova J, Kramara J, Bartek J. Tumors overexpressing RNF168 show altered DNA repair and responses to genotoxic treatments, genomic instability and resistance to proteotoxic stress. *Oncogene*. 2017 Apr 27;36(17):2405-2422. IF₍₂₀₁₇₎: 6.854

CONFERENCE TALKS

Zdenek Skrott, Martin Mistrik, Boris Cvek, Pavla Pouckova, Jiri Bartek. The activity of disulfiram towards breast cancer. X. Diagnostic, Predictive and Experimental Oncology Days. 2. - 3. 12. 2014 Olomouc.

Zdenek Skrott. Alcohol abuse drug disulfiram targets cancer via p97 segregate adaptor NPL4. Sanofi prize for pharmacy. 25.4. 2018 Prague.

Zdenek Skrott, Martin Mistrik, Dusana Majera, Tomas Ozdian, Jiri Bartek. Alcohol abuse drug disulfiram targets cancer via p97 segregate adaptor NPL4. 15th International Medical Postgraduate Conference. 22 – 23. 11. 2018. Hradec Králové.

Zdenek Skrott, Martin Mistrik, Klaus Kaae Andersen, Soren Friis, Dusana Majera, Tomas Ozdian, Jirina Bartkova, Peter Dzubak, Jindrich Sedlacek, Jing Li, Marian Hajduch, Boris Cvek, Raymond J. Deshaies, Jiri Bartek. Alcohol abuse drug disulfiram targets cancer via p97 segregate adaptor NPL4. XIV. Diagnostic, Predictive and Experimental Oncology Days. 19.-21. 11. 2018 Olomouc.

Zdenek Skrott, Martin Mistrik, Klaus Kaae Andersen, Soren Friis, Dusana Majera, Tomas Ozdian, Jirina Bartkova, Peter Dzubak, Jindrich Sedlacek, Jing Li, Marian Hajduch, Boris Cvek, Raymond J. Deshaies, Jiri Bartek. Alcohol abuse drug disulfiram targets cancer via p97 segregate adaptor NPL4. 10. PragueOnco. 23. -25. 1. 2019 Prague.

10 APPENDIX – FULL TEXT PUBLICATIONS RELATED TO THE THESIS

APPENDIX A

Skrott Z, Mistrik M, Andersen KK, Friis S, Majera D, Gursky J, Ozdian T, Bartkova J, Turi Z, Moudry P, Kraus M, Michalova M, Vaclavkova J, Dzubak P, Vrobel I, Pouckova P, Sedlacek J, Miklovcova A, Kutt A, Li J, Mattova J, Driessen C, Dou QP, Olsen J, Hajduch M, Cvek B, Deshaies RJ, Bartek J. Alcohol-abuse drug disulfiram targets cancer via p97 segregase adaptor NPL4. *Nature*. 2017 Dec 14;552(7684):194-199. IF₍₂₀₁₇₎: 41.577

Alcohol-abuse drug disulfiram targets cancer via p97 segregase adaptor NPL4

Zdenek Skrott^{1*}, Martin Mistrik^{1*}, Klaus Kaae Andersen², Søren Friis², Dusana Majera¹, Jan Gursky¹, Tomas Ozdian¹, Jirina Bartkova^{2,3}, Zsofia Turi¹, Pavel Moudry¹, Marianne Kraus⁴, Martina Michalova¹, Jana Vaclavkova¹, Petr Dzubak¹, Ivo Vrobel¹, Pavla Pouckova⁵, Jindrich Sedlacek⁶, Andrea Miklovcova⁷, Anne Kutt², Jing Li⁸, Jana Mattova⁵, Christoph Driessen⁴, Q. Ping Dou^{9,10}, Jørgen Olsen², Marian Hajduch¹, Boris Cvek^{6†}, Raymond J. Deshaies^{8,11†} & Jiri Bartek^{2,3}

Cancer incidence is rising and this global challenge is further exacerbated by tumour resistance to available medicines. A promising approach to meet the need for improved cancer treatment is drug repurposing. Here we highlight the potential for repurposing disulfiram (also known by the trade name Antabuse), an old alcohol-aversion drug that has been shown to be effective against diverse cancer types in preclinical studies. Our nationwide epidemiological study reveals that patients who continuously used disulfiram have a lower risk of death from cancer compared to those who stopped using the drug at their diagnosis. Moreover, we identify the ditiocarb-copper complex as the metabolite of disulfiram that is responsible for its anti-cancer effects, and provide methods to detect preferential accumulation of the complex in tumours and candidate biomarkers to analyse its effect on cells and tissues. Finally, our functional and biophysical analyses reveal the molecular target of disulfiram's tumour-suppressing effects as NPL4, an adaptor of p97 (also known as VCP) segregase, which is essential for the turnover of proteins involved in multiple regulatory and stress-response pathways in cells.

Despite advances in the understanding of cancer biology, malignant diseases have a high global toll. Furthermore, the increasing average human life expectancy is predicted to have demographic consequences, including an increase in the incidence of cancer. The high cancer-associated morbidity and mortality highlight the need for innovative treatments. Given the high costs, failure rate and long testing periods of developing new medicines, using drugs that are approved for the treatment of diverse diseases as candidate anti-cancer therapeutics represents a faster and cheaper alternative¹, benefitting from available clinically suitable formulations and evidence of tolerability in patients. Among promising cancer-killing drugs² is disulfiram (tetraethylthiuram disulfide, DSF), a drug that has been used for over six decades as a treatment for alcohol dependence³, with well-established pharmacokinetics, safety and tolerance at the US Food and Drug Administration (FDA)-recommended dosage⁴. In the body, DSF is metabolized to ditiocarb (diethyldithiocarbamate, DTC) and other metabolites, some of which inhibit liver aldehyde dehydrogenase⁵. Because DSF showed anti-cancer activity in preclinical models^{3,6–9} and because adjuvant DTC was used to treat high-risk breast cancer in a clinical trial¹⁰, DSF emerges as a candidate for drug repurposing in oncology. Additional advantages of DSF include a broad spectrum of malignancies sensitive to DSF, and its ability to also target the stem-like, tumour-initiating cells¹¹. Although the mechanism of DSF's anti-cancer activity remains unclear and it has been suggested that the drug inhibits proteasome activity^{6,12}, it has been shown that DSF chelates bivalent metals and forms complexes with copper (Cu), which enhances its anti-tumour activity^{6,13}. In addition to the lack of a well-defined mechanism of action in cancer cells, the main obstacles for DSF repurposing have

been: (i) uncertainty about the active metabolite(s) of DSF *in vivo*; (ii) the lack of assays to measure these active derivative(s) in tumours; (iii) missing biomarker(s) to monitor the impact of DSF in tumours and tissues; (iv) the lack of insights into the preferential toxicity towards cancer cells compared to normal tissues; and (v) the absence of a specific molecular target that could explain the potent anti-tumour activity of DSF. Here, we combine experimental approaches and epidemiology to address the important characteristics of DSF in relation to cancer, pursuing the goal of repurposing DSF for cancer therapy. We identify the active metabolite of DSF, and provide biological validation and mechanistic insights, including the discovery of a biologically attractive protein that has previously not been considered as the target for the anti-cancer activity of DSF.

Epidemiological analyses of DSF and cancer

The relative lack of cancer-related clinical trials with DSF^{10,14} prompted us to explore whether DSF use might reduce cancer mortality at a population level. Using the Danish nationwide demographic and health registries, we estimated hazard ratios of cancer-specific mortality associated with DSF use among patients with cancer for the first time during 2000–2013 (see Methods, Table 1 and Extended Data Fig. 1a). DSF users were categorized as (i) previous users, who were patients that were prescribed DSF for alcohol dependency only before their cancer diagnosis or (ii) continuing users, who were patients that were prescribed DSF both before and after diagnosis. As expected from the increase in cancer risk and the deleterious effect on prognosis¹⁵ caused by alcohol abuse, cancer-specific mortality was higher among previous DSF users than among patients with cancer who had never

¹Institute of Molecular and Translational Medicine, Faculty of Medicine and Dentistry, Palacky University, Olomouc, Czech Republic. ²Danish Cancer Society Research Center, DK-2100 Copenhagen, Denmark. ³Science for Life Laboratory, Division of Genome Biology, Department of Medical Biochemistry and Biophysics, Karolinska Institute, Stockholm, Sweden. ⁴Kantonsspital St Gallen, Department Oncology/Hematology, St Gallen, Switzerland. ⁵Institute of Biophysics and Informatics, First Faculty of Medicine, Charles University, 120 00 Prague 2, Czech Republic. ⁶Department of Cell Biology & Genetics, Palacky University, Olomouc, Czech Republic. ⁷Psychiatric Hospital, 785 01 Šternberk, Czech Republic. ⁸Division of Biology and Biological Engineering, Caltech, Pasadena, California 91125, USA. ⁹Barbara Ann Karmanos Cancer Institute and Department of Oncology, School of Medicine, Wayne State University, Detroit, Michigan, USA. ¹⁰School of Basic Medical Sciences, Affiliated Tumor Hospital of Guangzhou Medical University, Guangzhou 511436, China. ¹¹Howard Hughes Medical Institute, Caltech, Pasadena, California 91125, USA.

†Present addresses: Olomouc University Social Health Institute, Palacky University, Olomouc, Czech Republic (B.C.); Amgen, Thousand Oaks, California 91320, USA (R.J.D.).

*These authors contributed equally to this work.

Table 1 | Cancer-specific mortality associated with DSF use among Danish patients with cancer

Cancer type	Overall				Localized stage				Non-localized stage				Unknown stage			
	Number*	HR	95% CI	P value	Number*	HR	95% CI	P value	Number*	HR	95% CI	P value	Number*	HR	95% CI	P value
Any cancer†																
Previous users	3,038	1.00			1,429	1.00			1,054	1.00			555	1.00		
Continuing users	1,177	0.66	0.58–0.76	0.000	602	0.69	0.64–0.74	0.000	355	0.71	0.59–0.87	0.001	220	0.65	0.57–0.75	0.000
No prescriptions	236,950	0.68	0.64–0.73	0.000	113,354	0.59	0.57–0.61	0.000	73,933	0.80	0.73–0.88	0.000	49,663	0.66	0.62–0.71	0.000

Hazard ratios (HR) and 95% confidence intervals (CI) comparing continuing and previous users of DSF, relative to the time of their cancer diagnosis. For DSF exposure categories, statistics and clinical stages, see Methods.

*Number of patients included.

†Except cancers of the liver and kidney.

used DSF. Notably, we also found reduced cancer-specific mortality for cancer overall (Table 1), as well as for cancers of the colon, prostate and breast among continuing users compared to previous DSF users (Extended Data Fig. 1a). Stratification by clinical stage (Table 1) revealed reduced cancer-specific mortality with continuing use of DSF even among patients with metastatic disease. Although it is not possible to draw conclusions about causality, these findings supported the hypothesis that DSF may exert anti-cancer effects among patients suffering from common cancers, prompting us to perform pre-clinical analyses.

Anti-tumour activity of the DTC–copper complex

Because DSF anti-cancer activity has been suggested to be copper-dependent^{6,13}, we compared groups of mice injected with human MDA-MB-231 cancer cells, fed with a (i) normal diet; (ii) normal diet plus copper gluconate (CuGlu); (iii) normal diet plus DSF; or (iv) normal diet plus DSF and CuGlu (DSF/CuGlu); and tumour volume was measured over time (Fig. 1a and Extended Data Fig. 1b, c). Compared to matched controls, tumour volume in DSF- and DSF/CuGlu-treated groups at 32 days (at DSF doses equivalent to those used by alcoholics) were suppressed by 57% and 77%, respectively ($P = 0.0038$ in favour of the DSF/CuGlu treatment versus DSF alone). These results validate previous *in vitro*^{6,11,13} and *in vivo*^{6–9,13,16} studies, which indicated that DSF is an efficient anti-cancer agent and that copper potentiates its activity. As the reactive metabolite DTC forms complexes with metals, particularly copper¹⁷, we argued that a DTC–copper complex (bis (diethyldithiocarbamate)–copper (CuET)) forms *in vivo* (Extended Data Fig. 1d), providing the anti-cancer metabolite. To test this hypothesis, we developed a high-resolution

approach based on high-performance liquid chromatography–mass spectrometry to measure CuET in tissues, and readily detected CuET after a single oral dose of DSF (Extended Data Fig. 1e, f). Extracts from plasma, liver, brain and MDA-MB-231-xenografted tumours contained CuET in samples from mice treated for five days with DSF or DSF/CuGlu. The CuET levels in plasma and liver were slightly higher after DSF/CuGlu treatment compared to DSF alone. Notably, the CuET levels in the tumour specimens were almost an order of magnitude higher compared to corresponding levels in liver and brain tissues from the same animals (Fig. 1b), suggesting preferential accumulation of CuET in tumours. Importantly, we also confirmed formation of CuET in humans undergoing DSF treatment for alcoholism (Fig. 1c).

Next, we synthesized CuET and performed comparative cell culture and animal studies. Short-term (24-h) assays and long-term (colony-forming assay, CFA) assays consistently showed higher cytotoxicity of CuET than of the primary DSF metabolite DTC in various cancer cell lines (Fig. 1d and Extended Data Fig. 1g). The half-maximal lethal dose (LD_{50}) values of CuET in CFA experiments were ≤ 100 nM in three out of three tested breast cancer cell lines and similar potency was observed among cell lines derived from human lung, colon and prostate tumours (Extended Data Fig. 2a). These data were corroborated by tetrazolium dye ((2,3-bis-(2-methoxy-4-nitro-5-sulphophenyl)-2h-tetrazolium-5-carboxanilide) (XTT))-based 48-h cytotoxicity tests on a wider panel of cell types (Extended Data Fig. 2b). Unexpectedly, only the most sensitive cell lines (for example, AMO-1, Capan1) showed markers of apoptosis¹⁸, which included annexin V and activated caspases, whereas in most cell lines, for example, MDA-MB-231 and U2OS cells, CuET induced apoptosis-independent cell death (Extended Data Fig. 2c–f).

Direct therapeutic effects of CuET *in vivo* were then investigated using the MDA-MB-231 breast cancer (Fig. 1e) and AMO-1 myeloma (Fig. 1f) xenograft models treated intraperitoneally with a CuET–albumin formulation, with which the anti-tumour activity and good tolerability of this DSF metabolite was confirmed (Extended Data Fig. 1h, i).

CuET inhibits p97-dependent protein degradation

Next, we investigated the interaction between CuET and cellular protein degradation, one of the suggested explanations for anti-tumour effects of DSF^{6,12}. We confirmed that CuET induces phenotypic features shared with proteasome inhibitors, such as MG132 or bortezomib (BTZ), including accumulation of poly-ubiquitylated (poly-Ub) proteins (Fig. 2a and Extended Data Fig. 3a), rapid deubiquitylation of histone H2A (uH2A)¹⁹ (Extended Data Fig. 3b) and accumulation of ubiquitylated proteins in the cytoplasm¹⁹ (Extended Data Fig. 3c). Furthermore, TNF (also known as TNF α)-induced degradation of I κ B α (ref. 20) was blocked after 1-h treatment with CuET or BTZ (Fig. 2b). Finally, CuET inhibited degradation of Ub(G76V)–GFP (an ubiquitin–fusion degradation substrate)²¹ in a dose-dependent manner (Fig. 2c). However, although these data confirmed a defect in protein degradation, CuET had no effect on the CT-like, C-like or T-like activity of the 20S proteasome²² (Extended Data Fig. 3d, e). This was further corroborated by the lack of a stabilizing effect of CuET on p53 tumour suppressor protein in dicoumarol-treated cells, in which

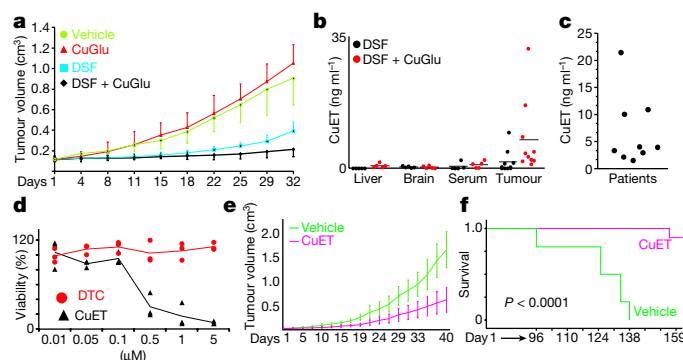


Figure 1 | Tumour-suppressing effects of DSF and CuET. **a**, Effects of orally administered DSF and CuGlu on subcutaneous growth of MDA-MB-231 tumours in mice. $n = 8$ mice per group. **b**, CuET levels in mouse tumours and tissues. $n = 5$ tissues, $n = 10$ tumours. **c**, CuET levels in human plasma after DSF treatment ($n = 9$ patients). **d**, Toxicity of DTC and CuET in MDA-MB-231 cells after 24 h treatment. $n = 3$ experiments. **e**, Effect of CuET on subcutaneous growth of MDA-MB-231 tumours in mice. $n = 20$ tumours. **f**, Survival of CuET- versus vehicle-treated mice with implanted AMO-1 xenografts. $n = 10$ animals per group. P value from a log-rank test. Data are mean \pm s.d. (**a**, **e**) or mean (**b**) linked means with individual values (**d**) or individual values (**c**).

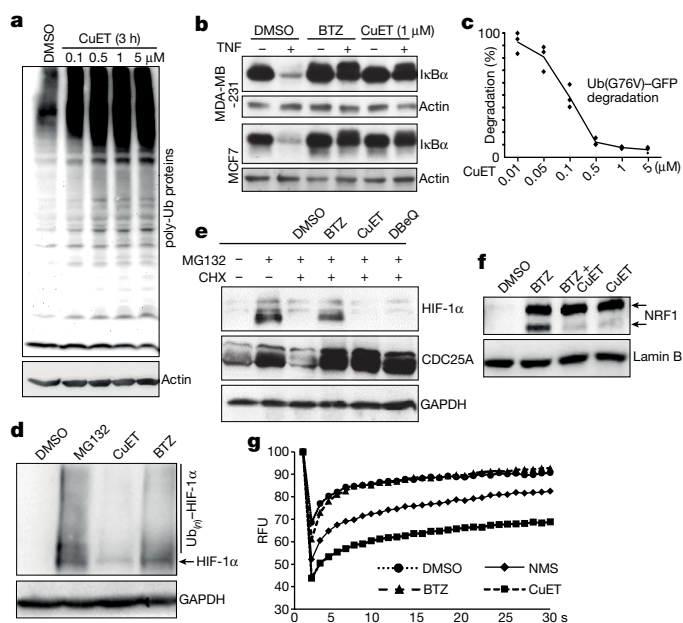


Figure 2 | CuET inhibits p97 segregase-dependent protein degradation.

a, CuET causes accumulation of poly-ubiquitylated proteins in MCF7 cells. **b**, TNF-induced I κ B α degradation is compromised after 1-h treatment with CuET or BTZ. **c**, Dose-dependent inhibition of Ub(G76V)-GFP degradation by CuET. HeLa cells were treated for 3 h. $n = 3$ experiments. **d**, HIF-1 α levels after 2-h treatments with MG132 (5 μ M), CuET (1 μ M), BTZ (1 μ M) in HeLa cells. **e**, Differential effect of BTZ (1 μ M), CuET (1 μ M) and DBE-Q (10 μ M) on CDC25A versus HIF-1 α in MG132-pretreated (4 h, 5 μ M), cycloheximide (CHX, 1 h, 50 μ g ml $^{-1}$)-exposed HeLa cells. **f**, BTZ (8 h, 1 μ M) induces NRF1 120-kDa (top arrow) and 110-kDa (bottom arrow) forms; whereas CuET (8 h, 0.5 μ M) only induced the non-cleaved 120-kDa form in NIH3T3 cells. **g**, FRAP quantification in U2OS Ub-GFP cells: slower mobility of accumulated cytoplasmic GFP-Ub after a 2-h pre-treatment with NMS873 (10 μ M), CuET (1 μ M) or BTZ (1 μ M). **a**, **b**, **d**-**g**. Data are representative of two independent biological experiments. Data are linked means and individual values (c) and relative mean signal of the bleached region from 12 cells per treatment (g).

p53 turnover depends on the core 20S proteasome independently of ubiquitin^{23,24}. In contrast to CuET, treatment with the 20S proteasome inhibitor BTZ stabilized p53 irrespective of dicoumarol (Extended Data Fig. 3f), indicating that 20S proteasome-dependent protein turnover remains operational with CuET treatment. Furthermore, CuET failed to inhibit 26S proteasome activity (Extended Data Fig. 3g), which was inferred from RPN11-dependent deubiquitylation²⁵. Collectively, these results suggest that CuET stabilizes ubiquitylated proteins by blocking a step upstream of the proteasome.

Next we considered p97-dependent processing of poly-Ub proteins, as this pathway operates upstream of the proteasome and its malfunction resembles phenotypes of proteasome inhibition²⁶. Unlike BTZ or MG132, CuET induced only modest accumulation (a small subfraction) of HIF-1 α (Fig. 2d), consistent with reported modest accumulation of HIF-1 α after knockdown of p97 compared to cells with inhibited proteasomes²⁷. Next, we pre-treated cells with MG132, followed by wash-off and 1-h cycloheximide (an inhibitor of translation) treatment combined with BTZ, CuET or DBE-Q (a direct inhibitor of p97 ATPase activity)²⁸. All tested inhibitors prevented degradation of CDC25A (a known p97 target)²⁹, whereas degradation of the mostly p97-independent target, that is, most of HIF-1 α ²⁷, was inhibited only by BTZ (Fig. 2e). Furthermore, consistent with cleavage of the 120-kDa species of the endoplasmic reticulum-tethered transcription factor NRF1 into an active 110-kDa form being a p97-dependent process³⁰, appearance of the cleaved NRF1 form was inhibited by both CuET and NMS873 (another p97 ATPase inhibitor) (Fig. 2f and Extended Data Fig. 4a, b).

These results suggest that the p97 pathway is compromised in cells treated with CuET.

Next, we asked whether CuET impairs the p97 segregase activity that extracts poly-Ub proteins from cellular structures, such as the endoplasmic reticulum, Golgi apparatus or chromatin for subsequent proteasomal degradation³¹. Using fluorescence recovery after photo-bleaching (FRAP) to investigate the mobility of accumulated poly-Ub proteins, we found that whereas GFP-ubiquitin in DMSO- or BTZ-treated cells diffused rapidly into bleached areas, this diffusion was slower after treatment with CuET or NMS873 (Fig. 2g and Extended Data Fig. 4c). This suggests that after treatment with CuET or NMS873 at least a subset of the accumulated poly-Ub proteins remains immobile, probably embedded into cellular structures. Consistently, upon detergent pre-extraction of mobile proteins, we observed greater immunofluorescence signals of extraction-resistant poly-Ub(K48) proteins (destined for proteasomal degradation) in NMS873- and CuET-treated cells compared to BTZ- or DMSO-treated controls (Extended Data Fig. 4d). Western blot analysis of endoplasmic reticulum-rich microsomal fractions also revealed enrichment of poly-Ub proteins after CuET and NMS873 treatment (Extended Data Fig. 4e). Malfunction of p97 segregase is furthermore associated with a cellular unfolded protein response (UPR)³². We confirmed UPR in cells treated with CuET or NMS873 by detecting increased markers of UPR induction, including the spliced form of XBP1s, ATF4 and phosphorylated (p-) eIF2 α ³³ (Extended Data Fig. 4f).

These studies are also of clinical relevance, because inhibition of p97 was suggested as an alternative treatment strategy for myeloma patients who had relapsed after therapy with BTZ (also known by the trade name Velcade)³⁴ or carfilzomib (CFZ)³⁵. Thus, we performed cytotoxicity tests with CuET on a panel of BTZ- or CFZ-adapted and non-adapted human cell lines or on cells derived from samples of patients with myeloma before therapy and with BTZ therapy. All pairs of adapted and non-adapted cells showed similar sensitivity to CuET treatment, in contrast to BTZ (Extended Data Fig. 5a-d). These results suggest that treatment with DSF (best combined with copper) or CuET might become a feasible therapeutical option for patients with relapsed, BTZ-resistant multiple myeloma.

CuET binds and immobilizes NPL4

To elucidate how CuET inhibits the p97 pathway, we first used an assay of p97 ATPase activity²⁸. In contrast to treatment with NMS873, CuET had no effect on p97 ATPase activity (Extended Data Fig. 6a). Because NPL4 and UFD1 proteins are key components of the p97 segregase³¹, we examined whether CuET might target the pathway through these cofactors. Ectopic overexpression of NPL4-GFP, but not UFD1-GFP or p97-GFP, reduced CuET cytotoxicity, suggesting that NPL4 is a candidate target of CuET (Fig. 3a and Extended Data Fig. 6b). An analogous 'rescue effect' of ectopic NPL4-GFP was apparent from the reduction in accumulation of poly-Ub proteins caused by CuET (Extended Data Fig. 6c).

As shown by live-cell imaging, 2-3-h exposure to CuET induced prominent nuclear clustering of NPL4-GFP, but not of UFD1-GFP or p97-GFP (Fig. 3b). Within 2-3 h, most of cellular NPL4-GFP became immobilized in nuclear clusters and also in cytoplasmic areas, as shown by FRAP (Fig. 3c). CuET-induced immobilization of endogenous NPL4 was confirmed by accumulation, which was detectable by western blot, in the detergent-insoluble fractions from various cell lines (Fig. 3d) and by immunofluorescence on pre-extracted cells (Extended Data Fig. 6d). Notably, the immobilization of NPL4 was also detectable in pre-extracted sections of cryopreserved tumours from mice treated with DSF or DSF and CuGlu, thus providing a potential biomarker of CuET activity towards the p97 pathway *in vivo* (Fig. 3e).

NPL4 is an attractive candidate for CuET binding, because this protein contains two zinc finger domains: a C-terminal NZF (NPL4-zinc finger) and a putative zinc finger-NPL4³⁶, which bind bivalent metals and metal complexes that might chemically resemble CuET³⁷.

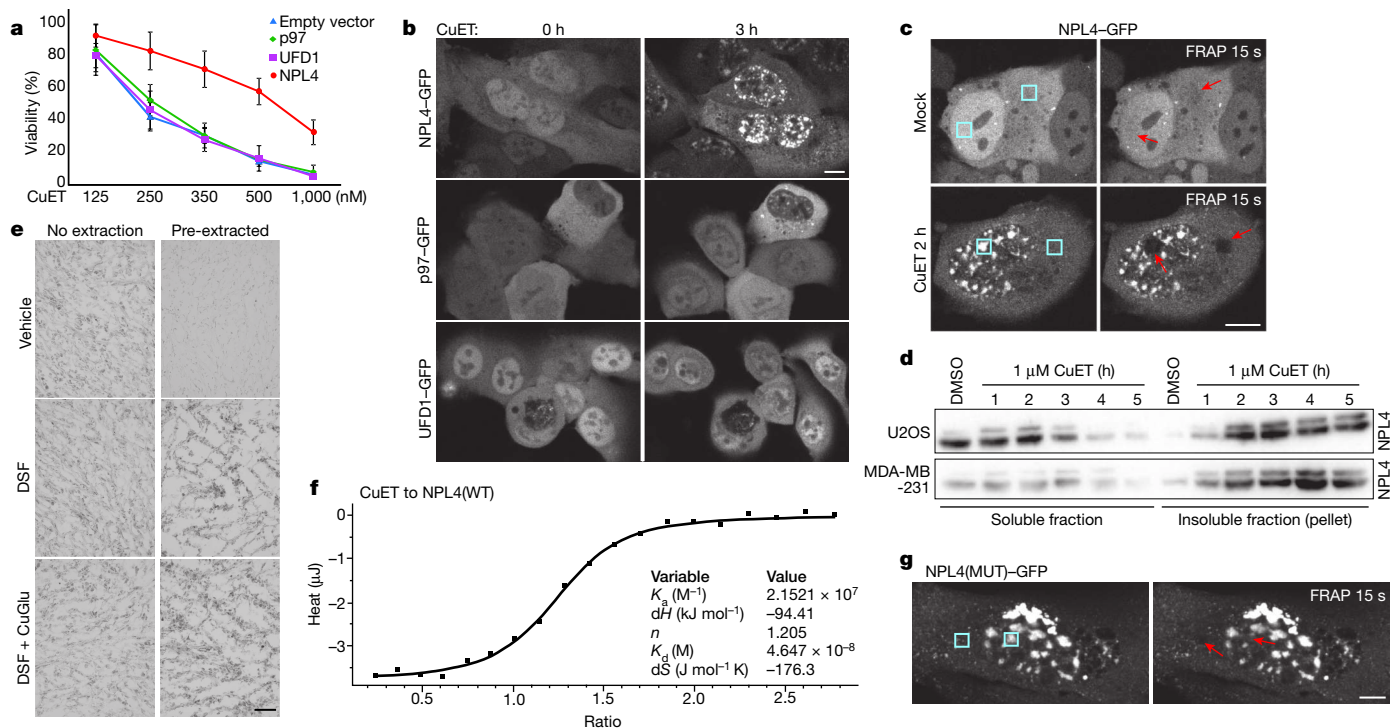


Figure 3 | CuET binds to and immobilizes NPL4. **a**, Ectopic NPL4-GFP, but not p97-GFP or UFD1-GFP rescues CuET toxicity in U2OS cells treated for 24 h. $n = 3$ experiments. Data are mean \pm s.d. **b**, CuET (1 μ M) induces intranuclear clustering of NPL4-GFP, but not p97-GFP or UFD1-GFP. **c**, CuET-induced (1 μ M) immobilization of NPL4-GFP (FRAP) in U2OS cells treated for 2 h. Blue boxes, areas before bleaching; arrows, after bleaching. **d**, NPL4 enrichment in Triton X-100-insoluble fractions

after CuET (1 μ M) treatment. **e**, Immunohistochemistry demonstrates the non-extractable NPL4 in MDA-MB-231 tumours from mice treated with DSF or DSF and CuGlu. **f**, ICT shows that CuET binds to purified NPL4(WT). **g**, Spontaneous intranuclear clustering and immobilization of NPL4(MUT)-GFP using FRAP in U2OS cells. Blue boxes, areas before bleaching; arrows, after bleaching. Scale bars, 10 μ m (**b**, **c**, **g**) or 50 μ m (**e**). **b-g**. Data are representative of two independent experiments.

Using isothermal calorimetry analysis (ITC)³⁸, we observed a standard dose-response-dependent binding curve (Fig. 3f) compatible with one binding site for CuET on wild-type NPL4 (NPL4(WT)), and a K_d in nanomolar concentrations for the NPL4-CuET interaction. Next, we used mutagenesis to test whether the putative ZF-NPL4 domain has any role in the potential NPL4-CuET interaction. The putative zinc finger domain was preferred, because an endogenous larger form of NPL4 that lacks the C-terminal NZF sequence exists in human cells. This larger NPL4 form is detectable as an upper band on western blots (Fig. 3d) and it is immobilized after CuET treatment, suggesting that the C-terminal NZF is not necessary for the interaction with CuET. No ITC interaction was found with a NPL4 mutant (NPL4(MUT)) (Extended Data Fig. 6f) in which both histidines and both cysteines in the putative zinc finger domain were substituted by alanines (Extended Data Fig. 6e). We used drug affinity responsive target stability (DARTS) as another, independent approach, which is based on altered protease susceptibility of target proteins upon drug binding³⁹. Consistently, exposure to CuET caused a differential pronase-dependent proteolysis pattern of NPL4(WT) but not NPL4(MUT) (Extended Data Fig. 6g). These results indicate that NPL4 is directly targeted by CuET and an intact putative zinc finger domain of NPL4 is essential for this interaction.

Notably, ectopically expressed NPL4(MUT)-GFP formed immobile nuclear clusters spontaneously in untreated cells, reminiscent of events seen in cells upon CuET treatment (Fig. 3c, g). Moreover, unlike ectopic NPL4(WT)-GFP, ectopically expressed NPL4(MUT)-GFP not only did not render cells resistant to CuET but also was toxic to the acceptor cells (Extended Data Fig. 6h). We also confirmed that multiple CuET-induced cellular phenotypes were mimicked by the ectopic NPL4(MUT)-GFP model, including accumulation of poly-Ub proteins and UPR activation (Extended Data Fig. 6i).

NPL4 aggregates trigger a heat-shock response

Although the nuclear NPL4 clusters occupied DAPI-unlabelled areas of chromatin (Extended Data Fig. 6d) co-localization with DAPI-excluded structures, such as nucleoli and nuclear speckles, were not found (Extended Data Fig. 7a). In late-G2 cells, NPL4 clusters were evidently excluded from the partially condensed chromatin (Extended Data Fig. 7b), suggesting that the NPL4 aggregates exclude chromatin rather than accumulating in specific nuclear areas. Both the nuclear clusters and the immobilized cytoplasmic NPL4 co-localized with poly-Ub proteins (confirmed by anti-Ub(K48) and FK2 antibodies), small ubiquitin-like modifiers (SUMOs) (only in nuclei) and with TDP43 protein⁴⁰ (Fig. 4a and Extended Data Fig. 7d), which are all features typical of aggregated defective proteins⁴¹. The same co-localization patterns were observed for spontaneous clusters formed by NPL4(MUT)-GFP showing that NPL4 aggregation is sufficient for the induction of these phenotypes even without CuET treatment (Extended Data Fig. 7c, e). Blockade of cellular ubiquitylation with a chemical inhibitor (MLN7243) of the E1 ubiquitin-activating enzyme failed to prevent either NPL4-GFP nuclear aggregation or cytoplasmic immobilization (Extended Data Fig. 7d), excluding the immobilization of NPL4 via recognition of ubiquitylated and SUMOylated substrates, but rather suggesting that immobilized NPL4 attracts ubiquitylated proteins or proteins that subsequently become ubiquitylated and/or SUMOylated. A key protein commonly associated with intracellular protein aggregates is HSP70, a chaperone implicated in aggregate processing⁴². Indeed, pre-extracted cells showed co-localization of HSP70 with both CuET-induced NPL4(WT)-GFP and spontaneous NPL4(MUT)-GFP aggregates (Fig. 4b, c). Both the CuET-induced NPL4(WT) aggregates and spontaneous NPL4(MUT) aggregates also co-localized with p97 (Extended Data Fig. 7f, g), as is particularly evident after pre-extraction. In the NPL4-GFP model, the amount of p97 immunoreactivity within

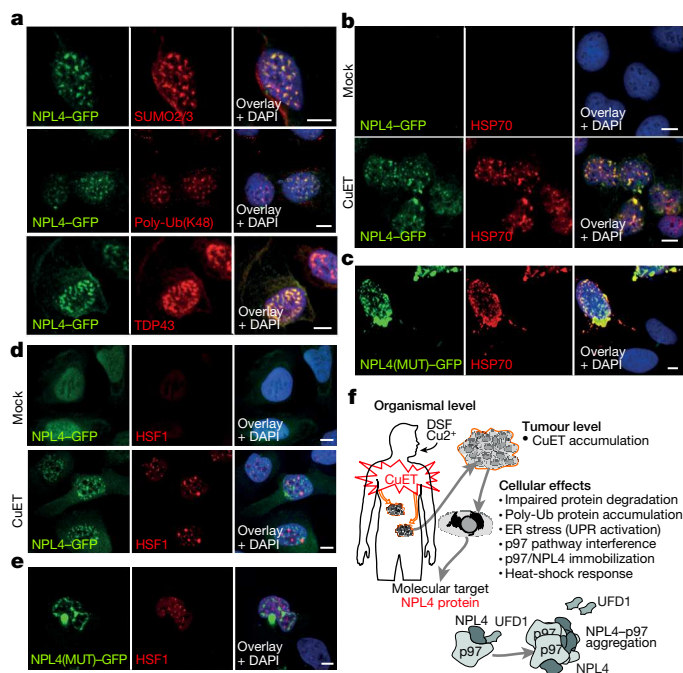


Figure 4 | NPL4 protein aggregation triggers HSR. **a**, NPL4–GFP co-localizes with SUMO2/3, poly-Ub(K48) and TDP43 in U2OS cells. Cells were treated with 1 μ M CuET for 3 h and pre-extracted. **b**, NPL4–GFP co-localizes with HSP70 in mock- and CuET-treated U2OS cells. Cells were treated with 1 μ M CuET for 3 h and pre-extracted. **c**, NPL4(MUT)–GFP co-localizes with HSP70 in U2OS cells after pre-extraction. **d**, CuET-induced HSF1 stress bodies. NPL4–GFP U2OS cells were treated with 1 μ M CuET for 3 h. **e**, HSF1 stress bodies in U2OS cells expressing NPL4(MUT)–GFP. **f**, Model of DSF anti-cancer activity in patients. Scale bars, 10 μ m. **a–e**, Data are representative of two independent experiments.

the NPL4–GFP clusters correlated with the GFP signal intensity, suggesting that p97 is immobilized via its interaction with NPL4. The other NPL4-binding partner, UFD1, was almost undetectable in detergent-insoluble pellets of CuET-treated or NPL4(MUT)–GFP-expressing cells despite clear p97 immobilization (Extended Data Fig. 8a, b), suggesting that UFD1 cannot bind to, or becomes only loosely attached to, the aggregated NPL4–p97 complex. Notably, non-extractable cellular p97 is detectable after CuET treatment (Extended Data Fig. 8c), including in stained tumour sections from mice treated with DSF or DSF and CuGlu, providing an additional candidate marker for CuET activity *in vivo* (Extended Data Fig. 8d).

Because aggregation of misfolded or damaged proteins triggers cellular heat-shock response (HSR) through an HSF1-dependent mechanism⁴³, we confirmed that CuET treatment indeed triggered a robust HSR accompanied by characteristic HSF1 nuclear stress foci (Fig. 4d) that were also detectable in cells spontaneously aggregating NPL4(MUT)–GFP (Fig. 4e). HSR markers, including accumulation of heat-shock proteins and a phosphorylation shift in HSF1, were detectable by western blot (Extended Data Fig. 8e, f).

Discussion

Our results help to explain the anti-cancer activity of the alcohol-abuse drug disulfiram. We propose a model for DSF cytotoxic activity, featuring rapid conversion of DSF into CuET, which accumulates in tumours. After entering cells, CuET binds NPL4 and induces its aggregation, consequently disabling the vital p97–NPL4–UFD1 pathway and inducing a complex cellular phenotype leading to cell death (Fig. 4f). Supporting CuET as the active metabolite is the correlation of CuET concentrations (active in the nanomolar range) with the biological effects and functional impact on the targeted pathway(s) *in vivo*. In addition, CuET is the only known metabolite of DSF containing copper ions, a metal

that enhances the anti-tumour effects of DSF; it is unlikely that another DSF metabolite could represent the major anti-cancer agent as levels of non-CuET metabolites should be lowered by copper addition. We also present a method for CuET detection in tissues and plasma, as well as data suggesting that preferential accumulation of CuET in tumours may contribute to cancer cell toxicity, consistent with the high therapeutic tolerability of DSF³, as documented even after years of daily administration at doses comparable to those we used in our mouse experiments. Considering the numerous studies on DSF and diverse opinions about the potential target of its anti-cancer effects⁴⁴, identification of NPL4, a key component of the p97–NPL4–UFD1 segregase complex, as the molecular target of CuET is surprising. The CuET–NPL4 interaction leads to rapid formation of protein aggregates and immobilization of this otherwise very mobile multifunctional protein complex, resulting in a severe phenotype, induction of HSR and eventually cell death. While additional potential targets of CuET cannot be excluded, the malfunction of the p97 pathway due to the NPL4–p97 aggregate formation explains the major cell phenotypes and the consequent cell death. Our work also reconciles the controversial studies^{6,12}, suggesting that the proteasome is the DSF target, by demonstrating that neither 20S nor 26S proteasome, but the processing of ubiquitylated proteins by the NPL4-dependent segregase, is targeted by CuET. Our results support the notion that the p97–NPL4 pathway is a promising therapeutic target in oncology^{45,46}. Indeed, reports on p97 overabundance correlating with progression and metastasis of carcinomas of the breast, colon and prostate^{47–49} are consistent with our present nationwide epidemiological analysis, which revealed an association between continued use of DSF and favourable prognosis, an intriguing finding that should be investigated further, particularly given the currently limited therapeutic options for patients with metastatic cancer. From a broader perspective, our study illustrates the potential of multifaceted approaches to drug repurposing, providing novel mechanistic insights, identification of new cancer-relevant targets and encouragement for further clinical trials, here with DSF, an old, safe and public domain drug⁴ that might help to save lives of patients with cancer worldwide.

Online Content Methods, along with any additional Extended Data display items and Source Data, are available in the online version of the paper; references unique to these sections appear only in the online paper.

Received 1 October 2015; accepted 8 November 2017.

Published online 6 December 2017.

- Collins, F. S. Mining for therapeutic gold. *Nat. Rev. Drug Discov.* **10**, 397 (2011).
- Pantziarka, P. *et al.* The repurposing drugs in oncology (ReDO) project. *Ecancermedalscience* **8**, 442 (2014).
- Iljin, K. *et al.* High-throughput cell-based screening of 4910 known drugs and drug-like small molecules identifies disulfiram as an inhibitor of prostate cancer cell growth. *Clin. Cancer Res.* **15**, 6070–6078 (2009).
- Cvek, B. Nonprofit drugs as the salvation of the world's healthcare systems: the case of Antabuse (disulfiram). *Drug Discov. Today* **17**, 409–412 (2012).
- Shen, M. L., Johnson, K. L., Mays, D. C., Lipsky, J. J. & Naylor, S. Determination of *in vivo* adducts of disulfiram with mitochondrial aldehyde dehydrogenase. *Biochem. Pharmacol.* **61**, 537–545 (2001).
- Liu, D., Cui, Q. C., Yang, H. & Dou, Q. P. Disulfiram, a clinically used anti-alcoholism drug and copper-binding agent, induces apoptotic cell death in breast cancer cultures and xenografts via inhibition of the proteasome activity. *Cancer Res.* **66**, 10425–10433 (2006).
- Zha, J. *et al.* Disulfiram targeting lymphoid malignant cell lines via ROS–JNK activation as well as Nrf2 and NF- κ B pathway inhibition. *J. Transl. Med.* **12**, 163 (2014).
- Safi, R. *et al.* Copper signaling axis as a target for prostate cancer therapeutics. *Cancer Res.* **74**, 5819–5831 (2014).
- Liu, P. *et al.* Liposome encapsulated disulfiram inhibits NF- κ B pathway and targets breast cancer stem cells *in vitro* and *in vivo*. *Oncotarget* **5**, 7471–7485 (2014).
- Dufour, P. *et al.* Sodium dithiocarbamate as adjuvant immunotherapy for high risk breast cancer: a randomized study. *Biotherapy* **6**, 9–12 (1993).
- Yip, N. C. *et al.* Disulfiram modulated ROS–MAPK and NF- κ B pathways and targeted breast cancer cells with cancer stem cell-like properties. *Br. J. Cancer* **104**, 1564–1574 (2011).

12. Lövborg, H. *et al.* Inhibition of proteasome activity, nuclear factor- κ B translocation and cell survival by the antialcoholism drug disulfiram. *Int. J. Cancer* **118**, 1577–1580 (2006).
13. Allensworth, J. L. *et al.* Disulfiram (DSF) acts as a copper ionophore to induce copper-dependent oxidative stress and mediate anti-tumor efficacy in inflammatory breast cancer. *Mol. Oncol.* **9**, 1155–1168 (2015).
14. Nechushtan, H. *et al.* A phase IIb trial assessing the addition of disulfiram to chemotherapy for the treatment of metastatic non-small cell lung cancer. *Oncologist* **20**, 366–367 (2015).
15. Jin, M. *et al.* Alcohol drinking and all cancer mortality: a meta-analysis. *Ann. Oncol.* **24**, 807–816 (2013).
16. Li, Y. *et al.* Copper improves the anti-angiogenic activity of disulfiram through the EGFR/Src/VEGF pathway in gliomas. *Cancer Lett.* **369**, 86–96 (2015).
17. Suzuki, Y. *et al.* The origin of an EPR signal observed in dithiocarbamate-loaded tissues. Copper(ii)-dithiocarbamate complexes account for the narrow hyperfine lines. *Biochim. Biophys. Acta* **1335**, 242–245 (1997).
18. Kepp, O., Galluzzi, L., Lipinski, M., Yuan, J. & Kroemer, G. Cell death assays for drug discovery. *Nat. Rev. Drug Discov.* **10**, 221–237 (2011).
19. Doll, C. *et al.* RNF168 binds and amplifies ubiquitin conjugates on damaged chromosomes to allow accumulation of repair proteins. *Cell* **136**, 435–446 (2009).
20. Li, J. M., Wu, H., Zhang, W., Blackburn, M. R. & Jin, J. The p97–UFD1L–NPL4 protein complex mediates cytokine-induced I κ B α proteolysis. *Mol. Cell. Biol.* **34**, 335–347 (2014).
21. Chou, T. F. & Deshaies, R. J. Quantitative cell-based protein degradation assays to identify and classify drugs that target the ubiquitin–proteasome system. *J. Biol. Chem.* **286**, 16546–16554 (2011).
22. Kisselev, A. F. & Goldberg, A. L. Monitoring activity and inhibition of 26S proteasomes with fluorogenic peptide substrates. *Methods Enzymol.* **398**, 364–378 (2005).
23. Asher, G., Lotem, J., Cohen, B., Sachs, L. & Shaul, Y. Regulation of p53 stability and p53-dependent apoptosis by NADH quinone oxidoreductase 1. *Proc. Natl Acad. Sci. USA* **98**, 1188–1193 (2001).
24. Asher, G., Tsvetkov, P., Kahana, C. & Shaul, Y. A mechanism of ubiquitin-independent proteasomal degradation of the tumor suppressors p53 and p73. *Genes Dev.* **19**, 316–321 (2005).
25. Verma, R. *et al.* Role of Rpn11 metalloprotease in deubiquitination and degradation by the 26S proteasome. *Science* **298**, 611–615 (2002).
26. Dai, R. M. & Li, C. C. Valosin-containing protein is a multi-ubiquitin chain-targeting factor required in ubiquitin–proteasome degradation. *Nat. Cell Biol.* **3**, 740–744 (2001).
27. Alexandru, G. *et al.* UBXD7 binds multiple ubiquitin ligases and implicates p97 in HIF1 α turnover. *Cell* **134**, 804–816 (2008).
28. Chou, T. F. *et al.* Reversible inhibitor of p97, DBE9, impairs both ubiquitin-dependent and autophagic protein clearance pathways. *Proc. Natl Acad. Sci. USA* **108**, 4834–4839 (2011).
29. Riemer, A. *et al.* The p97–Ufd1–Npl4 ATPase complex ensures robustness of the G2/M checkpoint by facilitating CDC25A degradation. *Cell Cycle* **13**, 919–927 (2014).
30. Radhakrishnan, S. K., den Besten, W. & Deshaies, R. J. p97-dependent retrotranslocation and proteolytic processing govern formation of active Nrf1 upon proteasome inhibition. *eLife* **3**, e01856 (2014).
31. Meyer, H., Bug, M. & Bremer, S. Emerging functions of the VCP/p97 AAA-ATPase in the ubiquitin system. *Nat. Cell Biol.* **14**, 117–123 (2012).
32. Magnaghi, P. *et al.* Covalent and allosteric inhibitors of the ATPase VCP/p97 induce cancer cell death. *Nat. Chem. Biol.* **9**, 548–556 (2013).
33. Samali, A., Fitzgerald, U., Deegan, S. & Gupta, S. Methods for monitoring endoplasmic reticulum stress and the unfolded protein response. *Int. J. Cell Biol.* **2010**, 830307 (2010).
34. Auner, H. W. *et al.* Combined inhibition of p97 and the proteasome causes lethal disruption of the secretory apparatus in multiple myeloma cells. *PLoS ONE* **8**, e74415 (2013).
35. Soriano, G. P. *et al.* Proteasome inhibitor-adapted myeloma cells are largely independent from proteasome activity and show complex proteomic changes, in particular in redox and energy metabolism. *Leukemia* **30**, 2198–2207 (2016).
36. Lass, A., McConnell, E., Fleck, K., Palamarchuk, A. & Wójcik, C. Analysis of Npl4 deletion mutants in mammalian cells unravels new Ufd1-interacting motifs and suggests a regulatory role of Npl4 in ERAD. *Exp. Cell Res.* **314**, 2715–2723 (2008).
37. Voráčková, I., Suchanová, S., Ulbrich, P., Diehl, W. E. & Ruml, T. Purification of proteins containing zinc finger domains using immobilized metal ion affinity chromatography. *Protein Expr. Purif.* **79**, 88–95 (2011).
38. Holdgate, G. *et al.* Biophysical methods in drug discovery from small molecule to pharmaceutical. *Methods Mol. Biol.* **1008**, 327–355 (2013).
39. Lomenick, B. *et al.* Target identification using drug affinity responsive target stability (DARTS). *Proc. Natl Acad. Sci. USA* **106**, 21984–21989 (2009).
40. Becker, L. A. *et al.* Therapeutic reduction of ataxin-2 extends lifespan and reduces pathology in TDP-43 mice. *Nature* **544**, 367–371 (2017).
41. Guo, L. *et al.* A cellular system that degrades misfolded proteins and protects against neurodegeneration. *Mol. Cell* **55**, 15–30 (2014).
42. Kim, Y. E., Hipp, M. S., Bracher, A., Hayer-Hartl, M. & Hartl, F. U. Molecular chaperone functions in protein folding and proteostasis. *Annu. Rev. Biochem.* **82**, 323–355 (2013).
43. Dai, C. & Sampson, S. B. HSF1: guardian of proteostasis in cancer. *Trends Cell Biol.* **26**, 17–28 (2016).
44. Cvek, B. Targeting malignancies with disulfiram (Antabuse): multidrug resistance, angiogenesis, and proteasome. *Curr. Cancer Drug Targets* **11**, 332–337 (2011).
45. Deshaies, R. J. Proteotoxic crisis, the ubiquitin–proteasome system, and cancer therapy. *BMC Biol.* **12**, 94 (2014).
46. Anderson, D. J. *et al.* Targeting the AAA ATPase p97 as an approach to treat cancer through disruption of protein homeostasis. *Cancer Cell* **28**, 653–665 (2015).
47. Cui, Y. *et al.* High expression of valosin-containing protein predicts poor prognosis in patients with breast carcinoma. *Tumour Biol.* **36**, 9919–9927 (2015).
48. Yamamoto, S. *et al.* Expression of valosin-containing protein in colorectal carcinomas as a predictor for disease recurrence and prognosis. *Clin. Cancer Res.* **10**, 651–657 (2004).
49. Tsujimoto, Y. *et al.* Elevated expression of valosin-containing protein (p97) is associated with poor prognosis of prostate cancer. *Clin. Cancer Res.* **10**, 3007–3012 (2004).

Supplementary Information is available in the online version of the paper.

Acknowledgements We thank J. Škvor, M. Zadinová, J. Večerka and D. Doležal for help with animal experiments, Jana Vrbkova for statistical analysis, D. Fridecky and T. Adam for help with HPLC, I. Protivankova and M. Grønng Nielsen for technical assistance. This work was supported by grants from the Kellner Family Foundation, Czech National Program of Sustainability, Grant Agency of the Czech Republic, MEYS CR project Czech-Biolmaging, the Czech Health Research Council, of the Danish Cancer Society, the Danish National Research Foundation (project CARD), the Danish Council for Independent Research, the Novo Nordisk Foundation, the Czech Cancer League, the Swedish Research Council, Cancerfonden of Sweden, the European Commission (EATRIS), the Czech Ministry of Education, youth and sports (OPVKCZ), Cancer Research Czech Republic and the Howard Hughes Medical Institute.

Author Contributions Z.S., M.Mis., B.C., R.J.D. and J.Barte. conceived the study. Z.S. and M.Mis. performed most biochemical and microscopy experiments and wrote the manuscript. D.M. established the expression cell lines and performed most cytotoxicity tests. T.O., P.D. and I.V. performed the HPLC experiments. K.K.A., S.F. and J.O. performed the epidemiological analyses. J.Bartk. performed the immunohistochemical analyses. J.V. and P.D. performed DARTS experiments. P.M. performed cell death analyses. Z.T. performed cytotoxicity tests and heat-shock response analyses. A.K. performed cytotoxicity tests. A.M. designed and performed phlebotomies of patients treated with Antabuse. M.Mic. performed the ITC. J.G. performed FACS analyses, cell death assays and cell sorting. J.S. performed 20S proteasome assays. J.L. performed 26S proteasome assays. M.K. and C.D. performed the cytotoxicity experiments on myeloid- and patient-derived cell lines. P.P., J.M. and M.H. performed mouse experiments. J.Barte., B.C., Q.P.D. and R.J.D. helped to design the experiments, interpreted the data and wrote/edited the manuscript. All authors approved the manuscript.

Author Information Reprints and permissions information is available at www.nature.com/reprints. The authors declare competing financial interests: details are available in the online version of the paper. Readers are welcome to comment on the online version of the paper. Publisher's note: Springer Nature remains neutral with regard to jurisdictional claims in published maps and institutional affiliations. Correspondence and requests for materials should be addressed to J.Barte. (jb@cancer.dk), B.C. (cvekb@seznam.cz) and R.J.D. (deshaies@caltech.edu).

Reviewer Information Nature thanks P. Brossart and the other anonymous reviewer(s) for their contribution to the peer review of this work.

METHODS

The experiments were not randomized.

Epidemiological analyses and access to health registers. We conducted a population-based cohort study by combining Danish nationwide demographic and health registers. This study was approved by the Danish Data Protection Agency and Statistics Denmark's Scientific Board. As the epidemiological study was based solely on register data and did not involve any contact with patients, no ethical approval was required from the Danish Scientific Ethical Committee⁵⁰. The cohort consisted of all Danes aged 35–85 years with a first-time diagnosis of cancer between January 2000 and December 2013. Because DSF (Antabuse) is a relative contra-indication among individuals with liver or kidney diseases, we excluded patients with cancers of the liver or kidney from the cohort. Cohort members were categorized according to use of DSF into two main groups: (i) those who filled at least one prescription of DSF within five years before the cancer diagnosis, but did not fill DSF prescription(s) during the first year after the diagnosis (previous users), that is, individuals suffering from alcoholism but taking DSF only before their cancer diagnosis; and (ii) those who used DSF before their cancer diagnosis and also filled one or more DSF prescriptions during the first year after the cancer diagnosis (continuing users), that is, individuals who underwent DSF therapy both before and after the cancer diagnosis. We also defined a category of patients with cancer who did not fill prescription(s) for DSF either before or after (≤ 1 year) the cancer diagnosis (never users). In the main analyses, we calculated hazard ratios and 95% confidence intervals estimating cancer-specific mortality among continuing DSF users compared to previous DSF users based on a Cox model regressing on both propensity scores and disulfiram use. By including propensity scores in the regression, we used demographic data and comorbid conditions/diagnostic codes as well as prescription data for selected concomitant drugs, to balance baseline characteristics of previous and continuing users of DSF and to adjust estimated hazard ratios of cancer-specific mortality associated with DSF use⁵¹. The patients with cancer were followed from one year after the diagnosis until death, migration or end of study (31 December 2014). The propensity scores thus estimate the probability of being treated with DSF in the exposure window 0–1 year after the cancer diagnoses conditional on the following other covariates in the calculation of propensity scores using logistic regression: gender, age at diagnosis, calendar time, highest achieved education and disposable income; medical histories of diabetes mellitus, chronic obstructive pulmonary disease, ischaemic heart disease, congestive heart failure, cerebrovascular disease, atrial fibrillation or atrial flutter, dementia and ulcer disease; and use of non-steroidal anti-inflammatory drugs (NSAIDs; including aspirin), non-aspirin antithrombotic agents (anticoagulants), statins, antihypertensive medication, other cardiovascular drugs, anti-diabetics and psychotropic drugs. In the Cox model, the propensity score is further included as a restricted cubic spline to model possible nonlinearities, in addition to the categorical disulfiram use, which is the variable of interest. Analyses were run for cancer overall and for breast, prostate and colon cancer, separately. Furthermore, all analyses were stratified by stage (localized, non-localized or unknown). Statistical significance of DSF use was evaluated by likelihood ratio tests. We used the software R for statistical computing⁵².

In vivo tumour experiments. The human breast cancer cell line MDA-MB-231 was injected (10^7 cells transplanted subcutaneously) to grow tumours in athymic NU/NU female mice (AnLab Ltd) with a body weight of 23.6–26.9 g, aged 12 weeks. Inclusion criteria were: female, appropriate age and weight (15–30 g). Exclusion criteria were: tumour size must not exceed 20 mm (volume $4,000 \text{ mm}^3$) in any direction in an adult mouse, the tumour mass should not proceed to the point where it significantly interferes with normal bodily functions, or causes pain or distress owing to its location, persistent self-induced trauma, rapid or progressive weight loss of more than 25%, for seven days. In none of the experiments were these approved ethical limits exceeded. After the tumours grew to $0.114\text{--}0.117 \text{ cm}^3$ on average, mice were randomly divided into four groups, each of eight mice, and treated as follows: (i) normal diet; (ii) normal diet plus oral administration of 0.15 mg kg^{-1} copper gluconate (CuGlu); (iii) normal diet plus oral administration of 50 mg kg^{-1} DSF; (iv) normal diet plus oral administration of 0.15 mg kg^{-1} CuGlu and 50 mg kg^{-1} DSF. Administration of compounds was carried out as a blinded experiment (all information about the expected outputs and the nature of used compounds were kept from the animal technicians). CuGlu was administered each day in the morning (08:00) and DSF each day in the evening (19:00) to mimic a clinical trial combining DSF and CuGlu in treatment of tumours involving the liver (NCT00742911). After treatment began, mice were weighed and their tumours measured twice per week. At day 32, mice were euthanized, and the tumours were removed and frozen at -80°C . The experiment was evaluated by comparing growth curves of tumours in the experimental groups with those in controls. The rates of tumour growth inhibition (TGI) were calculated by the formula $\text{TGI} = (1 - V_{\text{treated}}/V_{\text{control}})$ where V_{treated} is the mean of tumour volumes in the treated group and V_{control} is the mean of tumour volumes in the control group).

Mean tumour volume values at specific time intervals were statistically evaluated. To test directly the effect of CuET, we used MDA-MB-231 and AMO-1 models. MDA-MB-231 was injected (5×10^6 cells were transplanted subcutaneously) to grow tumours in SCID mice (ENVIGO) aged 10 weeks (± 2 weeks). AMO-1 xenografts were expanded in SCID mice. Each group consisted of 10 animals, each bearing two tumours. CuET was formulated in bovine serum albumin solution (1%) to a final concentration of 1 mg ml^{-1} . CuET was applied intraperitoneally with a schedule of five days on and two days off. All aspects of the animal study met the accepted criteria for the care and experimental use of laboratory animals, and protocols were approved by the Animal Research Committee of the 1st Faculty of Medicine Charles University in Prague and Ethical Committee of Faculty of Medicine and Dentistry, Palacky University in Olomouc. For HPLC-MS and immunohistochemistry analysis, we used MDA-MB-231 xenografted mice treated with the same DSF and DSF plus copper gluconate regime as described for the anti-cancer activity assessment with the notable difference that mice were euthanized after five days of treatment.

HPLC-MS analysis of CuET. The HR-MRM analysis was performed on a HPLC-ESI-QTOF system consisting of HPLC chromatograph Thermo UltiMate 3000 with AB Sciex TripleTOF 5600+ mass spectrometer, using the DuoSpray ESI source operated at an ion source voltage of 5,500 V, ion source gas flow rates of 40 units, curtain gas flow rate of 30 units, declustering potential of 100 V and temperature 400°C . Data were acquired in product ion mode with two parent masses (358.9 and 360.9) for analysis of CuET. Chromatographic separation was done by PTFE column, which was especially designed for analysis of strong metal chelators filled by C18 sorbent (IntellMed, IM_301). Analysis was performed at room temperature and with a flow rate of $1,500 \mu\text{l min}^{-1}$ with isocratic chromatography. Mobile phase consisted of HPLC grade acetone (Lachner) 99.9%, HPLC water (Merck Millipore) 0.1% and 0.03% HPLC formic acid (Sigma-Aldrich). Acquired mass spectra were evaluated in software PeakView 1.2. Extracted ion chromatograms of transitions 88.0 and 116.0 (common for both parent masses) with a 0.1 mass tolerance were Gaussian smoothed with width of two points. Peak area was then recorded and recalculated to ng ml^{-1} according to the calibration curve.

Sample preparation for HPLC-MS analysis. Liquid nitrogen-frozen biological samples were cut into small pieces using a scalpel. Samples (30–100 mg) were immediately processed by homogenization in 100% acetone in a ratio of 1:10 sample: acetone (for plasma or serum the ratio was 1:4). Homogenization was done in a table-top homogenizer (Retsch MM301) placed in a cold room (4°C) in 2-ml Eppendorf tubes with 2 glass balls (5 mm) for 1 min at 30 Hz. The tube was immediately centrifuged at 4°C , $20,000g$ for 2 min. Supernatant was decanted into a new 1.5-ml Eppendorf tube and immediately centrifuged for 30 min using a small table-top centrifuge (BioSan FVL-2400N) placed inside a -80°C freezer. Supernatant was quickly decanted into a glass HPLC vial and kept at -80°C for no longer than 6 h. Just before the HPLC analysis, the vial was placed into a pre-cooled (4°C) LC-sample rack and immediately analysed. To enable an approximate quantification of analysed CuET, a calibration curve was prepared. Various amounts of CuET were spiked in plasma, frozen in liquid nitrogen, and placed at -80°C to mimic sample processing. Standards were then processed as the samples described above. To measure circulating CuET concentrations, mice were given a single oral dose of DSF (50 mg kg^{-1}) and euthanized at different time points. Serum was collected and frozen for analysis.

Blood collection from humans for HPLC-MS analysis of CuET. Blood samples were collected before and 3 h after oral application of DSF (Antabuse, 400 mg) dissolved in water. Phlebotomy needles were specific for metal analysis—Sarstedt Safety Kanule $21G \times 1\frac{1}{2}$ inches, 85.1162.600. Collection tubes were specific for metal analysis—Sarstedt, S-Monovette 7.5 ml LH, 01.1604.400. Immediately after blood collection samples were centrifuged in a pre-cooled centrifuge (4°C at 1,300g for 10 min). After centrifugation, tubes were placed on ice and the plasma fraction was immediately aliquoted into the 1.5-ml Eppendorf tubes with approximately $500 \mu\text{l}$ per tube. The tubes with plasma were immediately frozen on dry ice and later stored in -80°C . Blood samples were collected from volunteers who gave informed consent and were undergoing Antabuse therapy because of alcohol abuse. Participants were four males (aged 34, 38, 41, 60 years) and five females (aged 37, 56, 46, 59, 63 years). All individuals were freshly diagnosed for alcohol-use disorder and were scheduled for Antabuse therapy. Blood samples were collected before and after the first use of Antabuse. All relevant ethical regulations were followed for the study. The study, including the collection of blood samples, was approved by the Ethical Committee of Faculty of Medicine and Dentistry, Palacky University in Olomouc.

Cell lines. Cell lines were cultured in appropriate growth medium supplemented with 10% fetal bovine serum (FBS) and penicillin-streptomycin; and maintained in a humidified, 5% CO_2 atmosphere at 37°C . Cell lines cultured in DMEM medium were: HCT116 (ATCC), DU145 (ECACC), PC3 (ECACC), T47D (NCI60),

HS578T (NCI60), MCF7 (ECACC), MDA-MB-231 (ATCC), U2OS (ECACC), HeLa (ATCC), NIH-3T3 (ATCC), CAPAN-1 (ATCC), A253 (ATCC), FaDu (ATCC), h-TERT-RPE1 (ATCC), HeLa-Ub(G76V)-GFP-ODD-Luc²¹. Cell lines cultured in RPMI1640 medium were: NCI-H358 (ATCC), NCI-H52 (ATCC), HCT-15 (ATCC), AMO-1 (ATCC), MM-1S (ATCC), ARH77 (ATCC), RPMI8226 (ATCC), OVCAR-3 (NCI60), CCRF-CEM (ATCC), K562 (ATCC), 786-0 (NCI60). Cell lines cultured in EMEM medium were: U87-MG (ATCC), SiHA (ATCC). Cell line A549 (ATCC) was cultured in F12K medium, HT29 (ATCC) in McCoy's medium and LAPC4 (provided by Z. Culig, University of Innsbruck) in IMDM medium supplemented with metribolone R1881 (Sigma-Aldrich). RWPE-1 (ATCC) cells were cultured in a keratinocyte serum-free medium supplemented with bovine pituitary extract and human recombinant epidermal growth factor (Thermo Fisher Scientific). BTZ- and CFZ-resistant multiple myeloma cell lines were previously described in ref. 35. Cell lines were tested for mycoplasma contamination and authenticated by STR method. None of the cell lines used in this study is listed in the database of commonly misidentified cell lines maintained by ICLAC.

Stable cell line construction. For construction of all stably transfected cell lines we used the U2OS cell line (ECACC). For U2OS Ub-GFP, we used the commercial Ub-GFP EGFP-C1 vector (Addgene); for U2OS NPL4-GFP, we used the commercial NPLOC4-GFP pCMV6-AC-GFP vector (Origene); for U2OS p97-GFP, we used the commercial VCP-GFP pCMV6-AC-GFP vector (Origene); and for U2OS UFD1-GFP, we used the commercial UFD1L-GFP pCMV6-AC-GFP vector (Origene). Cells were transfected using Promega FugeneHD according to the manufacturer's instructions. Cells were further cultured in the appropriate antibiotics (geneticin, 400 µg ml⁻¹). Medium with geneticin was replaced every 2–3 days until the population of resistant cells was fully established. Cells were further refined by sorting for cells expressing GFP (BD FACS Aria). For preparation of inducible NPL4(MUT)-GFP cells, U2OS cells were transfected with a pcDNA6/TR plasmid (Invitrogen, V1025-20) using the FugeneHD transfection reagent (Promega, E2311) according to the manufacturer's protocol. To generate a cell line that stably expressed the Tet repressor, U2OS cells were cultured in selective medium with blasticidin (10 µg ml⁻¹) for 10 days. Blasticidin-resistant colonies were picked, expanded and screened for clones that exhibited the lowest basal levels and highest inducible levels of expression. Next, the most suitable clones were transfected with the PCDNA4/TO expression vector encoding the mutated NPL4-GFP protein using the Fugene transfection reagent. Cells were cultured in medium with zeocin (500 µg ml⁻¹) to select clones that contain pcDNA4/TO-mutated NPL4-GFP. The NPL4(MUT)-GFP-encoding plasmid was obtained from Geneti Biotech. To induce expression of protein, cells were incubated with doxycycline (Sigma-Aldrich) 1 µg ml⁻¹ for 16–48 h.

Colony-formation assay. Cells were seeded into six-well plates at 100–300 cells per well (depending on the cell line). The next day, cells were treated with compounds as indicated in the specific experiments and kept in culture for 7–14 days. Colonies were visualized by crystal violet and counted.

XTT assay. Cells were plated at a density of 10,000 per well in a 96-well plate. The next day, cells were treated as indicated. After 24 h, an XTT assay was performed according to the manufacturer's instructions (Applichem). XTT solution was added to the medium and incubated for 30–60 min, and then the dye intensity was measured at the 475 nm wavelength using a spectrometer (TECAN, Infinite M200PRO). Results are shown as mean ± s.d. from three independent experiments, each performed in triplicate. For LD₅₀ analysis across the panel of cell lines listed in Extended Data Fig. 2b, cell lines were treated with various doses (at least five doses) for 48 h. LD₅₀ values were calculated using Graphpad Prism software based on survival curves from at least two independent experiments.

Annexin V staining. Cell cultures were treated as indicated and collected by trypsinization. Initial culture medium and washing buffer were collected to include detached cells. Cells were centrifuged (250g, 5 min) and re-suspended in a staining buffer (140 mM NaCl, 4 mM KCl, 0.75 mM MgCl₂, 10 mM HEPES) containing 2.5 mM CaCl₂, Annexin V-APC (1:20, BD Biosciences) and 2.5 µg ml⁻¹ 7-AAD (BD Biosciences) for 15 min on ice in the dark. Samples were analysed by flow cytometry using BD FACSVerser (BD Biosciences) and at least 10,000 events were acquired per sample. Collected data were processed using BD FACSSuite (BD Biosciences) and exported into Microsoft Excel.

Caspases 3/7 assay. Activity of caspase-3 and -7 was quantified by cleavage of fluorogenic substrate CellEvent Caspase-3/7 Green Detection Reagent (Thermo Fisher Scientific). In brief, samples prepared in the same staining buffer as described for annexin V staining above, supplemented with 2% FBS, 0.5 µM CellEvent Caspase-3/7 Green Detection Reagent and incubated for 45 min at room temperature in the dark. Subsequently, 0.5 µg ml⁻¹ DAPI was added and samples were analysed by flow cytometry using BD FACSVerser (BD Biosciences) and at least 10,000 events were acquired per sample. Collected data were processed using BD FACSSuite (BD Biosciences) and exported into Microsoft Excel.

Viability assay of multiple myeloma cells. The CellTiter 96 MTS-assay (Promega) was used according to the manufacturer's instructions to determine the cell viability of BTZ (Janssen Cilag), CFZ and CuEt in cell lines and the absorbance of the formazan product was measured in 96-well microplates at 492 nm. The assay measures dehydrogenase enzyme activity found in metabolically active cells.

For patient cells, the more sensitive luminescent CellTiterGlo assay (Promega) was used to determine cell viability, measured by ATP production of metabolically active cells. The primary myeloma cell samples were obtained after written informed consent and approval by the independent ethics review board (St Gallen ethics committee—Ethikkommission Ostschiweiz), in accordance with ICH-GCP and local regulations. Malignant plasma cells were retrieved by PBMC isolation from a patient with multiple myeloma progressing under BTZ-containing therapy, based on IMWG criteria (BTZ-resistant) and an untreated patient with multiple myeloma (BTZ-sensitive). The purity of the cell samples was >80% myeloma cells, as assessed by morphology.

Immunoblotting and antibodies. Equal amounts of cell lysates were separated by SDS-PAGE on hand-cast or precast tris-glycine gradient (4–20%) gels (Life Technologies), and then transferred onto a nitrocellulose membrane. The membrane was blocked with 5% bovine milk in Tris-buffered saline containing 0.1% Tween-20 for 1 h at room temperature, and then incubated overnight at 4 °C or for 1 h at room temperature, with one of the following primary antibodies (all antibodies were used in the system under study (assay and species) according to the instructions of the manufacturer): anti-ubiquitin (1:1,000; Cell Signaling, 3933), anti-H2A, acidic patch (1:1,000; Merck Millipore, 07-146), anti-monoubiquityl-H2A (1:1,000; Merck Millipore, clone E6C5), anti-IκBα (1:500; Santa Cruz Biotechnology, sc-371), anti-p53 (1:500; Santa Cruz Biotechnology, clone DO-1), anti-HIF-1α (1:1,000; BD Biosciences, 610958), anti-CDC25A (1:500; Santa Cruz Biotechnology, clone DCS-120), anti-NRF1 (1:1,000; Cell Signaling, clone D5B10), anti-VCP (1:2,000; Abcam, ab11433), anti-VCP (1:1,000; Novus Bio, NBP100-1557), anti-NPLOC4 (1:1,000; Novus Bio, NBP1-82166), anti-ubiquitin lys48-specific (1:1,000; Merck Millipore, clone Apu2), anti-β-actin (1:2,000; Santa Cruz Biotechnology, sc-1616; or 1:500, Santa Cruz Biotechnology, sc-87778), anti-GAPDH (1:1,000; GeneTex, clone 1D4), anti-lamin B (1:1,000; Santa Cruz Biotechnology, sc-6217), anti-calnexin (1:500; Santa Cruz Biotechnology, sc-11397), anti-α-tubulin (1:500; Santa Cruz Biotechnology, sc-5286), anti-XBP1 (1:500; Santa Cruz Biotechnology, sc-7160), UFD1 (1:500; Abcam, ab155003), cleaved PARP1 (1:500; Cell Signaling, 9544), p-eIF2α (1:500; Cell Signaling, 3597), ATF4 (1:500; Merck Millipore, ABE387), HSP90 (1:500; Enzo, ADI-SPA-810), HSP70 (1:500; Enzo, ADI-SPA-830), HSF1 (1:500; Cell Signaling, 4356), p-HSP27 (1:1,000; Abcam, 155987), HSP27 (1:1,000; Abcam, 109376) followed by detection by secondary antibodies: goat anti-mouse IgG-HRP (GE Healthcare), goat anti-rabbit (GE Healthcare), donkey anti-goat IgG-HRP (Santa Cruz Biotechnology, sc-2020). Bound secondary antibodies were visualized by ELC detection reagent (Thermo Fisher Scientific) and images were recorded by imaging system equipped with CCD camera (ChemiDoc, Bio-Rad) operated by Image Laboratory software or developed on film (Amersham).

Immunofluorescence staining. Cells were grown in 24-well plates with a 0.170-mm glass bottom (In Vitro Scientific). Where indicated, the cells were pre-extracted before fixation with pre-extraction buffer (10 mM PIPES pH 6.8, 100 mM NaCl, 1.5 mM MgCl₂, 300 mM sucrose, 0.5% Triton X-100, 1 mM DTT, 5 µg ml⁻¹ leupeptin, 2 µg ml⁻¹ aprotinin, 0.1 mM PMSF) for 20 min at 4 °C, washed by PBS and then immediately fixed with 4% formaldehyde for 15 min at room temperature. Cells were stained with primary antibodies: anti-ubiquitylated conjugated mouse FK2 antibody (1:500; Enzo, BML-PW8810), anti-VCP (1:500; Abcam, ab11433), anti-NPL4 (1:500; Novus Bio, NBP1-82166), HSP70 (1:100; Enzo, ADI-SPA-830), HSF1 (1:500; Cell Signaling, 4356), anti-ubiquitin lys48-specific (1:500; Merck Millipore, clone Apu2), SUMO2/3 (1:500; Abcam, ab3742), TDP43 (1:300; Proteintech, 10782-2-AP) and appropriate Alexa Fluor 488- and 568-conjugated secondary antibodies (Invitrogen, 1:1,000). Cytochrome c was stained using an Alexa Fluor 555-conjugated mouse anti-cytochrome c antibody according to the manufacturer's protocol (BD Pharmingen, 558700).

Microscopy, FRAP and image analysis. Samples were analysed using a Zeiss Axioimager Z.1 platform equipped with the Elyra PS.1 super-resolution module for structured illumination (SIM) and the LSM780 module for CLSM. High resolution images were acquired in super-resolution mode using a Zeiss Pln Apo100×/1.46 oil objective (total magnification, 1,600×) with appropriate oil (Immersion 518F). SR-SIM setup involved five rotations and five phases for each image layer and up to seven z-stacks (101 nm) were acquired per image. The CLSM setup for FRAP and life cells acquisition had a c-Apo 40×/1.2 W water immersion objective. Bleaching of regions of interest (ROIs) was performed using an Argon 488 nm laser. Lower resolution images of fixed samples were acquired using a Plan Apo 63×/1.4 oil objective (total magnification 1,008×). FRAP and image acquisitions were performed using Zeiss Zen 11 software. For FRAP, internal Zen's 'Bleach'

and 'Regions' modules were used. Data from FRAP analysis involving multiple bleached ROIs were exported into Microsoft Excel and plotted. Basic processing of acquired images, such as contrast and brightness settings, was done in Adobe Photoshop on images exported as TIFFs. Quantitative microscopy-based cytometry of the immunofluorescence-stained samples was performed using an automatic inverted fluorescence microscope BX71 (Olympus) using ScanR Acquisition software (Olympus) and analysed with ScanR Analysis software (Olympus).

Cell fractionation for Triton-X100 insoluble pellets. Cells were treated as indicated, washed in cold PBS and lysed in lysis buffer (50 mM HEPES pH 7.4, 150 mM NaCl, 2 mM MgCl₂, 10% glycerol, 0.5% Triton X-100, protease inhibitor cocktail by Roche) for 10 min gently agitating at 4 °C. Then, cells were scraped into Eppendorf tubes and kept for another 10 min on ice with intermittent vortexing. After that, the lysate was centrifuged at 20,000g for 10 min at 4 °C. The insoluble fraction and supernatant were separately re-suspended in 1 × LSB buffer.

Isolation of microsomal fraction. After the desired treatment in cell culture, cells were washed with cold PBS and lysed (250 mM sucrose, 20 mM HEPES pH 7.4, 10 mM KCl, 1.5 mM MgCl₂, 1 mM EDTA, 1 mM DTT, protease inhibitor cocktail). Lysates were homogenized by Potter-Elvehjem PTFE homogenizer and kept on ice for 20 min. The homogenates were subjected to serial centrifugation steps (720g and 10,000g for 5 min each, and 100,000g for 1 h). Pellets and supernatants from the last ultracentrifugation step were resuspended in the 1 × LSB buffer and used for western blot analysis.

Immunoperoxidase staining of pre-extracted tissue sections. Frozen sections (4–5 μm thick) from xenograft-grown, cryopreserved tumour tissues were cut on a cryostat and placed on commercial adhesion slides (SuperFrost Plus, Menzel, Germany) and air-dried for 2 h at room temperature. The dried sections were carefully covered with the cold extraction buffer: 50 mM Tris-HCl (pH 7.5), 150 mM NaCl, 1 mM MgCl₂, 5% glycerol, 1 mM DTT, 1% Triton X-100, 1% IGEPAL, protease inhibitor cocktail (Phos Stop Easy pack, 04906837001, Roche) or cold PBS (controls) and incubated in a cold room for 20 min. Pre-extracted and control PBS-treated sections were gently washed three times in cold PBS, and fixed in 4% paraformaldehyde fixative for 15 min, followed by another three washes in PBS. Washed sections were then subject to a sensitive immunoperoxidase staining protocol, using the primary rabbit monoclonal antibody against VCP antibody (EPR3307(2)) (1:10,000; ab109240, Abcam) and rabbit polyclonal antibody against NPLOC4 (1:500; NBP1-82166, Novus Biologicals) and Vectastain Elite kit as secondary reagents (Vector Laboratories, USA), followed by a nickel-sulfate-enhanced diaminobenzidine reaction without nuclear counterstaining, mounted and microscopically evaluated and representative images documented by an experienced oncopathologist.

Isothermal titration calorimetry (ITC). Experiments were performed at 25 °C with a Nano ITC Low Volume (TA Instruments) and analysed by Nano Analyze Software v.2.3.6. During all measurements, injections of 2.5 μl of ligand (16 μM) were titrated into 250 μl protein (2 μM) with time intervals of 300 s, a stirring speed of 250 r.p.m. All ITC experiments were conducted with degassed buffered solutions 20 mM HEPES buffer pH 7.3, in the presence of 1% DMSO. Purified GST-NPL4(WT) and GST-NPL4(MUT) proteins were used in ITC experiment.

Drug affinity responsive target stability (DARTS). DARTS was performed according to a modified published protocol³⁸. Purified GST-NPL4(WT) and GST-NPL4(MUT) proteins were diluted by 100 mM phosphate buffer, pH 7.4 to final concentration of 0.03 μg μl⁻¹. The proteins were treated with CuET (final concentration of 5 μM; dissolved in DMSO) for 1 h and equal amounts of DMSO were added to the solutions, which served as control samples. Pronase (Sigma-Aldrich) was dissolved in TNC buffer (50 mM Tris-Cl, 50 mM NaCl, 10 mM CaCl₂, pH 7.5). The 0.025 μg of pronase was added to 50 μl of protein solution and incubated for 1 h at 37 °C. Samples without pronase served as the non-digested controls. The pronase reaction was stopped by addition of 5 × SDS loading buffer; the samples were boiled at 95 °C for 15 min and loaded on SDS-PAGE gels. After SDS-PAGE, gels were silver-stained and scanned on a GS-800 Calibrated Densitometer (Bio-Rad) or used for western blot analysis.

20S proteasome activity. To measure proteasome activity in cell extracts, cell lines were seeded in 100-mm Petri dishes at a density of 3 × 10⁶ cells per dish. After 24 h, cells were washed twice with 2 ml of ice-cold PBS and scraped in to 1,000 μl ice-cold PBS. The cells were then isolated and suspended in buffer (50 mM HEPES (pH 7.5), 150 mM NaCl, 1% Triton X-100 and 0.1 μM PMSF) and then centrifuged at 15,000 r.p.m. for 15 min at 4 °C. The cell lysates (10 μg) were incubated with 20 μM of substrates for measurement of chymotrypsin-like, trypsin-like and caspase-like activities (Suc-LLVT-AMC, Ac-RLR-AMC and Z-LLE-AMC (Boston Biochem)) in 90 μl of assay buffer (30 mM Tris-HCl, 0.035% sodium dodecylsulfate (pH 7.4)) in the presence CuET (1 μM and 5 μM) and BTZ (1 μM) for the investigation of proteasome inhibition; BTZ or an equivalent volume of solvent (DMSO) was used as a control. After 2 h of incubation at 37 °C, inhibition of proteasome activity was measured by the release of hydrolysed free AMC groups by fluorimeter at

380/460 nm (TECAN, Infinite M200PRO). To measure proteasome activity in live cells, the cells were seeded in 24-well plate at a density of 0.2 × 10⁶ cells per well. Cell lines were treated with CuET (1 μM and 5 μM), vehicle control or 1 μM BTZ for 1 h. After incubation, cells were twice washed with 0.5 ml of 1 × ice-cold PBS and scraped into 100 μl ice-cold lysis buffer and then centrifuged at 15,000 r.p.m. for 15 min at 4 °C. Subsequently, the cell extract (10 μg) was incubated with 20 μM substrates to measure chymotrypsin-like, trypsin-like and caspase-like activities in assay buffer (30 mM Tris-HCl (pH 7.4)). After 2 h of incubation at 37 °C, inhibition of proteasome enzymatic activities was measured by the release of hydrolysed free AMC as described above.

Ub(G76V)-GFP degradation. HeLa Ub(G76V)-GFP-ODD-Luc cells expressing Ub(G76V)-GFP were seeded at a density of 10⁴ cells per well in 96-well plates. The next day, cells were treated with 4 μM MG132 for 3 h. After that, the medium was discarded and cells were washed twice with PBS and then incubated with the tested compound in the presence of 30 μg ml⁻¹ cycloheximide for another 3 h. The GFP signal was acquired using an ImageXpress automated microscope. For each well, four images were taken (corresponding to 200–250 cells). Cells were analysed every 30 min during 3 h of treatment. Normalized GFP signal intensity was calculated using the following formula: (test compound – background)/(basal GFP signal intensity × background) where 'test compound' is defined as the mean GFP signal intensity of Ub(G76V)-GFP-expressing cells treated with the test compound. 'Background' is defined as the background GFP signal intensity of HeLa cells. 'Basal GFP signal intensity' is defined as mean GFP signal intensity of Ub(G76V)-GFP-expressing cells treated with DMSO. The degradation rate constant (*k*) was obtained from the slope of the linear range of plotting ln(normalized GFP signal intensity) versus time ranging from 90 to 180 min. The percentage of remaining *k* for each compound is calculated using the following formula (test compound/DMSO control) × 100.

p97 ATPase activity assay. P97 ATPase assay was performed as described previously²⁸. A total of 250 nM of p97 protein was diluted in assay buffer (50 mM Tris-HCl pH 7.4, 20 mM MgCl₂, 0.5 mM DTT). Test compounds were added in DMSO (final concentration of DMSO was 5%). After 10 min of incubation, the reaction was started with ATP (100 μM final concentration) followed by a 1-h incubation at room temperature. The reaction was stopped by adding Bioluminescence solution (Enzo) and free phosphate was measured according to the manufacturer's instructions. Results are expressed as the percentage of activity of the control (a well containing only DMSO).

26S proteasome activity. The RPN11 assay is described in PubChem (AID588493). In brief, a synthetic fluorescently labelled substrate, Ub4pepOG, was used to measure RPN11 activity. Fluorescence polarization assay was performed in a low-volume 384-well solid black plate in the presence of (i) 5 μl of the compound 1,10-phenanthroline or CuEt in 3% DMSO or 3% DMSO control; (ii) 5 μl of BioMol 26S proteasome; and (iii) 5 μl of substrate (15 nM Ub4pepOG). Fluorescence polarization is measured using a plate reader with excitation of 480 nm and emission of 520 nm filter set. The activity was normalized to DMSO control and fit to a dose-response curve.

Protein expression and purification. All proteins were expressed in *E. coli* BL21 (DE3) cells (Novagen). p97-His (pET28a vector) and Ufd1-His (pET28a vector) expression were induced by 1 mM IPTG (Life Technologies) at an OD₆₀₀ of 0.6 for 10 h at 22 °C. NPL4(WT) and NPL4(MUT) (pGEX-2TK) were induced by 0.4 mM IPTG at an OD₆₀₀ of 0.8 overnight at 16 °C. For p97 and UFD1, the bacterial pellet was suspended in buffer (50 mM Tris-HCl pH 8.0, 300 mM NaCl, 2.5 mM MgCl₂, 20 mM imidazole, 5% glycerol) and lysed by sonication and centrifuged (14,000g for 20 min). Proteins were purified by Ni-NTA chromatography (Qiagen) according to the manufacturer's instructions. For p97, the protein was further purified by gel filtration (Superdex 200, GE Healthcare). For GST-NPL4(WT) and GST-NPL4(MUT), the bacterial pellet was suspended in phosphate buffer (PBS, 0.1% Triton X-100, 300 mM NaCl) and lysed by sonication and centrifuged (14,000g for 10 min). Proteins were purified by glutathione sepharose 4B (Life Technologies) according to the manufacturer's protocol. The proteins were further purified by gel filtration (Superdex 200, GE Healthcare).

Chemicals. CuET was prepared by direct synthesis from water solutions of diethyldithiocarbamate sodium salt and copper(II) chloride as described previously⁵³. CuET for *in vivo* experiments was prepared equally with a slight modification. The reaction between diethyldithiocarbamate sodium salt and copper(II) chloride was performed in a sterile 1% aqueous solution of bovine serum albumin. The resulting solution was used directly. The following chemicals were purchased from commercial vendors: tetraethylthiuram disulfide (disulfiram, DSF) (Sigma-Aldrich), sodium diethyldithiocarbamate trihydrate (Sigma-Aldrich), copper D-gluconate (Sigma-Aldrich), BTZ (Velcade, Janssen-Cilag International N.V.), MG132 (Sigma-Aldrich), DBE-Q (Sigma-Aldrich), NMS873 (Abmole), cycloheximide (Sigma-Aldrich), dicoumarol (Sigma-Aldrich), 1,10-phenanthroline (Sigma) and MLN7243 (Active Biochem).

Statistical analyses and reproducibility. For the epidemiological study, we calculated hazard ratios and 95% confidence intervals estimating cancer-specific mortality, based on a Cox model regressing of both propensity scores and disulfiram use, balancing baseline characteristics of previous and continuing users of DSF and adjusting estimated hazard ratios of cancer-specific mortality associated with DSF use⁵¹. The propensity score estimates were conditional on multiple covariates, based on using logistic regression (see 'Epidemiological analyses and access to health registers' for specifics of cohorts and covariates). In the Cox model, the propensity score is further included as a restricted cubic spline to model possible nonlinearities, in addition to the categorical disulfiram use as the variable of interest. Statistical significance of DSF use was evaluated by likelihood ratio tests, using the software R for statistical computing⁵².

For evaluation of the animal studies, STATISTICA software, v.12 (StatSoft) was used to estimate sample size. For a power of 80%, the level of significance set at 5%, 4 groups and RMSSE = 0.8, seven mice per group were estimated. For usage of non-parametrical statistical methods, the number of eight mice per group was finally planned. The differences between tumour volumes were statistically analysed by non-parametrical Kruskal–Wallis test, not requiring any assumptions of normality and homoscedascity. To test the effect of CuET treatment on survival of AMO-1-xenografted mice, a Kaplan–Meier graph and log-rank statistical test were

used. For other experiments, the statistics, such as number of repetitions, centre value and error bars, are specified in figure legends.

Data availability. Most data generated or analysed during this study are included in the article and its Supplementary Information. Uncropped images of all gels and blots can be found in Supplementary Fig. 1. Source Data for all graphs are provided in the online version of the paper. Additional datasets generated during and/or analysed during the current study and relevant information are available from the corresponding authors upon reasonable request.

50. Thygesen, L. C., Daasnes, C., Thaulow, I. & Brønnum-Hansen, H. Introduction to Danish (nationwide) registers on health and social issues: structure, access, legislation, and archiving. *Scand. J. Public Health* **39** (Suppl), 12–16 (2011).
51. Rosenbaum, P. R. & Rubin, D. B. The central role of the propensity score in observational studies for causal effects. *Biometrika* **70**, 41–55 (1983).
52. R Core Team. *R: A language and environment for statistical computing*. R Foundation for Statistical Computing <https://www.R-project.org/> R v.3.2.3 (2015-12-10) (R Foundation for Statistical Computing, 2016).
53. Cvek, B., Milacic, V., Taraba, J. & Dou, Q. P. Ni(II), Cu(II), and Zn(II) diethyldithiocarbamate complexes show various activities against the proteasome in breast cancer cells. *J. Med. Chem.* **51**, 6256–6258 (2008).

APPENDIX B

Skrott Z, Cvek B. Linking the activity of bortezomib in multiple myeloma and autoimmune diseases. *Crit Rev Oncol Hematol.* 2014 Nov;92(2):61-70. IF₍₂₀₁₄₎: 4.027

Linking the activity of bortezomib in multiple myeloma and autoimmune diseases

Zdeněk Škrott, Boris Cvek*

Department of Cell Biology and Genetics, Faculty of Science, Palacky University, Slechtitelu 11, 78371 Olomouc, Czech Republic

Accepted 2 May 2014

Contents

1. Introduction.....	61
2. Mechanism of action of bortezomib <i>in vitro</i>	62
3. Discrepancy between preclinical and clinical evaluations.....	62
4. Bortezomib's activity in immunological disorders.....	63
5. Proteostasis as a determining factor of sensitivity to bortezomib.....	64
6. Bortezomib resistance.....	64
7. Conclusions.....	66
Conflict of interest statement.....	66
Reviewers.....	66
Acknowledgments.....	66
References.....	66
Biographies.....	70

Abstract

Since their introduction to the clinic 10 years ago, proteasome inhibitors have become the cornerstone of anti-multiple myeloma therapy. Despite significant progress in understanding the consequences of proteasome inhibition, the unique activity of bortezomib is still unclear. Disappointing results from clinical trials with bortezomib in other malignancies raise the question of what makes multiple myeloma so sensitive to proteasome inhibition. Successful administration of bortezomib in various immunological disorders that exhibit high antibody production suggests that the balance between protein synthesis and degradation is a key determinant of sensitivity to proteasome inhibition because a high rate of protein production is a shared characteristic in plasma and myeloma cells. Initial or acquired resistance to bortezomib remains a major obstacle in the clinic as *in vitro* data from cell lines suggest a key role for the $\beta 5$ subunit mutation in resistance; however the mutation was not found in patient samples. Recent studies indicate the importance of selecting for a subpopulation of cells that produce lower amounts of paraprotein during bortezomib therapy.

© 2014 Elsevier Ireland Ltd. All rights reserved.

Keywords: Multiple myeloma; Bortezomib; Resistance; Ubiquitin-proteasome system; Autoimmune diseases; Proteostasis

1. Introduction

More than 10 years ago, the FDA (US Food and Drug Administration) approved a first-in-class proteasome

inhibitor, bortezomib (Velcade), for the treatment of refractory and relapsed multiple myeloma. Subsequently, proteasome inhibition-based regimens have become a front-line therapeutic strategy for multiple myeloma patients [1]. Bortezomib, formerly known as PS-341, was first described as an inhibitor of inflammation [2], but its strong cytotoxic effect toward tumor cell lines changed the research

* Corresponding author. Tel.: +420 585634904.

E-mail address: cvekb@seznam.cz (B. Cvek).

focus of this drug to cancer therapy. Preclinical investigations and phase 1 trial results suggested that some malignancies, including multiple myeloma, appeared to be sensitive to bortezomib treatment [3,4]. After these initial studies, phase 2 trials [5,6] confirmed the positive effect on multiple myeloma patient survival, and bortezomib treatment progressed to a phase 3 trial, in which the superiority of bortezomib over the standard of care was demonstrated [7]. Although originally approved as a single agent, bortezomib is currently used predominantly in combination with other drugs [8]. The high occurrence of initial and acquired resistance to bortezomib treatment accelerated the development of a second generation of proteasome inhibitors with improved activity and safety profiles. Recently, the FDA approved a new proteasome inhibitor, carfilzomib (Kyprolis), for the treatment of refractory and relapsed multiple myeloma patients who have received at least two prior therapies [9,10], and proteasome inhibitors developed by other groups have entered clinical trials [11–13].

Multiple myeloma is not the only malignancy treatable with bortezomib. It has been approved as a second-line therapy also for mantle cell lymphoma [14], and has shown promising activity in Waldenström's macroglobulinemia as a single agent [15,16] or as part of a combination therapy [17] for MALT lymphoma [18,19] and cutaneous T-cell lymphoma [20]. Preclinical studies suggested bortezomib as a favorable candidate for the treatment of solid tumors; however, these promising results did not translate to the clinic [21]. Negative results from most of the clinical trials with non-hematological and even hematological tumors raised the question of what makes multiple myeloma so sensitive to proteasome inhibition. This question is still not fully understood; however, significant progress in recent years has brought new light to the unique mechanism of bortezomib activity in multiple myeloma.

2. Mechanism of action of bortezomib *in vitro*

It is generally believed that the ubiquitin-proteasome system (UPS) is responsible for the degradation of the majority of cellular proteins. Prior to destruction, proteins are usually marked by a polyubiquitin chain that serves as a recognition signal for proteasomes [22]. The constitutive 26S proteasome is composed of a regulatory 19S particle that mediates substrate recognition, deubiquitination, unfolding, and protein hydrolysis by the 20S core particle. The 20S proteasome contains three proteolytic subunits: $\beta 1$, $\beta 2$, and $\beta 5$ ($\beta 5$ is inhibited by bortezomib) with caspase-, trypsin-, and chymotrypsin-like activity, respectively [23]. In addition to inhibiting the $\beta 5$ subunit, high concentrations of bortezomib also target the $\beta 1$ subunit expressing caspase-like activity, with a minimal effect on the trypsin-like activity of $\beta 2$ [24].

Proteasome-mediated protein degradation is a fundamental process for maintaining the viability and homeostasis of the cell. In addition to degrading short-lived regulatory

proteins, the proteasome prevents the accumulation of non-functional, damaged or misfolded and thus potentially toxic proteins. Moreover, the role of the UPS is not limited to proteolysis but also includes the involvement in multiple signaling cascades, cell cycle control, and DNA-damage response [25]. Not surprisingly, by inhibiting the proteasome, bortezomib has profound effects on a multitude of cellular processes, some of which may contribute to its anti-cancer activity. Bortezomib has been shown to cause the accumulation of the cell cycle inhibitors p21 and p27 [26,27] and to induce Bcl-2 protein family and p53-dependent or -independent apoptosis [28–31]. As mentioned above, bortezomib was first described to suppress inflammation through the inhibition of NF- κ B, a key pro-inflammatory and tumor promoting transcription factor [32]. Inactive NF- κ B is bound by inhibitory protein I- κ B, sequestering NF- κ B to its cytoplasmic localization. Upon activation, I- κ B is ubiquitinated and subsequently degraded in the proteasome, thus allowing NF- κ B to translocate to the nucleus and induce the transcription of genes involved in proliferation, angiogenesis, or the suppression of apoptosis [33]. As expected, bortezomib treatment leads to the accumulation of I- κ B, inhibition of NF- κ B nuclear translocation, and suppression of target genes, which has been confirmed in multiple myeloma [34] and other cancer cell lines [35–38]. NF- κ B is often overexpressed [39–41] and constitutively active in multiple myeloma, providing the rationale for bortezomib treatment; thus, NF- κ B inhibition was believed to be predominantly responsible for the anti-cancer activity of bortezomib [42].

In addition, by mediating the degradation of misfolded proteins by ERAD (endoplasmic reticulum-associated degradation), proteasomes prevent cells from ER-stress and the unfolded-protein response (UPR) [43], which triggers apoptosis if unmitigated [44]. Not surprisingly, bortezomib treatment induced terminal UPR in various cancer cell lines [45–47], including multiple myeloma [48,49], revealing another important aspect of the mechanism of action of bortezomib.

3. Discrepancy between preclinical and clinical evaluations

As mentioned above, bortezomib activity in multiple myeloma was believed to be related to the transcription factor NF- κ B from the beginning of its clinical use. The proteasome is required for both canonical and non-canonical NF- κ B activation [50], and as NF- κ B is frequently upregulated in multiple myeloma and further increased upon chemotherapy, the efficacy of bortezomib was generally explained by the inhibition of the transcription factor. Indeed, tumors containing an activating mutation in NF- κ B signaling appeared to have a better response to proteasome inhibitors [39]. However, further studies made this assumption more questionable. First, in an intestinal epithelial cell line, various proteasome inhibitors, including MG-132 or lactacystin, not only failed

to inhibit NF- κ B but activated IKK kinase phosphorylation of I- κ B, thus inducing its degradation, which led to the nuclear translocation of NF- κ B [51]. Second, pharmacological inactivation of NF- κ B by the selective IKK inhibitor PS-1145 displayed lower toxic effects on multiple myeloma cells compared to bortezomib treatment, possibly indicating that NF- κ B inhibition only accounts for a fraction of bortezomib's cell-killing activity [52]. Finally, Hideshima et al. illustrated that bortezomib and other proteasome inhibitors significantly inhibit I- κ B expression, induce IKK kinase, and activate the canonical NF- κ B pathway in primary multiple myeloma cell lines. Moreover, co-treatment of cells with bortezomib and IKK inhibitors potentiated bortezomib anticancer effect [53]. Together, these results argue against a critical role for NF- κ B inhibition in bortezomib's mechanism of action on multiple myeloma, and suggest the need for another explanation.

In preclinical studies with cell lines derived from a wide range of solid tumors, low concentrations of bortezomib have been shown to be toxic for most of the cell lines *in vitro* and in mouse xenografts [54,55]. Unexpectedly, bortezomib failed as a monotherapy in almost all phase 2 clinical trials with non-hematological malignancies [56]. One possible explanation for this obvious discrepancy may be that cancer cell lines differ from their counterparts in tissues in important aspects [57]; this type of affected process could be the global turnover rate of cellular proteins. Comparative transcriptomic and proteomic studies revealed a significantly upregulated expression of genes involved in protein synthesis and degradation, including proteasomes, in cultured cell lines compared to tumor tissue or primary cells [58,59]. Most of the upregulated genes in the cultured cell lines were associated with higher proliferation rates, where macromolecule processing and the degradation machinery play a critical role [60]. These findings provide a possible reason for why cell lines are so sensitive to proteasome inhibition and proteotoxic stress compared to tumor tissues. Another explanation for such disappointing results in clinical trials is insufficient drug delivery and thus poor proteasome inhibition in solid and poorly accessible tumors. Indeed, according to a study in mice [61], proteasome inhibition and the anticancer effect of bortezomib negatively correlates with tumor vascularization and architecture. An additional possibility is that solid tumors may be primarily resistant to the relatively short and mild proteasome inhibition that is clinically achievable with bortezomib, as higher drug doses and inhibition would likely lead to serious adverse effects [62].

New light could be shed on to this question with the second-generation proteasome inhibitor ixazomib, also called MLN9078 [63], which showed better pharmacodynamics compared to bortezomib in preclinical solid tumor-derived xenograft models [64]. The improvement is likely due to better physicochemical properties of ixazomib, namely, a shorter half-life of proteasome dissociation, enabling the molecule to be more sufficiently distributed into tissues, sustaining its inhibitory activity [64]. The anticancer activity of ixazomib, already confirmed in

preclinical studies [65,66] and even in clinical trials [67,68] with multiple myeloma, has also been evaluated in a phase 1 study with non-hematological malignancies [69]. Ixazomib was present in all tumor biopsies, and 86% of them showed a significant post-treatment accumulation of ATF-3, a marker of the unfolded-protein response [69]. These results bring promises to the further investigation of novel proteasome inhibitors for the management of solid tumors despite the poor activity of carfilzomib against various solid tumors in phase 1/2 clinical trial [70].

Notwithstanding the future of new proteasome inhibitors in the treatment of solid tumors, the sharp contrast in the activity of bortezomib toward multiple myeloma and other non-hematological malignancies may reveal critical characteristics for determining tumor sensitivity to proteasome inhibition. Importantly, multiple myeloma is not the only disease treatable with bortezomib, as bortezomib was also successfully used therapeutically for some immunological disorders [71]. Clinical features shared by both groups of relatively distinct illnesses may help us to understand the mechanism of bortezomib's action in a more detailed manner.

4. Bortezomib's activity in immunological disorders

As it becomes clearer that it is mainly the high-rate of protein production that determines the sensitivity of certain cell types to proteasome inhibition, bortezomib has been suggested to specifically target non-malignant cells. Plasma cells and their neoplasms are known to produce and secrete extremely high amount of antibodies, *i.e.*, >3000 molecules/cell/second, and the upregulation of the proteins involved in ER stress and UPR indicates a strong dependency of plasma cells on sufficient protein degradation [71,72]. Importantly, plasma cells, especially long-lived ones, play a key role in several antibody-mediated autoimmune diseases, such as systemic lupus erythematosus (SLE) [73], myasthenia gravis (MG) [74] or autoimmune hemolytic anemia [75], and as non-proliferating cells, they are particularly difficult to target pharmacologically [76]. In preclinical models, bortezomib and other proteasome inhibitors have been successfully used in SLE-like mice [77–80], experimental autoimmune MG rats [81] and experimental hemophilia-A mice that develop anti-factor VIII antibodies [82]. In the SLE model, bortezomib depleted both short-lived and long-lived plasma cells by the activation of terminal UPR, reduced dsDNA-specific antibodies and prolonged the survival of mice. Similar bortezomib activity toward plasma cells was confirmed in others studies, highlighting the promises of clinical application of proteasome inhibitors in these types of disorders. More importantly, based on a few case reports and some small trials (summarized in Ref. [71]), it seems that bortezomib can be used in clinical practice, bringing benefits to patients with rheumatoid arthritis, autoimmune hemolytic anemia or SLE. The most discussed and extensively studied application of bortezomib is most likely in recipients of

renal transplantation to prevent antibody-mediated rejection [83]. Interestingly, the efficacy of bortezomib treatment was also confirmed in less frequent diseases. For example, bortezomib induced complete and partial responses in TEMPI syndrome [84], a recently described illness that has characteristics that include monoclonal gammopathy of IgG κ , suggesting a critical role for paraprotein in the pathophysiology of the syndrome [85]. Additionally, treatment with bortezomib resulted in a rapid clinical response in a patient with refractory thrombotic thrombocytopenic purpura associated with the depletion of inhibitory autoantibodies against ADAMTS13, a metalloproteinase that cleaves the von Willebrand factor, which is produced by plasma cells [86].

In summary, based on the efficacy of bortezomib against the diseases mentioned above, which share the characteristic of a high-rate antibody production, it seems highly probable that the excessive production of proteins and thus a strong need to efficiently degrade the damaged and misfolded ones determines the sensitivity of certain cell types, including multiple myeloma cells, to proteasome inhibition.

5. Proteostasis as a determining factor of sensitivity to bortezomib

Based on transcriptomic and proteomic studies, it seems that the proteasome level is markedly upregulated in a vast majority of cancers [87–90]. Despite tight co-regulation in these cancers, there are also some differences in the proteasome pool or overall activity, and interestingly, a consistently higher proteasome activity was found in two of three breast cancer cell lines that were relatively more resistant to bortezomib [91]. In line with these results, the balance between the proteasomal load *versus* its capacity determines the sensitivity of multiple myeloma cells to proteasome inhibitors [92].

Proteasome expression varies among established cell lines or primary patient-derived clones and a lower proteasome level is negatively correlated with the workload, resulting in higher stress and thus a higher sensitivity to bortezomib [92]. Importantly, even different rates of antibody synthesis can determine the sensitivity of multiple myeloma cells to proteasome inhibition, and an increase in Ig synthesis further sensitizes these cells to bortezomib [93]. In addition, protein synthesis imposes a large burden on proteasome-dependent degradation, as almost 30% of newly synthesized proteins are immediately degraded by the proteasome [94,95]; hence, both sides of proteostasis, *i.e.*, protein synthesis and degradation, contribute to determine the sensitivity of certain cell types to proteasome inhibitors [96]. Interestingly, plasma cells lose a significant portion of their proteasome expression during differentiation, whereas antibody synthesis increases, resulting in imbalanced proteostasis, suggesting the involvement of the exquisite sensitivity of plasma cells to proteasome inhibition [77,97]. These results indicate a rationale for combining proteasome inhibitors with other ER-stressors,

such as HDAC inhibitors [98,99], p97 inhibitors [100] or HSPs inhibitors [101] to increase sensitivity or to overcome resistance. This approach has been successful for multiple myeloma and others malignancies [102,103].

6. Bortezomib resistance

The introduction of proteasome inhibitor bortezomib and the immunomodulatory agent thalidomide to the clinic resulted in the prolonged overall survival of multiple myeloma patients, with a portion of these patients sustaining remission for many years [104]. Despite these improvements, initial and acquired resistance still represents a major challenge because a majority of patients suffer from relapse. Although the recently approved agents carfilzomib and pomalidomide have brought promise to overcome drug resistance [9,105], there is a strong need to identify the physiological mechanisms underlying this critical but poorly understood area. There are many hypotheses to explain resistance to proteasome inhibition, including the altered accumulation of pro-apoptotic proteins Noxa and Bim or the activation of the AKT pathway [106]. However, the most discussed mechanism behind acquired resistance to bortezomib is the up-regulation or mutation of proteasome subunits [107]. This type of data comes from many recent studies (reviewed in Ref. [107]) elucidating bortezomib resistance in several cancer cell lines by continued exposure to the drug. The most prominent feature observed in these types of experiments was a mutation in the bortezomib-binding pocket of the β 5 subunit of the proteasome core particle harboring CT-like activity. Several mutations of the PSMB5 gene expressing β 5 were described, usually leading to the improper binding of the drug and thus insufficient target inhibition [108–110]. Additionally, bortezomib-resistant cell lines generated by continuous exposure to the drug often express a high amount of the β 5 subunit, suggesting another mechanism of resistance to proteasome inhibition. This mechanism for the development of resistance was described for multiple myeloma cell lines and cell lines derived from a variety of other hematological and non-hematological malignancies [110–113]. Despite thorough verification, under experimental conditions, the clinical relevance of the PSMB5 mutation or overexpression of the β 5 subunit remains largely unclear.

Recently, a study [114] with patients participating in an APEX clinical trial treated with single agent bortezomib or high dose dexametasonone has brought light to the poorly understood area of clinical resistance to bortezomib. This study addressed whether variations in the PSMB5 gene determine initial or acquired resistance to bortezomib and whether they affect long-term outcomes of treatment. Interestingly, the genotype frequency of non-synonymous SNPs (single nucleotide polymorphism) in PSMB genes in pre- and post-treatment multiple myeloma samples did not differ from the average population and no unique non-synonymous SNPs were found in post-treatment samples, including patients who

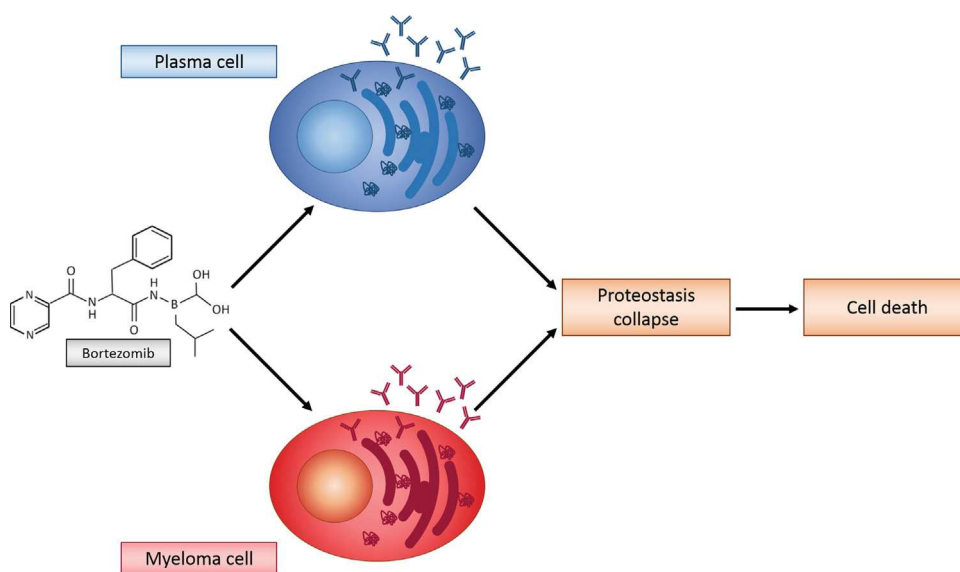


Fig. 1. The high-rate production of antibodies determines the sensitivity of plasma and myeloma cells to bortezomib.

were initially sensitive to bortezomib and then relapsed after prolonged therapy. The study also did not find any correlation between SNP variants of the PMSB5 gene and resistance or clinical outcome, supporting the previous observation [115]. Moreover, the PSMB5 A108T variant commonly found in many bortezomib-resistant cell lines was not observed in any of the pre- or post-treatment samples collected from 10 patients deemed relatively insensitive to bortezomib or from 6 patients who were initially sensitive but relapsed prior to sample collection [114]. The results from this study suggest that acquired resistance to bortezomib is not linked to the PSMB5 gene variants and indicate a different mechanism.

As bortezomib-induced apoptosis is associated with a terminal unfolded-protein response, it has been suggested [115,116] that aggresome formation, which normally sequesters ubiquitinated misfolded proteins and leads them to autophagy-mediated degradation, helps cells to survive while under proteasome inhibition. Interestingly, HDAC inhibitors, abrogating the formation of aggresomes, exhibit synergistic cell-killing activity with bortezomib and are able to overcome bortezomib resistance [98,117]. In accordance with these pre-clinical results, several clinical trials in phase 1 or 2 with the pan-HDAC inhibitors vorinostat or panobinostat revealed significant responses in heavily pretreated patients, even those who were bortezomib-refractory [99,118,119]. The ability of HDAC inhibitors to overcome resistance to bortezomib, both in experimental models and in patients, suggests a critical role for the impaired accumulation of ubiquitinated proteins in the acquired resistance to proteasome inhibition.

As multiple myeloma cells and their physiological counterparts, plasma cells, produce high amounts of immunoglobulin, it is not surprising that they depend on ERAD (endoplasmic reticulum-associated degradation),

which is impeded by proteasome inhibitors (Fig. 1). It seems probable that the elevated secretion of antibodies is a critical factor underlying the unique sensitivity of multiple myeloma to proteasome inhibition in the clinic. It is also possible that the insufficient production of immunoglobulin proteins mediates the resistance to bortezomib. Indeed, it has been reported that bortezomib-resistant cell lines secrete lower levels of proteins than bortezomib-sensitive ones [92]. In a mouse model of multiple myeloma, bortezomib treatment led to a selection of CD93 and CD69 negative cells, which correspond to mature B cells expressing fewer Ig molecules than CD93 and CD69 positive plasma cells. Moreover, bortezomib-sensitive cells are predominantly CD93 and CD69 positive, whereas the resistant cells are CD93 and CD69 negative (irrespective if primarily or secondary). Additionally, LPS-prompted plasma cell maturation re-sensitized bortezomib-resistant cells, accompanied by the increased production of Ig and the expression of CD93 and CD69 markers [120] (supporting a previous study [121] in which 2-methoxyestriol induced plasma cell maturation to overcome resistance to bortezomib). Notably, CD93 has been revealed as a biomarker of outcome in multiple myeloma patients [120].

The crucial role of plasma cell maturation in acquired resistance to bortezomib has been supported in a recently published study [122]. Using tumor samples from multiple myeloma patients, the authors showed Xbp1s, a mediator of UPR and plasma cell maturation, to be involved in clinical resistance to bortezomib (Fig. 2). In accordance with the requirement for Xbp1s signaling for bortezomib toxicity *in vitro* [121,122], Xbp1s is suppressed in bortezomib-refractory primary cells [121], and Xbp1s level correlates with patient outcome [123]. Moreover, Xbp1s negative cells, which correspond to multiple myeloma B cells or

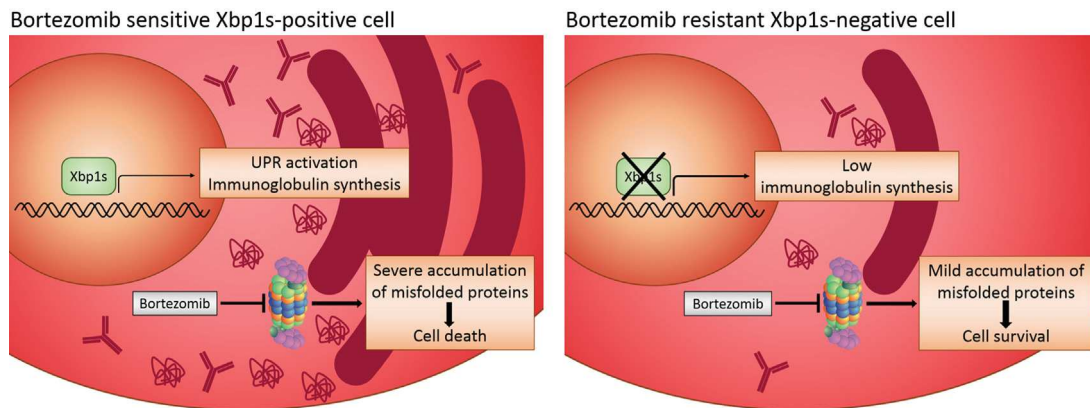


Fig. 2. *The role of Xbp1s in clinical resistance to bortezomib.* Xbp1s induces genes involved in immunoglobulin production and UPR related to organelle biogenesis, protein folding and ERAD. As Xbp1s positive myeloma cells produce high amounts of immunoglobulin, they depend on ERAD, which is impeded by bortezomib. Xbp1s negative myeloma cells produce less immunoglobulins and exhibit less basal ER-stress, which makes them more vulnerable when ERAD is inhibited by bortezomib. UPR-unfolded protein response; ERAD-endoplasmic reticulum-associated degradation.

pre-plasmablasts, are enriched in bortezomib-refractory samples and seem to survive therapeutic application of bortezomib. A subpopulation of Xbp1s negative cells express lower amounts of Ig and exhibits fewer UPR markers, suggesting decreased ER-stress and less dependency on the UPR pathway than Xbp1s positive plasma cells [122]. Whereas no PMSB5 mutation was identified in 20 tumor samples, two Xbp1 mutations were observed [124]. Together, these results are of great importance, indicating that resistance to bortezomib may be reversible and highlighting the need for a new drug able to specifically target a selected Xbps1 negative population after bortezomib treatment.

7. Conclusions

In summary, a growing body of evidence suggests that the ratio of protein synthesis and degradation is a critical determinant of the initial sensitivity to bortezomib-containing therapies, and importantly, this ratio may also play a role in the mechanisms conferring acquired resistance. Successful administration of bortezomib in various immunological diseases together with an improved dose schedule and subcutaneous administration of bortezomib resulting in less neurotoxicity opens the door for the introduction of proteasome inhibitors to other non-malignant disorders. Despite the fact that carfilzomib, alternative proteasome inhibitors ab-154 [125] and RA190 [126] or a USP7 specific inhibitor [127] are able to overcome the resistance to bortezomib in experimental studies, the clinical experience with recently approved carfilzomib and ongoing trials with various proteasome inhibitors will most likely uncover the future of management of bortezomib-refractory patients. Recent studies emphasize the application of next generation of ER-stressors, such as proteasome or HDAC inhibitors, or alternative treatment approaches that are able to kill the bortezomib-selected population of pre-plasmablasts.

Conflict of interest statement

The author declares no conflict of interest.

Reviewers

Dr Rodger Tiedemann, Hematology/Oncology, Princess Margaret Hospital, Toronto, ON, M5G 2C1, Canada.

Simone Cenci, M.D., Staff Scientist, San Raffaele Scientific Institute, Genetics and Cell Biology, Via Olgettina 58, I-20132 Milano, Italy.

Acknowledgments

This work was financed by project OP VK CZ.1.07/2.3.00/20.0062 ‘An inexpensive drug Antabuse as anticancer remedy: mechanism of action and clinical trials’ from resources of European Union and the Czech Republic.

References

- [1] Moreau P, Richardson PG, Cavo M, Orłowski RZ, San Miguel JF, Palumbo A, Harousseau JL. Proteasome inhibitors in multiple myeloma: 10 years later. *Blood* 2012;120(5):947–59.
- [2] Palombella VJ, Conner EM, Fuseler JW, et al. Role of the proteasome and NF-kappaB in streptococcal cell wall-induced polyarthritis. *Proc Natl Acad Sci USA* 1998;95(26):15671–6, 22.
- [3] Aghajanian C, Soignet S, Dizon DS, et al. A phase I trial of the novel proteasome inhibitor PS341 in advanced solid tumor malignancies. *Clin Cancer Res* 2002;8(8):2505–11.
- [4] Orłowski RZ, Stinchcombe TE, Mitchell BS, et al. Phase I trial of the proteasome inhibitor PS-341 in patients with refractory hematologic malignancies. *J Clin Oncol* 2002;20(22):4420–7.
- [5] Richardson PG, Barlogie B, Berenson J, Singhal S, Jagannath S, Irwin D, Rajkumar SV, Srkalovic G, Alsina M, Alexanian R, Siegel D, Orłowski RZ, Kuter D, Limentani SA, Lee S, Hideshima T, Esseltine

- DL, Kauffman M, Adams J, Schenkein DP, Anderson KC. A phase 2 study of bortezomib in relapsed, refractory myeloma. *N Engl J Med* 2003;348(26):2609–17.
- [6] Jagannath S, Barlogie B, Berenson J, et al. A phase 2 study of two doses of bortezomib in relapsed or refractory myeloma. *Br J Haematol* 2004;127(2):165–72.
- [7] Richardson PG, Sonneveld P, Schuster MW, et al. Bortezomib or high-dose dexamethasone for relapsed multiple myeloma. *N Engl J Med* 2005;352(24):2487–98.
- [8] Kouroukis CT, Baldassarre FG, Haynes AE, Imrie K, Reece DE, Cheung MC. Bortezomib in multiple myeloma: a practice guideline. *Clin Oncol (R Coll Radiol)* 2014;26(2):110–9.
- [9] Herndon TM, Deisseroth A, Kaminskas E, et al. U.S. Food and Drug Administration approval: carfilzomib for the treatment of multiple myeloma. *Clin Cancer Res* 2013;19(17):4559–63.
- [10] Kortuem KM, Stewart AK. Carfilzomib. *Blood* 2013;121(6):893–7.
- [11] Richardson PG, Spencer A, Cannell P, et al. Phase 1 clinical evaluation of twice-weekly marizomib (NPI-0052), a novel proteasome inhibitor, in patients with relapsed/refractory multiple myeloma (MM). *Blood* 2011;118(21):140–1.
- [12] Berdeja JG, Richardson PG, Lonial S, et al. Phase 1/2 study of oral MLN9708, a novel, investigational proteasome inhibitor, in combination with lenalidomide and dexamethasone in patients with previously untreated multiple myeloma (MM). *Blood* 2011;118(21):223.
- [13] Richardson PG, Baz R, Wang L, et al. Investigational agent MLN9708, an oral proteasome inhibitor, in patients (pts) with relapsed and/or refractory multiple myeloma (MM): results from the expansion cohorts of a phase 1 dose-escalation study. *Blood* 2011;118(21):140.
- [14] Kane RC, Dagher R, Farrell A, et al. Bortezomib for the treatment of mantle cell lymphoma. *Clin Cancer Res* 2007;13(18):5291–4.
- [15] Chen CI, Kouroukis CT, White D, et al. Bortezomib is active in patients with untreated or relapsed Waldenström's macroglobulinemia: a phase II study of the National Cancer Institute of Canada Clinical Trials Group. *J Clin Oncol* 2007;25(12):1570–5.
- [16] Treon SP, Hunter ZR, Matous J, et al. Multicenter clinical trial of bortezomib in relapsed/refractory Waldenström's macroglobulinemia: results of WMCTG Trial 03-248. *Clin Cancer Res* 2007;13(11):3320–5.
- [17] Dimopoulos MA, García-Sanz R, Gavratiopoulou M, et al. Primary therapy of Waldenström macroglobulinemia (WM) with weekly bortezomib, low-dose dexamethasone, and rituximab (BDR): long-term results of a phase 2 study of the European Myeloma Network (EMN). *Blood* 2013;122(19):3276–82.
- [18] Troch M, Jonak C, Müllauer L, et al. A phase II study of bortezomib in patients with MALT lymphoma. *Haematologica* 2009;94(5):738–42.
- [19] Conconi A, Martinelli G, Lopez-Guillermo A, et al. Clinical activity of bortezomib in relapsed/refractory MALT lymphomas: results of a phase II study of the International Extranodal Lymphoma Study Group (IELSG). *Ann Oncol* 2011;22(3):689–95.
- [20] Zinzani PL, Musuraca G, Tani M, et al. Phase II trial of proteasome inhibitor bortezomib in patients with relapsed or refractory cutaneous T-cell lymphoma. *J Clin Oncol* 2007;25(27):4293–7.
- [21] Cvek B. Proteasome inhibitors. *Prog Mol Biol Transl Sci* 2012;109:161–226.
- [22] Finley D. Recognition and processing of ubiquitin-protein conjugates by the proteasome. *Annu Rev Biochem* 2009;78:477–513.
- [23] Cvek B, Dvorak Z. The ubiquitin-proteasome system (UPS) and the mechanism of action of bortezomib. *Curr Pharm Des* 2011;17(15):1483–99.
- [24] Dick LR, Fleming PE. Building on bortezomib: second-generation proteasome inhibitors as anti-cancer therapy. *Drug Discovery Today* 2010;15(5-6):243–9.
- [25] Goldberg AL. Protein degradation and protection against misfolded or damaged proteins. *Nature* 2003;426:895–9.
- [26] Hideshima T, Richardson P, Chauhan D, et al. The proteasome inhibitor PS-341 inhibits growth, induces apoptosis, and overcomes drug resistance in human multiple myeloma cells. *Cancer Res* 2001;61(7):3071–6.
- [27] Chen Q, Xie W, Kuhn DJ, et al. Targeting the p27 E3 ligase SCF(Skp2) results in p27- and Skp2-mediated cell-cycle arrest and activation of autophagy. *Blood* 2008;111(9):4690–9.
- [28] Hideshima T, Mitsiades C, Akiyama M, et al. Molecular mechanisms mediating antimyeloma activity of proteasome inhibitor PS-341. *Blood* 2003;101(4):1530–4.
- [29] Mitsiades N, Mitsiades CS, Poulaki V, et al. Molecular sequelae of proteasome inhibition in human multiple myeloma cells. *Proc Natl Acad Sci USA* 2002;99(22):14374–9.
- [30] Pei XY, Dai Y, Grant S. The proteasome inhibitor bortezomib promotes mitochondrial injury and apoptosis induced by the small molecule Bcl-2 inhibitor HA14-1 in multiple myeloma cells. *Leukemia* 2003;17(10):2036–45.
- [31] Qin JZ, Ziffra J, Stennett L, et al. Proteasome inhibitors trigger NOXA-mediated apoptosis in melanoma and myeloma cells. *Cancer Res* 2005;65(14):6282–93.
- [32] Karin M. Nuclear factor- κ B in cancer development and progression. *Nature* 2006;441(7092):431–6.
- [33] Hayden MS, Ghosh S. Shared principles in NF- κ B signaling. *Cell* 2008;132(3):344–62.
- [34] Hideshima T, Chauhan D, Schlossman R, Richardson P, Anderson KC. The role of tumor necrosis factor- α in the pathophysiology of human multiple myeloma: therapeutic applications. *Oncogene* 2001;20(33):4519–27.
- [35] Allen C, Saigal K, Nottingham L, Arun P, Chen Z, Van Waes C. Bortezomib-induced apoptosis with limited clinical response is accompanied by inhibition of canonical but not alternative nuclear factor κ B subunits in head and neck cancer. *Clin Cancer Res* 2008;14(13):4175–85.
- [36] Jazirehi AR, Economou JS. Proteasome inhibition blocks NF- κ B and ERK1/2 pathways, restores antigen expression, and sensitizes resistant human melanoma to TCR-engineered CTLs. *Mol Cancer Ther* 2012;11(6):1332–41.
- [37] Pham LV, Tamayo AT, Yoshimura LC, Lo P, Ford RJ. Inhibition of constitutive NF- κ B activation in mantle cell lymphoma B cells leads to induction of cell cycle arrest and apoptosis. *J Immunol* 2003;171(1):88–95.
- [38] Bersani F, Taulli R, Accornero P, et al. Bortezomib-mediated proteasome inhibition as a potential strategy for the treatment of rhabdomyosarcoma. *Eur J Cancer* 2008;44(6):876–84.
- [39] Keats JJ, Fonseca R, Chesi M, et al. Promiscuous mutations activate the noncanonical NF- κ B pathway in multiple myeloma. *Cancer Cell* 2007;12(2):131–44.
- [40] Annunziata CM, Davis RE, Demchenko Y, et al. Frequent engagement of the classical and alternative NF- κ B pathways by diverse genetic abnormalities in multiple myeloma. *Cancer Cell* 2007;12(2):115–30.
- [41] Demchenko YN, Glebov OK, Zingone A, Keats JJ, Bergsagel PL, Kuehl WM. Classical and/or alternative NF- κ B pathway activation in multiple myeloma. *Blood* 2010;115(17):3541–52.
- [42] Orłowski RZ, Kuhn DJ. Proteasome inhibitors in cancer therapy: lessons from the first decade. *Clin Cancer Res* 2008;14(6):1649–57.
- [43] Smith MH, Ploegh HL, Weissman JS. Road to ruin: targeting proteins for degradation in the endoplasmic reticulum. *Science* 2011;334(6059):1086–90.
- [44] Tabas I, Ron D. Integrating the mechanisms of apoptosis induced by endoplasmic reticulum stress. *Nat Cell Biol* 2011;13(3):184–90.
- [45] Nawrocki ST, Carew JS, Dunner Jr K, et al. Bortezomib inhibits PKR-like endoplasmic reticulum (ER) kinase and induces apoptosis via ER stress in human pancreatic cancer cells. *Cancer Res* 2005;65(24):11510–9.

- [46] Fribley A, Zeng Q, Wang CY. Proteasome inhibitor PS-341 induces apoptosis through induction of endoplasmic reticulum stress-reactive oxygen species in head and neck squamous cell carcinoma cells. *Mol Cell Biol* 2004;24(22):9695–704.
- [47] Fels DR, Ye J, Segan AT, et al. Preferential cytotoxicity of bortezomib toward hypoxic tumor cells via overactivation of endoplasmic reticulum stress pathways. *Cancer Res* 2008;68(22):9323–30.
- [48] Lee AH, Iwakoshi NN, Anderson KC, Glimcher LH. Proteasome inhibitors disrupt the unfolded protein response in myeloma cells. *Proc Nat Acad Sci USA* 2003;100:9946–51.
- [49] Obeng EA, Carlson LM, Gutman DM, Harrington Jr WJ, Lee KP, Boise LH. Proteasome inhibitors induce a terminal unfolded protein response in multiple myeloma cells. *Blood* 2006;107(12):4907–16.
- [50] Palombella VJ, Rando OJ, Goldberg AL, Maniatis T. The ubiquitin-proteasome pathway is required for processing the NF-kappa B1 precursor protein and the activation of NF-kB. *Cell* 1994;78(5):773–85.
- [51] Nemeth ZH, Wong HR, Odoms K, et al. Proteasome inhibitors induce inhibitory kappa B (I kappa B) kinase activation, I kappa B alpha degradation, and nuclear factor kappa B activation in HT-29 cells. *Mol Pharmacol* 2004;65(2):342–9.
- [52] Hideshima T, Chauhan D, Richardson P, et al. NF-(B as a therapeutic target in multiple myeloma. *J Biol Chem* 2002;277(19):16639–47.
- [53] Hideshima T, Ikeda H, Chauhan D, et al. Bortezomib induces canonical nuclear factor-kappaB activation in multiple myeloma cells. *Blood* 2009;114(5):1046–52.
- [54] Holbeck SL, Collins JM, Doroshow JH. Analysis of Food and Drug Administration-approved anticancer agents in the NCI60 panel of human tumor cell lines. *Mol Cancer Ther* 2010;9(5):1451–60.
- [55] Milano A, Iaffaioli RV, Caponigro F. The proteasome: a worthwhile target for the treatment of solid tumours? *Eur J Cancer* 2007;43(7):1125–33.
- [56] Caravita T, de Fabritiis P, Palumbo A, Amadori S, Boccadoro M. Bortezomib: efficacy comparisons in solid tumors and hematologic malignancies. *Nat Clin Pract Oncol* 2006;3(7):374–87.
- [57] Borrell B. How accurate are cancer cell lines? *Nature* 2010;463(7283):858.
- [58] Sandberg R, Ernberg I. The molecular portrait of in vitro growth by meta-analysis of gene-expression profiles. *Genome Biol* 2005;6(8):R65.
- [59] Pan C, Kumar C, Bohl S, Klingmueller U, Mann M. Comparative proteomic phenotyping of cell lines and primary cells to assess preservation of cell type-specific functions. *Mol Cell Proteomics* 2009;8(3):443–50.
- [60] Powers ET, Morimoto RI, Dillin A, Kelly JW, Balch WE. Biological and chemical approaches to diseases of proteostasis deficiency. *Annu Rev Biochem* 2009;78:959–91.
- [61] Williamson MJ, Silva MD, Terkelsen J, et al. The relationship among tumor architecture, pharmacokinetics, pharmacodynamics, and efficacy of bortezomib in mouse xenograft models. *Mol Cancer Ther* 2009;8(12):3234–43.
- [62] Driscoll JJ, Minter A, Driscoll DA, Burris JK. The ubiquitin + proteasome protein degradation pathway as a therapeutic strategy in the treatment of solid tumor malignancies. *Anticancer Agents Med Chem* 2011;11(2):242–6.
- [63] Cvek B. Ixazomib citrate, proteasome inhibitor oncolytic. *Drug Future* 2012;37(8):561–5.
- [64] Kupperman E, Lee EC, Cao Y, et al. Evaluation of the proteasome inhibitor MLN9708 in preclinical models of human cancer. *Cancer Res* 2010;70(5):1970–80.
- [65] Chauhan D, Tian Z, Zhou B, et al. In vitro and in vivo selective antitumor activity of a novel orally bioavailable proteasome inhibitor MLN9708 against multiple myeloma cells. *Clin Cancer Res* 2011;17(16):5311–21.
- [66] Tian Z, Zhao JJ, Tai YT, et al. Investigational agent MLN9708/2238 targets tumor-suppressor miR33b in MM cells. *Blood* 2012;120(19):3958–67.
- [67] Richardson PG, Berdeja JG, Niesvizky R, et al. Oral weekly MLN9708, an investigational proteasome inhibitor, in combination with lenalidomide and dexamethasone in patients (pts) with previously untreated multiple myeloma (MM): a phase I/II study. *J Clin Oncol* 2012;30(suppl) (abstr 8033).
- [68] Lonial S, Baz RC, Wang M, et al. Phase I study of twice-weekly dosing of the investigational oral proteasome inhibitor MLN9708 in patients (pts) with relapsed and/or refractory multiple myeloma (MM). *J Clin Oncol* 2012;30(suppl) (abstr 8017).
- [69] Smith DC, Sullivan D, Infante JR, et al. MLN9708, an investigational proteasome inhibitor, in patients (pts) with solid tumors: Updated phase I results. *J Clin Oncol* 2012;30(suppl) (abstr e13603).
- [70] Papadopoulos KP, Burris 3rd HA, Gordon M, et al. A phase I/II study of carfilzomib 2-10-min infusion in patients with advanced solid tumors. *Cancer Chemother Pharmacol* 2013;72(4):861–8.
- [71] Gomez AM, Willcox N, Molenaar PC, et al. Targeting plasma cells with proteasome inhibitors: possible roles in treating myasthenia gravis. *Ann NY Acad Sci* 2012;1274:48–59.
- [72] Lifter J, Kincade PW, Choi YS. Subpopulations of chicken B lymphocytes. *J Immunol* 1976;117(6):2220–5.
- [73] Lipsky PE. Systemic lupus erythematosus: an autoimmune disease of B cell hyperactivity. *Nat Immunol* 2001;2(9):764–6.
- [74] Díaz-Manera J, Martínez-Hernández E, Querol L, et al. Long-lasting treatment effect of rituximab in MuSK myasthenia. *Neurology* 2012;78(3):189–93.
- [75] Gehrs BC, Friedberg RC. Autoimmune hemolytic anemia. *Am J Hematol* 2002;69(4):258–71.
- [76] Hoyer BF, Manz RA, Radbruch A, Hiepe F. Long-lived plasma cells and their contribution to autoimmunity. *Ann NY Acad Sci* 2005;1050:124–33.
- [77] Cascio P, Oliva L, Cerruti F, et al. Dampening Ab responses using proteasome inhibitors following in vivo B cell activation. *Eur J Immunol* 2008;38(3):658–67.
- [78] Neubert K, Meister S, Moser K, et al. The proteasome inhibitor bortezomib depletes plasma cells and protects mice with lupus-like disease from nephritis. *Nat Med* 2008;14(7):748–55.
- [79] Ichikawa HT, Conley T, Muchamuel T, et al. Beneficial effect of novel proteasome inhibitors in murine lupus via dual inhibition of type I interferon and autoantibody-secreting cells. *Arthritis Rheum* 2012;64(2):493–503.
- [80] Seavey MM, Lu LD, Stump KL, Wallace NH, Ruggeri BA. Novel, orally active, proteasome inhibitor, delanzomib (CEP-18770), ameliorates disease symptoms and glomerulonephritis in two pre-clinical mouse models of SLE. *Int Immunopharmacol* 2012;12(1):257–70.
- [81] Gomez AM, Vrolix K, Martínez-Martínez P, et al. Proteasome inhibition with bortezomib depletes plasma cells and autoantibodies in experimental autoimmune myasthenia gravis. *J Immunol* 2011;186(4):2503–13.
- [82] Meslier Y, Andre S, Dimitrov JD, et al. Bortezomib delays the onset of factor VIII inhibitors in experimental hemophilia A, but fails to eliminate established anti-factor VIII IgG-producing cells. *J Thromb Haemost* 2011;9(4):719–28.
- [83] Sadaka B, Alloway RR, Shields AR, Schmidt NM, Woodle ES. Proteasome inhibition for antibody-mediated allograft rejection. *Semin Hematol* 2012;49(3):263–9.
- [84] Schroyens W, O'Connell C, Sykes DB. Complete and partial responses of the TEMPI syndrome to bortezomib. *N Engl J Med* 2012;367(8):778–80.

- [85] Sykes DB, Schroyens W, O'Connell C. The TEMPI syndrome—a novel multisystem disease. *N Engl J Med* 2011;365(5):475–7.
- [86] Shortt J, Oh DH, Opat SS. ADAMTS13 antibody depletion by bortezomib in thrombotic thrombocytopenic purpura. *N Engl J Med* 2013;368(1):90–2.
- [87] Deng S, Zhou H, Xiong R, et al. Over-expression of genes and proteins of ubiquitin specific peptidases (USPs) and proteasome subunits (PSs) in breast cancer tissue observed by the methods of RFDD-PCR and proteomics. *Breast Cancer Res Treat* 2007;104(1):21–30.
- [88] Geiger T, Wehner A, Schaab C, Cox J, Mann M. Comparative proteomic analysis of eleven common cell lines reveals ubiquitous but varying expression of most proteins. *Mol Cell Proteomics* 2012;11(3) (M111.014050) <http://www.ncbi.nlm.nih.gov/pubmed/?term=Geiger+T%2C+Wehner+A>
- [89] Ross DT, Scherf U, Eisen MB, et al. Systematic variation in gene expression patterns in human cancer cell lines. *Nat Genet* 2000;24(3):227–35.
- [90] Moghaddas Gholami A, Hahne H, Wu Z, et al. Global proteome analysis of the NCI-60 cell line panel. *Cell Rep* 2013;4(3):609–20.
- [91] Codony-Servat J, Tapia MA, Bosch M, et al. Differential cellular and molecular effects of bortezomib, a proteasome inhibitor, in human breast cancer cells. *Mol Cancer Ther* 2006;5(3):665–75.
- [92] Bianchi G, Oliva L, Cascio P, et al. The proteasome load versus capacity balance determines apoptotic sensitivity of multiple myeloma cells to proteasome inhibition. *Blood* 2009;113(13):3040–9.
- [93] Meister S, Schubert U, Neubert K, et al. Extensive immunoglobulin production sensitizes myeloma cells for proteasome inhibition. *Cancer Res* 2007;67(4):1783–92.
- [94] Schubert U, Anton LC, Gibbs J, Norbury CC, Yewdell JW, Bennink JR. Rapid degradation of a large fraction of newly synthesized proteins by proteasomes. *Nature* 2000;404(6779):770–4.
- [95] Qian SB, Princiotta MF, Bannink JR, Yewdell JW. Characterization of rapidly degraded polypeptides in mammalian cells reveals a novel layer of nascent protein quality control. *J Biol Chem* 2006;281(1):392–400.
- [96] Cenci S, Oliva L, Cerruti F, et al. Pivotal advance: protein synthesis modulates responsiveness of differentiating and malignant plasma cells to proteasome inhibitors. *J Leukoc Biol* 2012;92(5):921–31.
- [97] Cenci S, Mezghrani A, Cascio P, et al. Progressively impaired proteasomal capacity during terminal plasma cell differentiation. *EMBO J* 2006;25(5):1104–13.
- [98] Santo L, Hideshima T, Kung AL, et al. Preclinical activity, pharmacodynamic, and pharmacokinetic properties of a selective HDAC6 inhibitor, ACY-1215, in combination with bortezomib in multiple myeloma. *Blood* 2012;119(11):2579–89.
- [99] Richardson PG, Schlossman RL, Alsina M, et al. PANORAMA 2: panobinostat in combination with bortezomib and dexamethasone in patients with relapsed and bortezomib-refractory myeloma. *Blood* 2013;122(14):2331–7.
- [100] Auner HW, Moody AM, Ward TH, et al. Combined inhibition of p97 and the proteasome causes lethal disruption of the secretory apparatus in multiple myeloma cells. *PLoS One* 2013;8(9):e74415.
- [101] Mitsiades CS, Mitsiades NS, McMullan CJ, et al. Antimyeloma activity of heat shock protein-90 inhibition. *Blood* 2006;107(3):1092–100.
- [102] Yerlikaya A, Okur E, Eker S, Erin N. Combined effects of the proteasome inhibitor bortezomib and Hsp70 inhibitors on the B16F10 melanoma cell line. *Mol Med Rep* 2010;3(2):333–9.
- [103] Sonnemann J, Marx C, Becker S, et al. p53-dependent and p53-independent anticancer effects of different histone deacetylase inhibitors. *Br J Cancer* 2014;110(3):656–67.
- [104] Orlowski RZ. Novel agents for multiple myeloma to overcome resistance in phase III clinical trials. *Semin Oncol* 2013;40(5):634–51.
- [105] Lacy MQ, McCurdy AR. Pomalidomide. *Blood* 2013;122(14):2305–9.
- [106] McConkey DJ, Zhu K. Mechanisms of proteasome inhibitor action and resistance in cancer. *Drug Resist Updat* 2008;11(4–5):164–79.
- [107] Kale AJ, Moore BS. Molecular mechanisms of acquired proteasome inhibitor resistance. *J Med Chem* 2012;55(23):10317–27.
- [108] Ri M, Iida S, Nakashima T, et al. Bortezomib-resistant myeloma cell lines: a role for mutated PSMB5 in preventing the accumulation of unfolded proteins and fatal ER stress. *Leukemia* 2010;24(8):1506–12.
- [109] Franke NE, Niewerth D, Assaraf YG, et al. Impaired bortezomib binding to mutant $\beta 5$ subunit of the proteasome is the underlying basis for bortezomib resistance in leukemia cells. *Leukemia* 2012;26(4):757–68.
- [110] Oerlemans R, Franke NE, Assaraf YG, et al. Molecular basis of bortezomib resistance: proteasome subunit beta5 (PSMB5) gene mutation and overexpression of PSMB5 protein. *Blood* 2008;112(6):2489–99.
- [111] Suzuki E, Demo S, Deu E, et al. Molecular mechanisms of bortezomib resistant adenocarcinoma cells. *PLoS One* 2011;6(12):e27996.
- [112] Balsas P, Galan-Malo P, Marzo I, Naval J. Bortezomib resistance in a myeloma cell line is associated to PSM $\beta 5$ overexpression and polyploidy. *Leuk Res* 2012;36(2):212–8.
- [113] Lu S, Yang J, Song X, et al. Point mutation of the proteasome beta5 subunit gene is an important mechanism of bortezomib resistance in bortezomib-selected variants of Jurkat T cell lymphoblastic lymphoma/leukemia line. *J Pharmacol Exp Ther* 2008;326(2):423–31.
- [114] Lichter DI, Danaee H, Pickard MD, et al. Sequence analysis of β -subunit genes of the 20S proteasome in patients with relapsed multiple myeloma treated with bortezomib or dexamethasone. *Blood* 2012;120(23):4513–6.
- [115] Politou M, Karadimitris A, Terpos E, Kotsianidis I, Apperley JF, Rahemtulla A. No evidence of mutations of the PSMB5 (beta-5 subunit of proteasome) in a case of myeloma with clinical resistance to bortezomib. *Leuk Res* 2006;30(2):240–1.
- [116] Catley L, Weisberg E, Kiziltepe T, et al. Aggresome induction by proteasome inhibitor bortezomib and alpha-tubulin hyperacetylation by tubulin deacetylase (TDAC) inhibitor LBH589 are synergistic in myeloma cells. *Blood* 2006;108(10):3441–9.
- [117] Mitsiades CS, Mitsiades NS, McMullan CJ, et al. Transcriptional signature of histone deacetylase inhibition in multiple myeloma: biological and clinical implications. *Proc Natl Acad Sci USA* 2004;101(2):540–5.
- [118] Weber DM, Graef T, Hussein M, et al. Phase I trial of vorinostat combined with bortezomib for the treatment of relapsing and/or refractory multiple myeloma. *Clin Lymphoma Myeloma Leuk* 2012;12(5):319–24.
- [119] San-Miguel JF, Richardson PG, Gunther A, et al. Phase Ib study of panobinostat and bortezomib in relapsed or relapsed and refractory multiple myeloma. *J Clin Oncol* 2013;31(29):3696–703.
- [120] Stessman HA, Mansoor A, Zhan F, Linden MA, Van Ness B, Baughn LB. Bortezomib resistance can be reversed by induced expression of plasma cell maturation markers in a mouse in vitro model of multiple myeloma. *PLoS One* 2013;8(10):e77608.
- [121] Gu JL, Li J, Zhou ZH, et al. Differentiation induction enhances bortezomib efficacy and overcomes drug resistance in multiple myeloma. *Biochem Biophys Res Commun* 2012;420(3):644–50.
- [122] Leung-Hagesteijn C, Erdmann N, Cheung G, et al. Xbp1s-negative tumor B cells and pre-plasmablasts mediate therapeutic proteasome inhibitor resistance in multiple myeloma. *Cancer Cell* 2013;24(3):289–304.
- [123] Ling SC, Lau EK, Al-Shabeeb A, et al. Response of myeloma to the proteasome inhibitor bortezomib is correlated with the unfolded protein response regulator XBP-1. *Haematologica* 2012;97(1):64–72.

- [124] Chapman MA, Lawrence MS, Keats JJ, et al. Initial genome sequencing and analysis of multiple myeloma. *Nature* 2011;471(7339):467–72.
- [125] Tian Z, D'Arcy P, Wang X, et al. A novel small molecule inhibitor of deubiquitylating enzyme USP14 and UCHL5 induces apoptosis in multiple myeloma and overcomes bortezomib resistance. *Blood* 2014;123(5):706–16.
- [126] Anchoori RK, Karanam B, Peng S, et al. A bis-benzylidene piperidone targeting proteasome ubiquitin receptor RPN13/ADRM1 as a therapy for cancer. *Cancer Cell* 2013;24(6):791–805.
- [127] Chauhan D, Tian Z, Nicholson B, et al. A small molecule inhibitor of ubiquitin-specific protease-7 induces apoptosis in multiple myeloma cells and overcomes bortezomib resistance. *Cancer Cell* 2012;22(3):345–58.

Biographies


Zdeněk Škrott is a master's student in cell and molecular biology at Department of Cell Biology & Genetics, Palacký University Olomouc. He is involved in research on an old drug disulfiram as an anticancer drug inhibiting proteasome-dependent degradation.

Boris Cvek (Ph.D.) is a researcher at Department of Cell Biology & Genetics, Palacký University Olomouc. His main research topics are proteasome inhibitors and repurposing of old drugs for new uses.

APPENDIX C

Majera D, **Skrott Z**, Bouchal J, Bartkova J, Simkova D, Gachechiladze M, Steigerova J, Kurfurstova D, Gursky J, Korinkova G, Cwierka K, Hodny Z, Mistrik M, Bartek J. Targeting genotoxic and proteotoxic stress-response pathways in human prostate cancer by clinically available PARP inhibitors, vorinostat and disulfiram. *Prostate*. 2019 Mar;79(4):352-362. IF₍₂₀₁₇₎: 3.347

Targeting genotoxic and proteotoxic stress-response pathways in human prostate cancer by clinically available PARP inhibitors, vorinostat and disulfiram

Dusana Majera PhD¹  | Zdenek Skrott MSC¹ | Jan Bouchal PhD²  |
 Jirina Bartkova MD, PhD^{3,4} | Dana Simkova PhD² | Mariam Gachechiladze MD, PhD² |
 Jana Steigerova PhD² | Daniela Kurfurstova MD, PhD² | Jan Gursky PhD¹ |
 Gabriela Korinkova PhD² | Karel Cwierotka MD, PhD⁵ | Zdenek Hodny MD, PhD⁶ |
 Martin Mistrik PhD¹ | Jiri Bartek MD, PhD^{1,3,4,6}

¹ Laboratory of Genome Integrity, Institute of Molecular and Translational Medicine, Faculty of Medicine and Dentistry, Palacky University, Olomouc, Czech Republic

² Department of Clinical and Molecular Pathology, Institute of Molecular and Translational Medicine, Faculty of Medicine and Dentistry, Palacky University, Olomouc, Czech Republic

³ Danish Cancer Society Research Center, Copenhagen, Denmark

⁴ Division of Genome Biology, Department of Medical Biochemistry and Biophysics, Science for Life Laboratory, Karolinska Institute, Stockholm, Sweden

⁵ Department of Oncology, Faculty of Medicine and Dentistry, Palacky University, University Hospital, Olomouc, Czech Republic

⁶ Department of Genome Integrity, Institute of Molecular Genetics of the CAS, v.v.i., Prague, Czech Republic

Correspondence

Jiri Bartek, MD, PhD, Danish Cancer Society Research Center, Copenhagen, Denmark
 Email: jb@cancer.dk

Jan Bouchal, PhD, Department of Clinical and Molecular Pathology, Institute of Molecular and Translational Medicine, Faculty of Medicine and Dentistry, Palacky University, Olomouc, Czech Republic.
 Email: jan.bouchal@upol.cz

Martin Mistrik, PhD, Laboratory of Genome Integrity, Institute of Molecular and Translational Medicine, Faculty of Medicine and Dentistry, Palacky University, Olomouc, Czech Republic
 Email: martin.mistik@upol.cz

Funding information

The Danish cancer society; the Novo Nordisk Foundation; Palacky University, Grant numbers: IGA-LF-2018-001, IGA-LF-2018-034; the Swedish research council and Cancer Fonden; the Danish council for independent research; Czech Ministry of Education, Grant number: DRO-61989592; Czech National Program of Sustainability, Grant number: LO1304; Czech Ministry of Health, Grant numbers: AZV 16-32030, DRO-FNOL00098892, NV15-28628A;

Background: Castration-resistant prostate cancer (PCa) represents a serious health challenge. Based on mechanistically-supported rationale we explored new therapeutic options based on clinically available drugs with anticancer effects, including inhibitors of PARP1 enzyme (PARPi), and histone deacetylases (vorinostat), respectively, and disulfiram (DSF, known as alcohol-abuse drug Antabuse) and its copper-chelating metabolite CuET that inhibit protein turnover.

Methods: Drugs and their combination with ionizing radiation (IR) were tested in various cytotoxicity assays in three human PCa cell lines including radio-resistant stem-cell like derived cells. Mechanistically, DNA damage repair, heat shock and unfolded protein response (UPR) pathways were assessed by immunofluorescence and immunoblotting.

Results: We observed enhanced sensitivity to PARPi/IR in PC3 cells consistent with lower homologous recombination (HR) repair. Vorinostat sensitized DU145 cells to PARPi/IR and decreased mutant p53. Vorinostat also impaired HR-mediated DNA repair, as determined by Rad51 foci formation and downregulation of TOPBP1 protein, and overcame radio-resistance of stem-cell like DU145-derived cells. All PCa models responded well to CuET or DSF combined with copper. We demonstrated that DSF interacts with copper in the culture media and forms adequate levels of CuET indicating that DSF/copper and CuET may be considered as comparable treatments. Both DSF/copper and CuET evoked hallmarks of UPR in PCa cells, documented by upregulation of ATF4, CHOP and phospho-eIF2 α , with ensuing heat

Kellner Family Foundation; Czech-Biolmaging,
Grant number: LM2015062

shock response encompassing activation of HSF1 and HSP70. Further enhancing the cytotoxicity of CuET, combination with an inhibitor of the anti-apoptotic protein survivin (YM155, currently undergoing clinical trials) promoted the UPR-induced toxicity, yielding synergistic effects of CuET and YM155.

Conclusions: We propose that targeting genotoxic and proteotoxic stress responses by combinations of available drugs could inspire innovative strategies to treat castration-resistant PCa.

KEYWORDS

disulfiram, PARP, prostate cancer, proteotoxic stress, vorinostat

1 | INTRODUCTION

Prostate cancer (PCa) is the most frequently diagnosed malignancy in men and one of the major causes of cancer-related death in developed countries.¹ PCa is initially androgen-dependent and responds to androgen deprivation therapies, however, the disease ultimately progresses into a hormone-independent and largely incurable stage with metastases to the bones, lung, brain, or liver.

Aberrations in the DNA damage response (DDR) machinery are common in cancer and represent potential targets for therapeutic intervention.² PARP1 activity is important in sensing and signaling DNA damage that arises both endogenously, for example, through generation of oxidative DNA lesions and DNA single-strand breaks (SSBs), or exogenously, such as due to ionizing radiation (IR) exposure or treatment with various chemotherapeutics. Exposure of cycling cells to inhibitors of PARP1 (PARPi) causes excessive unrepaired SSBs and acceleration of DNA replication³ leading to replication stress and formation of DNA double-strand breaks (DSBs), toxic lesions preferentially repaired by homologous recombination (HR). HR defects due to mutations or silencing of factors such as BRCA1/2 sensitize cells to PARPi, as shown for ovarian, breast and also metastatic prostate cancer.⁴

Defects in DNA damage sensors, signaling kinases or nucleotide excision repair also sensitize to PARPi⁴ suggesting that the therapeutic potential of PARPi might extend beyond the BRCA1/2-defective tumors. There is also an urgent need to identify and validate potential biomarkers to predict sensitivity of individual tumors to PARPi, exemplified for PCa by the fusion oncogene TMPRSS2-ERG or loss of the PTEN tumor suppressor.^{5,6}

PCa is a heterogeneous disease reflecting both genetic and epigenetic alterations.⁷ Six epigenetics-modulating drugs targeting DNA methylation or histone deacetylation have been approved for cancer treatment.⁷ Since epigenetic regulation is complex, preclinical studies are required to generate patient stratification hypotheses and identify predictive biomarkers. Epigenetic reprogramming after loss of Rb and p53 tumor suppressors diminishes androgen receptor expression and is associated with resistance to antiandrogen therapy.^{8,9} From this point of view, both PC3 and DU145 cells,

lacking AR and possessing mutations in tumor suppressors, represent relevant models of a subgroup of aggressive prostate cancer.

Another approach to PCa treatment could be drug repurposing, with potentially multifaceted benefits for clinical implementation of new treatment options. DSF is among such possible candidates, showing anti-tumor activity in multiple studies. Recently, we discovered the molecular target and mode of action of DSF, thereby strengthening DSF's potential as an anticancer drug.¹⁰ Many cancers become resistant to monotherapy through diverse mechanisms, posing a major challenge in contemporary oncology. Drug combination could overcome resistance to single compounds, thus it is vital to find the drugs that act synergistically and are well tolerated.¹¹

Here, we describe differential responses to PARPi and IR in cellular models of aggressive PCa: PC3 (typical for loss of p53 and PTEN), DU145 (mutated p53 and Rb) and radioresistant stem-like PCa cells.¹² Moreover, we show that HDAC inhibition alters expression of HR proteins and potentiates cytotoxicity of IR, and that DSF's active metabolite, diethyldithiocarbamate-copper complex (CuET), activates heat shock response and UPR, showing synergistic toxic effect in combination with a survivin inhibitor-YM155 in human PCa models.

2 | MATERIAL AND METHODS

2.1 | Cell lines

DU145 and PC3 cell lines were cultured in DMEM medium, LNCaP in RPMI medium and LAPC4 in IMDM. DMEM, RPMI, and IMDM media were supplemented with 10% fetal bovine serum and penicillin/streptomycin. IMDM medium was additionally supplemented with 1 nM R1881. RWPE-1 cells were cultured in a keratinocyte serum-free medium supplemented with the bovine pituitary extract and human recombinant epidermal growth factor (Thermo Scientific, Waltham, MA). EP156T cells were cultured as described previously.¹³ All cell cultures were maintained in humidified 5% CO₂ atmosphere at 37°C. LAPC4, EP156T and RWPE1 cells were kindly provided by Prof. Zoran Culig and Prof. Helmut Klocker (Innsbruck Medical University). Other cell lines were purchased from the European Collection of Cell

Cultures (ECACC) and authenticated by AmpflSTR™ Identifier PCR Amplification Kit (Applied Biosystems, Foster City, CA).

2.2 | Colony forming and cell viability assays

For clonogenic cell survival assay, cells were plated in 6-well plates at 200–500 cells per plate. Next day the cells received appropriate treatment and kept in culture for 7–14 days. Colonies of approximately 50 cells were visualized by 1% crystal violet in 96% ethanol, and their number and total area were counted. Results were confirmed in three independent experiments. For XTT assay, cells were plated at a density of 10 000 per well in a 96-well plate. The next day, cells were treated as indicated. After 48 h, an XTT assay was performed according to the manufacturer's instructions (Applchem, Darmstadt, Germany). XTT solution was added to the medium and incubated for 30–60 min, and then the dye intensity was measured at the 475 nm wavelength using a spectrometer (TECAN, Infinite M200PRO, Mannedorf, Switzerland).

2.3 | Ionizing radiation and chemicals

The KU58948 inhibitor was obtained from AstraZeneca (London, UK). Vorinostat, MK132, nutlin 3, DSF, tunicamycin, thapsigargin and CuCl₂ were purchased from Sigma-Aldrich, YM155 from Selleckchem and copper diethyldithiocarbamate (CuET) from TCI Chemicals. Ionizing radiation was delivered using Xstrahl RS research cabinet gamma irradiator.

2.4 | Immunoblotting

Equal amounts of cell lysates were separated by SDS-PAGE on handcast or precast gel (Invitrogen, Carlsbad, CA), and then transferred onto nitrocellulose membrane. The membrane was blocked with 5% milk in Tris-buffered saline containing 0.1% Tween 20 for 1 h at room temperature, and then incubated overnight at 4°C or 1 h at room temperature with one of the following primary antibodies against: p53 (FL-393, Cell Signaling, Danvers, MA), Rad51 (ab63801, Abcam, Cambridge, UK), GAPDH (GTX30666, GeneTex), alpha-tubulin (H-300, Santa Cruz, Dallas, TX), BRCA1 (D-9, Santa Cruz), KU70 (N3H10, Santa Cruz), KU80 (ab3107, Abcam), DNA-PKcs (clone 18-2 Thermo Scientific), lamin B (M-20, Santa Cruz), TopBP1 (A300-111A, Bethyl, Montgomery, TX), BRCA2 (A300-005A, Bethyl), ATF4 (ABE387, Merck-Millipore), CHOP (L63F7, Cell Signaling), p-eIF2a (S51, Cell signalling), HSP70 (C92FBA-5, Enzo), followed by detection by secondary antibodies: goat-anti mouse and goat-anti rabbit (GE Healthcare). HRP conjugated secondary antibodies were visualized by ECL detection reagent (Thermo Scientific).

2.5 | Immunofluorescence staining

After appropriate treatment cells were fixed with 4% formaldehyde for 15 min at room temperature, washed with PBS and permeabilized with 0.5% Triton X-100 in PBS for 5 min. The samples on the plastic inserts cutted directly from cultivation plates using CNC machine were then immunostained with primary antibodies against Rad51 (ab63201,

Abcam), cyclin A (6E6, Leica), BRCA1 (D-9, Santa Cruz), p53 (FL-393, Santa Cruz), HSF1 (4356S Cell Signaling), followed by a fluorochrome-conjugated secondary antibodies: Alexa Fluor-488 or Alexa Fluor-568 (Invitrogen). Nuclei were visualized by Hoechst 33342 at room temperature for 5 min before mounting. Images were automatically recorded using an inverted fluorescence microscope BX71 (Olympus) and ScanR Acquisition software (Olympus), analyzed with ScanR Analysis software (Olympus), and evaluated with Statistica software (StatSoft).

2.6 | Small RNA interference

DU145 cells were transfected with anti-p53 siRNA (Eurofins Genomics-GUC CAG AUG AAG CUC CCA GAA) and NT siRNA (Eurofins Genomics-UAA UGU AUU GGA ACG CAU A) using Lipofectamine RNAiMAX transfection reagent (Invitrogen) according to manufacturer's recommended protocol. After 24 h, cells were either collected for Western blot analysis or used for immunofluorescence analysis.

2.7 | Cell cycle analysis

Cells were harvested at indicated times after treatment (both adherent and detached cells were collected) and fixed in cold 70% ethanol. After treatment with RNaseA, samples were stained with propidium iodide (PI). Cellular DNA content was analyzed using flow cytometer BD FACSVerser (BD Biosciences), and collected data were processed using BD FACSuite (BD Biosciences). At least 10 000 cells per sample were analyzed.

2.8 | Caspases 3/7 assay

Activity of caspase-3 and -7 was quantified by cleavage of fluorogenic substrate CellEvent™ Caspase-3/7 Green Detection Reagent (ThermoFisher Scientific). Briefly, samples were prepared in staining buffer (140 mM NaCl, 4 mM KCl, 0.75 mM MgCl₂, 10 mM HEPES) supplemented with 2% FBS, 0.5 μM CellEvent™ Caspase-3/7 Green Detection Reagent and incubated for 45 min at room temperature in the dark. Subsequently, 0.5 μg/mL DAPI was added and samples were analyzed by flow cytometry using BD FACSVerser (BD Biosciences), at least 10 000 events were acquired per sample. Collected data were processed by BD FACSuite (BD Biosciences).

2.9 | Measurement of CuET formation in vitro

To measure the formation of diethyldithiocarbamate-copper complex (CuET) in vitro a complete cell culture medium (DMEM, 10% FBS, 1% penicillin/streptomycin) was incubated with 1 μM disulfiram or 1 μM disulfiram plus 1 μM copper (ii) chloride, and 1 μM CuET as a control. After 3 h of incubation in 37 °C, 5% CO₂, the samples were vortexed and mixed with acetone in a ratio 1:250. The mixture was centrifuged 18 000g for 2 min at 4°C. The CuET complex in supernatant was analyzed by HPLC-MS method as described previously.¹⁰ The quantification of CuET complex was calculated according to the calibration curve.

3 | RESULTS

3.1 | DU145 cells show more efficient HR repair after PARPi and IR compared to more responsive PC3 cells

The standard-of-care therapy for localized PCa is radical prostatectomy followed by fractionated radiotherapy. In patients with disseminated PCa, androgen deprivation is achieved either by surgical or chemical castration. However, tumors often become castration-resistant as

disease progresses.¹⁴ Human PC3 and DU145 cell lines both lack androgen receptors and thus represent useful models for PCa patients with androgen-independent tumor growth.⁸

Recent findings showed high response rates to PARPi treatment in patients with PCa defective in DNA repair genes.⁴ Using colony formation assays that mimic effects of long-lasting therapy, we found PC3 cells more sensitive to the PARPi than DU145 cells (Figure 1A), while normal prostate epithelial RWPE1 and EP156T cells did not respond within the 1000 nM range (Supplementary Figures S1A and S1B). As PARP inhibitors are also candidate radiosensitizers, we tested

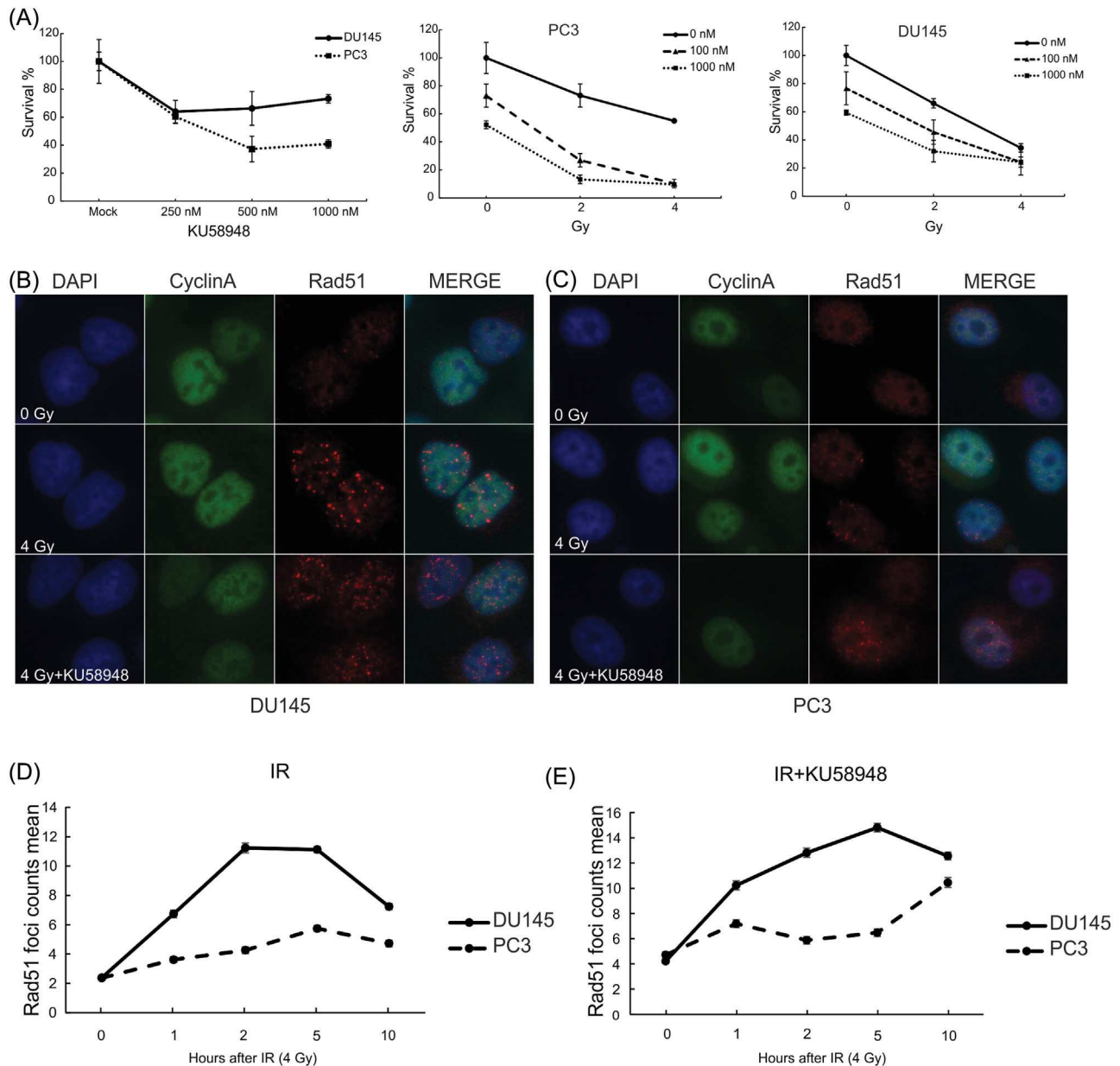


FIGURE 1 Rad51 foci formation is more effective in DU145 than in more responsive PC3 cells after KU58948 pre-treatment and IR. (A) PC3 and DU145 cells were treated with various concentrations of KU58948 and incubated for 8 days in colony formation assay. Next, cells were irradiated with different doses after 24 h pre-treatment with the KU58948 and incubated for 8-days in colony formation assay. Error bars represent SD of mean ($n = 3$). For immunofluorescence analysis, DU145 (B) and PC3 (C) cells were treated with 1 μ M KU58948 inhibitor for 24 h followed by IR (4 Gy) and fixed at different time points (0, 1, 2, 5, and 10 h). Images are representative from 2 h time points. Rad51 foci formation in cyclin A-positive DU145 cells was more effective than in PC3 cells (D and E). [Color figure can be viewed at wileyonlinelibrary.com]

combined PARPi and IR to explore potential additive/synergic effects. DU145 and PC3 cells were pre-treated with 100 nM and 1 μ M PARPi and irradiated after 24 h. Although PC3 cells were less responsive than DU145 to IR alone, the combination with PARPi was more effective in PC3 than in DU145 cells (Figure 1A). These data suggest that PC3 cells respond well to PARPi monotherapy or combined with IR, while DU145 respond rather poorly, a phenomenon which we decided to study further mechanistically.

PARPi is particularly effective in treatment of breast and ovarian cancer with BRCA1/2 mutations.¹⁵ BRCA1 along with Rad51 and other factors mediate HR, a high-fidelity DNA repair of DNA DSBs during S and G2 phases of the cell cycle. As PC3 cells responded well to PARPi and the combination with IR compared to DU145 cells, the functional status of HR- repair was examined using immunofluorescence analysis of RAD51 foci as marker of active HR. These experiments involved pre-treatment of cells with PARPi for 24 h, subsequent IR (4 Gy) and further incubation for 1, 2, 5, or 10 h. Fixed cells were then co-stained for RAD51 and the S/G2 marker cyclin A to focus on the HR-relevant cell-cycle phases (Figures 1B and 1C).¹⁶ Quantification showed reduced RAD51 foci in PC3 cells compared to DU145 in cyclin A-positive cells (Figures 1D and 1E) supporting the hypothesis of insufficient HR to explain higher sensitivity of PC3 cells to PARPi. These data are consistent with the notion that HR defects sensitize cancer cells to PARPi, alone or combined with IR¹⁷ and extend this concept to PCa.

3.2 | Vorinostat treatment overcomes DU145 cell resistance towards IR and PARPi

Since DU145 cells display relative resistance to PARPi and the combined PARPi/IR treatment (Figure 1A), we sought to identify a drug able to sensitize this PCa model to PARPi. DU145 harbours p53 mutations (P223L and V274F) thereby providing a model matching PCa patients harbouring p53 mutation with limited treatment options and adverse prognosis.¹⁸ We chose the FDA-approved histone deacetylase inhibitor vorinostat (also known as SAHA), reportedly preferentially cytotoxic towards cancer cells with mutated p53.¹⁹ Indeed, DU145 cells responded well to vorinostat (Figure 2A) and were more sensitive compared to PC3 (Supplementary Figure S2A). In DU145 cells, vorinostat caused activation of apoptosis markers caspases 3/7 (Supplementary Figure S2E) and G2/M arrest, as determined by flow cytometry (Supplementary Figure S2D) and accumulation of prometaphase cells (Supplementary Figure S2B). Unfortunately, in the short-term viability assay normal prostate epithelial cells RWPE-1 and EP156T respond similarly, thereby questioning the therapeutic window of vorinostat monotherapy (Supplementary Figures S2F and S2G). Mechanistically, vorinostat treatment should evoke degradation of the accumulated mutant p53 protein reverting its anti-apoptotic effect.¹⁹ Indeed, downregulation of p53 by vorinostat (Figures 2C and 2E) was mediated by increased p53 degradation, rescuable by proteasome inhibitor MG132 or nutlin, an inhibitor of MDM2 ubiquitin ligase for p53 (Figure 2D). Importantly, pre-treatment with vorinostat also sensitized the DU145 cells to IR and PARPi (Figures 2B and S2C) suggesting possible impact of

vorinostat on the DDR machinery. This phenomenon was further explored as combinations of IR and/or PARPi with vorinostat could potentially represent feasible treatment strategies.

3.3 | Vorinostat downregulates HR factors and sensitizes radio-surviving PCa cells to IR

To elucidate how vorinostat potentiates the effects of IR and PARPi, we assessed its impact on the DDR pathways. First, as HDACs regulate gene expression, we examined the levels of multiple HR factors after vorinostat treatment, and observed modest yet noticeable decreases of BRCA1, BRCA2, Rad51, and TopBP1 proteins (Figure 3G). Interestingly, despite the lower total BRCA1 level (Figure 2F), the ability to form IR-induced BRCA1 foci remained unchanged (Figures 2G and 2H). Notably, vorinostat pre-treatment prevented formation of IR-induced Rad51 foci in cyclin A-positive cells (Figures 3A and 3B), suggesting robust impairment of HR explaining the acquired sensitivity to PARPi. This effect is unlikely attributable to vorinostat-mediated downregulation of mutant p53, because direct downregulation of mut-p53 in DU145 cells by siRNA did not reproduce such phenotype (Figures 3C-E). Interestingly, Ku70, Ku80, and DNA-PK, proteins involved in DSB repair via non-homologous end joining (NHEJ), remained unaffected upon vorinostat treatment (Figure 3F) consistent with differential transcription control of genes involved in distinct DNA repair pathways.²⁰ As radio-resistance in PCa represents a significant issue that lacks suitable cellular models, our team developed a model of radiosurviving PCa cells obtained by exposure of parental DU145 cells to clinically relevant daily fractions of IR to a cumulative dose of 64 Gy (2 Gy applied every 24 h for 32 days). This treatment is not 100% toxic and selects for a radiation-surviving, stem-like cell population.^{12,21} Importantly, pre-treatment with vorinostat sensitised such cells to IR in colony formation assay (Supplementary Figure S2H) further suggesting vorinostat as an interesting option for combined IR treatment.

3.4 | Disulfiram as a candidate drug for PCa treatment

Prostate, as a mainly secretory organ, is especially dependent on proper function of endoplasmic reticulum (ER) and ER-associated degradation (ERAD). ERAD malfunction or insufficiency leads to ER stress and activation of the unfolded protein response (UPR).²² Several factors of ERAD machinery are upregulated in PCa,²³ and UPR activation in PCa has been recently demonstrated, providing a possible vulnerability exploitable therapeutically.²⁴ We have recently shown that DSF targets cancer via inhibition of the p97/NPL4 pathway, essential for ERAD.¹⁰ DSF's anticancer activity depends on copper²⁵ and we showed that in vivo, DSF becomes converted into diethyldithiocarbamate, a strong copper chelator forming a stable (CuET) the ultimate anticancer metabolite of DSF.¹⁰ CuET accumulates in tumors and paralyzes p97/NPL4-dependent processing of proteins, leading to strong proteotoxic stress, UPR and heat shock

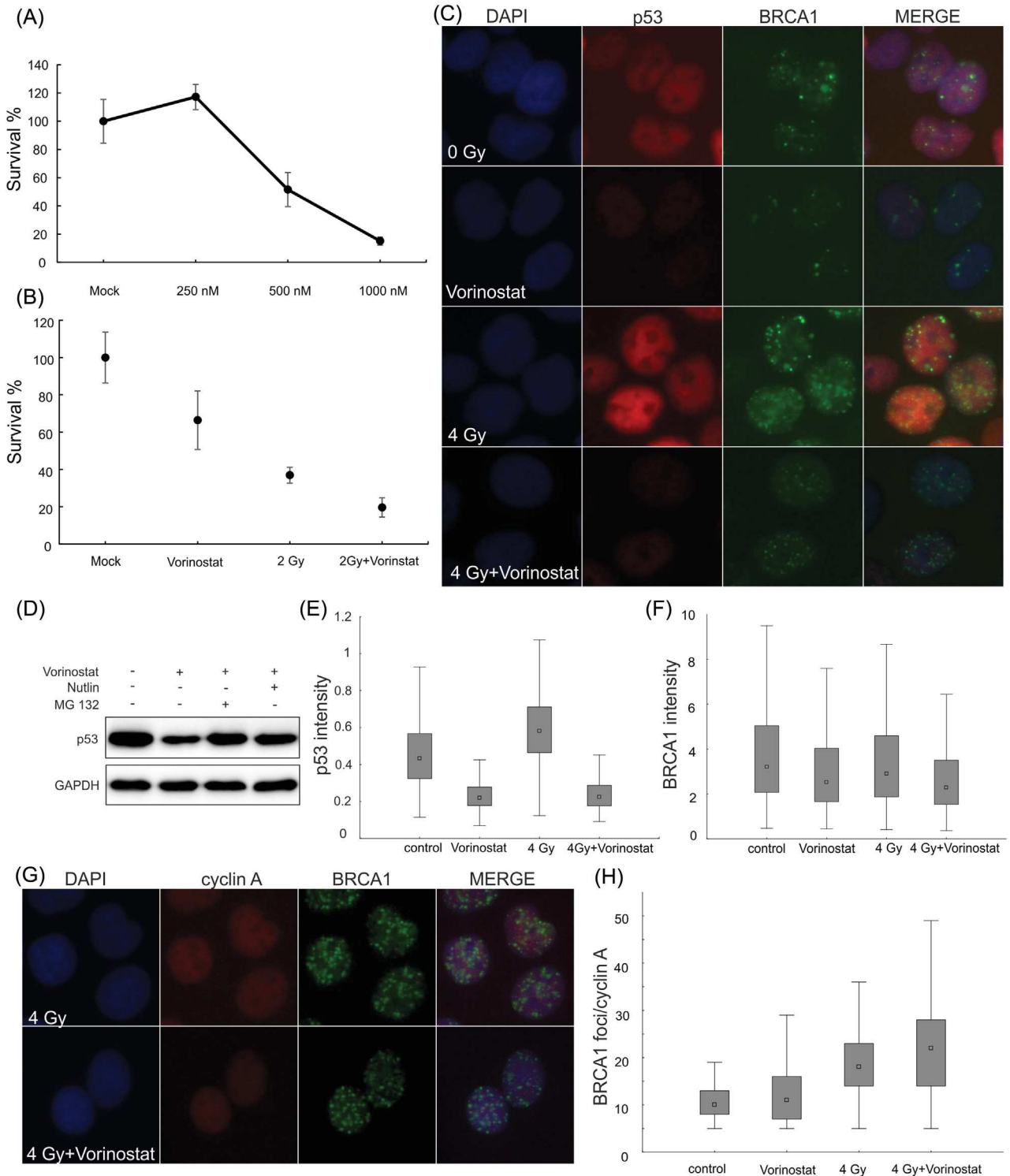


FIGURE 2 BRCA1 foci are formed in cyclin A-positive DU145 cells upon DNA damage after IR and vorinostat treatment, whereas p53 is downregulated. DU145 cell line was treated with vorinostat at indicated concentrations (A) and in combination with IR (2 Gy) and 500 nM vorinostat (B). Cell viability was measured by clonogenic cell survival assay for 8 days. Error bars represent SD of mean ($n = 3$). Next, cells were treated with 5 μ M vorinostat for 24 h, irradiated with 4 Gy and fixed after 5 h. Immunofluorescent staining of p53 and BRCA1 (C) was quantified for their intensity (E and F). One-day treatment with 5 μ M vorinostat downregulated p53 levels in DU145 cells which was abrogated by proteasome inhibitor MG132 or MDM2 inhibitor nutlin (D). Quantification of BRCA1 foci formation in cyclin A-positive DU145 cells (H) after IR and/or vorinostat was evaluated by immunofluorescence analysis (G). [Color figure can be viewed at wileyonlinelibrary.com]

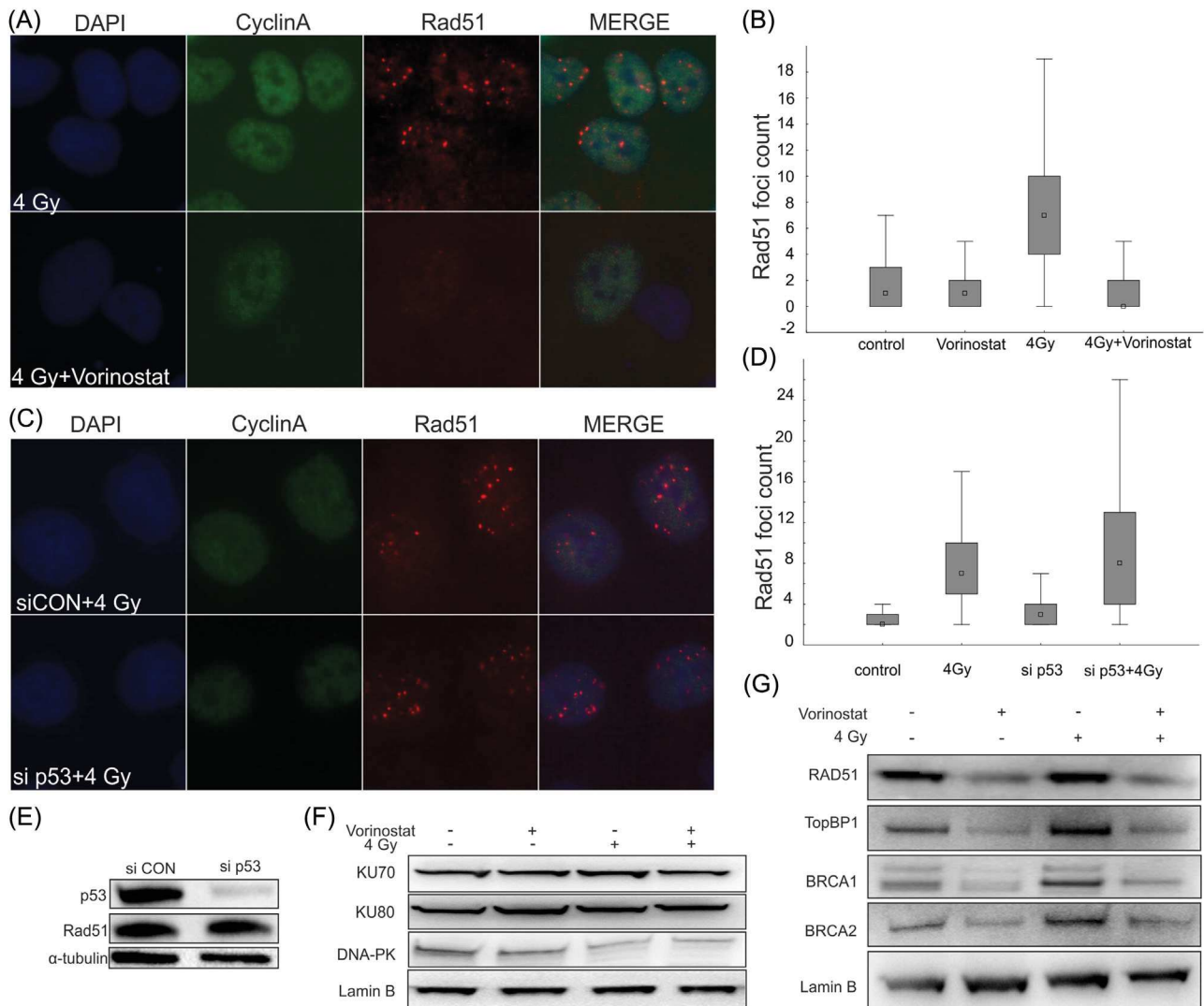


FIGURE 3 Vorinostat downregulates BRCA1 and Rad51 proteins. (A) Cells were treated with 5 μ M vorinostat for 24 h, irradiated with 4 Gy and fixed after 5 h. Rad51 foci were determined by immunofluorescence analysis. (B) Quantification of Rad51 foci formation was assessed in cyclin A-positive cells. (C) Next, cells were treated with siRNA (control or p53-targeting) for 48 h and formation of Rad51 was determined after IR (4 Gy) followed by 5 h of incubation. (D) Quantification of Rad51 foci was measured in cyclin A-positive cells after downregulation of p53. (E) Downregulation of mutated p53 had no impact on Rad51 protein levels. (G) Rad51, TopBP1, BRCA1 and BRCA2 were downregulated after 24 h of treatment with 5 μ M vorinostat, whereas Ku70, Ku80 and DNA-PK remained unchanged (F) as determined by Western blotting analysis. [Color figure can be viewed at wileyonlinelibrary.com]

responses (HSR).¹⁰ Since this drug is clinically used and well tolerated, it is an ideal candidate for repurposing. Specifically for PCa, DSF might be an interesting therapeutic candidate as it scored highly in PCa cell line models.²⁶

First, we treated DU145, PC3 and radiosurviving DU145 cells by DSF, DSF + CuCl₂, CuCl₂ alone or CuET for 48 h to test for cytotoxicity. All cell lines responded with similar sensitivity within nanomolar range (IC₅₀ around 200 nM) to DSF + CuCl₂ and CuET (Figure 4A). To further explore the comparable potencies of DSF + CuCl₂ and CuET, we assessed whether CuET forms also in vitro, in media containing DSF and CuCl₂. Indeed, we confirmed that CuET complex forms efficiently, indicating that the cell culture effects under DSF + CuCl₂ treatment are attributable to CuET (Figure 4B). DSF treatment alone was moderately toxic, likely

reflecting the presence of copper ions in standard growth media, forming some CuET. Notably, unlike treatments with PARPi or HDACi there was an obvious lack of differential responses among the otherwise very heterogeneous cell lines, suggesting a mechanism of action independent of the p53 status or DNA repair defects. To confirm that PCa cells treated by DSF + CuCl₂ and CuET are experiencing stress phenotypes similar to other cellular models,¹⁰ PCa cells were first examined for activation of HSR. Immunofluorescence analysis confirmed a robust HSR manifested by formation of HSF1 nuclear stress foci²⁷ (Figures 4C and 4D) and increase of heat shock protein 70 (HSP70), the main HSR effector, in all tested cell lines (Figure 4E). The PCa cells also strongly activate UPR manifested by elevated ATF4, CHOP, and phospho-eIF2 α , established UPR markers²² (Figures 5A and 5B).

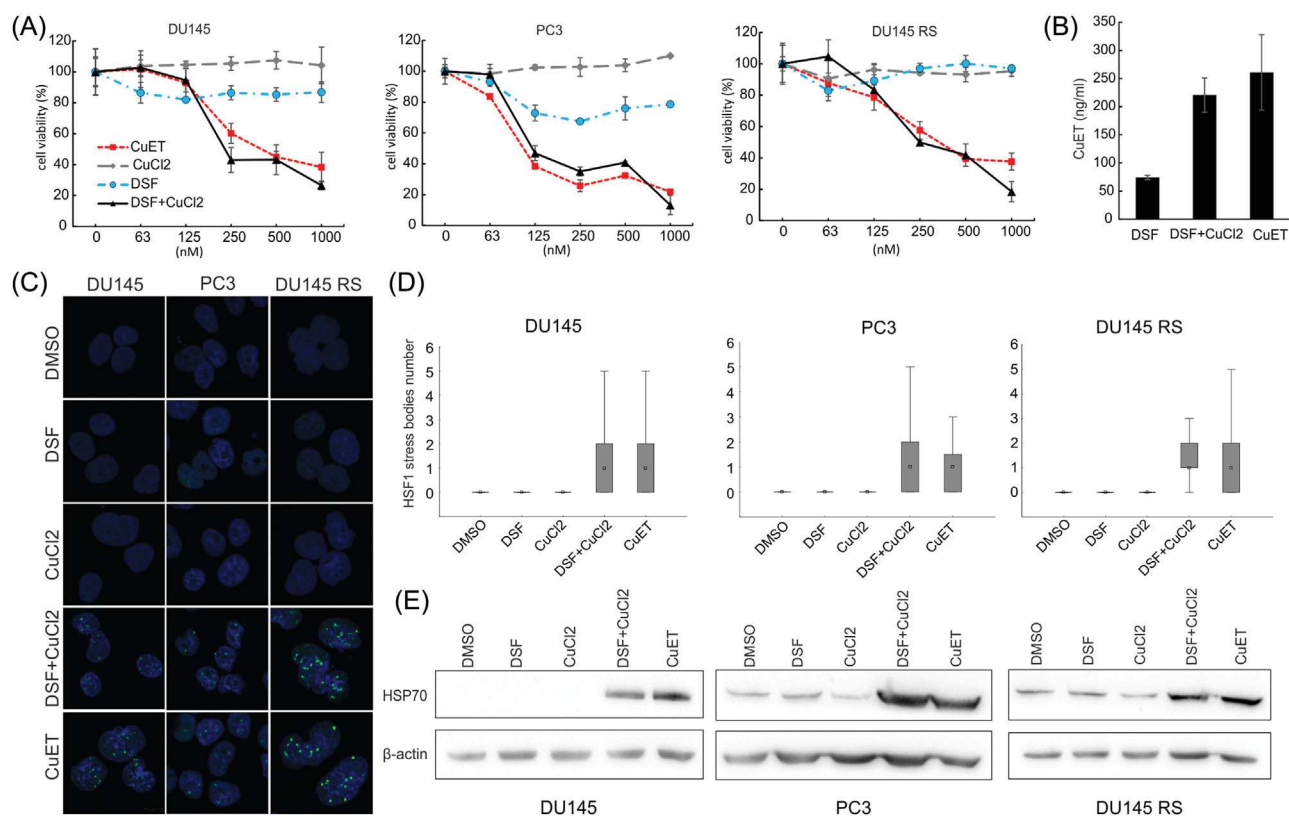


FIGURE 4 Disulfiram plus copper and CuET show cytotoxic effect in prostate cancer cell lines and activates heat shock response. (A) DU145, PC3 and radiosurviving DU145 cell lines were treated with DSF, copper chloride, DSF plus copper chloride or CuET with indicated concentrations and evaluated in 48 h by XTT assay. (B) Amount of CuET complex in the media was analyzed by HPLC-MS. (C) Cells were treated with indicated compounds (500 nM all) or their combinations and stained for HSF1. (D) HSF1 stress nuclear foci were quantified using ScanR. (E) Western blotting analysis revealed increase of HSP70, the main HSR effector, after the treatment with CuET or DSF + CuCl₂. [Color figure can be viewed at wileyonlinelibrary.com]

3.5 | Disulfiram toxicity synergizes with chemical inhibition of survivin

DSF's toxicity for PCa cell lines^{26,28} inspired a small pharmacodynamic clinical trial in PCa patients with non-metastatic recurrent prostate cancer.²⁹ The trial failed to show either global demethylation as a presumed pharmacodynamic marker²⁸ or significant changes in PSA levels, consequently concluding that such DSF monotherapy was inefficient in PCa patients. Such failure might reflect, at least in part, the fact that copper was not included into this trial, thus limiting DSF's anticancer activity that is otherwise apparent from preclinical studies including mouse models.^{10,30} A new Phase Ib study of intravenous copper loading combined with oral DSF administration in metastatic castration resistant prostate cancer was launched recently, which should provide more conclusive information about DSF efficacy in patients (ClinicalTrials.gov Identifier: NCT02963051). As DSF alone could be insufficient for eradication of PCa cells in vivo combined therapy could provide a better option. Because UPR, robustly induced by DSF + CuCl₂ and CuET treatments, strongly activates cell death, such candidate combinational treatment strategy could exploit inhibition of pro-survival proteins that are known to be overexpressed in cancers, such as survivin.³¹ Chemical inhibitor of survivin, YM155, showed anticancer activity in preclinical cancer models including

PCa³² and is being evaluated in clinical trials.³³ Interestingly, synergistic toxicity between YM155 and common UPR inducers thapsigargin and tunicamycin has been recently reported.³⁴ However, these two UPR inducers are very toxic and unsuitable for clinical applications.³⁵ On the other hand, DSF (combined with copper) is relatively well tolerated and thus provides a viable option to potentiate survivin inhibitors. Motivated by this rationale, DSF + CuCl₂ and CuET were first compared with thapsigargin and tunicamycin and very good potency in UPR induction was confirmed (Figures 5A and 5B). Next, DU145 and PC3 cells were treated with indicated combinations of DSF (with copper) and YM155. Combination of the drugs led to reduced survival of both DU145 and PC3 cells. (Figures 5C and 5D) revealing moderate synergy as computed using CompuSyn algorithm³⁶ (Figure 5E). Thus combination of two clinically available drugs, YM155 and DSF (supplemented with copper) represents a readily available and potentially efficient treatment option for PCa and also other cancer patients.

4 | DISCUSSION

Therapy of advanced PCa still poses a serious challenge in oncology, making any innovative and better alternative treatments highly

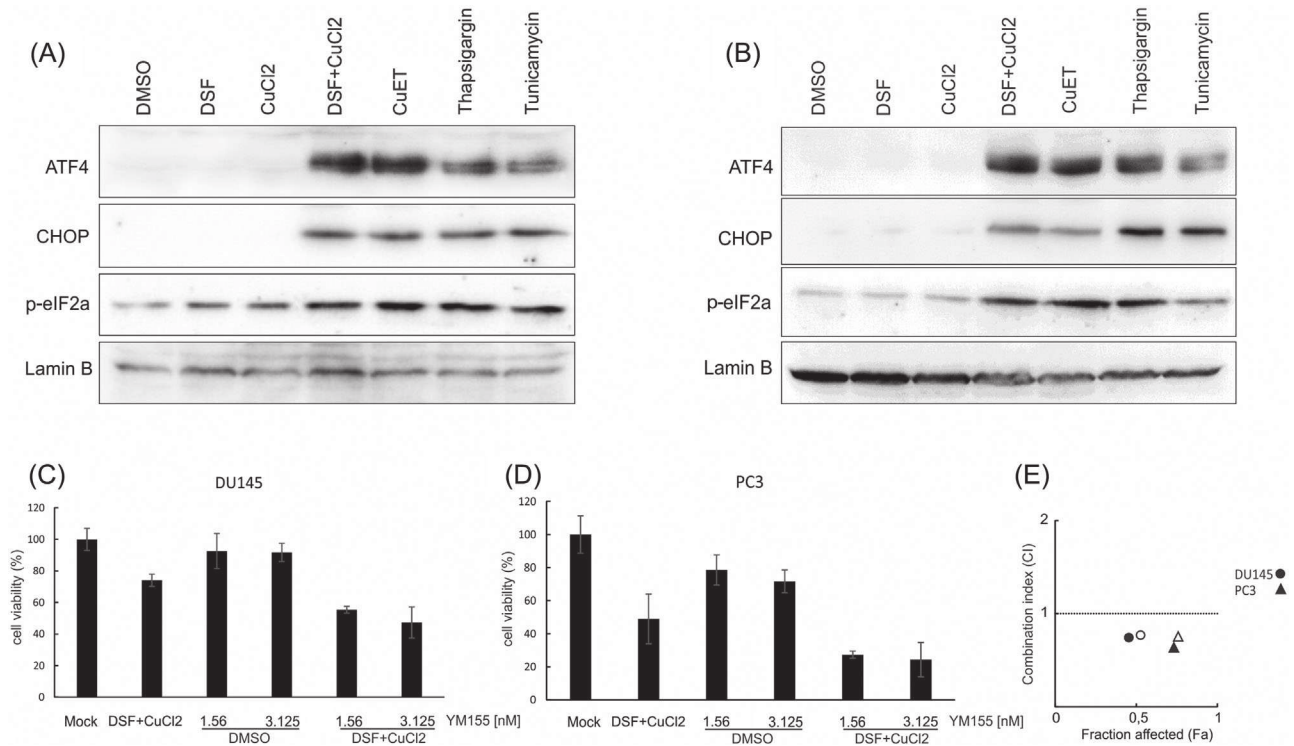


FIGURE 5 Disulfiram activates UPR and kills DU145 and PC3 cell lines in a synergistic manner with survivin inhibitor YM155. DU145 (A) and PC3 (B) cells were treated with 500 nM concentration of indicated compounds for 8 h and cell lysates were analyzed for ATF4, CHOP, p-eIF2a and lamin B. (C and D) Next, cells were treated with 500 nM DSF + CuCl₂ and with indicated concentrations of survivin inhibitor and analyzed for synergy in CompuSyn (E). Circles and triangles refer to DU145 and PC3 cells, respectively. Fill and empty objects indicate combinations of DSF + CuCl₂ with lower and higher concentration of survivin inhibitor, respectively

desirable. Here we chose two well-characterized cellular models (PC3, DU145) and one experimentally derived model (termed radio-surviving DU145) of castration resistant PCa to explore new therapeutic options. We concentrated on anticancer drugs currently entering or in clinical trials such as PARPi, vorinostat, and DSF, the latter with recently revealed mechanism of action through interference with p97/NPL4- mediated protein turnover. IR was added in some experimental setups as it is known that the standard androgen deprivation treatment may benefit from combination with radiotherapy in locally advanced prostate cancer.³⁷

Compared to DU145, PC3 cells showed higher sensitivity to PARPi and IR. Analogous observations were published by others and the differential sensitivity was associated in part with PTEN loss and induction of senescence in PC3 cells.^{38–40} Here, we add another clue as PC3 cells show low Rad51 foci formation after PARPi and IR suggesting defects in HR-promoted DNA repair. Defects in HR are regarded as a major prerequisite for synthetic lethality in combination with PARPi.⁴¹ Based on a phase II clinical trial, combined with next-generation sequencing of DNA repair genes, the PARPi olaparib (Lynparza) received an FDA designation of breakthrough therapy.^{4,42} Our present results suggest a potential for PARPi in treating PCa, guided by immunohistochemical and/or ex vivo biopsy evaluation of HR biomarkers such as RAD51 foci formation.⁴³ These approaches, while technically challenging, have a potential for clinical implementation as

predictive biomarkers for treatment with PARPi, complementary to genetic analyses of *BRCA1/2*, *ATM* or *TPR228-ERG*.^{4,6,42} Olaparib has also been recently reported to be effective in combination with, and as maintenance therapy after, first-line endocrine therapy of prostate cancer.⁴⁴

Different therapeutic approaches will be required for castration-resistant PCa cases that are HR repair proficient. Based on our current data, we propose another treatment strategy, involving HDAC inhibitors such as vorinostat. DU145 are among the cell lines with gain-of function p53 mutations,^{18,45} associated with preferential sensitivity to HDAC inhibition.¹⁹ Indeed, these cells responded well to vorinostat, particularly when combined with IR, as also noticed by others.⁴⁶ Consistent with the literature, we observed reduced p53, and modest downregulation of BRCA1, BRCA2 and Rad51 after vorinostat treatment by immunoblotting. For the first time, we report that vorinostat downregulates also TOPBP1 which is important for Rad51 loading to chromatin during HR.⁴⁷ Indeed, pre-treatment with vorinostat resulted in less efficient DNA repair by HR, as documented by lower counts of Rad51 foci in cyclin A-positive cells. Downregulation of mutated p53 by siRNA altered neither Rad51 foci nor the RAD51 protein level, indicating that the effect of HDAC inhibition by vorinostat is more pleiotropic affecting also the HR-promoted DNA repair processes. Consistently, other HDAC inhibitors, MS-275 and FK228, impaired HR repair.⁴⁸ The vorinostat-induced DNA repair defect was further corroborated in our experiments of combined treatment with IR and PARPi.

As targeting proteotoxic stress pathways represents an emerging promising therapeutic approach for PCa,²⁴ we also tested DSF that impairs protein degradation.¹⁰ DSF repurposing for cancer treatment is currently tested in at least eight clinical trials (according to ClinicalTrials.gov) involving various cancers including PCa. Despite DSF monotherapy failed in a clinical trial in PCa patients with non-metastatic recurrent PCa,²⁹ this study did not combine DSF with copper, which is required for DSF's anticancer activity in vitro^{25,49} and potentiates its activity in vivo.^{10,30} Another intriguing option for future treatment is concomitant DSF (ideally supplemented with copper) with other anticancer drugs or IR. Such combinations show promising results in preclinical models^{50,51} and also in a few clinical trials.^{52,53} In this study, we demonstrated toxicity of the CuET complex, the main anticancer metabolite of disulfiram in vivo¹⁰ as well as potency of DSF in combination with copper. These treatments also induced cellular responses which were reported for other cell lines, including UPR and HSR pathway activation. Such strong activation of UPR prompted us to test the combination of DSF with a survivin inhibitor YM155, reported as being highly potent in combination with UPR inducers thapsigargin and tunicamycin.³⁴ YM155 is a novel anticancer drug undergoing clinical trials and it was already tested as a monotherapy in castration-resistant PCa patients, yet with a rather limited effect.³³ The observed synergy between YM155 and CuET/DSF + CuCl₂, reported in our present study, provides a further rationale for additional preclinical and/or clinical investigations, with potential implications also for other human malignancies, beyond the treatment of PCa.

5 | CONCLUSIONS

Combined IR/PARPi effectively killed HR-impaired PCa cells. Vorinostat treatment reduced levels of HR factors including TOPBP1, with ensuing enhanced sensitivity to IR and PARPi. DSF/copper was effective against all PCa models, triggering proteotoxic stress, UPR and heat shock pathway activation, highlighting a rationale for combinatorial therapy blocking anti-apoptotic responses by survivin inhibitors. We propose that targeting genotoxic stress and proteotoxic stress responses by combinations of available drugs could inspire innovative strategies to treat castration-resistant PCa.

ACKNOWLEDGMENTS

We thank Kamila Nemcova for technical assistance with cell culture and immunoblotting. PARPi was kindly provided by Astra Zeneca. The study was supported by grants from the Kellner Family Foundation, Czech National Program of Sustainability LO1304, MEYS CR (LM2015062 Czech-Biolmaging and DRO-61989592), Czech Ministry of Health NV15-28628A, DRO-FNOL00098892 and AZV 16-32030A, University of Palacky IGA-LF-2018-001 and 034, the Danish cancer society, the Novo Nordisk Foundation, the Danish council for independent research, the Swedish research council and Cancer Fonden.

CONFLICTS OF INTEREST

The authors have no conflicts of interest to disclose.

ORCID

Dusana Majera  <http://orcid.org/0000-0002-9238-3437>

Jan Bouchal  <http://orcid.org/0000-0003-4842-1720>

REFERENCES

- Torre LA, Bray F, Siegel RL, Ferlay J, Lortet-Tieulent J, Jemal A. Global cancer statistics, 2012. *CA Cancer J Clin*. 2015;65:87–108.
- Kurfurstova D, Bartkova J, Vrtel R, et al. DNA damage signalling barrier, oxidative stress and treatment-relevant DNA repair factor alterations during progression of human prostate cancer. *Mol Oncol*. 2016;10:879–894.
- Maya-Mendoza A, Moudry P, Merchut-Maya JM, Lee M, Strauss R, Bartek J. High speed of fork progression induces DNA replication stress and genomic instability. *Nature*. 2018;559:279–284.
- Mateo J, Carreira S, Sandhu S, et al. DNA-repair defects and olaparib in metastatic prostate cancer. *N Engl J Med*. 2015;373:1697–1708.
- Mendes-Pereira AM, Martin SA, Brough R, et al. Synthetic lethal targeting of PTEN mutant cells with PARP inhibitors. *EMBO Mol Med*. 2009;1:315–322.
- Brenner JC, Ateeq B, Li Y, et al. Mechanistic rationale for inhibition of Poly(ADP-Ribose) polymerase in ETS gene fusion-positive prostate cancer. *Cancer Cell* 2011;19:664–678.
- Graça I, Pereira-Silva E, Henrique R, Packham G, Crabb SJ, Jerónimo C. Epigenetic modulators as therapeutic targets in prostate cancer. *Clin Epigenetics*. 2016;8:98.
- Ku SY, Rosario S, Wang Y, et al. Rb1 and Trp53 cooperate to suppress prostate cancer lineage plasticity, metastasis, and antiandrogen resistance. *Science*. 2017;355:78–83.
- Mu P, Zhang Z, Benelli M, et al. SOX2 promotes lineage plasticity and antiandrogen resistance in TP53 – and RB1 – deficient prostate cancer. *Science*. 2017;355:84–88.
- Skrrott Z, Mistrik M, Andersen KK, et al. Alcohol-abuse drug disulfiram targets cancer via p97 segregase adaptor NPL4. *Nature*. 2017;552:194–199.
- Al-Lazikani B, Banerji U, Workman P. Combinatorial drug therapy for cancer in the post-genomic era. *Nat Biotechnol*. 2012;30:679–692.
- Kyjacova L, Hubackova S, Krejčíková K, et al. Radiotherapy-induced plasticity of prostate cancer mobilizes stem-like non-adherent, Erk signaling-dependent cells. *Cell Death Differ*. 2015;22:898–911.
- Kogan I, Goldfinger N, Milyavsky M, et al. HTERT-immortalized prostate epithelial and stromal-derived Cells. *Cancer Res*. 2006;66:3531–3540.
- Santer FR, Erb HH, McNeill RV. Therapy escape mechanisms in the malignant prostate. *Semin Cancer Biol*. 2015;35:133–144.
- Fong PC, Boss DS, Yap TA, et al. Inhibition of poly(ADP-Ribose) polymerase in tumors from BRCA mutation carriers. *N Engl J Med*. 2009;361:123–134.
- Mistrik M, Oplustilova L, Lukas J, Bartek J. Low-dose DNA damage and replication stress responses quantified by optimized automated single-cell image analysis. *Cell Cycle*. 2009;8:2592–2599.
- Oplustilova L, Wolanin K, Mistrik M, et al. Evaluation of candidate biomarkers to predict cancer cell sensitivity or resistance to PARP-1 inhibitor treatment. *Cell Cycle*. 2012;11:3837–3850.
- Gurova KV, Rokhlin OW, Budanov AV, et al. Cooperation of two mutant p53 alleles contributes to Fas resistance of prostate carcinoma cells. *Cancer Res*. 2003;63:2905–2912.

19. Li D, Marchenko ND, Moll UM. SAHA shows preferential cytotoxicity in mutant p53 cancer cells by destabilizing mutant p53 through inhibition of the HDAC6-Hsp90 chaperone axis. *Cell Death Differ*. 2011;18:1904–1913.
20. Polkinghorn WR, Parker JS, Lee MX, et al. Androgen receptor signaling regulates DNA repair in prostate cancers. *Cancer Discov*. 2013;3:1245–1253.
21. Guggenberger F, van de Werken HJG, Erb HH, et al. Fractionated radiation of primary prostate basal cells results in downplay of interferon stem cell and cell cycle checkpoint signatures. *Eur Urol*. 2018;74:847–849.
22. Storm M, Sheng X, Arnoldussen YJ, Saatcioglu F. Prostate cancer and the unfolded protein response. *Oncotarget*. 2016;7:54051–54066.
23. Erzurumlu Y, Ballar P. Androgen mediated regulation of endoplasmic reticulum-associated degradation and its effects on prostate cancer. *Sci Rep*. 2017;7:40719.
24. Nguyen HG, Conn CS, Kye Y, et al. Development of a stress response therapy targeting aggressive prostate cancer. *Sci Transl Med*. 2018;10:eaar2036.
25. Chen D, Cui QC, Yang H, Dou QP. Disulfiram, a clinically used anti-alcoholism drug and copper-binding agent, induces apoptotic cell death in Breast cancer cultures and xenografts via inhibition of the proteasome activity. *Cancer Res*. 2006;66:10425–10433.
26. Ilijin K, Ketola K, Vainio P, et al. High-throughput cell-based screening of 4910 known drugs and drug-like small molecules identifies disulfiram as an inhibitor of prostate cancer cell growth. *Clin Cancer Res*. 2009;15:6070–6078.
27. Biamonti G, Vourc'h C. Nuclear stress bodies. *Cold Spring Harb Perspect Biol*. 2010;2:a000695.
28. Lin J, Haffner MC, Zhang Y, et al. Disulfiram is a DNA demethylating agent and inhibits prostate cancer cell growth. *Prostate*. 2011;71:333–343.
29. Schweizer MT, Lin J, Blackford A, et al. Pharmacodynamic study of disulfiram in men with non-metastatic recurrent prostate cancer. *Prostate Cancer Prostatic Dis*. 2013;16:357–361.
30. Safi R, Nelson ER, Chitneni SK, et al. Copper signaling axis as a target for prostate cancer therapeutics. *Cancer Res*. 2014;74:5819–5831.
31. Altieri DC. Survivin, cancer networks and pathway-directed drug discovery. *Nat Rev Cancer*. 2008;8:61–70.
32. Nakahara T, Takeuchi M, Kinoyama I, et al. YM155, a novel small-molecule survivin suppressant, induces regression of established human hormone-Refractory prostate tumor xenografts. *Cancer Res*. 200;8014–8021.
33. Tolcher AW, Quinn DI, Ferrari A, et al. A phase II study of YM155, a novel small-molecule suppressor of survivin, in castration-resistant taxane-pretreated prostate cancer. *Ann Oncol*. 2012;23:968–973.
34. Leli NM, Dey S, Brady L, Koumenis C. Identifying novel regulators of the Unfolded Protein Response (UPR) by genome-scale CRISPR-Cas9 knockout screens. *Cancer Res*. 2017;77:Abstract nr 1247.
35. Foufelle F, Fromenty B. Role of endoplasmic reticulum stress in drug-induced toxicity. *Pharmacol Res Perspect*. 2016;4:e00211.
36. Chou T-C. Theoretical basis, experimental design, and computerized simulation of synergism and antagonism in drug combination studies. *Pharmacol Rev*. 2006;58:621–681.
37. Warde P, Mason M, Ding K, et al. Combined androgen deprivation therapy and radiation therapy for locally advanced prostate cancer. *Lancet*. 2011;378:2104–2111.
38. Barreto-Andrade JC, Efimova EV, Maucri HJ, et al. Response of human prostate cancer cells and tumors to combining PARP inhibition with ionizing radiation. *Mol Cancer Ther*. 2011;10:1185–1193.
39. Chatterjee P, Choudhary GS, Sharma A, et al. PARP inhibition sensitizes to low dose-Rate radiation TMPRSS2-ERG fusion gene-Expressing and PTEN-Deficient prostate cancer cells. Tofilon PJ, ed. *PLoS ONE*. 2013;8:e60408.
40. Fraser M, Zhao H, Luoto KR, et al. PTEN deletion in prostate cancer cells does not associate with loss of RAD51 function. *Clin Cancer Res*. 2012;18:1015–1027.
41. Lord CJ, Ashworth A. The DNA damage response and cancer therapy. *Nature*. 2012;481:287–294.
42. Helleday T. PARP inhibitor receives FDA breakthrough therapy designation in castration resistant prostate cancer: beyond germline BRCA mutations. *Ann Oncol*. 2016;27:755–757.
43. Naipal KAT, Verkaik NS, Ameziane N, et al. Functional ex vivo assay to select homologous recombination-deficient breast tumors for PARP inhibitor treatment. *Clin Cancer Res*. 2014;20:4816–4826.
44. Feiersinger GE, Trattng K, Leitner PD, et al. Olaparib is effective in combination with, and as maintenance therapy after, first-line endocrine therapy in prostate cancer cells. *Mol Oncol*. 2018;12:561–576.
45. Goh AM, Coffill CR, Lane DP. The role of mutant p53 in human cancer. *J Pathol*. 2011;223:116–126.
46. Chinnaiyan P, Vallabhaneni G, Armstrong E, Huang S-M, Harari PM. Modulation of radiation response by histone deacetylase inhibition. *Int J Radiat Oncol*. 2005;62:223–229.
47. Moudry P, Watanabe K, Wolanin KM, et al. TOPBP1 regulates RAD51 phosphorylation and chromatin loading and determines PARP inhibitor sensitivity. *J Cell Biol* 2016;212:281–288.
48. Fukuda T, Wu W, Okada M, et al. Class I histone deacetylase inhibitors inhibit the retention of BRCA1 and 53BP1 at the site of DNA damage. *Cancer Sci*. 2015;106:1050–1056.
49. Brar SS, Grigg C, Wilson KS, et al. Disulfiram inhibits activating transcription factor/cyclic AMP-responsive element binding protein and human melanoma growth in a metal-dependent manner in vitro, in mice and in a patient with metastatic disease. *Mol Cancer Ther*. 2004;1049–1060.
50. Wang Y, Li W, Patel SS, et al. Blocking the formation of radiation induced breast cancer stem cells. *Oncotarget*. 2014;5:3743–3755.
51. Lun X, Wells JC, Grinshtein N, et al. Disulfiram when combined with copper enhances the therapeutic effects of temozolomide for the treatment of glioblastoma. *Clin Cancer Res*. 2016;22:3860–3875.
52. Nechushtan H, Hamamreh Y, Nidal S, et al. A phase IIb trial assessing the addition of disulfiram to chemotherapy for the treatment of metastatic non-Small cell lung cancer. *Oncologist*. 2015;20:366–367.
53. Huang J, Campian JL, Gujar AD, et al. Final results of a phase I dose-escalation, dose-expansion study of adding disulfiram with or without copper to adjuvant temozolomide for newly diagnosed glioblastoma. *J Neurooncol*. 2018;138:105–111.

SUPPORTING INFORMATION

Additional supporting information may be found online in the Supporting Information section at the end of the article.

How to cite this article: Majera D, Skrott Z, Bouchal J, et al. Targeting genotoxic and proteotoxic stress-response pathways in human prostate cancer by clinically available PARP inhibitors, vorinostat and disulfiram. *The Prostate*. 2019;79:352–362. <https://doi.org/10.1002/pros.23741>

APPENDIX D

Chroma K, Mistrik M, Moudry P, Gursky J, Liptay M, Strauss R, **Skrott Z**, Vrtel R, Bartkova J, Kramara J, Bartek J. Tumors overexpressing RNF168 show altered DNA repair and responses to genotoxic treatments, genomic instability and resistance to proteotoxic stress. *Oncogene*. 2017 Apr 27;36(17):2405-2422. IF₍₂₀₁₇₎: 6.854

ORIGINAL ARTICLE

Tumors overexpressing RNF168 show altered DNA repair and responses to genotoxic treatments, genomic instability and resistance to proteotoxic stress

K Chroma¹, M Mistrik^{1,5}, P Moudry^{1,2,5}, J Gursky¹, M Liptay¹, R Strauss², Z Skrott¹, R Vrtel³, J Bartkova^{2,4}, J Kramara¹ and J Bartek^{1,2,4}

Chromatin DNA damage response (DDR) is orchestrated by the E3 ubiquitin ligase ring finger protein 168 (RNF168), resulting in ubiquitin-dependent recruitment of DDR factors and tumor suppressors breast cancer 1 (BRCA1) and p53 binding protein 1 (53BP1). This ubiquitin signaling regulates pathway choice for repair of DNA double-strand breaks (DSB), toxic lesions whose frequency increases during tumorigenesis. Recruitment of 53BP1 curbs DNA end resection, thereby limiting homologous recombination (HR) and directing DSB repair toward error-prone non-homologous end joining (NHEJ). Under cancer-associated ubiquitin starvation conditions reflecting endogenous or treatment-evoked proteotoxic stress, the ubiquitin-dependent accrual of 53BP1 and BRCA1 at the DNA damage sites is attenuated or lost. Challenging this current paradigm, here we identified diverse human cancer cell lines that display 53BP1 recruitment to DSB sites even under proteasome inhibitor-induced proteotoxic stress, that is, under substantial depletion of free ubiquitin. We show that central to this unexpected phenotype is overabundance of RNF168 that enables more efficient exploitation of the residual-free ubiquitin. Cells with elevated RNF168 are more resistant to combined treatment by ionizing radiation and proteasome inhibition, suggesting that such aberrant RNF168-mediated signaling might reflect adaptation to chronic proteotoxic and genotoxic stresses experienced by tumor cells. Moreover, the overabundant RNF168 and the ensuing unorthodox recruitment patterns of 53BP1, RIF1 and REV7 (monitored on laser micro-irradiation-induced DNA damage) shift the DSB repair balance from HR toward NHEJ, a scenario accompanied by enhanced chromosomal instability/micronuclei formation and sensitivity under replication stress-inducing treatments with camptothecin or poly(ADP-ribose) polymerase (PARP) inhibitor. Overall, our data suggest that the deregulated RNF168/53BP1 pathway could promote tumorigenesis by selecting for a more robust, better stress-adapted cancer cell phenotype, through altered DNA repair, fueling genomic instability and tumor heterogeneity. Apart from providing insights into cancer (patho)biology, the elevated RNF168, documented here also by immunohistochemistry on human clinical tumor specimens, may impact responses to standard-of-care and some emerging targeted cancer therapies.

Oncogene (2017) 36, 2405–2422; doi:10.1038/onc.2016.392; published online 14 November 2016

INTRODUCTION

Reflecting the process of oncogenic transformation and the ensuing biological consequences, cancer cells are generally exposed to enhanced endogenous stresses such as replication stress/DNA damage and proteotoxic stress. Such environment provides selective pressures for tumors to adapt, through selection of features that allow cancer cell survival and proliferation at the expense of genomic instability and potential vulnerabilities in the form of dependencies on various stress-support pathways.^{1–3} For example, nascent tumor cells in early stages of tumorigenesis experience increased replication stress and incidence of DNA lesions including the highly toxic DNA double-strand breaks (DSBs), and such DNA damage is sensed and acted upon by the cell's DNA damage response (DDR) machinery.^{2,4,5} Although such checkpoint response provides a biological anticancer barrier capable of preventing tumor growth

through induction of cellular senescence or cell death,^{6–8} some tumors escape the barriers and progress to aggressive malignancy. One way how cancers breach the DDR barrier is through selection of mutations in the ataxia telangiectasia mutated (ATM)-Chk2-p53 pathway,^{4,6} however, in many cases the adaptation mechanisms that help cancer cells cope with diverse stresses and thereby support tumor progression remain poorly understood.

Given that tumor cells are exposed to higher loads of DSBs, because of both endogenous replication stress and impact of standard-of-care treatments including radiotherapy and multiple chemotherapeutic drugs, cancer cell responses to DSBs are crucial for cancer development and treatment response. Mammalian cells respond to DSBs by activating a multi-component signaling cascade that relies on several protein posttranslational modifications including phosphorylation, ubiquitination, methylation, sumoylation and poly(ADP ribosylation) to orchestrate the DSB

¹Institute of Molecular and Translational Medicine, Faculty of Medicine and Dentistry, Palacky University, Olomouc, Czech Republic; ²Genome Integrity Unit, Danish Cancer Society Research Center, Copenhagen, Denmark; ³Department of Clinical Genetics, University Hospital Olomouc, Olomouc, Czech Republic and ⁴Department of Medical Biochemistry and Biophysics, Science For Life Laboratory, Division of Translational Medicine and Chemical Biology, Karolinska Institute, Solna, Sweden. Correspondence: Dr J Kramara, Institute of Molecular and Translational Medicine, Faculty of Medicine and Dentistry, Palacky University, Hnevotinska 5, Olomouc 775 15, Czech Republic or Professor J Bartek, Genome Integrity Unit, Danish Cancer Society Research Center, Strandboulevarden 49, Copenhagen DK-2100, Denmark. E-mail: juraj.kramara@upol.cz or jb@cancer.dk

⁵These authors contributed equally to this work.

Received 6 June 2016; revised 14 August 2016; accepted 12 September 2016; published online 14 November 2016

signaling and repair.⁹ Closely linked with DSB-induced phosphorylation signaling by the ATM kinase, ubiquitination of diverse proteins on damaged chromatin, mediated by E3 ubiquitin ligases ring finger protein 8 (RNF8) and ring finger protein 168 (RNF168), is critical for proper cellular response to DSBs.¹⁰ RNF8 is recruited to DSB sites through binding to phosphorylated mediator of DNA damage checkpoint 1 (MDC1), an adaptor protein that recognizes the initial DSB signal—the ATM-phosphorylated histone variant H2A.X¹¹ (γ H2AX). RNF8 catalyzes lysine K63-linked ubiquitination of histone H1, which promotes recruitment of the other key E3 ligase, RNF168.¹² The RNF8/RNF168-driven ubiquitinations create a platform for binding of two essential effectors (and tumor suppressors) to the DSB site: p53 binding protein 1 (53BP1) and breast cancer 1 (BRCA1).^{13,14} These two proteins control the DSB repair pathway choice: 53BP1 promotes repair by the non-homologous end joining (NHEJ) pathway, whereas BRCA1 may oppose or facilitate (depending on distinct protein complexes of BRCA1) the homologous recombination (HR) repair. Both BRCA1 and 53BP1 exert their control over the repair pathway choice by regulating DSB end resection. Although 53BP1 licenses NHEJ by limiting resection and dominates in G1 phase, some BRCA1 complexes counteract 53BP1 by removing it from the sites of damage in S phase thereby enabling DNA resection and HR initiation.^{15–17} The exact mechanism of resection inhibition by 53BP1 remains enigmatic, however several 53BP1 interacting factors have been identified recently that have been implicated in resection control, including RIF1 and REV7.^{18–21} Upregulated 53BP1 recruitment in S phase because of absence of functional BRCA1 precludes the error-free HR and licenses inappropriate mutagenic NHEJ at replication-associated DSBs instead, resulting in enhanced chromosomal instability.²² Hence, cells with aberrant S-phase recruitment of 53BP1, such as BRCA1-deficient tumors, exhibit sensitivity toward chemotherapeutic agents that cause damage of replicating DNA, including poly(ADP-ribose) polymerase (PARP) inhibitors (PARPis).¹⁵

The exact nature of 53BP1 recruitment to the DNA damage sites has been elucidated only recently. It has been shown that along with the dimethylated histone H4K20, 53BP1 also reads H2AK15 monoubiquitination catalyzed by RNF168 upon DNA damage.^{23,24} Another layer of regulation represent proteins that compete for the H4K20 mark with 53BP1 and thus oppose 53BP1's recruitment to chromatin. Three such proteins have been reported, the JMJD2A and JMJD2B demethylases and the polycomb protein L3MBTL. All are removed from chromatin upon DNA damage by the ubiquitin–proteasome system (UPS) in an RNF168-dependent manner. Clearance of the competing proteins exposes the H4K20 mark and allows 53BP1 binding to chromatin.^{25,26} Collectively, RNF168 appears to be crucial for both recruitment modes of 53BP1 and thereby for shifting the DSB repair balance toward NHEJ. The central role of RNF168 in DSB signaling is also consistent with the clinical phenotype of its homozygous inactivating mutation, leading to a grave human disease highly reminiscent of the ATM kinase deficiency-associated neurodegeneration, immunodeficiency and cancer-prone syndrome of Ataxia Telangiectasia.²⁷ As a powerful signal amplifier at damaged chromatin, RNF168 requires a careful control over its abundance and function, a requirement documented by negative regulation of RNF168 by two ubiquitin ligases—TRIP12 and UBR5 that target RNF168 for proteasomal degradation.²⁸ Depletion of these proteins causes, in an additive manner, accumulation of RNF168 to supraphysiological levels and enhances the accrual of 53BP1 and other genome caretakers on chromatin.²⁸

According to current understanding in the field, depletion of the cellular-free ubiquitin pool that occurs as a consequence of proteotoxic stress abrogates the ubiquitin-dependent aspects of DSB response such as recruitment of 53BP1.^{29,30} Under proteotoxic stress, ubiquitin is redistributed within the cell, the bulk being trapped in cytoplasmic protein conjugates because of

the limited recycling capacity of the proteasome. Consequently, the free ubiquitin level in the nucleus is depleted and ubiquitin-dependent nuclear processes such as the DSB signaling are attenuated.²⁹ A typical phenotypic manifestation of DDR attenuation under ubiquitin depletion conditions is a failure to recruit the 53BP1 and BRCA1 proteins to the sites of damage.³⁰ As mentioned above, most tumors experience at least partly enhanced endogenous proteotoxic stress, a scenario most prominent in multiple myeloma.¹ The endogenous proteotoxic stress is a consequence of cancer-related gross changes in chromosome number, gene copy number, aberrant protein overproduction exemplified by the immunoglobulin-producing myelomas and/or transcription variants that boost the production of aberrant proteins thus overloading the UPS.¹ Hence, proteotoxic stress seems to be intimately linked to cancer and has been listed as one of the emerging cancer hallmarks.³ Exacerbating the endogenous proteotoxic stress by proteasome inhibitors has proven to be a viable strategy in treatment of multiple myeloma and it may be applicable also to other cancers.¹ Nevertheless, a broader use of proteasome inhibitors in cancer treatment has so far been hampered by limited efficiency of proteasome inhibition *in vivo* and frequent emergence of resistance.¹

While analyzing responses to diverse stresses among a range of human cell types, we identified a subset of cancer cell lines that did not follow the established pattern of limited DSB response under enhanced proteotoxic stress. Through a combination of functional DDR-related, biochemical and cell biology approaches, we pinpointed aberrant ubiquitin signaling centered around overabundance of RNF168 as the mechanistic basis of this paradigm-shifting cancer-associated phenotype. These results, as well as implications of these findings for our understanding of tumorigenesis and responses of cancer cells to diverse treatments are presented below.

RESULTS

53BP1 is recruited to DNA damage sites despite proteotoxic stress in MDA-MB-231 cells

In an attempt to identify vulnerabilities of triple-negative carcinomas, a subset of breast tumors with poor prognosis, often aberrant DSB repair and currently lacking any targeted treatment option, we examined diverse aspects of the DDR machinery in the human triple-negative breast cancer model cell line MDA-MB-231. In sharp contrast to the current consensus in the field, inhibition of proteasome activity that depletes the pool of free cellular ubiquitin did not abrogate recruitment of the 53BP1 protein to ionizing radiation induced foci (IRIF). Indeed, in the MDA-MB-231 cell line exposed to IR after a 2-h pre-treatment with the proteasome inhibitor MG132 formation of 53BP1-positive IRIF was not diminished compared with controls with active proteasome, as over 40 % of cells formed > 5 53BP1 IRIFs (Figures 1a and b). In contrast, in the control U2OS sarcoma cell line, the same treatment abrogated 53BP1 IRIF formation completely (Figures 1a and b). Another control cell type, a primary diploid human fibroblast strain (BJ) responded in the same manner as the U2OS cells (Figures 1a and b). Collectively, these results indicated that in the MDA-MB-231 cells, the 53BP1 DSB response pathway displays an exceptional resistance to depletion of free ubiquitin.

Unorthodox DSB response in MDA-MB-231 cells is limited to downstream steps of the pathway

We reasoned that the MDA-MB-231 cells might exhibit a non-standard response to core proteasome inhibition resulting in a less pronounced drop in free ubiquitin levels thus enabling sustained 53BP1 IRIF formation. Nevertheless, immunoblotting analysis of total ubiquitin showed accumulation of high-molecular weight ubiquitin conjugates and depletion of free ubiquitin in both

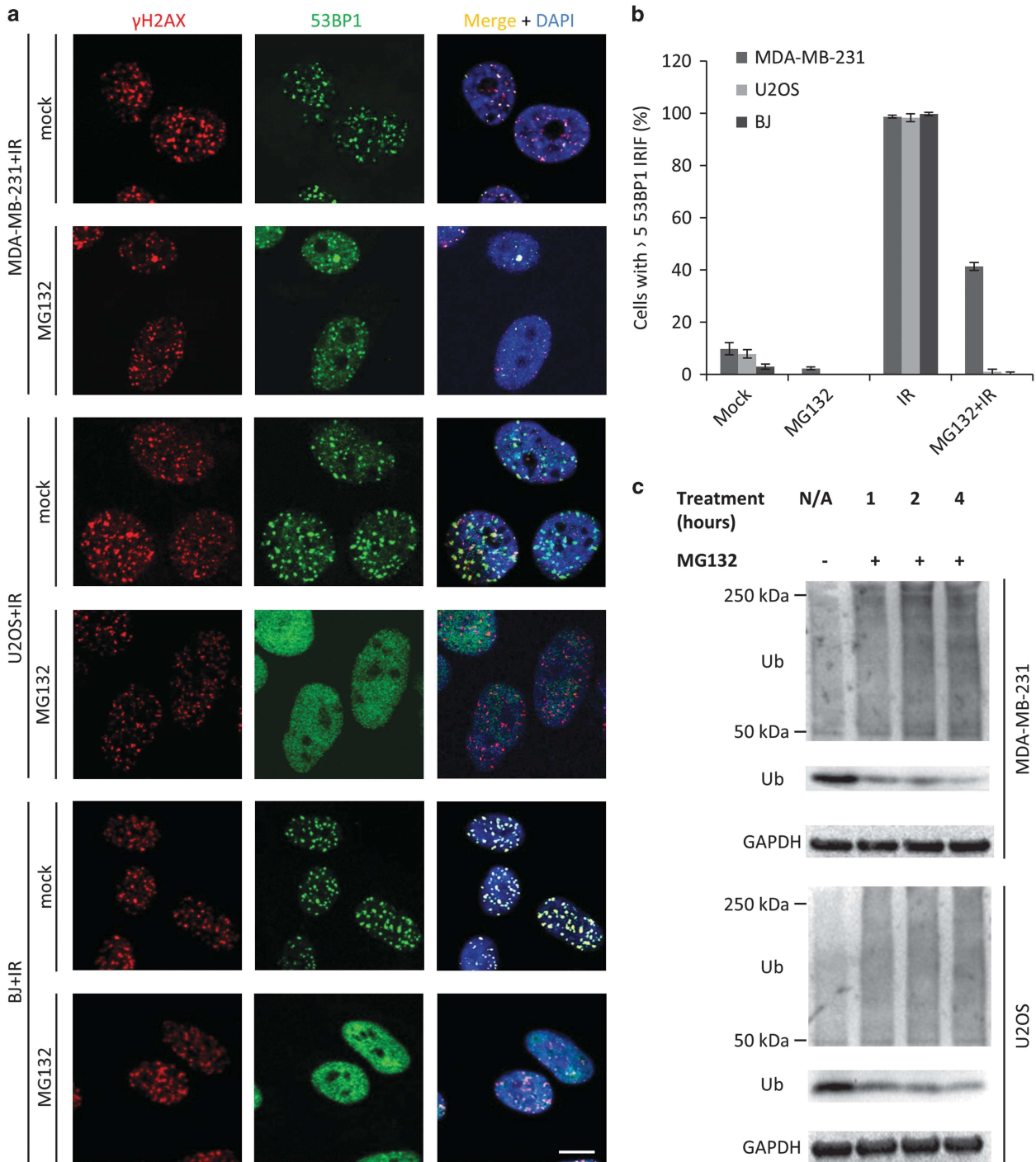


Figure 1. 53BP1 is recruited to DNA damage sites despite proteotoxic stress in MDA-MB-231 cells. **(a)** MDA-MB-231, U2OS and BJ cells were mock- or MG132 (5 μ M) treated for 2 h and subsequently irradiated with 2 Gy. One hour post-irradiation, the cells were fixed and immunostained for γ H2AX and 53BP1. Scale 10 μ m. **(b)** Cells with > 5 53BP1 IRIFs were scored for all three lines after mock, MG132 or either of the treatments combined with irradiation (2 Gy). **(c)** MDA-MB-231 and U2OS cells were mock and MG132 treated, lysed at various time points and subsequently probed for free ubiquitin and ubiquitin conjugate levels using immunoblotting. In **(b)**, results are mean \pm s.d. of three independent experiments.

MDA-MB-231 and U2OS control upon MG132 treatment (Figure 1c). Along with free ubiquitin depletion, accumulation of such protein-ubiquitin conjugates is a sign of proteasome inhibition, indicating that altered sensitivity to proteasome inhibitors is unlikely to cause the observed MDA-MB-231 phenotype.

Analogous to the known response in U2OS cells,¹³ the MG132-treated MDA-MB-231 cells also displayed the disappearance of ubiquitin conjugates (detected by the FK2 antibody) at sites of IR-inflicted DNA damage (Figures 2a and b). It has been shown that upon proteasome inhibition, ubiquitin is largely lost from histones and other nuclear proteins and shuttled to cytoplasmic proteins

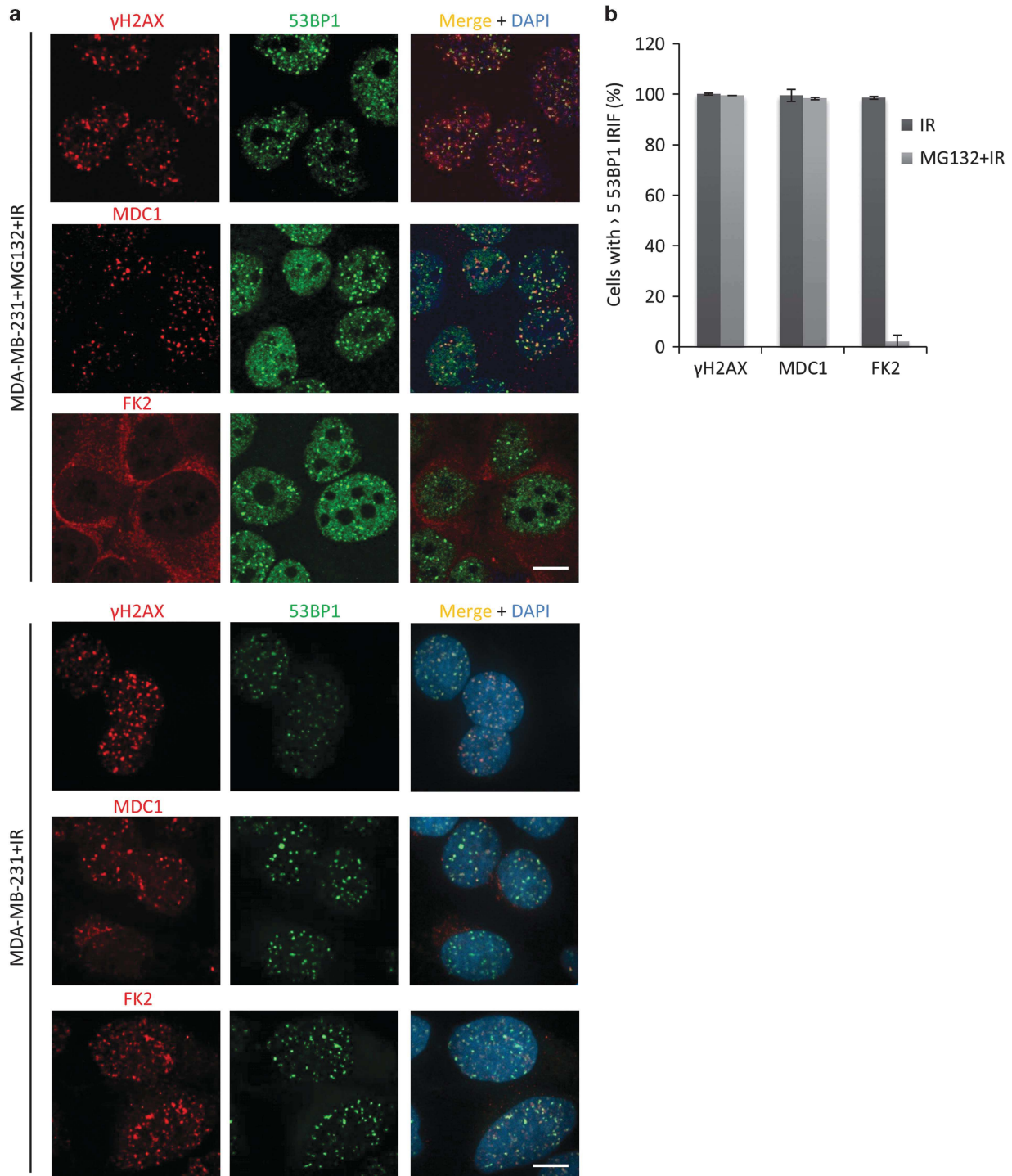


Figure 2. Probing DSB response upstream of 53BP1 in MG132-treated MDA-MB-231 and U2OS cells. **(a)** MDA-MB-231 cells were pretreated with MG132 for 2 h, irradiated with 2 Gy and 1 h post-irradiation immunostained for the indicated proteins or protein modifications known to be present in IRIFs. Scale 10 μ m. **(b)** Graphical summary of nuclei with > 5 γ H2AX, FK2 or MDC1 IRIFs, scored in cells bearing > 5 53BP1 IRIFs. Results are mean \pm s.d. of three independent experiments.

awaiting degradation in the proteasome complex.²⁹ This result again shows that MDA-MB-231 cells respond to proteasome inhibition in an apparently standard way leading to depletion of the free nuclear ubiquitin pool, without any obvious compensatory mechanism that would facilitate the sustained 53BP1 accrual at the sites of DNA damage.

Importantly, additional key DDR factors acting upstream of 53BP1 such as γ H2AX and recruitment of MDC1 were observed in

IRIFs (Figures 2a and b) in both mock-treated and proteasome inhibitor-treated cells. This suggested that the upstream steps of the DSB response pathway react to proteasome inhibition largely in a standard mode in MDA-MB-231 cells.

To further assess the chromatin DSB response pathway at the level of 53BP1 and its associated proteins in the proteasome-inhibited cells, we probed the MDA-MB-231 and the control U2OS cells for recruitment of two known 53BP1 effectors—RIF1^{19,21} and

REV7,²⁰ to laser micro-irradiation induced DNA damage sites. In contrast to U2OS, MG132 pretreated MDA-MB-231 cells showing 53BP1 accumulation in laser-induced 'stripes' also displayed RIF1 and REV7 accrual at such sites of micro-irradiation (Figures 3a and b). These results imply that the upstream steps of the DSB response pathway operate normally, and the unorthodox DSB response in the MDA-MB-231 cells under proteotoxic stress is shared by 53BP1 and its downstream effectors.

UDR motif-mutated 53BP1 is not recruited to DSB sites under proteotoxic stress

53BP1 binds to two chromatin modifications at the DSBs—dimethylated histone H4 (H4K20) and ubiquitinated histone H2A (H2AK15Ub).^{23,24} The H2AK15Ub mark is recognized by the ubiquitin damage response (UDR) domain at the C-terminal part of 53BP1.²⁴ We utilized a UDR motif-mutated 53BP1 incapable of binding the H2AK15Ub mark to test whether ubiquitin was indeed required for 53BP1 accumulation at DSBs under conditions of proteotoxic stress in the MDA-MB-231 line. Although a 53BP1 wild-type green fluorescent protein (GFP) fusion protein was recruited to IRIFs, cells expressing the GFP-tagged UDR mutant (L1619A)²⁴ did not form 53BP1 IRIFs (Figure 4). Furthermore, a GFP-tagged Tudor domain 53BP1 mutant (D1521R)²⁴ behaved similarly and was not recruited to IRIFs (Figure 4). Taken together, this implied that in the MDA-MB-231 cells, 53BP1 recruitment still depends on each of the two intact modules that recognize H4K20 and H2AK15Ub, respectively, even when levels of cellular-free ubiquitin become limiting.

The proteotoxic stress-resistant DSB response depends on ubiquitin signaling, particularly RNF168

As the DSB response in the MDA-MB-231 cells is still fueled by ubiquitin under proteotoxic stress, a mechanism should exist that provides sufficient amount of ubiquitin to sustain the process. One plausible way of bypassing an acute decrease in free ubiquitin levels is overexpression of the E2 and/or E3 ubiquitin conjugating enzymes/ligases. Elevated pool of an E2 conjugating enzyme that was charged with ubiquitin before the drop in free ubiquitin level might serve as a temporary reservoir for downstream processes. On the other hand, an overexpressed E3 ligase might outcompete other E3 ligases in the uptake of residual ubiquitin under conditions of proteotoxic stress. Hence, we examined the levels of the key DSB response related ubiquitin conjugating enzyme UBC13 (UBE2N) and E3 ligases RNF8 and RNF168 in the MDA-MB-231 cells. Strikingly, all three enzymes displayed elevated levels in this cell line (Figure 5a). When normalized to glyceraldehyde 3-phosphate dehydrogenase (GAPDH), both RNF8 and RNF168 showed more than twofold higher levels than those in the U2OS cells, whereas UBC13 level was even higher—more than fivefold above the U2OS cells (Figure 5b). The overabundance of these three enzymes was even more profound when the normal diploid BJ cells were compared with MDA-MB-231 cells: more than fourfold for UBC13, sixfold for RNF8 and more than eightfold in the case of RNF168 (Figure 5b). Importantly, the level of the 53BP1 protein was comparable in all three cell types (Figure 5b).

Quantitative PCR and cycloheximide chase experiments indicated that the overabundance of RNF168 in the MDA-MB-231 cells reflected transcriptional upregulation rather than increased protein stability (Supplementary Figures S1A and B). In addition to transcriptional upregulation, an increase in RNF168 translation efficiency and/or transcript stability likely contribute to the observed RNF168 protein overabundance in MDA-MB-231 cells as transcriptional upregulation alone (a 2.5-fold increase compared with U2OS, Supplementary Figure S1A) is unlikely to account for the high RNF168 protein levels given the faster protein turnover of RNF168 in these cells (deduced from the

almost fourfold shorter RNF168 protein half-life in MDA-MB-231 compared with U2OS, Supplementary Figure S1B). Indeed, the accelerated turnover of RNF168 protein was consistent with overabundant TRIP12 and UBR5 (Supplementary Figure S1C), the two enzymes critical for ubiquitin/proteasome-mediated degradation of RNF168.²⁸ The elevated TRIP12 and UBR5 might reflect a fine-tuning mechanism in MDA-MB-231 cells, possibly providing a negative feedback loop to limit the overabundant RNF168 to levels that are not overly harmful to cells, a scenario that occurs upon experimental gross overexpression of RNF168.²⁸ Consistently, depletion of either TRIP12 or UBR5 in MDA-MB-231 led to an even more pronounced DSB response phenotype resistant to proteasome inhibition (Supplementary Figure S1D), possibly due to further increase in the abundance of RNF168. As to additional components of the ubiquitin-mediated DSB signaling, we found enhanced abundance of HERC2 (Supplementary Figure S1C), another ubiquitin ligase that promotes 53BP1 recruitment at DSBs,³¹ whereas there was little if any alteration of the negative regulators JMJD2A, L3MBTL1 or RNF169 proteins³² (negative data, not shown).

Overall, these results supported the functional significance of the RNF168-centered ubiquitin-mediated signaling pathway in the altered DSB response in MDA-MB-231 cells. This notion was further supported by functional experiments, in which small interfering RNA (siRNA)-mediated knockdown of UBC13, RNF8 or RNF168 completely abolished the proteotoxic stress-resistant DSB response phenotype in the proteasome inhibitor-treated MDA-MB-231 cells (Figures 5c and d).

Based on available mechanistic insights²⁸ and the pronounced clinical phenotype of RNF168 deficiency,²⁷ we hypothesized that the RNF168 ligase could be central to the unorthodox DSB response phenotype in MDA-MB-231 cells. Partial knockdown of RNF168 with increasing amounts of siRNA resulted in a gradual decrease of cells capable of forming >5 53BP1 IRIFs (Figure 6a). Importantly, this phenotype could be rescued by expression of siRNA-resistant WT, but not the mutant version of RNF168 (C16S, in the RING domain) that abolishes the enzymatic activity of the protein (Figure 6b).

If RNF168 has a central role in the studied DSB response phenotype, overexpression of the enzyme in a cell line incapable of sustaining DSB signaling under proteotoxic stress might mimic the situation seen in MDA-MB-231 cells. Indeed, an U2OS-derived cell line overexpressing a RNF168-GFP fusion protein exhibited 53BP1 IRIF formation in nearly all nuclei even after proteasome inhibition (Figures 6c–e). As in the case of MDA-MB-231 cells, the number of 53BP1 IRIF-positive cells correlated with the level of RNF168 (Supplementary Figure S2) and, consistent with the pathway hierarchy,^{5,13} the phenotype was dependent on RNF8 (Supplementary Figure S3). Of note, changes in RNF8 levels had a less profound effect on the phenotype compared with the more marked impact of RNF168 abundance, thereby supporting the major role of RNF168 in the proteotoxic stress-resistant DSB response (Supplementary Figure S3). Furthermore, ectopic expression of the RNF168 (C16S) mutant in the U2OS cell line did not result in the proteotoxic stress-resistant phenotype (Supplementary Figure S4), as opposed to expression of the WT protein (Figures 6c and d and Supplementary Figure S4). These results also parallel the scenario seen in MDA-MB-231 cells, where the ectopic RNF168 C16S RING mutant was incapable of rescuing the loss of the phenotype caused by knockdown of endogenous RNF168. Overall, these data were consistent with the emerging key role of RNF168 abundance in the proteotoxic stress-resistant DSB response.

The proteotoxic stress-resistant DSB response cancer phenotype is more common

Next, we asked whether the emerging phenotype observed in the triple-negative breast cancer cells MDA-MB-231 is unique or more widespread, and tested a panel of proteasome inhibitor-treated

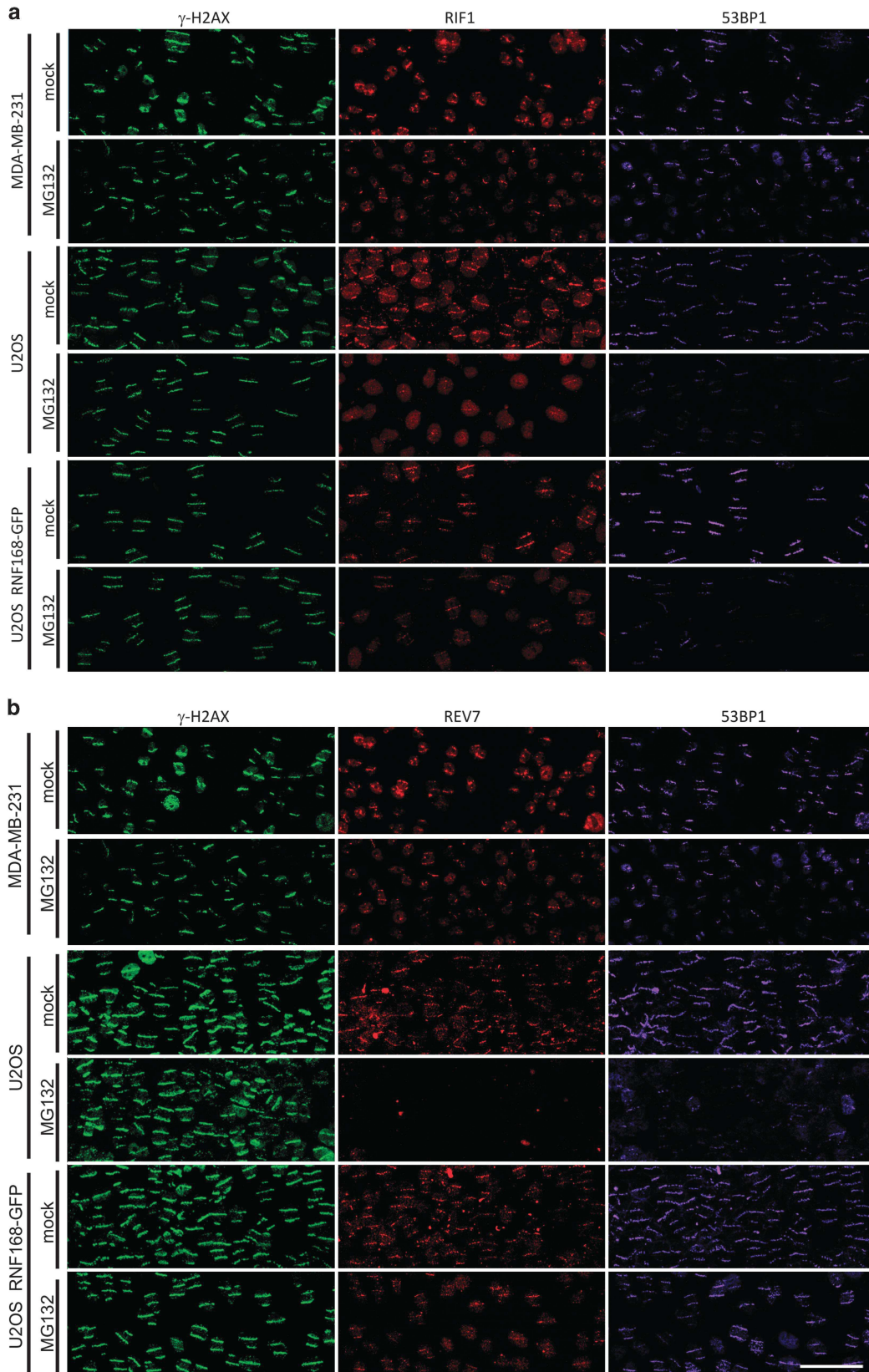


Figure 3. Probing DSB response downstream of 53BP1 in MG132-treated MDA-MB-231, U2OS and U2OS RNF168-GFP cells. (a) Mock or MG132-treated (5 μ M, 2 h) MDA-MB-231, U2OS and U2OS RNF168-GFP cells were laser-microirradiated and immunostained for γ H2AX, 53BP1 and RIF1. (b) As in (a), but staining for γ H2AX, 53BP1 and REV7. Scale bar 50 μ m.

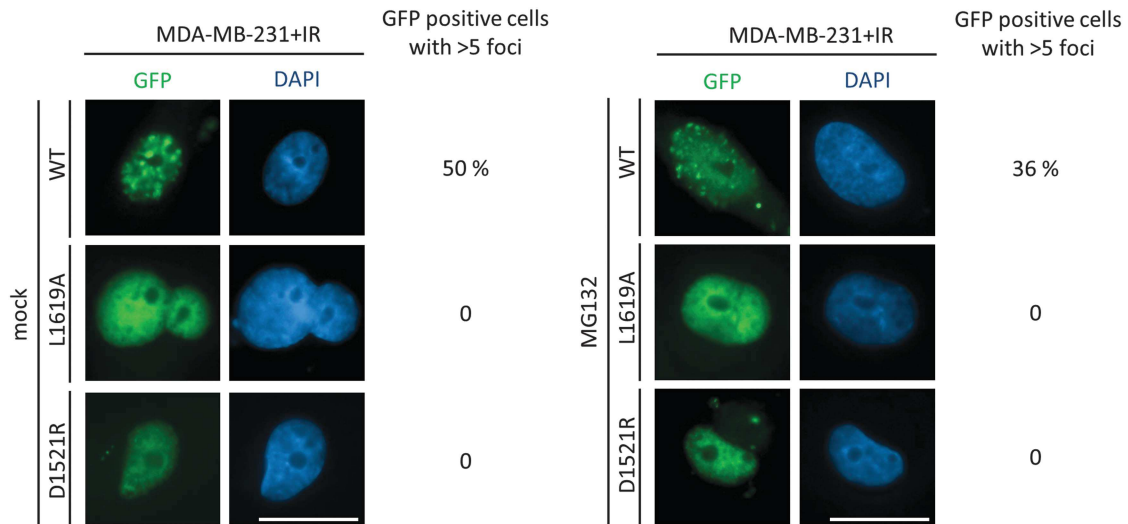


Figure 4. 53BP1 recruitment to sites of damage in MDA-MB-231 is methylation and ubiquitination dependent. MDA-MB-231 cells transfected with siRNA against 53BP1 and expression vectors for the indicated siRNA-resistant GFP-tagged versions of 53BP1 were mock or MG132 treated (2 h, 5 μ M), irradiated with 2 Gy and after 1 h processed for GFP imaging. Scale 20 μ m. Results are mean of two independent experiments.

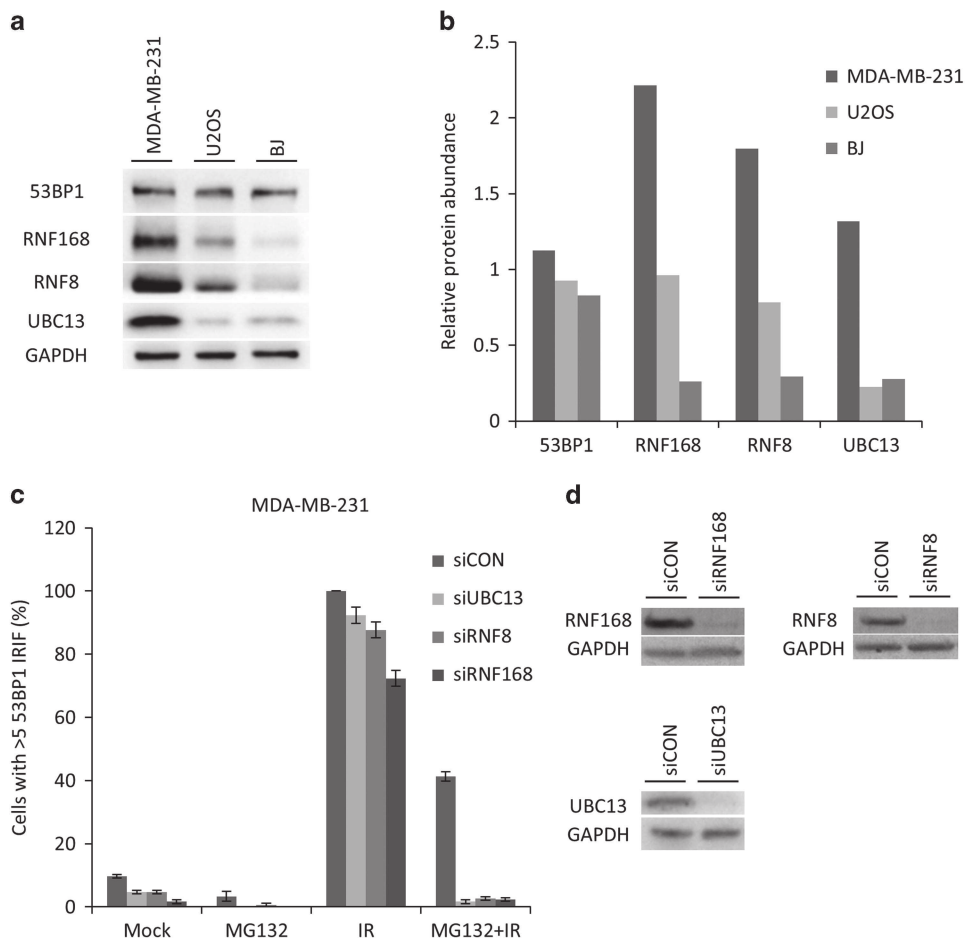
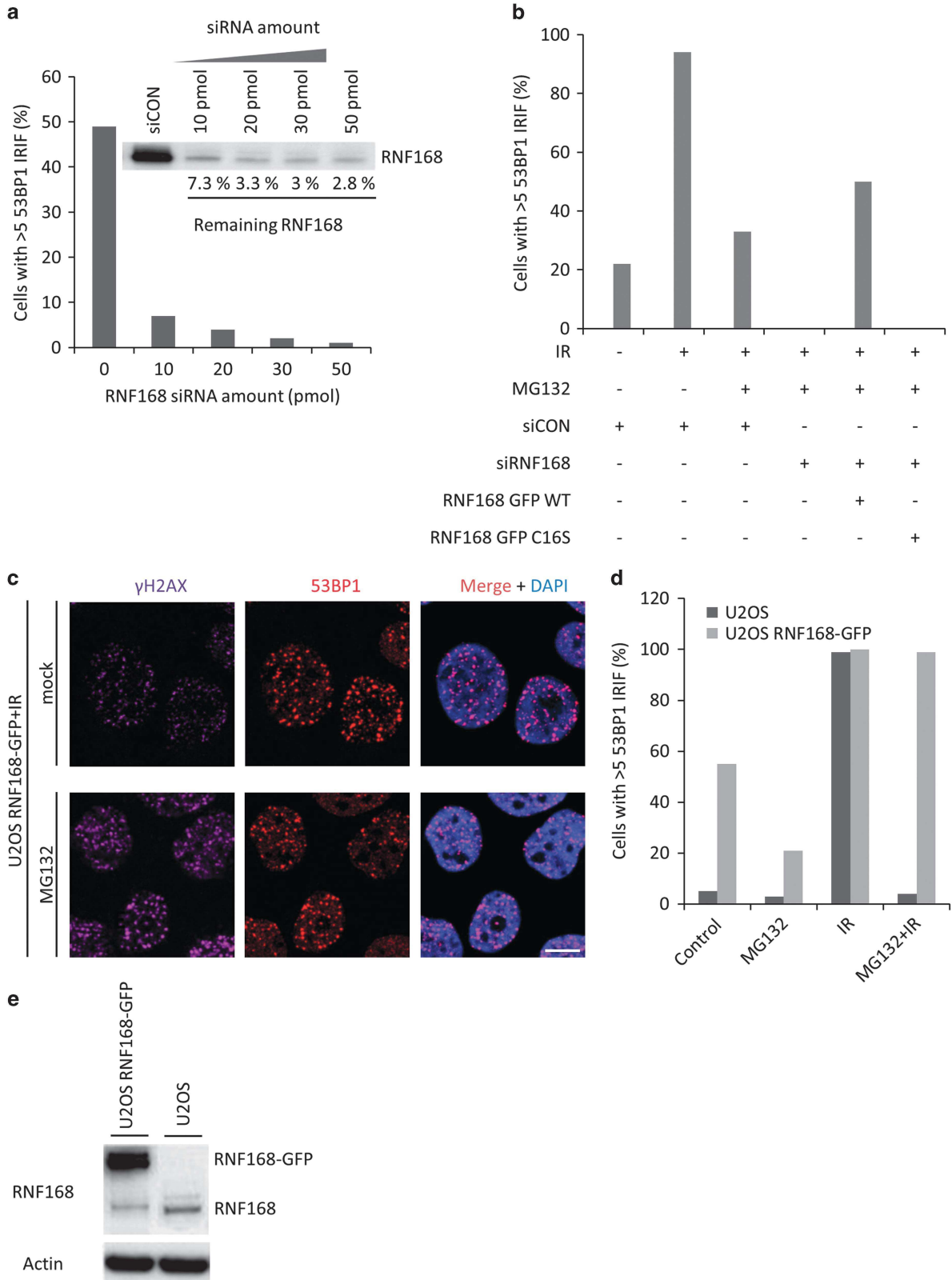


Figure 5. Elevated levels and impact of ubiquitin-mediated DSB signaling-related enzymes in MDA-MB-231 cells. **(a)** MDA-MB-231, U2OS and BJ cell lysates were analyzed by immunoblotting for abundance of 53BP1 and the major DSB ubiquitin signaling enzymes RNF8, RNF168 and UBC13. **(b)** Protein abundance was calculated using densitometric analysis of the immunoblot shown in **a**. Band intensities were normalized to corresponding GAPDH bands. **(c)** MDA-MB-231 cells were transfected with indicated siRNAs, mock and MG132 treated (2 h, 5 μ M) with and without irradiation (2 Gy) and 1 h post-irradiation stained for 53BP1. Cells with >5 53BP1 IRIF were scored. Results are mean \pm s.d. of three independent experiments **(d)** Knockdown efficiency in **(c)** was verified by probing corresponding cell lysates by immunoblotting using indicated antibodies.

human cancer cell lines for occurrence of 53BP1 IRIF. Strikingly, we observed the proteotoxic stress-resistant DSB response analogous to MDA-MB-231 cells also in two other cell lines, the breast cancer-derived MCF7 cells and cervical cancer-derived HeLa cells, whereas MDA-MB-436, another breast cancer cell line, was

phenotypically similar to the control U2OS cells (Figure 7a). Notably, all cell lines displaying the proteotoxic stress-resistant DSB response showed elevated RNF168 (Figures 7b and c). The protein levels of RNF8 and UBC13 in MCF7 and HeLa cells showed only a slight if any increase, in contrast to the more pronounced



elevation of RNF168 (Figure 7b). The combination of enhanced RNF168 and 'normal' levels of RNF8 and UBC13 was therefore reminiscent of the scenario seen in the engineered RNF168-GFP overexpressing U2OS cell line (Figure 7b), which also shares the altered DSB response phenotype. Consistently, the selectively enhanced level of RNF168 in the RNF168-GFP overexpressing U2OS cell line also resulted in the recruitment to DSBs of the 53BP1-dependent RIF1 and REV7 proteins under conditions of proteasome inhibition (Figures 3a and b). Overall, these results further supported the central role of the RNF168 ligase in the altered DSB response phenotype.

Given the wider occurrence of the proteotoxic stress-resistant DSB response, we asked whether it might represent some kind of phenotypic adaptation beneficial for tumor cells. Cancer cells experience a higher load of intrinsic genotoxic stress including DSBs^{2,4} and enhanced proteotoxic stress¹ that might possibly attenuate the ubiquitin-mediated DSB response pathway because of chronic limitation of free ubiquitin. We hypothesized that a proteotoxic stress-resistant DSB response may help to counteract the adverse effects of proteotoxic stress on DSB signaling and thereby support tumor cell viability. When four cell lines from our panel were treated with MG132 and subsequently irradiated, their survival positively correlated with their respective abilities to sustain the DSB response under such proteotoxic stress conditions. The cell lines MDA-MB-231 and MCF7 that display the proteotoxic stress-resistant DSB response showed significantly higher survival compared with the control U2OS and BJ cells (Figure 7e). Also, consistent with the above-mentioned hypothesis about the potential adaptive value of the proteotoxic stress-resistant DSB response during tumor progression, partial short hairpin RNA (shRNA)-mediated knockdown of RNF168 lowered the tolerance to combined proteasome inhibition and IR treatment in MDA-MB-231 cells (data not shown).

One of the most prominent signs of chronic proteotoxic stress is accumulation of ubiquitin-conjugated proteins because of cellular protein quality control and UPS overload. The accumulation is readily detectable by immunoblotting and immunostaining techniques using antibodies recognizing protein-conjugated ubiquitin. To examine whether the heightened resistance to combined irradiation and proteasome inhibition (Figure 7e) correlated with higher loads of endogenous proteotoxic stress, we compared the levels of conjugated ubiquitin in our panel of cell lines (Figure 7d) by immunoblotting using an antibody against K48 linked ubiquitin. Pronounced conjugate accumulation in both MDA-MB-231 and MCF7 cells was apparent compared with BJ and U2OS cells (Figure 7d). This finding was consistent with our hypothesis that the increased tolerance to simultaneous irradiation and proteasome inhibition in the MDA-MB-231 and MCF7 lines might reflect adaptation to chronic proteotoxic stress.

Proteasome inhibitors have been successfully used in the treatment of multiple myeloma and other hematological malignancies.³³ Besides pro-apoptotic effects, one of the proposed modes of action of these inhibitors is further exacerbation of the high intrinsic proteotoxic stress in the immunoglobulin-

producing myeloma cells thus causing a lethal unfolded protein response.¹ Given the high endogenous levels of proteotoxic stress in myeloma cells, we asked whether myelomas show a similarly 'adapted' DSB response, reminiscent of some carcinoma cell lines such as MDA-MB-231. We therefore probed two human myeloma cell lines, AMO1 and MMS1, for their ability to form 53BP1 IRIFs after MG132 treatment. Strikingly, the proteotoxic stress-resistant DSB response phenotype in these myeloma cell lines was even more pronounced than in the MDA-MB-231 cells, as 60% and 90% of AMO1 and MMS1 myeloma cells, respectively, formed more than five 53BP1 IRIFs under proteasome inhibition conditions (Figures 8a and b). Similarly to MDA-MB-231 and other cancer cell lines that share the proteotoxic stress-resistant DSB response, the ability to sustain 53BP1 IRIF formation after MG132 treatment correlated with elevated RNF168. Protein levels of RNF168 in AMO1 and MMS1 cells exceeded not only those seen in BJ and U2OS cells, but even that in MDA-MB-231 cells (Figure 8c). As expected, both AMO1 and MMS1 cell lines showed grossly elevated levels of intrinsic proteotoxic stress manifested by accumulation of poly-ubiquitinated proteins and the BIP protein—an established marker of proteotoxic stress and UPR activation (Figure 8c).³⁴ Taken together, these results further support the possibility that the proteotoxic stress-resistant DSB response indeed represents an adaptation to chronic proteotoxic stress experienced by tumors.

To validate the relevance of our findings obtained in experiments with cultured cell lines on clinical material, we performed an immunohistochemical analysis of the abundance of the central element of the pathway, RNF168 on archival paraffin sections from a cohort of carcinomas of the head and neck, uterine cervix and anus, and the corresponding normal human stratified epithelial tissues as matching controls. The rationale for using this material included the following main arguments: (i) the above tumor types often harbor human papillomavirus oncogenes and therefore match HeLa cells that we found positive for the proteotoxic stress-resistant DSB response phenotype; (ii) as normal breast epithelium contains only rare proliferating cells, the stratified epithelium provides a more rigorous control tissue as there are clearly defined layers of constantly proliferating cells, thereby avoiding a bias of comparing proliferating breast tumors (relevant to MDA-MB-231 and MCF7 cell lines in our panel) with largely nonproliferating normal breast tissue. As can be seen from the representative examples of the immunohistochemical staining patterns (Supplementary Figure S5), the abundance of RNF168 was clearly higher in the cancer tissues ($n=25$) compared with normal epithelium ($n=18$), whereas the expression of 53BP1, used as an internal control protein, was comparable in both cancerous and normal tissues (Supplementary Figure S5).

Overall, these results indicate that the observed proteotoxic stress-resistant DSB response phenotype is shared by a subset of human cancer cell lines, and its main feature—the overabundance of RNF168, is also observed in clinical tumor specimens.

Figure 6. The proteotoxic stress-resistant DSB response phenotype depends on RNF168. **(a)** MDA-MB-231 cells were transfected with increasing amounts of RNF168 siRNA, treated with 5 μM MG132 (2 h), irradiated (2 Gy) and 1 h post-irradiation stained for 53BP1. Nuclei with > 5 53BP1 IRIFs were scored. Inset—siRNA transfected MDA-MB-231 cells were lysed and analyzed by immunoblotting for remaining RNF168 level. **(b)** MDA-MB-231 cells were co-transfected with control or RNF168 siRNA and siRNA-resistant plasmids carrying GFP-tagged WT or the C16S RING mutant version of RNF168. Transfected cells were mock or MG132 treated (2 h, 5 μM), irradiated (2 Gy) and 1 h post-irradiation stained for 53BP1 and scored for nuclei with > 5 53BP1 IRIFs. **(c)** U2OS RNF168-GFP cells were pre-treated with MG132 for 2 h, irradiated with 2 Gy and 1 h post-irradiation immunostained for γH2AX and 53BP1. Scale bar 10 μm . **(d)** U2OS RNF168-GFP cells were mock or MG132 treated (2 h, 5 μM), irradiated (2 Gy) and 1 h post-irradiation stained for 53BP1 and scored for nuclei with > 5 53BP1 IRIFs. The chart shows one of three consistent repeats. **(e)** U2OS and U2OS RNF168-GFP cells were lysed and probed for RNF168 levels by immunoblotting. The total level of RNF168 in U2OS RNF168-GFP is approximately fivefold higher than in U2OS. In **(a, b and d)**, the charts show one out of three consistent experiments.

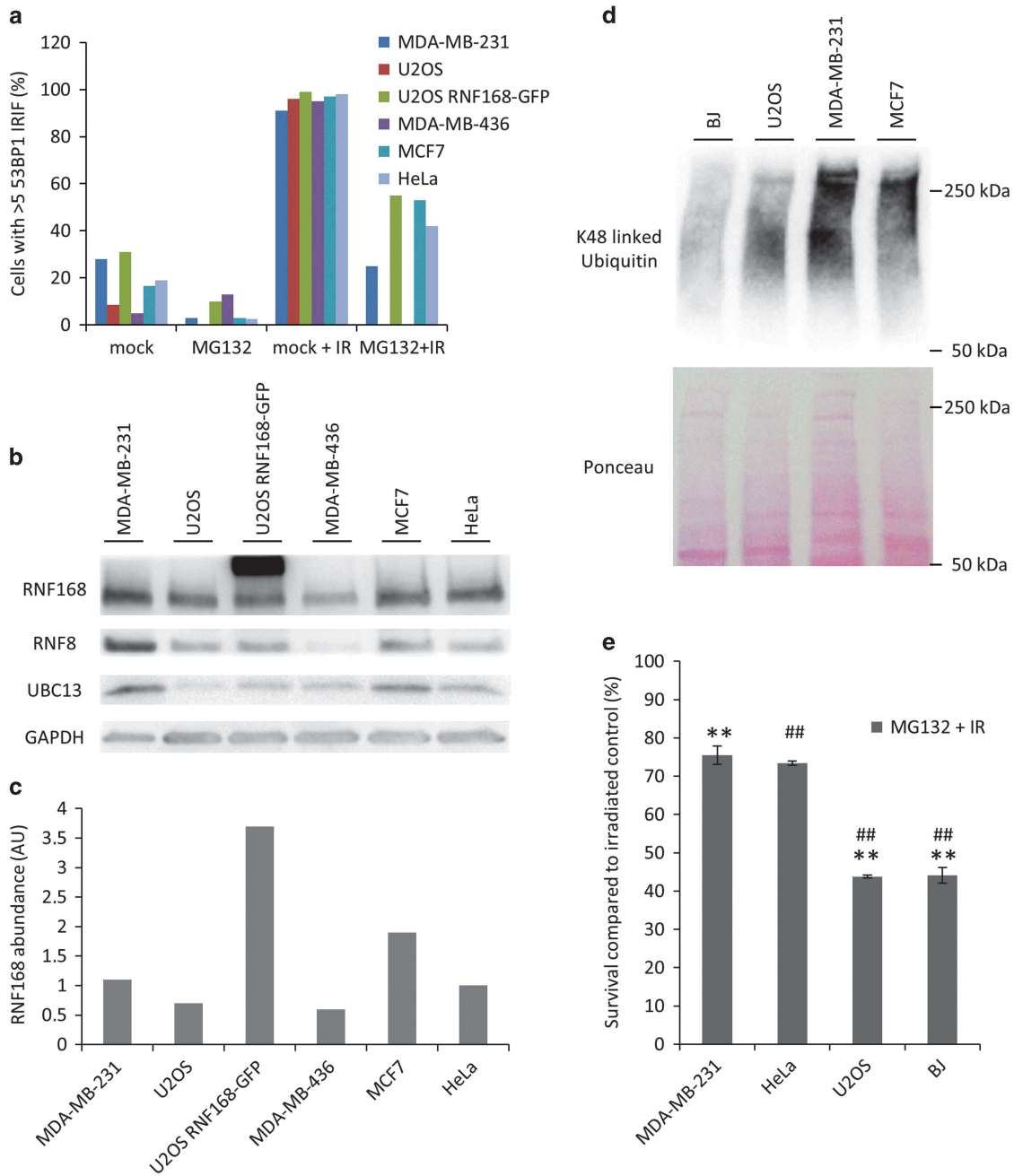


Figure 7. The proteotoxic stress-resistant DSB response phenotype is shared by other cancer cell lines. **(a)** Indicated cells lines were mock- and MG132 treated (2 h, 5 μ M), either with or without irradiation (2 Gy) and 1 h post-irradiation stained for 53BP1. Nuclei with >5 53BP1 IRIFs were scored. **(b)** Lysates prepared from the lines in **(a)** were probed for RNF8, RNF168 and UBC13 levels by immunoblotting. **(c)** RNF168 band intensity was quantified and normalized according to the total protein levels in the indicated lines. **(d)** Indicated cell lines were probed for the level of conjugated K48 linked ubiquitin by immunoblotting. Equal protein amounts were loaded for all the cell lines. **(e)** Indicated cell lines displaying various levels of RNF168 expression were pretreated with 5 μ M MG132 (2 h), irradiated with 2 Gy and 1 h post-treatment seeded to Petri dishes. Six days post-irradiation, the cells were trypsinized and counted using an automated cell counter. In **(a)** and **(e)**, results are mean \pm s.d. of three independent experiments. Statistical significance was determined with two-tailed unpaired Student's *t*-test; **,#*p* < 0.005.

Overabundant RNF168 shifts DSB repair toward NHEJ, enhances genomic instability and vulnerability to PARPis and camptothecin

The results obtained so far suggested that MDA-MB-231 and some other cancer cell lines capable of DSB signaling despite proteotoxic stress may deviate from normal cells and from other cancer cell lines in various aspects of their genome integrity control. To explore this emerging concept further, we first assessed the response of MDA-MB-231 cells to PARPi, a strategy

that causes DNA damage mainly during S phase and which showed promise in treatment of a subset of triple-negative breast tumors in clinical trials.^{35,36} Immunofluorescence analysis showed that while > 60% of S-phase MDA-MB-231 cells treated by a PARPi displayed over 10 53BP1-positive foci per nucleus, in U2OS the fraction of such cells was significantly lower (Figures 9a and b). Given the similar cell cycle phase profiles of both cell lines (data not shown) and the fact that the DSBs caused by PARPi commonly occur during S phase and are preferentially repaired by HR the

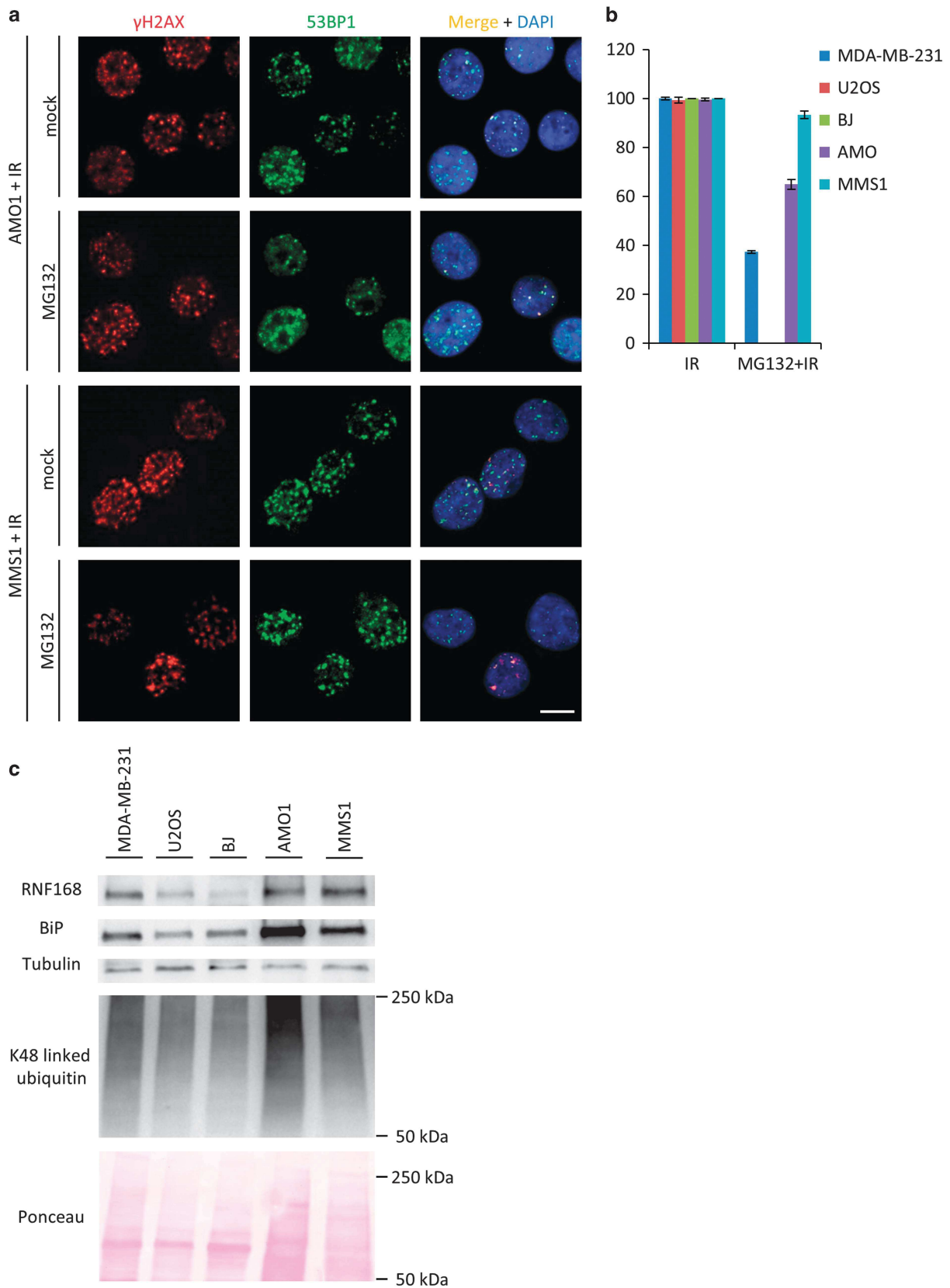
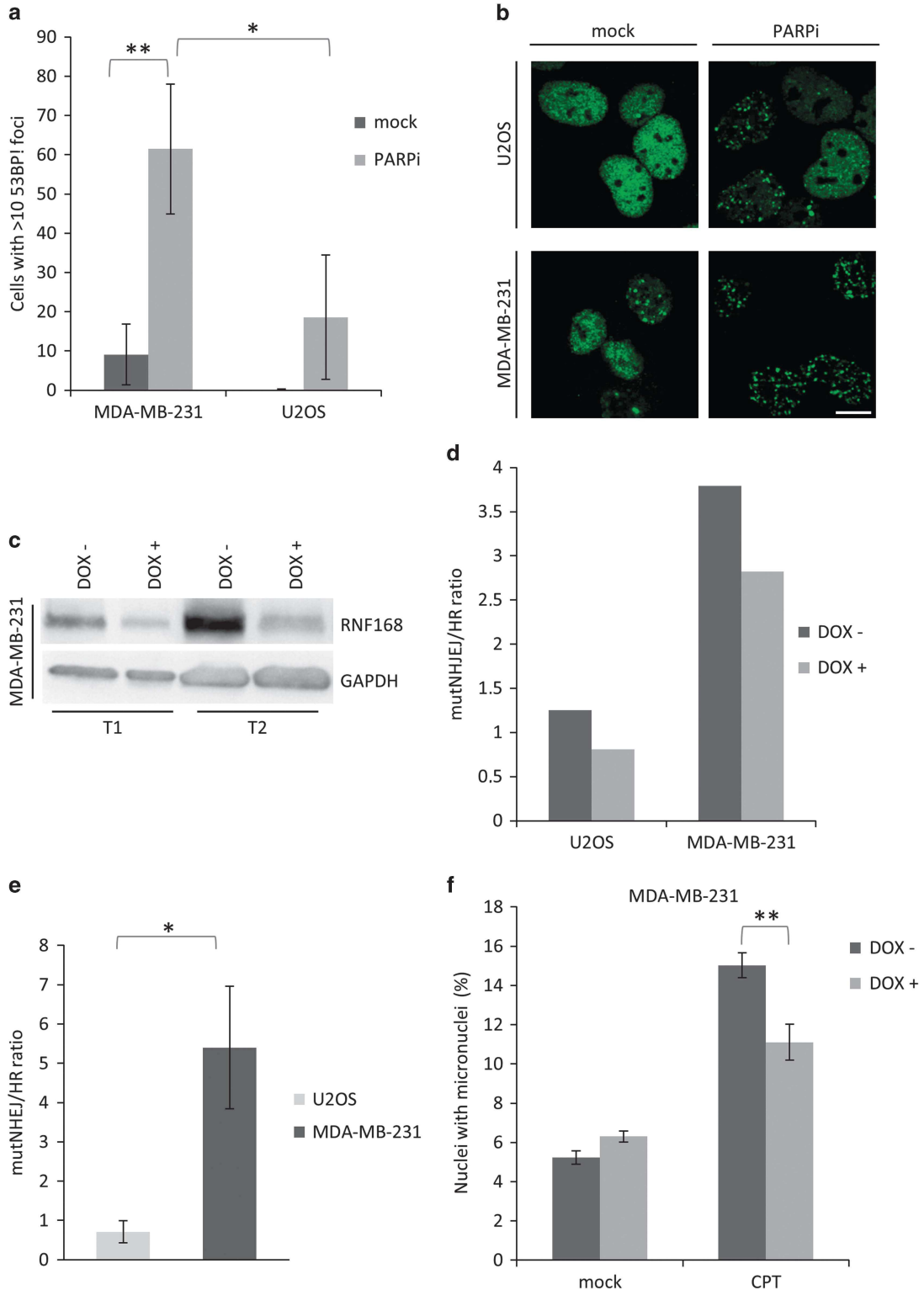


Figure 8. Multiple myeloma cell lines exhibit the RNF168-fueled proteotoxic stress-resistant DSB response. **(a and b)** AMO1 and MMS1 cell lines were mock- and MG132-treated (2 h, 5 μ M), either with or without irradiation (2 Gy) and 1h post-irradiation stained for 53BP1. Nuclei with > 5 53BP1 IRIFs were scored. Scale 10 μ m. **(c)** Indicated cell lines were probed for the level of conjugated K48 linked ubiquitin, RNF168 and BiP by immunoblotting. Equal protein amounts were loaded for all the cell lines. In **(b)**, results are mean \pm s.d. of three independent experiments.

efficiency of which is affected by 53BP1 recruitment,^{15,37} these results suggested that such unscheduled recruitment of 53BP1 might alter the balance between the major DSB repair pathways. The latter possibility would also be consistent with the ability of 53BP1 to promote mutagenic NHEJ (mutNHEJ) by blocking DSB end resection, resulting in hypersensitivity toward chemotherapeutic agents that damage DNA in S-phase cells, including

PARPis and topoisomerase inhibitors.^{15,37} To address such possibilities in a syngeneic system, we first generated clones of MDA-MB-231 cells expressing a doxycycline (DOX)-inducible shRNA against RNF168, and validated the partial knockdown of RNF168 in these models by immunoblotting (Figure 9c). Next, we assessed the ratio of mutNHEJ/HR repair modes by introducing into the RNF168-regulatable cell lines the so-called Traffic light



system,³⁸ a reporter that enables flow cytometric analysis of repair pathway choice at individual I-SceI induced DNA breaks. Quantification of red (mutNHEJ) and green (HR) events then provides information on the overall activity proportion of the two pathways in the analyzed cell population. A representative example of such experiment shown in Figure 9d indeed supports the RNF168-dependent repair shift, as the cells with DOX-induced partial RNF168 knockdown showed a lower mutNHEJ/HR ratio. Furthermore, consistent with the high and low levels of RNF168, respectively, the mutNHEJ/HR ratio was more than sixfold higher in the parental MDA-MB-231 cells compared with the parental U2OS cells (Figure 9e).

Excessive mutNHEJ leads to frequent chromosome aberrations and genome rearrangements that might contribute to tumor heterogeneity.^{22,39} To examine whether the RNF168-driven upregulation of mutNHEJ makes the MDA-MB-231 line more prone to genome rearrangements, we used the DOX-inducible RNF168 knockdown model in MDA-MB-231 cells and compared numbers of micronuclei in DOX-induced and non-induced cells pretreated by a topoisomerase I inhibitory drug camptothecin (CPT). The number of micronuclei was indeed significantly lower in the DOX-induced cells with lowered RNF168 level and hence a more proficient HR repair because of less robust recruitment of 53BP1 (Figure 9f). These results support a plausible scenario that the aberrantly upregulated RNF168 protects cancer cells from adverse effects of proteotoxic stress on the DDR, however, only at the cost of increased genomic instability.

As the altered balance of DSB repair pathway choice toward higher mutNHEJ and the ensuing chromosomal instability can impact cell viability under exposure to S-phase genotoxic insults that require HR for efficient DNA repair,²² we next tested sensitivity of the MDA-MB-231 cells with inducible RNF168 knockdown toward CPT. Strikingly, the DOX-induced cells with decreased RNF168 levels were significantly less sensitive to CPT (Figure 10a) than the non-induced counterpart cells. We interpret the observed decrease in CPT sensitivity upon RNF168 knockdown as further evidence for upregulation of NHEJ and the ensuing genomic instability in the MDA-MB-231 cells driven by RNF168 overabundance.

Surprisingly, the MDA-MB-231 knockdown cell line did not show a significant change in sensitivity toward PARP1 inhibition, which is also known to be particularly toxic to cells with deregulated NHEJ.¹⁵ We reasoned that this might be caused by only moderate degree of RNF168 knockdown achieved in the MDA-MB-231 cells. To address this possibility, we also established and tested a MCF7-derived RNF168 knockdown cell line for sensitivity to CPT and the KU58948 PARP1 inhibitor. Indeed, MCF7 cells that share with MDA-MB-231 cells also the RNF168-fueled proteotoxic stress-resistant DSB response proved to be more amenable to the DOX-inducible RNF168 knockdown as the RNF168 level dropped >3.5-fold upon DOX treatment (Figure 10b). Another important reason for including MCF7 was the fact that, along with MDA-MB-231, MCF7 cells exhibited significant PARPi sensitivity, despite both

these cell lines are BRCA1/BRCA2 proficient.¹⁵ We hypothesized that the observed sensitivity to PARPi might be at least partly attributable to the RNF168 overabundance and the ensuing shift of the mutNHEJ/HR ratio, thereby creating a partial, relative 'HR deficiency' despite the proficient BRCA1/2 genes. Consistent with such possibility, the MCF7 cells showed significantly decreased sensitivity toward both CPT and the PARPi upon induction of RNF168 knockdown (Figure 10c). Thus, apart from providing another piece of evidence for aberrant upregulation of NHEJ in these cell lines, this result might also represent an important clue for better understanding of PARPi sensitivity in BRCA1/2-proficient tumors.

DISCUSSION

From a broader perspective, our present study contributes to better understanding of genome integrity maintenance and points to previously unrecognized wide occurrence and impact of aberrant ubiquitin-mediated signaling of DNA damage under proteotoxic stress, with the ensuing consequences for genomic instability and responses to cancer treatment. Our results suggest that human tumors can be widely categorized into two subsets, featuring 'standard' and 'proteotoxic stress-resistant' responses to DNA breakage, respectively. The latter tumor category, discovered and characterized here, may represent an adaptive scenario of 'conditional/secondary' rather than 'genetically caused/primary' HR deficiency, with implications for genomic instability and selective advantages, but also potential vulnerabilities of such cancers.

First, from the mechanistic point of view of the chromatin response to DSB, we show that overabundance of the RNF168 ubiquitin ligase, sometimes accompanied by enhanced levels of additional E2/E3 enzymes, renders the DSB signaling insensitive to depletion of free ubiquitin levels resulting from proteotoxic stress. According to the current paradigm scenario typical for normal cells and some cancers, exemplified by the widely used human U2OS sarcoma cell line model, DSB signaling is grossly attenuated when free ubiquitin levels become limiting upon proteasome inhibition-induced proteotoxic stress. Therefore, it seemed counterintuitive that we could observe sustained recruitment of 53BP1 and its partner proteins REV7 and RIF1 after proteasome inhibition. Although 53BP1 recruitment is regulated also by other modifications including NEDDylation and acetylation^{40,41} and NEDDylation was suggested to compensate for ubiquitination when proteasome is inhibited⁴² our own experiments using inhibitors of NEDD conjugation and deacetylation did not support this possibility (our unpublished data). Based on our results, we propose a model whereby ubiquitin is still used under proteotoxic stress to relay the DSB chromatin signaling, provided that the RNF168 E3 ligase is overabundant and hence can preferentially channel the remaining available ubiquitin to the RNF168-mediated pathway (Figure 11). Notably, whereas experimentally

Figure 9. Overabundant RNF168 causes unscheduled 53BP1 recruitment, increased mutNHEJ pathway activity and micronuclei formation. **(a)** MDA-MB-231 and U2OS cells were mock or PARPi (10 μ M, 24 h) treated, immunostained for 53BP1 and cyclin A. Cyclin A-positive cells with >10 53BP1 foci were scored. **(b)** Representative images of 53BP1 immunostained cells from **(a)**. Scale 10 μ M. **(c)** The MDA-MB-231 DOX-inducible knockdown cells were pretreated with DOX (DOX, 100 ng/ml; 72 h: T1 or 96 h: T2), lysed and probed for RNF168. After the 72 h pre-treatment, the RNF168 levels were >2.5 times lower in the DOX-treated cells compared with controls (T1). The endpoint (96-h knockdown) RNF168 levels are shown in the T2 panel. **(d)** The effect of RNF168 level on the mutNHEJ/HR ratio was assessed in the MDA-MB-231 and U2OS cell lines bearing the DOX-inducible RNF168 knockdown and the Traffic light reporter. Stable reporter cell lines were pretreated with DOX as in **(a)** and subsequently transduced with a lentivirus carrying an HR repair template and an I-SceI gene. Five days post-transduction, cells were examined by flow cytometry for mCherry and GFP signal. The NHEJ/HR ratio was calculated by correlating the numbers of red (NHEJ) and green (HR). **(e)** Analogous to **(d)**, assessed in the parental U2OS and MDA-MB-231 cell lines only. **(f)** MDA-MB-231 cells were pretreated with DOX as above, then mock or CPT treated (10 nM, 24 h) and nuclei/micronuclei were counterstained with DAPI. Fraction of micronuclei in the DAPI-stained objects was determined. In **(a, e and f)**, results are mean \pm s.d. of three independent experiments. Statistical significance was determined with two-tailed unpaired Student's *t*-test; **P* < 0.05; ***P* < 0.005.

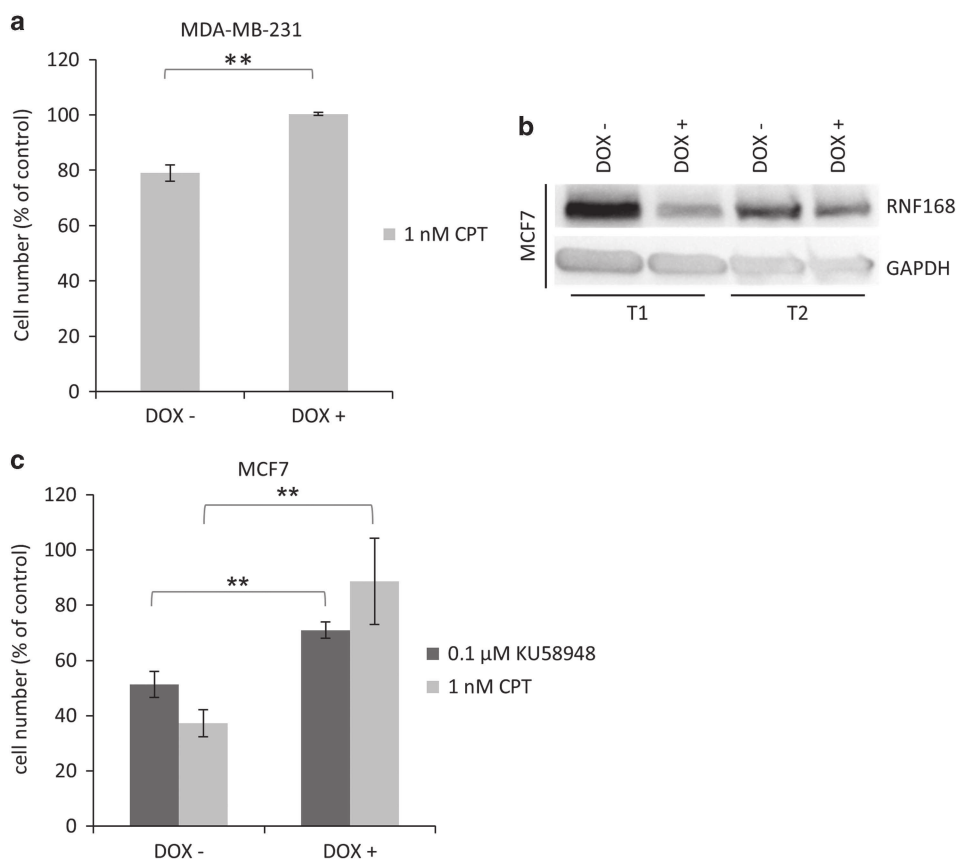


Figure 10. RNF168 overabundance sensitizes MDA-MB-231 and MCF7 cells to CPT and PARPi. **(a)** Sensitivity of the MDA-MB-231 RNF168 knockdown cells toward CPT was assessed by a cell survival assay. The cells were pretreated with DOX as above and then treated with 1 nM CPT. After 6 days, the cells were trypsinized and counted using an automated cell counter. **(b)** The MCF7 DOX-inducible knockdown cell line was pretreated with DOX (DOX, 100 ng/ml; 72 h: T1 or 96 h: T2), lysed and probed by immunoblotting for RNF168. After the 72 h pre-treatment, the RNF168 levels were > 3.5-fold lower in the DOX-induced cells than in the non-treated control cells (T1). **(c)** Sensitivity of the MCF7 RNF168 knockdown cells toward CPT and KU58948 was assessed as in **(a)**. In **(a)** and **(c)**, results are mean \pm s.d. of three independent experiments. Statistical significance was determined with two-tailed unpaired Student's *t*-test; ***P* < 0.005.

induced ectopic overexpression of RNF168 can rescue the otherwise abolished DSB recruitment of 53BP1 (as well as recruitment of RIF1 and REV7) under proteotoxic stress in cells with moderate, physiological levels of endogenous RNF168 (Figures 6c and d, 3a and b), recruitment of the RAP80-BRCA1 complex to DSB lesions is not rescued under such circumstances (our unpublished results). This striking difference between the two branches of the chromatin response to DSBs further supports our recent report on a functional interplay between JMJD1C demethylase, RNF8 and the MDC1 scaffold protein as a selective mechanism required to recruit the RAP80-BRCA1 complex, but not 53BP1.⁴³ Considered in the context of our present study, the 'hyper-activity' of the overabundant RNF168 that is sufficient to rescue the 53BP1 recruitment under proteotoxic stress is not enough to allow recruitment of RAP80-BRCA1, as the latter branch of the DSB chromatin response critically depends on RNF8-mediated ubiquitination of MDC1, rather than histone ubiquitination by RNF168, as well as on additional protein modifications.⁴³ Such a dichotomy in ubiquitin-mediated recruitment of 53BP1 versus RAP80-BRCA1 is also consistent with the recent report from the Halazonetis laboratory that 53BP1 recruitment in proteasome inhibitor-treated cells may be partially rescued by fusing a bulky moiety to the H2AX histone.⁴⁴ This presumably opens up chromatin in the vicinity of DSBs and thus partially restores residual chromatin ubiquitination that in turn enables 53BP1 accrual at DNA lesions.⁴⁴ Analogous to the differential responses to overexpression of RNF168 in our present study, recruitment of

the RAP80-BRCA1 complex to IRIFs under proteasome inhibition conditions was also not rescued by the chromatin opening strategy. Furthermore, our data are also consistent with the notion that the FK2 antibody detected ubiquitin conjugates at the DSB sites may reflect preferential reactivity with RNF8-mediated ubiquitination of MDC1, whereas the histone ubiquitin products catalyzed by RNF168 may not be accessible to antibodies because of nucleosome compaction.⁴³ Such interpretation can also help explain that upon replacement of endogenous RNF168 with a catalytically inactive RNF168 variant, the FK2 antibody foci remained detectable, whereas ubiquitination of histone H2AX was abolished.⁴⁵

We suggest that our experiments can shed some light also on the competition based mode of 53BP1 recruitment that reportedly requires the two competing demethylases, JMJD2A and JMJD2B to be removed from chromatin flanking the DSBs and degraded in order to expose the H4K20me2 that can be subsequently bound by the 53BP1's tandem TUDOR domains.²⁶ As we have observed sustained 53BP1 recruitment under conditions of proteasome inhibition, it seems unlikely that the two demethylases have to be degraded to allow for 53BP1 recruitment to chromatin. We favor a model in which the clearance of the competing proteins from the DSB-flanking chromatin is sufficient and does not have to be accompanied by their degradation in order to permit 53BP1 recruitment. According to such modified model, the RNF168-mediated ubiquitination of JMJD2A and JMJD2B would serve primarily as a chromatin eviction signal and the subsequent

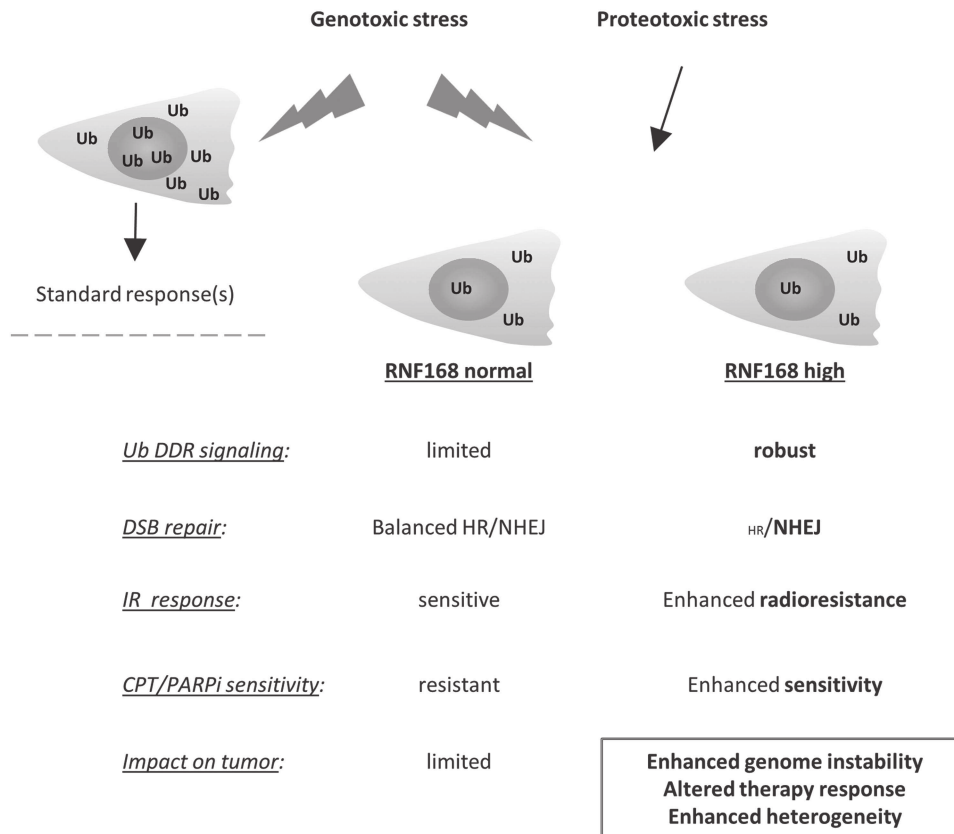


Figure 11. Model summarizing the proteotoxic stress-resistant DSB response and its impact on cancer cells. Changes in chromosome or gene copy number and transcription (de)regulation in cancer cells result in protein overproduction that overwhelms the cellular protein quality control, causing chronic proteotoxic stress and diminishing levels of free ubiquitin. The limited free ubiquitin supply has to be shared by diverse ubiquitin-dependent processes whose efficiency, including that of DSB signaling, is impaired. This is manifested by increased radiosensitivity. Overexpression of RNF168 (and other key DSB response ubiquitin-related enzymes) in the proteotoxic stress-resistant cells shifts the free ubiquitin equilibrium toward DSB signaling thus increasing radioresistance. Overexpression of RNF168 and concomitant robust 53BP1 recruitment promotes mutNHEJ at the expense of HR repair, rendering the cells sensitive to topoisomerase and PARPis, and leading to enhanced genomic instability. Such changes collectively impact tumor heterogeneity, progression and responses to therapy.

degradation of these demethylases is not essential for 53BP1 recruitment.

In the absence of BRCA1 that limits 53BP1 chromatin loading during S phase, the RNF168-driven 53BP1 recruitment precludes DSB end resection and thereby HR, whereas boosting DNA repair by the mutagenic NHEJ pathway.^{22,46,47} Unexpectedly, our findings show that BRCA1-proficient cells bearing overabundant RNF168 mimic, at least to some extent, the BRCA1-deficient phenotype by displaying lower levels of HR at the expense of upregulated mutNHEJ. We show that this is most likely caused by aberrantly enhanced 53BP1 recruitment in S-phase cells that is fueled by the excess of RNF168. Albeit not tested in our present study, it is predictable based on the published work in mouse B cells and embryonic fibroblasts, which the overabundant RNF168 inhibits efficient DSB end resection and fuels DSB repair by the mutagenic NHEJ pathway.²² The RNF168 overexpression seems to derail the physiological balance of the DSB repair pathways toward 53BP1 recruitment and mutNHEJ. We speculate that this imbalance leads to 'conditional HR deficiency' especially under chronic proteotoxic stress conditions, and might account for (or contribute to) the observed increased sensitivity of certain BRCA1-proficient (and principally also HR-proficient) tumors such as subsets of triple-negative breast carcinomas, toward PARPis.^{35,48}

The unexpectedly wide occurrence of the proteotoxic stress-resistant DDR among different tumor cell lines raises a question

whether it might represent a means of adaptation or provide some selective advantage(s) during tumorigenesis. Cancer cells suffer from increased endogenous proteotoxic stress that stems from such features as aneuploidy, mutation overload and hence accumulation of altered proteins, and variation of gene copy number and levels of transcription.^{1,3} We propose that apart from placing a significant burden on the protein quality control mechanisms,³ proteotoxic stress also impacts on DSB response via attenuating the ubiquitin driven signaling at damaged chromatin. Of note, the load of endogenous DSBs increases during cell transformation and tumor progression because of enhanced replication stress evoked by diverse oncogenes and loss of some tumor suppressors.^{6,7,49–51} Given its pathophysiological significance, aberrations in the DSB ubiquitination signaling pathway might profoundly affect genome integrity of tumor cells. Our findings show that attenuation of DSB signaling because of proteotoxic stress might be circumvented by upregulation of one or more key ubiquitin ligases involved in the DDR, particularly RNF168. Importantly, this concept was further supported by observation of the proteotoxic stress-resistant DSB response in multiple myeloma cells, an established model of cancer-related proteotoxic stress. It has been also reported that breast cancers exhibit elevated levels of some E2 ubiquitin conjugating enzymes.⁵² Taken together, this implies that upregulation of some ubiquitin-mediated cellular processes might represent a more general strategy to overcome adverse effects of cancer-

associated proteotoxic stress. UPS has a major role in the regulation of several key tumorigenesis driving processes, such as cellular proliferation, apoptosis and stress tolerance.^{1,53} Hence, it is likely that these pathways are sensitive to proteotoxic stress and tumor cells have evolved compensatory mechanisms such as the upregulation of specific enzymes of the UPS. In terms of potential selective advantages during tumorigenesis, the acquired overabundance of RNF168 can help enhance survival of cancer cells under combined proteotoxic and replication stresses, fuel error-prone DNA repair, genomic instability and thereby intratumor heterogeneity (Figure 11), all features likely to promote tumor progression and aggressivity.

It remains to be elucidated how cancer cells acquire the elevated expression of RNF168 and/or other ubiquitin ligases and conjugating enzymes. Analogous to other tumor-associated changes in gene expression, the most likely candidates are mutations in gene regulatory sequences, genome rearrangements or transcription suppressor/activator mutations. One of the likely candidates that might drive the cancer-related RNF168 overexpression is the family of FOXO transcription factors known to regulate various stress response genes including components of the DDR machinery.^{54,55} Dysregulation of the FOXO3a transcription factor occurs in both breast cancer and hematological malignancies,⁵⁴ which implies that this protein (and possibly other FOXO family members) might fuel the elevated RNF168 expression in tumors. Regardless of the molecular mechanism, it will also be conceptually interesting to find out when during tumor progression such overexpression of RNF168 occurs, relative to the reported activation of the DSB-responsive checkpoint anticancer barrier and its interplay with the ARF-p53 checkpoint pathway.^{2,4,8,53}

Last but not least, our present results indicate that such possibly adaptive upregulation of RNF168 may have important implications for responses of tumors to standard-of-care as well as some emerging targeted treatments. On one hand, we show that tumor cells with the proteotoxic stress-resistant DSB response phenotype are more resistant to ionizing radiation under conditions of enhanced proteotoxic stress. At the same time, however, the altered balance among the DSB repair pathways appears to generate a kind of adaptive, conditional HR deficiency, and thereby unmask some potentially exploitable vulnerabilities to S-phase genotoxic drugs such as CPT or PARPis. In the light of our present findings, combined immunohistochemical detection of RNF168 and markers of proteotoxic stress such as conjugated ubiquitin or the BiP chaperone might be exploited as candidate biomarkers to identify the subsets of patients whose tumors may display the proteotoxic stress-resistant phenotype described here, and possibly help decisions about personalized cancer therapy in the future.

MATERIALS AND METHODS

Cell culture and generation of DSBs

Most cell lines used in this work were cultured in Dulbecco's modified Eagle's medium, supplemented with 10% fetal bovine serum (PAA, Pasching, Austria) and penicillin/streptomycin (Sigma-Aldrich, St Louis, MO, USA) in a humidified atmosphere of 5% CO₂ at 37 °C. For MCF7, AMO1 and MMS1 culturing, the standard cell culture medium was RPMI-1640 with the same supplements as above. All cell lines were purchased from ATCC (Manassas, VA, USA) with the exception of U2OS RNF168-GFP that was established previously.¹³

X-ray irradiation was done using the YXLON.SMART 160E/1.5 device (YXLON, Horsens, Denmark) at the following settings: 150 kV, 6 mA, 11 mGy/s.

Micro-irradiation

Laser micro-irradiation was performed on a Zeiss Axioimager Z.1 instrument equipped with a laser scanning LSM780 module (Zeiss, Oberkochen, Germany). A UV-A laser (355 nm 65 mW) was used to induce the DNA

damage. BrDU presensitization and irradiation of the cells was done as described previously.⁵⁶ Subsequent immunofluorescent detection of recruited proteins was essentially done as in Xu *et al.*²⁰

Plasmids and RNA interference

Most plasmids were transfected using the FuGENE 6 (Roche, Basel, Switzerland) reagent following the manufacturer's instructions. When required, plasmid DNA was transfected by nucleofection using the Neon (Life Technologies, Carlsbad, CA, USA) device at settings recommended by the manufacturer for the respective cell line. The pGFP-53BP1-FI-wt, pGFP-53BP1-FI-L1619A and pGFP-53BP1-FI-D1521 plasmids carrying the 53BP1 UDR and Tudor domains mutations were a gift from D Durocher (Samuel Lunenfeld Research Institute, Ontario, Canada). The pAcGFP-C1-RNF168 plasmids harboring the C16S RING and MIU mutations were described previously.¹³ The Traffic light repair template, the I-SceI lentiviral constructs³⁸ as well as the lentivirus production plasmids pMD2.G and psPAX2 (D Trono, unpublished) were purchased from Addgene (Cambridge, MA, USA; plasmids no's 31476, 31482, 12259 and 12260). The inducible shRNA RNF168 knockdown lentiviral plasmids were constructed as described in Wiederschain *et al.*⁵⁷ using following oligonucleotides (5'-3'): shRNA RNF168 sense CCGGGGCGAAGAGCGATGGAGGACTCGAGTCCTCCATCGCTCTTCGCTTTT; shRNA RNF168 antisense AATTA AAAAGGC GAAGAGCGATGGAGGACTCGAGTCTCCATCGCTCTTCGCC (Generi Biotech, Hradec Kralove, Czech Republic). The backbone pLKO-Tet-On Puro^{57,58} plasmid was obtained from Addgene (plasmid no. 21915).

siRNA's were transfected with the Lipofectamine RNAiMAX (Invitrogen, Carlsbad, CA, USA) reagent following the manufacturer's instructions. siRNAs were purchased from Thermo Fisher Scientific (Waltham, MA, USA): siCON-negative control, siRNA#1 (ID#4390843), siRNF168 (ID #126171), siRNF8 (ID#17200) and from MWG Operon (Ebersberg, Germany): 53BP1DD2013 GAGAGCAGAUGAUCCUUUAtt (5'-3').

Oligonucleotides and quantitative PCR

The abundance of RNF168 mRNA level was probed by quantitative PCR using a Nano LightCycler (Roche) instrument and following oligos (5'-3'): RNF168qPCR_F1 CAGGGCAAGACACAGAAATAGA; RNF168qPCR_R1 GGCAC CACAGGCACATAA; RNF168qPCR_F2 CTCCTACAGCCTAGCATTTC and RNF168qPCR_R2 AGATCACAAAGCACTCCCTTTA (Generi Biotech). Following GAPDH, primers were used as an internal control: GAPDH—F GAAG ATGGTGATGGGATTTC; GAPDH—R GAAGGTGAAGGTCGGAGT (Generi Biotech) PCR product abundance was quantified using the LighCycler Nano software (Roche).

Chemicals and antibodies

The Bortezomib (PS-341), MG132 and CPT inhibitors were purchased from Sigma-Aldrich. The KU58948 PARP1 inhibitor was obtained from AstraZeneca (London, UK). Antibodies used in this study included following mouse monoclonal antibodies: γ H2AX (Merck Millipore, Billerica, MA, USA), RNF8 (B-2) (Santa Cruz Biotechnology, Santa Cruz, CA, USA), Ubc13, JMJD2A (KDM4A) (Thermo Fisher Scientific, Waltham, MA, USA), HERC2 (BD Transduction Laboratories, San Jose, CA, USA), MDC1, USP34 (Abcam, Cambridge, UK), GAPDH (GT239) (GeneTex, Hsinchu, Taiwan), β -actin (Sigma-Aldrich) and polyclonal rabbit: 53BP1, BRCA1 (Santa Cruz Biotechnology), TRIP12 (Abcam), UBR5 (Sigma-Aldrich), FK2 (Enzo Life Sciences, Farmingdale, NY, USA), RIF1 (Bethyl Laboratories, Montgomery, TX, USA), REV7 (BD Transduction Laboratories). The rabbit polyclonal antibodies to RNF168 and RNF169 were a gift from N Mailand (Center for Protein Research, Copenhagen, Denmark).

Immunoblotting

Cells were lysed in Laemmli sample buffer and the whole-cell lysates were subsequently separated on a 10% sodium dodecyl sulfate–polyacrylamide gel electrophoresis gel and transferred to a nitrocellulose membrane (GE Healthcare, Little Chalfont, UK). The membrane was blocked in 5% (w/v) skim milk in Tris-buffered saline supplemented with in 0.1% (v/v) Tween-20 and probed with a primary antibody. Subsequently, the membrane was incubated with horseradish peroxidase-labeled secondary anti-mouse or anti-rabbit antibodies (Santa Cruz Biotechnology) and the signals were visualized using ECL detection reagents (Thermo Fisher Scientific) and the ChemiDoc system (Bio-Rad, Hercules, CA, USA). Band intensity quantification was performed in the ImageJ software (<http://imagej.nih.gov/ij/>).

Immunofluorescence and micronuclei staining, microscopic analysis

Cells grown on 12-mm coverslips were fixed with 4% paraformaldehyde in phosphate-buffered saline (PBS) for 15 min and then permeabilized with PBS containing 0.2% (v/v) Triton X-100 for 5 min. Suspension cells were cytopinned onto microscopic slides before fixation using the Cyto-Tek Sakura instrument (Sakura Finetek, Torrance, CA, USA). Fixed cells were blocked with 5% (v/v) fetal bovine serum in PBS for 30 min and incubated overnight at 4 °C with primary antibodies (diluted in 5% (w/v) bovine serum albumin in PBS). Coverslips were washed three times in PBS supplemented with 0.1% (v/v) Tween-20, once with PBS and then incubated with an appropriate secondary goat anti-rabbit or goat anti-mouse Alexa Fluor 488 or Alexa Fluor 568 conjugated (Invitrogen) secondary antibody (diluted in 5% (w/v) bovine serum albumin in PBS) for 60 min at room temperature. Slips were then washed as above and mounted onto slides using the 4,6-diamidino-2-phenylindole (DAPI) containing Vectashield mounting reagent (Vector Laboratories, Burlingame, CA, USA). Coverslips for micronuclei analysis were fixed and washed as above, stained with DAPI diluted in PBS and subsequently mounted with the Vectashield reagent (without DAPI).

Slides were visualized by the Axio Observer.Z1/Cell Observer Spinning Disc microscopic system (Yokogawa, Tokyo, Japan and Zeiss) equipped with an Evolve 512 (Photometrix, Tucson, AZ, USA) EMCCD camera. Zeiss Plan Achromat 63x and 100x/1.40 NA objectives were used.

For quantitative image analysis, a series of random fields were recorded automatically using the ScanR imaging workstation (Olympus, Tokyo, Japan; with an EM charge-coupled device camera (C9100; Hamamatsu Photonics, Hamamatsu City, Japan), a U Plan S Achromat 40×/0.9 NA objective, and an image resolution of 200×200 nm/pixel). The number and intensity of micronuclei and IR-induced nuclear foci were quantified using the ScanR image analysis software (Olympus).

Generation of lentiviruses and lentiviral transduction

Lentiviruses were generated by co-transfecting 293T cells with 4 µg of pMD2.G, 7 µg of psPAX2 and 9 µg of a lentiviral plasmid of interest using the CaPO₄ precipitation method.⁵⁹ Six to eight hours post-transfection, the cells were washed briefly with pre-warmed PBS and medium was changed. Lentivirus containing supernatant was collected 48 h later. Target cells were transduced at multiplicity of infection of 1–10 with the supernatant supplemented with 4 µg/ml polybrene (Sigma-Aldrich). Twenty-four hours post-transduction, the medium was changed and when required, the cells were selected in 1 µg/ml puromycin.

Flow cytometric analysis of DNA repair pathway choice

Cells harboring the Traffic light reporter were seeded in a 12-well plate and 24-h later transduced with the I-SceI and GFP repair template containing construct using the procedure above. Seven days later, the cells were trypsinized, fixed with formaldehyde and analyzed by an Influx (BD Biosciences, San Jose, CA, USA) instrument. GFP was measured using a 488 nm laser for excitation and a 530/40 filter, whereas mCherry was excited using a 561 nm laser and acquired with a 610/20 filter. Data were analyzed using the FACS Software (BD Biosciences) software.

Cell cycle analysis

Cells were fixed in 70% ethanol and stained with propidium iodide for flow cytometric analysis. Fixed cells were analyzed on a FACS Verse instrument (BD Biosciences) and cell cycle distribution was assigned using the FACSuite software (BD Biosciences).

Long-term cell survival assay

In all, 1 × 10⁵ cells were seeded in triplicate to ø 6 cm plates and left to attach overnight. Next day, the medium was replaced by inhibitor or dimethylsulfoxide (mock) containing medium. Seven days later, the cells were trypsinized and cell number was scored using a Vi-Cell XR Cell Viability Analyzer (Beckman Coulter, Brea, CA, USA) equipped with the ViCELL XR software (Beckman Coulter).

The IR resistance of proteotoxic stress DDR-resistant lines was assessed as above with following modifications: attached cells were pretreated with 5 µM MG132 or dimethylsulfoxide (mock) for 2 h and subsequently irradiated with 2 Gy. Then medium was changed and cell survival was assayed as above 7 days later.

Statistical analysis

Differences in DNA repair pathway efficiency and cell survival assays were analyzed by Student's *t*-test. Variability and reproducibility among repeated experiments subjected to quantitative evaluations, such as immunofluorescence IRIF counts or quantitative PCR products is indicated by mean ± s.d. and shown as error bars in graphical summaries in the relevant figures.

ABBREVIATIONS

53BP1, p53 binding protein 1; BRCA1, breast cancer 1; DDR, DNA damage response; DSB, double-strand break; HR, homologous recombination; IRIF, ionizing radiation induced foci; NHEJ, non-homologous end joining; PARP1, poly(ADP-ribose) polymerase 1; RNF168, ring finger protein 168.

CONFLICT OF INTEREST

The authors declare no conflict of interest.

ACKNOWLEDGEMENTS

We thank Jan Bouchal, Katerina Bouchalova and our colleagues from the Laboratory of Genome Integrity for technical assistance, suggestions and comments on the manuscript. This work was supported by grants from the following foundations: Grant Agency of the Czech Republic 13-17555S, Czech National Program of Sustainability LO1304, the Kellner Family Foundation, the Norwegian Financial Mechanism CZ09 (Project PHOSCAN 7F14061), MEYS CR (LM2015062 Czech-Biologymaging), the internal grant IGA-LF-2016-030, the EU operation program CZ.1.07/2.3.00/30.0004, the Danish National Research Foundation (DNRF125, project CARD), Danish Cancer Society, the Swedish Research Council, the Lundbeck Foundation, Cancer Fonden, and the Danish Council for Independent Research.

REFERENCES

- 1 Deshaies RJ. Proteotoxic crisis, the ubiquitin-proteasome system, and cancer therapy. *BMC Biol* 2014; **12**: 94.
- 2 Halazonetis TD, Gorgoulis VG, Bartek J. An oncogene-induced DNA damage model for cancer development. *Science* 2008; **319**: 1352–1355.
- 3 Luo J, Solimini NL, Elledge SJ. Principles of cancer therapy: oncogene and non-oncogene addiction. *Cell* 2009; **136**: 823–837.
- 4 Bartek J, Bartkova J, Lukas J. DNA damage signalling guards against activated oncogenes and tumour progression. *Oncogene* 2007; **26**: 7773–7779.
- 5 Jackson SP, Bartek J. The DNA-damage response in human biology and disease. *Nature* 2009; **461**: 1071–1078.
- 6 Bartkova J, Horejsi Z, Koed K, Kramer A, Tort F, Zieger K *et al*. DNA damage response as a candidate anti-cancer barrier in early human tumorigenesis. *Nature* 2005; **434**: 864–870.
- 7 Bartkova J, Rezaei N, Liontos M, Karakaidos P, Kletsas D, Issaeva N *et al*. Oncogene-induced senescence is part of the tumorigenesis barrier imposed by DNA damage checkpoints. *Nature* 2006; **444**: 633–637.
- 8 Evangelou K, Bartkova J, Kotsinas A, Pateras IS, Liontos M, Velimezi G *et al*. The DNA damage checkpoint precedes activation of ARF in response to escalating oncogenic stress during tumorigenesis. *Cell Death Differ* 2013; **20**: 1485–1497.
- 9 Zhao Y, Brickner JR, Majid MC, Mosammaparast N. Crosstalk between ubiquitin and other post-translational modifications on chromatin during double-strand break repair. *Trends Cell Biol* 2014; **24**: 426–434.
- 10 Lukas J, Lukas C, Bartek J. More than just a focus: the chromatin response to DNA damage and its role in genome integrity maintenance. *Nat Cell Biol* 2011; **13**: 1161–1169.
- 11 Reinhardt HC, Yaffe MB. Phospho-Ser/Thr-binding domains: navigating the cell cycle and DNA damage response. *Nat Rev Mol Cell Biol* 2013; **14**: 563–580.
- 12 Thorslund T, Ripplinger A, Hoffmann S, Wild T, Uckelmann M, Villumsen B *et al*. Histone H1 couples initiation and amplification of ubiquitin signalling after DNA damage. *Nature* 2015; **527**: 389–393.
- 13 Doil C, Mailand N, Bekker-Jensen S, Menard P, Larsen DH, Pepperkok R *et al*. RNF168 binds and amplifies ubiquitin conjugates on damaged chromosomes to allow accumulation of repair proteins. *Cell* 2009; **136**: 435–446.
- 14 Stewart GS, Panier S, Townsend K, Al-Hakim AK, Kolas NK, Miller ES *et al*. The RIDDLE syndrome protein mediates a ubiquitin-dependent signaling cascade at sites of DNA damage. *Cell* 2009; **136**: 420–434.
- 15 Bunting SF, Callen E, Wong N, Chen HT, Polato F, Gunn A *et al*. 53BP1 inhibits homologous recombination in Brca1-deficient cells by blocking resection of DNA breaks. *Cell* 2010; **141**: 243–254.

- 16 Daley JM, Sung P. 53BP1, BRCA1, and the choice between recombination and end joining at DNA double-strand breaks. *Mol Cell Biol* 2014; **34**: 1380–1388.
- 17 Densham RM, Garvin AJ, Stone HR, Strachan J, Baldock RA, Daza-Martín M et al. Human BRCA1-BARD1 ubiquitin ligase activity counteracts chromatin barriers to DNA resection. *Nat Struct Mol Biol* 2016; **23**: 647–655.
- 18 Callen E, Di Virgilio M, Kruhlak MJ, Nieto-Soler M, Wong N, Chen HT et al. 53BP1 mediates productive and mutagenic DNA repair through distinct phosphoprotein interactions. *Cell* 2013; **153**: 1266–1280.
- 19 Chapman JR, Barral P, Vannier JB, Borel V, Steger M, Tomas-Loba A et al. RIF1 is essential for 53BP1-dependent nonhomologous end joining and suppression of DNA double-strand break resection. *Mol Cell* 2013; **49**: 858–871.
- 20 Xu G, Chapman JR, Brandsma I, Yuan J, Mistrik M, Bouwman P et al. REV7 counteracts DNA double-strand break resection and affects PARP inhibition. *Nature* 2015; **521**: 541–544.
- 21 Zimmermann M, Lotterberger F, Buonomo SB, Sfeir A, de Lange T. 53BP1 regulates DSB repair using Rif1 to control 5' end resection. *Science* 2013; **339**: 700–704.
- 22 Zong D, Callen E, Pegoraro G, Lukas C, Lukas J, Nussenzweig A. Ectopic expression of RNF168 and 53BP1 increases mutagenic but not physiological non-homologous end joining. *Nucleic Acids Res* 2015; **43**: 4950–4961.
- 23 Botuyan MV, Lee J, Ward IM, Kim JE, Thompson JR, Chen J et al. Structural basis for the methylation state-specific recognition of histone H4-K20 by 53BP1 and Crb2 in DNA repair. *Cell* 2006; **127**: 1361–1373.
- 24 Fradet-Turcotte A, Canny MD, Escibano-Diaz C, Orthwein A, Leung CC, Huang H et al. 53BP1 is a reader of the DNA-damage-induced H2A Lys 15 ubiquitin mark. *Nature* 2013; **499**: 50–54.
- 25 Acs K, Luijsterburg MS, Ackermann L, Salomons FA, Hoppe T, Dantuma NP. The AAA-ATPase VCP/p97 promotes 53BP1 recruitment by removing L3MBTL1 from DNA double-strand breaks. *Nat Struct Mol Biol* 2011; **18**: 1345–1350.
- 26 Mallette FA, Mattioli F, Cui G, Young LC, Hendzel MJ, Mer G et al. RNF8- and RNF168-dependent degradation of KDM4A/JMJD2A triggers 53BP1 recruitment to DNA damage sites. *EMBO J* 2012; **31**: 1865–1878.
- 27 Devgan SS, Sanal O, Doil C, Nakamura K, Nahas SA, Pettijohn K et al. Homozygous deficiency of ubiquitin-ligase ring-finger protein RNF168 mimics the radiosensitivity syndrome of ataxia-telangiectasia. *Cell Death Differ* 2011; **18**: 1500–1506.
- 28 Gudjonsson T, Altmeyer M, Savic V, Toledo L, Dinan C, Grofte M et al. TRIP12 and UBR5 suppress spreading of chromatin ubiquitylation at damaged chromosomes. *Cell* 2012; **150**: 697–709.
- 29 Dantuma NP, Groothuis TA, Salomons FA, Neeffjes J. A dynamic ubiquitin equilibrium couples proteasomal activity to chromatin remodeling. *J Cell Biol* 2006; **173**: 19–26.
- 30 Jacquemont C, Taniguchi T. Proteasome function is required for DNA damage response and fanconi anemia pathway activation. *Cancer Res* 2007; **67**: 7395–7405.
- 31 Bekker-Jensen S, Rendtlew Danielsen J, Fugger K, Gromova I, Nerstedt A, Lukas C et al. HERC2 coordinates ubiquitin-dependent assembly of DNA repair factors on damaged chromosomes. *Nat Cell Biol* 2010; **12**: 80–86. sup pp 1–12.
- 32 Panier S, Boulton SJ. Double-strand break repair: 53BP1 comes into focus. *Nat Rev Mol Cell Biol* 2014; **15**: 7–18.
- 33 Chauhan D, Hideshima T, Anderson KC. Proteasome inhibition in multiple myeloma: therapeutic implication. *Annu Rev Pharmacol Toxicol* 2005; **45**: 465–476.
- 34 Gething MJ. Role and regulation of the ER chaperone BiP. *Semin Cell Dev Biol* 1999; **10**: 465–472.
- 35 Livraghi L, Garber JE. PARP inhibitors in the management of breast cancer: current data and future prospects. *BMC Med* 2015; **13**: 188.
- 36 Ricks TK, Chiu HJ, Ison G, Kim G, McKee AE, Kluetz P et al. Successes and challenges of PARP inhibitors in cancer therapy. *Front Oncol* 2015; **5**: 222.
- 37 Bouwman P, Aly A, Escandell JM, Pieterse M, Bartkova J, van der Gulden H et al. 53BP1 loss rescues BRCA1 deficiency and is associated with triple-negative and BRCA-mutated breast cancers. *Nat Struct Mol Biol* 2010, biology **17**: 688–695.
- 38 Certo MT, Ryu BY, Annis JE, Garibov M, Jarjour J, Rawlings DJ et al. Tracking genome engineering outcome at individual DNA breakpoints. *Nat Methods* 2011; **8**: 671–676.
- 39 Rodgers K, McVey M. Error-prone repair of DNA double-strand breaks. *J Cell Physiol* 2016; **231**: 15–24.
- 40 Ma T, Chen Y, Zhang F, Yang CY, Wang S, Yu X. RNF111-dependent neddylation activates DNA damage-induced ubiquitination. *Mol Cell* 2013; **49**: 897–907.
- 41 Tang J, Cho NW, Cui G, Manion EM, Shanbhag NM, Botuyan MV et al. Acetylation limits 53BP1 association with damaged chromatin to promote homologous recombination. *Nat Struct Mol Biol* 2013; **20**: 317–325.
- 42 Hjerpe R, Thomas Y, Chen J, Zemla A, Curran S, Shpiro N et al. Changes in the ratio of free NEDD8 to ubiquitin triggers NEDDylation by ubiquitin enzymes. *Biochem J* 2012; **441**: 927–936.
- 43 Watanabe S, Watanabe K, Akimov V, Bartkova J, Blagoev B, Lukas J et al. JMJD1C demethylates MDC1 to regulate the RNF8 and BRCA1-mediated chromatin response to DNA breaks. *Nat Struct Mol Biol* 2013; **20**: 1425–1433.
- 44 Kocylowski MK, Rey AJ, Stewart GS, Halazonetis TD. Ubiquitin-H2AX fusions render 53BP1 recruitment to DNA damage sites independent of RNF8 or RNF168. *Cell Cycle* 2015; **14**: 1748–1758.
- 45 Mattioli F, Vissers JH, van Dijk WJ, Ikpa P, Citterio E, Vermeulen W et al. RNF168 ubiquitinates K13-15 on H2A/H2AX to drive DNA damage signaling. *Cell* 2012; **150**: 1182–1195.
- 46 Munoz MC, Lailier C, Gunn A, Cheng A, Robbiani DF, Nussenzweig A et al. RING finger nuclear factor RNF168 is important for defects in homologous recombination caused by loss of the breast cancer susceptibility factor BRCA1. *J Biol Chem* 2012; **287**: 40618–40628.
- 47 Munoz MC, Yanez DA, Stark JM. An RNF168 fragment defective for focal accumulation at DNA damage is proficient for inhibition of homologous recombination in BRCA1 deficient cells. *Nucleic Acids Res* 2014; **42**: 7720–7733.
- 48 Inbar-Rozensal D, Castiel A, Visochek L, Castel D, Dantzer F, Izraeli S et al. A selective eradication of human nonhereditary breast cancer cells by phenanthridine-derived polyADP-ribose polymerase inhibitors. *Breast Cancer Res* 2009; **11**: R78.
- 49 Burrell RA, McClelland SE, Endesfelder D, Groth P, Weller MC, Shaikh N et al. Replication stress links structural and numerical cancer chromosomal instability. *Nature* 2013; **494**: 492–496.
- 50 Di Micco R, Fumagalli M, Cicalese A, Piccinin S, Gasparini P, Luise C et al. Oncogene-induced senescence is a DNA damage response triggered by DNA hyper-replication. *Nature* 2006; **444**: 638–642.
- 51 Gorgoulis VG, Vassiliou LV, Karakaidos P, Zacharatos P, Kotsinas A, Liloglou T et al. Activation of the DNA damage checkpoint and genomic instability in human precancerous lesions. *Nature* 2005; **434**: 907–913.
- 52 Chen L, Madura K. Increased proteasome activity, ubiquitin-conjugating enzymes, and eEF1A translation factor detected in breast cancer tissue. *Cancer Res* 2005; **65**: 5599–5606.
- 53 Velimezi G, Lontos M, Vougas K, Roumeliotis T, Bartkova J, Sideridou M et al. Functional interplay between the DNA-damage-response kinase ATM and ARF tumour suppressor protein in human cancer. *Nat Cell Biol* 2013; **15**: 967–977.
- 54 Greer EL, Brunet A. FOXO transcription factors at the interface between longevity and tumor suppression. *Oncogene* 2005; **24**: 7410–7425.
- 55 Tran H, Brunet A, Grenier JM, Datta SR, Fornace AJ Jr., DiStefano PS et al. DNA repair pathway stimulated by the forkhead transcription factor FOXO3a through the Gadd45 protein. *Science* 2002; **296**: 530–534.
- 56 Mistrik M, Vesela E, Furst T, Hanzlikova H, Frydrych I, Gursky J et al. Cells and stripes: a novel quantitative photo-manipulation technique. *Sci Rep* 2016; **6**: 19567.
- 57 Wiederschain D, Wee S, Chen L, Loo A, Yang G, Huang A et al. Single-vector inducible lentiviral RNAi system for oncology target validation. *Cell Cycle* 2009; **8**: 498–504.
- 58 Wee S, Wiederschain D, Maira SM, Loo A, Miller C, deBeaumont R et al. PTEN-deficient cancers depend on PIK3CB. *Proc Natl Acad Sci USA* 2008; **105**: 13057–13062.
- 59 Tiscornia G, Singer O, Verma IM. Production and purification of lentiviral vectors. *Nat Protoc* 2006; **1**: 241–245.

Supplementary Information accompanies this paper on the Oncogene website (<http://www.nature.com/onc>)

APPENDIX E

Skrott Z, Majera D, Gursky J, Buchtova T, Hajduch M, Mistrik M, Bartek J. Disulfiram's anti-cancer activity reflects targeting NPL4, not inhibition of aldehyde dehydrogenase. *Oncogene*. 2019 Aug 7. *In press*. IF₍₂₀₁₈₎: 6.634



Disulfiram's anti-cancer activity reflects targeting NPL4, not inhibition of aldehyde dehydrogenase

Zdenek Skrott¹ · Dusana Majera¹ · Jan Gursky¹ · Tereza Buchtova¹ · Marian Hajduch¹ · Martin Mistrik¹ · Jiri Bartek^{1,2,3}

Received: 18 April 2019 / Revised: 27 June 2019 / Accepted: 22 July 2019
© The Author(s), under exclusive licence to Springer Nature Limited 2019

Abstract

Aldehyde dehydrogenase (ALDH) is a proposed biomarker and possible target to eradicate cancer stem cells. ALDH inhibition as a treatment approach is supported by anti-cancer effects of the alcohol-abuse drug disulfiram (DSF, Antabuse). Given that metabolic products of DSF, rather than DSF itself inhibit ALDH in vivo, and that DSF's anti-cancer activity is potentiated by copper led us to investigate the relevance of ALDH as the suggested molecular cancer-relevant target of DSF. Here we show that DSF does not directly inhibit ALDH activity in diverse human cell types, while DSF's in vivo metabolite, S-methyl-N,N-diethylthiocarbamate-sulfoxide inhibits ALDH activity yet does not impair cancer cell viability. Our data indicate that the anti-cancer activity of DSF does not involve ALDH inhibition, and rather reflects the impact of DSF's copper-containing metabolite (CuET), that forms spontaneously in vivo and in cell culture media, and kills cells through aggregation of NPL4, a subunit of the p97/VCP segregase. We also show that the CuET-mediated, rather than any ALDH-inhibitory activity of DSF underlies the preferential cytotoxicity of DSF towards BRCA1- and BRCA2-deficient cells. These findings provide evidence clarifying the confusing literature about the anti-cancer mechanism of DSF, a drug currently tested in clinical trials for repositioning in oncology.

Introduction

Cancer stem cells (CSCs) are believed to represent a major challenge to successful cancer therapy [1], due to CSCs'

ability to resist standard-of-care treatment modalities and fuel post-treatment relapse and metastatic spread [2]. CSCs can be detected through expression of several markers including aldehyde dehydrogenases (ALDHs) [3]. There are 19 putatively functional *ALDH* genes in the human genome [4], and several ALDH isoenzymes are used as markers of stem cells including CSC [5]. ALDH have diverse functions in normal tissues, including the pivotal role in catalysing endogenous and exogenous aldehydes into carboxylic acids [6]. If aldehydes are not metabolized, they may cause severe toxicity to the cells, including DNA damage by forming adducts [7]. Numerous studies reported that ALDH is overexpressed in cancer cells and implicated in metastatic spread [8–10]. Despite the above-mentioned reports on ALDH in CSCs, however, it remains unclear whether ALDH may serve as an actionable target for cancer treatment, and whether tumours are indeed addicted to ALDH function.

Recent efforts to eradicate CSCs have exploited the old anti-alcoholism drug DSF, used for decades as an ALDH inhibitor in clinical care [4]. Eradication of CSCs by DSF has been reported in numerous studies, the first of which reported DSF's toxicity for breast cancer cells with CSC-

These authors contributed equally: Zdenek Skrott, Dusana Majera

Supplementary information The online version of this article (<https://doi.org/10.1038/s41388-019-0915-2>) contains supplementary material, which is available to authorized users.

- ✉ Martin Mistrik
martin.mistik@upol.cz
- ✉ Jiri Bartek
jb@cancer.dk

¹ Institute of Molecular and Translational Medicine, Faculty of Medicine and Dentistry, Palacky University, Olomouc, Czech Republic

² Danish Cancer Society Research Center, Copenhagen, Denmark

³ Division of Genome Biology, Department of Medical Biochemistry and Biophysics, Science for Life Laboratory, Karolinska Institute, Stockholm, Sweden

like properties [11]. In recent years, multiple studies reported DSF as a drug toxic to cancer cells via inhibition of ALDH in a range of tumour types and models [12–20] and other studies have later build on these findings and used DSF combined with copper ions to target cancer cells [21–24]. However, the mechanism of ALDH inhibition by DSF is more complex, as metabolic products of DSF, not DSF itself, inhibit ALDH in vivo [4]. While well accepted in pharmacology, the latter fact has often been overlooked in the cancer-related studies focusing on DSF and ALDH, thereby causing potentially misleading interpretations of the results.

In vivo DSF is rapidly metabolized to diethyldithiocarbamate (DDTC), which is further converted to *S*-methyl-*N,N*-diethyldithiocarbamate (DETC) and *S*-methyl-*N,N*-diethyldithiocarbamate (Me-DDTC). Subsequent P450-catalyzed oxidation of DETC and Me-DDTC produces DETC-sulfoxide (DETC-SO) and *S*-methyl-*N,N*-diethylthiocarbamate-sulfoxide (Me-DTC-SO) and -sulfone (Me-DTC-SO₂), metabolites that are most likely directly involved in ALDH inhibition [25–29]. Importantly, when downstream steps of DSF metabolism are blocked by a chemical P450 inhibitor, liver ALDH remains uninhibited [30], thus unambiguously proving that not DSF itself, but its metabolites are the genuine inhibitors of ALDH in vivo. Despite this knowledge is published and accepted in some research fields, most cancer-focused studies regard DSF as a direct ALDH inhibitor. Notably, there are no published data with regard to any anti-cancer effects of the DSF metabolites that are responsible for ALDH inhibition. Further fuelling the confusion in this field, the vast majority of cancer-related studies report that DSF inhibits ALDH only when combined with copper ions [12–16], a fact that further underlines the extent of misunderstanding and lack of logic behind such approach with respect to the known mechanism of ALDH inhibition, a process that does not involve copper at all. On the other hand, it is well known that copper does potentiate DSF's anti-cancer toxicity [12, 31, 32], and we have recently uncovered that this reflects the in vivo formation of a copper-containing CuET (bis-diethyldithiocarbamate-copper) complex, the ultimate anti-cancer metabolite derived from DSF [33]. This conundrum surrounding the links among DSF, ALDH, copper and cancer toxicity prompted us to assess the role of ALDH as a potential target of DSF's anti-cancer activity in more detail, using genuine validated inhibitors of ALDH enzymatic activity, and thereby help to reconcile the often mis-interpreted findings in this field, with the goal to facilitate the future repositioning of DSF for treatment of cancer.

Results

DSF's toxicity for cancer cells is mediated by CuET formed in the culture media

Despite numerous pre-clinical studies and ongoing clinical trials, the mechanism of anti-cancer activity of DSF is still debated, as several targets and hypotheses have been proposed. Among them, the inhibition of ALDH is probably currently the most prevalent and accepted theory. ALDH is attractive not only as a generally accepted marker of stem cells, but also as an important protective enzyme metabolising potentially harmful aldehydes. However, the hypothesis that ALDH may represent a promising avenue to target cancer stem cells or cancer in general, remains to be rigorously tested.

Recently, preferential cytotoxicity of DSF for homologous recombination (HR) deficient cells have been reported [20]. Since DSF is regarded by some as a direct inhibitor of ALDH, the reported cytotoxicity in this study was attributed to increased acetaldehyde levels ensuing ALDH inhibition, and subsequent DNA damage induced by the crosslinking activity of the aldehydes. As direct inhibition of cellular ALDH by DSF is in fact highly unlikely (see Introduction) we decided to reproduce and re-analyse those intriguing results. First, we tried to recapitulate the reported preferential sensitivity of BRCA1 and BRCA2-deficient cell lines to DSF [20]. Indeed, the H1299 cell lines with doxycycline (DOX)-inducible shBRCA1 or shBRCA2 show efficient knockdown of these genes after DOX induction (Fig. 1a) and both models show also hypersensitivity of BRCA-depleted cells to olaparib (Supplementary Fig. 1a) a PARP1 inhibitor effective against HR deficient cancers [34]. In agreement with Tacconi et al. [20], we confirmed that BRCA1- and BRCA2-deficient cells are indeed more sensitive to DSF treatment compared to their BRCA-proficient counterparts (Fig. 1b). Importantly, we have recently described a new metabolite of DSF, CuET, which is formed in vivo and is responsible for DSF's anti-cancer activity [33], providing a meaningful explanation for why is the toxicity of DSF potentiated by copper supplementation. Thus we sought to investigate whether the CuET complex forms also in vitro, since standard cell culture media contain significant amounts of copper ions [35] and the complex biochemical environment in the medium may allow spontaneous formation of such complex. Indeed, we have confirmed that CuET is detectable in DSF-containing medium even without any additional copper supplementation (Fig. 1c). As predicted, addition of more copper to the medium increased the amount of formed CuET; conversely chelation of copper ions by a metal chelator,

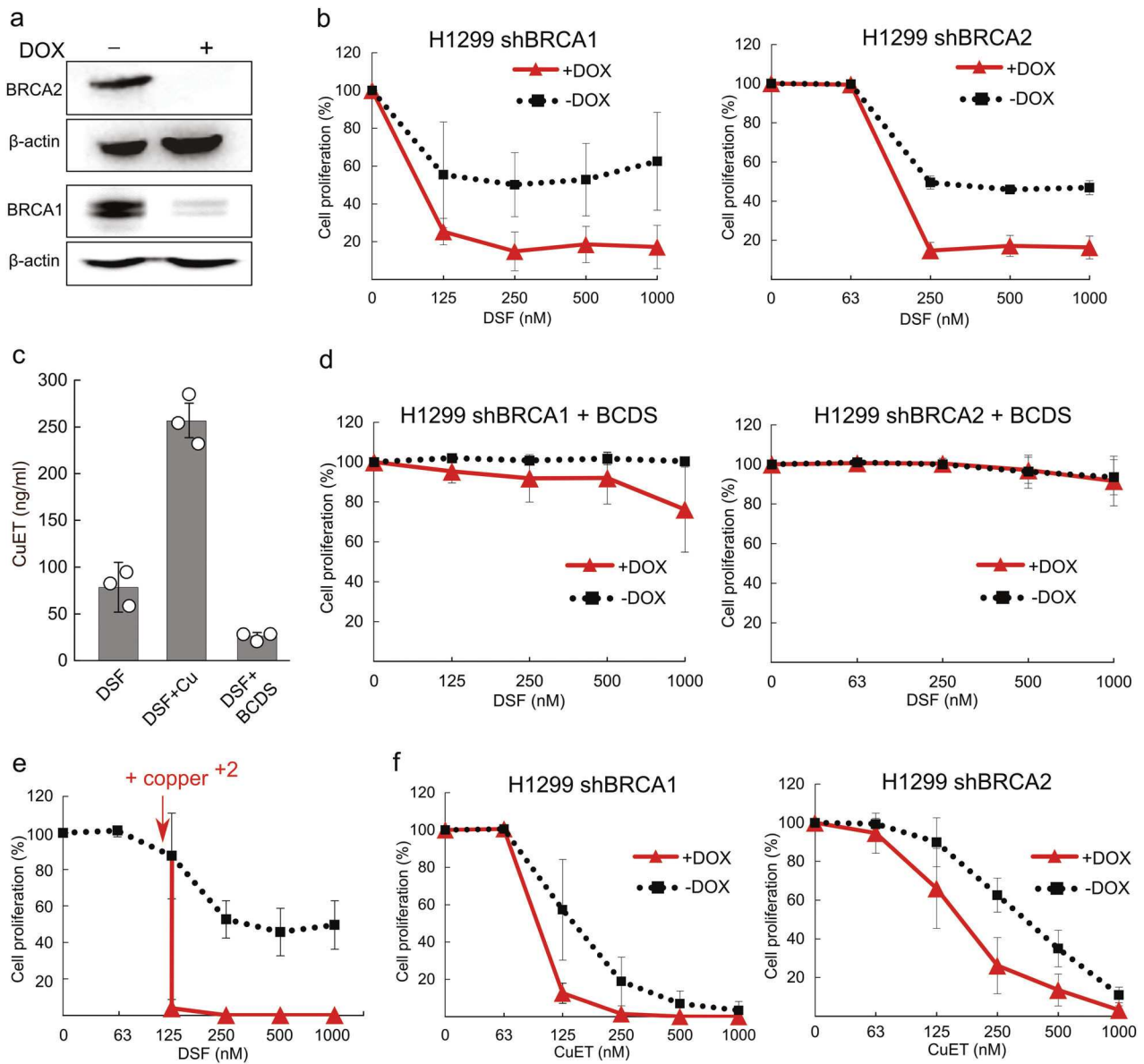


Fig. 1 Preferential cytotoxicity of disulfiram to BRCA1- and BRCA2-depleted H1299 cells is copper dependent. **a** H1299 cells expressing DOX-inducible shBRCA1 or shBRCA2 were cultivated for at least 3 days in DOX and protein expression was evaluated by Western blotting, confirming efficient knockdown of BRCA1 and BRCA2, respectively. **b** H1299 cells expressing DOX-inducible shBRCA1 or shBRCA2 were treated with DSF at indicated concentration for 5 days. **c** HPLC-MS analysis of CuET complex formed in the media

containing DSF, DSF with copper, or DSF with BCDS. **d** Cells as in **b** were treated with the combination of 10 μ M BCDS and DSF at indicated concentration for 5 days. **e** H1299 cells were treated with DSF or the combination of 1 μ M CuCl₂ and DSF at indicated concentrations for 5 days. **f** Cells as in **b** were treated with CuET at indicated concentration for 5 days. All graphs represent at least three independent experiments. Error bars represent SD

bathocuproinedisulfonic acid (BCDS), markedly reduced the levels of spontaneously formed CuET (Fig. 1c). Importantly, in line with our hypothesis and results of spontaneous formation of CuET, chelation of copper by BCDS completely reversed the cytotoxic effect of DSF in all tested cell lines irrespective of their BRCA1/2 status (Fig. 1d, Supplementary Fig. 1b). Another interesting aspect described by Tacconi et al. [20] was the observation that the cytotoxic effect of DSF reaches a certain plateau, which

cannot be overcome by increasing concentrations of the drug, a phenomenon attributed by the authors to limited solubility of the DSF. We also confirmed this plateau effect but we argued that this might be explained by an alternative mechanism, namely reflecting the limiting amounts of copper in culture media, which would enable only limited formation of CuET irrespective of increasing concentrations of DSF. To test the two alternative hypotheses, we added non-toxic extra amounts of copper ions to culture

medium. Supporting our hypothesis, we observed a reversal of the plateau effect, along with a striking potentiation of DSF toxicity (Fig. 1e). Finally, we directly tested the synthetic CuET complex. As expected, CuET treatment was highly potent and also recapitulated the preferential toxicity toward BRCA-impaired cell lines (Fig. 1f, Supplementary Fig. 1c). Taken together, these results demonstrate that DSF's cytotoxicity is fully dependent on copper ions and is mediated by the CuET complex, which is spontaneously formed in the medium, proportionally to the amounts of DSF and copper ions present in the cell culture environment.

Neither DSF nor CuET inhibit ALDH activity, contrary to DSF metabolite Me-DTC-SO

Given the fact that DSF's anti-cancer activity is commonly attributed to inhibition of ALDH, we wanted to test this hypothesis further. An important aspect of DSF as a drug is that it undergoes extensive metabolism resulting in several compounds, including S-methyl-N, N-diethylthiocarbamate-sulfoxide (Me-DTC-SO), which represents the most likely DSF's metabolite responsible for the inhibition of liver ALDH in vivo [25, 26]. However, no potential effect of Me-DTC-SO on cancer cells has so far been reported. First, we investigated the impact of CuET, DSF and Me-DTC-SO on ALDH activity. We selected two human cancer cell lines with high ALDH expression, K562 and A549, and used the well-established ALDEFLUOR assay to measure total ALDH activity in these cells [36]. Strikingly, in K562 cells ALDH activity was not impaired by either CuET or DSF treatment, in contrast to the Me-DTC-SO metabolite that inhibited ALDH with an efficacy similar to D-aminobenzaldehyde (DEAB), a commonly employed ALDH inhibitor used here as a positive control for ALDH inhibition (Fig. 2a, b). Consistently, neither CuET nor DSF decreased the percentage of ALDH positive cells, in contrast to Me-DTC-SO and DEAB (Fig. 2c). The same scenario was reproduced also in the A549 cells as neither CuET nor DSF mimicked the impact of the ALDH inhibitors, while Me-DTC-SO completely blocked the ALDH activity in all cells (Fig. 2d–f). Analogous data were seen in the BRCA1/2 knockdown H1299 cells whose overall ALDH activity is lower compared to K562 or A549 cell lines, again confirming that only Me-DTC-SO potently inhibited ALDH, while CuET and DSF had no direct measurable effect on ALDH activity (Supplementary Fig. 2a, b).

ALDH inhibitors are not toxic to cancer cells

Next, we tested the toxicity of Me-DTC-SO and DEAB, in concentrations efficiently inhibiting the ALDH activity. Strikingly, both compounds failed to suppress growth of

K562 and A549 cells (Fig. 3a). In contrast, CuET which does not inhibit ALDH reduced the growth of both cancer cell lines (Fig. 2b). Furthermore, the H1299 cells were highly responsive to CuET but fully resistant to both DEAB and Me-DTC-SO inhibitors, irrespectively of their BRCA1/2 status (Fig. 3c, d). Given the fact that DSF undergoes rapid transformation in vivo, it is very likely that both metabolites, CuET and Me-DTC-SO, exist in the body at the same time and their effects may potentially influence each other. To test if ALDH inhibition augments the toxicity of CuET, we combined CuET with Me-DTC-SO and DEAB at concentrations efficiently inhibiting ALDH and analysed the viability of cancer cells; however, no potentiation was observed (Fig. 3e). Taken together, these results clearly exclude ALDH inhibition as a possible explanation for DSF's anti-cancer activity and call for an alternative, mechanistically justified explanation. At the same time, our data caution that targeting the ALDH as an approach to cancer treatment should be further scrutinized.

Reduced ALDH activity readout of the ALDEFLUOR assay upon long-term exposure to DSF is an indirect consequence of toxicity

Our results excluding direct inhibition of ALDH by CuET and/or DSF sharply contrast with numerous previous studies claiming that DSF or DSF combined with copper inhibits ALDH activity in cultured cells [12–14, 19, 20], thereby raising the notion of how can such conflicting conclusions be reconciled. One key aspect shared by the studies that reported apparent effects of DSF or DSF/Cu treatments on ALDH activity were long exposure times to the drug (from many hours to several days). This seemed to us a rather odd approach for aiming to test direct enzymatic inhibitors for which a few-hour exposure should be sufficient. We argued that such long exposure times to a toxic and metabolized compound might generate confounding indirect effects and thereby complicate the interpretation of the final outcome, as many important cellular functions can be already hampered due to rather broad, non-specific phenotypes. Such late indirect effects could also bias the readout of the commonly used ALDEFLUOR assay, which requires cellular import of a fluorescent probe and its intracellular retention after cleavage by the ALDH enzyme. To test this idea, we compared ALDH activity at different time-points of drug exposure to evaluate the potential effect of reduced cellular fitness on the ALDEFLUOR assay readout. First, we measured ALDH activity after 3 h of incubation with the four relevant drugs, which was sufficient to suppress ALDH activity when the direct ALDH inhibitors DEAB and Me-DTC-SO were used, yet with no detectable ALDH-inhibitory effect of either CuET or DSF used in parallel experiments (Fig. 2a). Next, we tested not

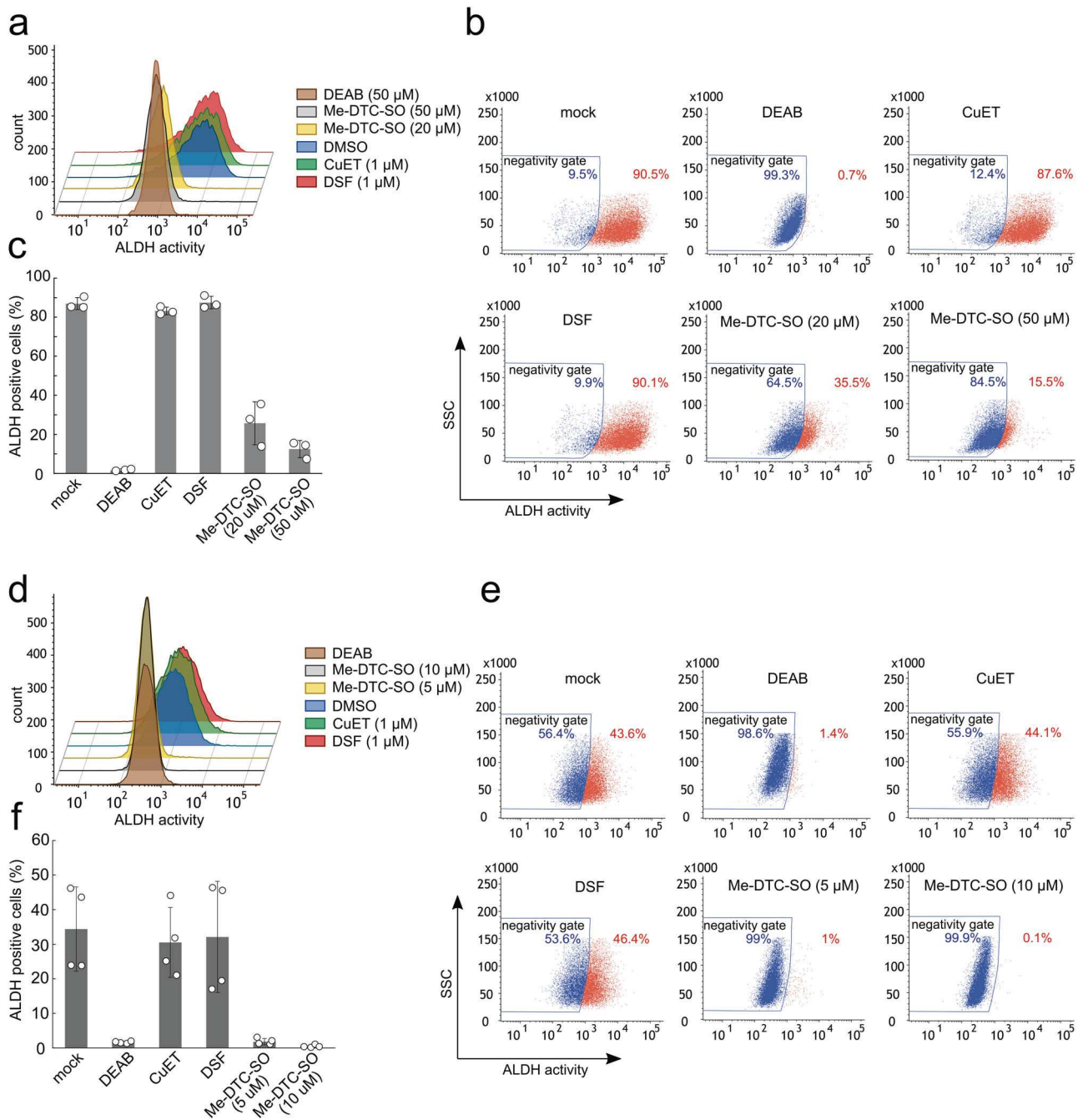


Fig. 2 ALDH activity in cells is inhibited by DSF's metabolite Me-DTC-SO, but not affected by DSF and CuET. **a**, **b** K562 cells were treated with indicated compounds and ALDH activity was quantified by ALDEFLUOR™ assay. Representative graphs and flow cytometry profile from three independent experiments are shown. **c** Number of

ALDH positive K562 cells. **d**, **e** A549 cells were treated with indicated compounds and ALDH activity was measured. Representative graphs and flow cytometry profile from four independent experiments are shown. **f** Number of ALDH positive A549 cells

only CuET as a compound of interest, but also bortezomib (BTZ), a compound that exerts its toxicity through specific inhibition of the 20 S proteasome and partly resembles the cellular effects induced by CuET [33]. Notably, BTZ's mechanism of action is completely unrelated to ALDH. Consistent with our previous results, DSF and CuET failed to inhibit ALDH activity after 3 h of exposure despite other

typical cellular phenotypes such as accumulation of poly-ubiquitinated proteins [33] are already well detectable in the cells treated for 3 h with the same concentration of DSF or CuET (Fig. 4a). As expected, also BTZ failed to score in the ALDH inhibition assay (Fig. 4b). Strikingly, however, after a prolonged treatment (20 h), both CuET and BTZ markedly reduced the ALDEFLUOR-assessed ALDH

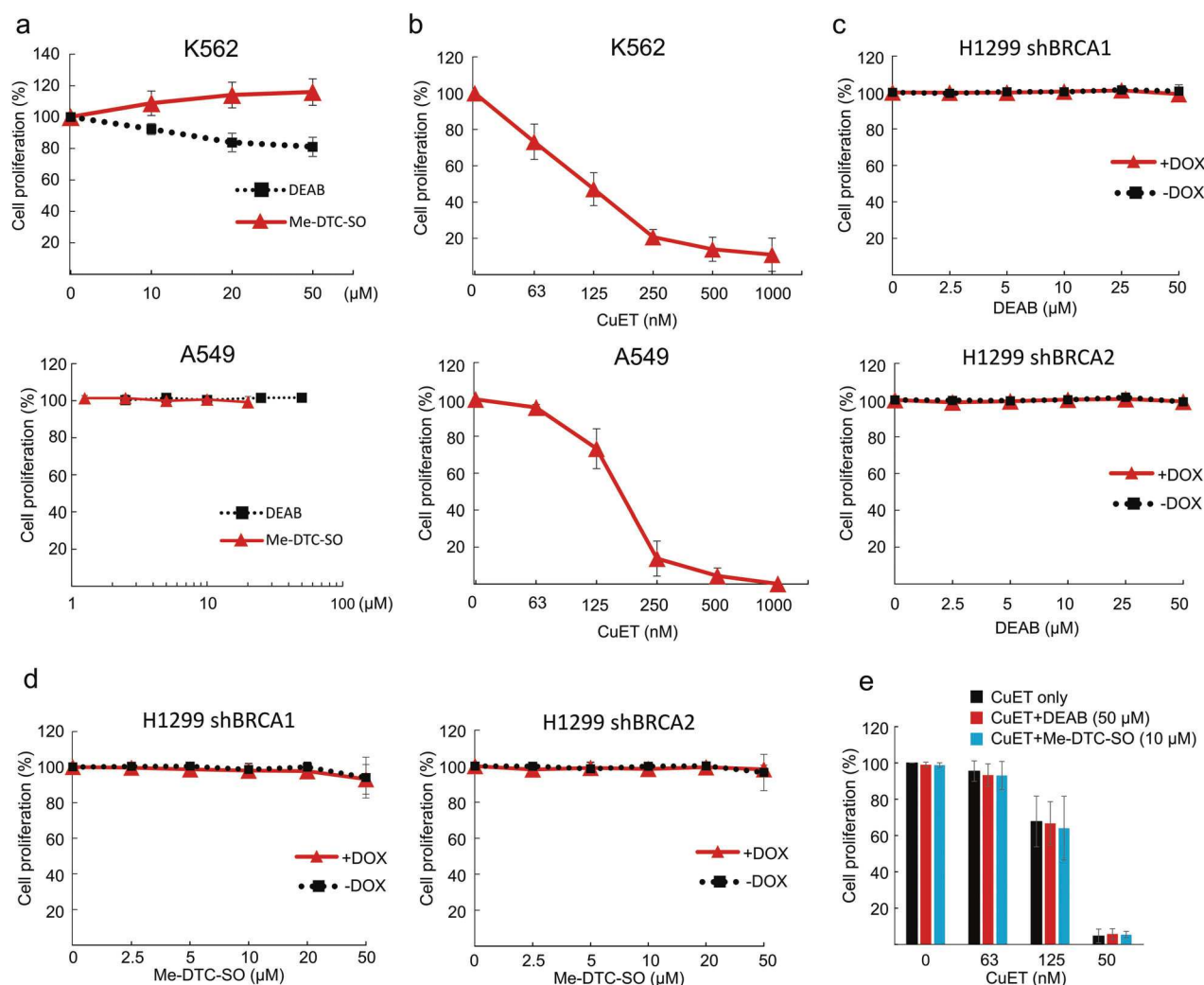


Fig. 3 Cytotoxicity of ALDH inhibitors and CuET. **a** Cytotoxicity of DEAB or Me-DTC-SO in A549 and K562 cells after 5 days of treatment. **b** Cytotoxicity of CuET in A549 and K562 cells after 5 days of treatment. All graphs represent at least three independent experiments. Error bars represent SD. **c** H1299 cells expressing DOX-

inducible shBRCA1 or shBRCA2 were treated with ALDH inhibitors DEAB and **d** Me-DTC-SO at indicated concentrations for 5 days. **e** Cytotoxicity of CuET, Me-DTC-SO and DEAB or their combination in A549 cells

activity readout (Fig. 4b) and clearly decreased the numbers of ALDH-positive cells (Fig. 4c, d). Such prolonged treatments also increased the numbers of permeabilised cells, an indirect marker of reduced cell fitness and increased cell death (Fig. 4e). Given that even BTZ, a compound never reported as an ALDH inhibitor, behaved similarly to CuET, we propose that the decrease of ALDH activity in such long-term treatment experiments is not caused by any direct interference with ALDH enzymatic activity, but it is rather a consequence of impaired cell fitness. All permeabilised cells were totally negative for ALDH activity (Supplementary Fig. 3b), which is understandable considering the principle of the ALDEFLUOR assay. Even the seemingly still ‘intact’ (nonpermeabilized) cells showed a lower ALDH activity readout suggesting that prolonged cellular stresses (at least the proteotoxic stress

caused by CuET- or BTZ-induced protein turnover impairment) is sufficient to indirectly affect the outcome of the ALDEFLUOR assay (Supplementary Fig. 3a), a fact that has been incorrectly interpreted by many as direct inhibition of ALDH by DSF. These results help explain the previous conflicting studies and exclude ALDH inhibition as a mechanism underlying DSF’s toxicity to cancer cells.

DSF toxicity is linked to NPL4 aggregation

We have recently reported that DSF is metabolised in vivo into the CuET complex, and showed that CuET represents the ultimate anti-cancer metabolite. CuET interferes with the cellular protein degradation machinery *via* targeting the NPL4 cofactor of the p97/VCP segregase, leading to NPL4

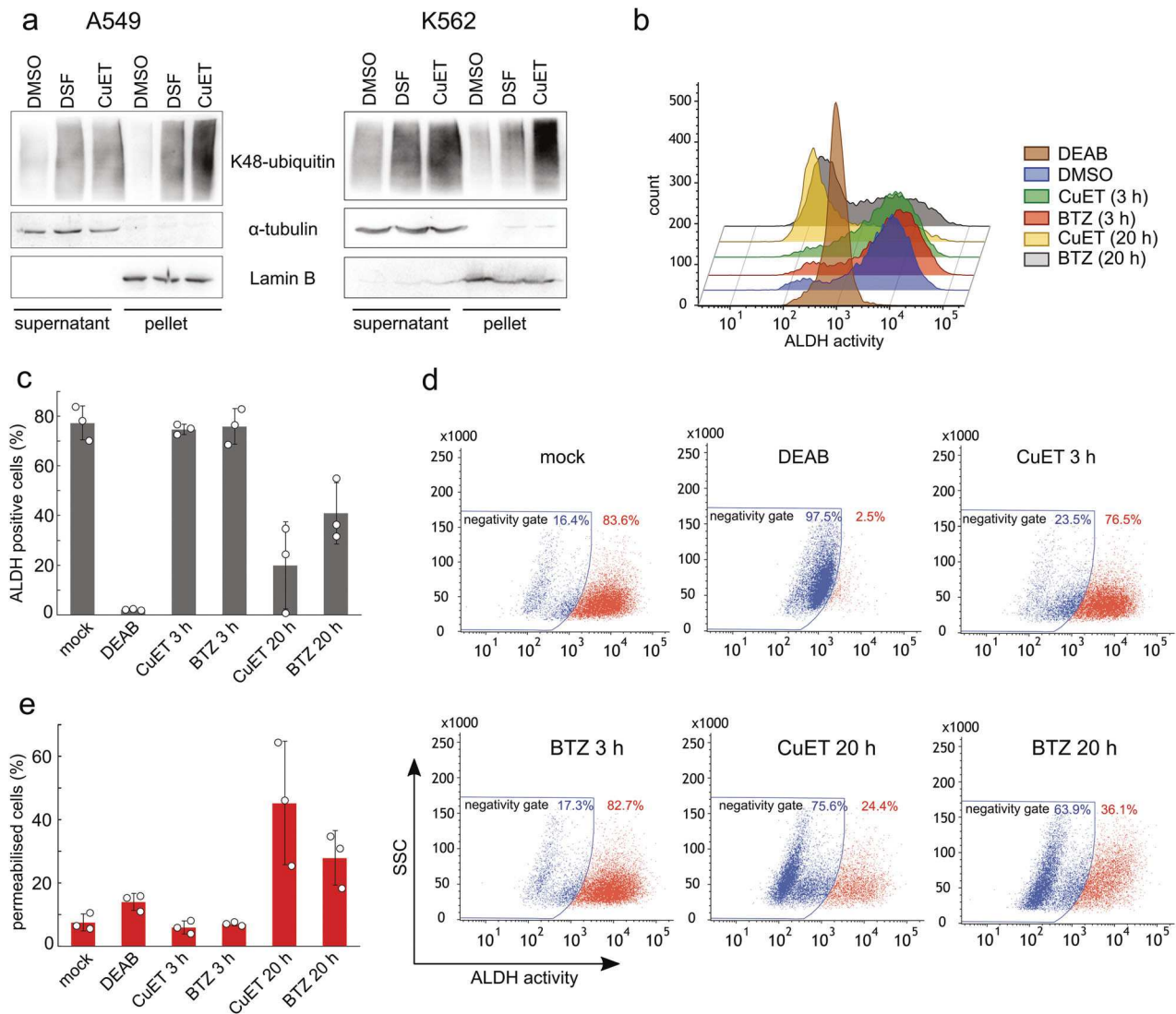


Fig. 4 CuET reduces ALDH activity after prolonged treatment. **a** Western blot analysis of immobilized and accumulated K48 poly-ubiquitin in CuET/DSF (1 μ M, 3 h) treated A549 and K562 cells. **b** K562 cells were treated with DEAB (50 μ M), CuET (1 μ M), BTZ (1 μ M) for indicated time and ALDH activity was quantified by ALDEFLUOR™ assay. Representative graphs from three independent

experiments are shown. **c** Number of ALDH positive K562 cells after indicated treatments. Error bars represent SD of three independent experiments. **d** Representative flow cytometry profile of K562 cells treated as in **b**. **e** Percentage of permeabilized K562 cells after indicated treatments was measured by DAPI staining using flow cytometry

aggregation, activation of stress responses and cell death [33]. Since CuET is formed from DSF also in vitro in culture media (Fig. 1c) and DSF's toxicity strictly depends on available copper ions (Fig. 1d, e), we examined whether DSF's cytotoxicity is also accompanied by NPL4 aggregation. We treated the cells with CuET, DSF, DSF combined with a copper chelator BCDS, and the two ALDH inhibitors: Me-DTC-SO and DEAB and assessed the NPL4 protein status. As expected, both CuET and DSF treatment led to formation of insoluble aggregated endogenous NPL4 resistant to pre-extraction (Fig. 5a). Chelation of copper ions by BCDS completely suppressed DSF's effect on NPL4 aggregation, thereby preserving the normal diffuse staining

pattern of NPL4 that was sensitive to cell pre-extraction. The same un-altered, extraction-sensitive diffuse staining of NPL4 was furthermore observed for mock treated cells, but also upon treatment by the two ALDH inhibitors Me-DTC-SO and DEAB (Fig. 5a, see Fig. 5b for signal quantification). These results were further corroborated using a NPL4-GFP expressing cell line showing the same effects on GFP tagged NPL4 protein (Supplementary Fig. 4a, b). Together with the other results of our present study, these data demonstrate that DSF's cytotoxicity does not involve ALDH inhibition, but rather it is attributable to CuET causing NPL4 aggregation, as recently described for the synthetic CuET complex [33].

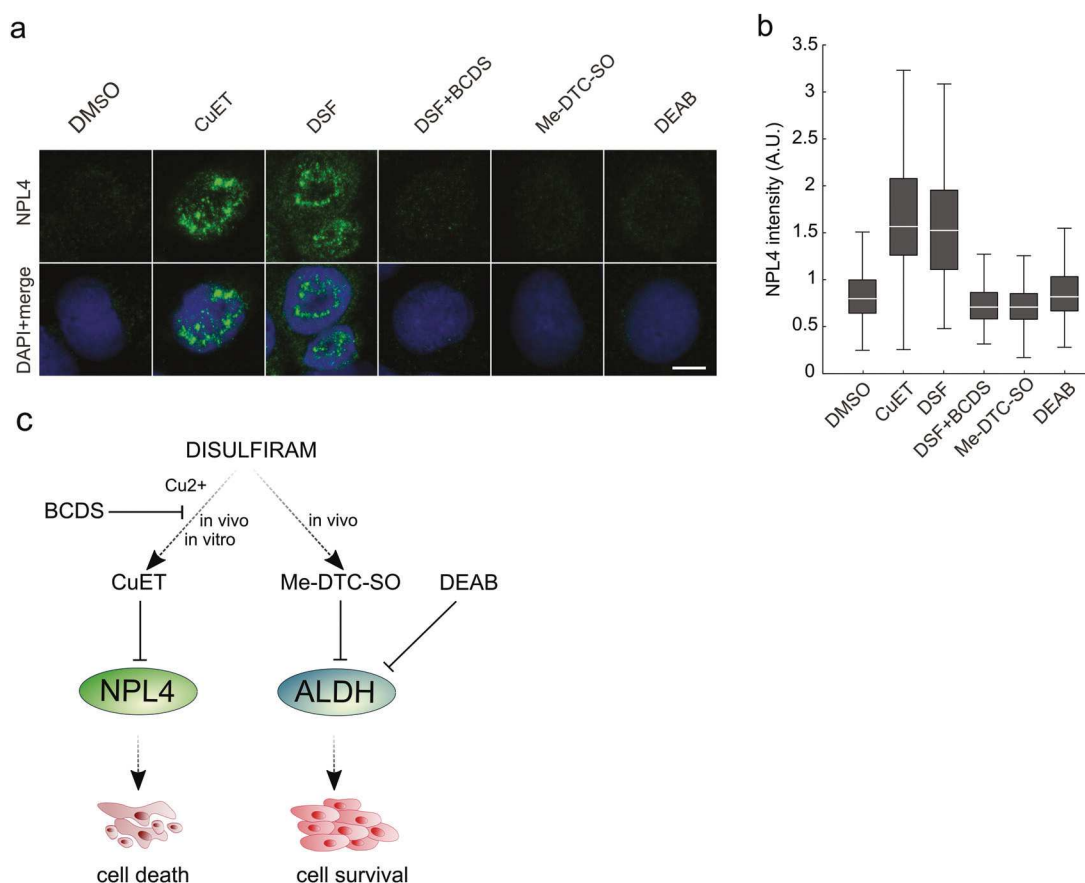


Fig. 5 DSF toxicity is caused by NPL4 aggregation. **a** A549 cells were treated with DMSO, DSF (1 μ M), CuET (500 nM), Me-DTC-SO (20 μ M), DSF with BCDS (10 μ M) and DEAB (50 μ M) for 4 h and NPL4 aggregation was visualized by immunofluorescence staining

after pre-extraction. **b** Quantification of nuclear NPL4 signal in more than 200 cells. **c** Schematic representation of the mechanism of action of disulfiram and its metabolites

Discussion

The alcohol-abuse drug DSF is a promising candidate for repurposing in cancer therapy, as documented by many pre-clinical studies and ongoing clinical trials. Proper knowledge of drug's mechanism of action is essential for both development of suitable biomarkers and selection of individual patients who might most benefit from such treatment. In this study, we therefore critically assessed the commonly accepted theory about DSF's mechanism of action in cancer cells, namely the inhibition of ALDH enzymes. Many publications attribute the anti-cancer effect of DSF to interference with ALDH, and others build their subsequent work on such conclusions. As ALDH was widely proposed to be a cancer target [37, 38], the hypothesis that DSF kills cancer cells *via* inhibition of ALDH seemed plausible and was widely accepted by experimental cancer researchers and oncologists. DSF is indeed well known as a drug averting alcoholism through ALDH enzyme inhibition in the human body. On the other hand, it is not DSF itself but rather some of its metabolites that directly inhibit ALDH, an

important fact that is much less appreciated and completely overlooked in cancer-related studies, thereby fuelling the misleading claims that DSF directly inhibits cellular ALDH. In sharp contrast, here we show that neither DSF nor CuET (which forms spontaneously both *in vivo* and *in cell culture* due to available copper ions) inhibits ALDH, contrary to the appropriate DSF's metabolite Me-DTC-SO that does inhibit ALDH. Importantly, the results of the cytotoxicity assays showed that the genuine ALDH inhibitors DEAB and Me-DTC-SO were not toxic to cancer cells at a concentration range that robustly inhibited the ALDH activity while treatments with CuET and DSF killed cancer cells efficiently. Furthermore, despite only a minor fraction of cells in culture (~20% in the H1299 cell line) are positive for ALDH activity, all cells respond well to CuET or DSF treatment. Furthermore, we have proven here that the cytotoxicity of DSF for human cancer cells requires the availability of copper and spontaneous formation of the CuET complex. The frequently observed potentiation of DSF activity by copper has been often attributed to ALDH inhibition, an unproven conclusion that lacks any rational

basis. Yet such major discrepancy has remained overlooked.

While some potential contribution of ALDH inhibition to the *in vivo* anti-cancer activity of DSF by the relevant metabolites cannot be entirely excluded, it should be emphasized that also under *in vivo* conditions, DSF's toxicity for cancer cells is potentiated by copper supplementation [12, 33] that leads to increased formation of CuET [33] at the expense of lower formation of the ALDH-inhibitory metabolites. Moreover, the ALDH hypothesis is also based only on results obtained in cell culture experiments, and it has so far not been proven under *in vivo* conditions, in tumour tissues. Importantly, in the Asian population a large number of people (approximately 540 million) carry a mutation in the *ALDH2* gene producing a defective enzyme [39] that causes alcohol-related symptoms largely resembling the therapeutic exposure to DSF. Yet, these people still suffer from common cancers with a similar frequency as the matched normal population [40]. In addition, normal stem cells physiologically express ALDH activity, but patients treated with DSF to prevent use of alcohol are medicated for many years with no evidence of stem cell exhaustion demonstrated by myelodysplasia or bone marrow failure [41]. As studies that employ DSF have become a key part of cancer research aiming to target ALDH in CSCs, our present results provide a fresh insight into this field that should motivate further thorough examination of the role played by ALDH in cancer cells. From the clinical perspective, inhibition of liver ALDH in cancer patients treated by DSF represents serious limitation for its widespread use. DSF must be excluded in all patients whose overall treatment requires administration of some alcohol-based substances. Those include patients receiving therapy with drugs where alcohol is used as an excipient (such as commonly used anti-cancer drugs gemcitabine or paclitaxel) or disinfectants (e.g., before surgery). Moreover, moderate alcohol consumption might be regarded by some patients as an important aspect of life quality, incompatible with a concomitant DSF treatment. Sensitive patients even do not tolerate alcohol-containing cosmetics or mouthwash under DSF therapy, again interfering with quality of life. Our results suggest that this limitation of DSF could be possibly overcome by direct application of CuET. However, on its own the CuET complex is highly lipophilic, water insoluble and thus unsuitable for clinical applications. In our previous work, we have overcome this limitation and developed an albumin-based formulation of CuET, which is prepared by single *in situ* reaction yielding CuET-albumin composition in an aqueous solution suitable for *in vivo* applications and demonstrating promising anti-tumour effects [33]. Consequently, other groups also reported formulations of CuET based on a similar principle and using

other pharmaceutically acceptable excipients [42, 43]. These results indicate, that direct application of CuET is in principle feasible and represents a potential strategy to target cancer. At the same time, our present study should inspire further research into the proposed ability of DSF to target CSCs, in light of our findings that the anti-cancer effect of DSF is mediated by CuET and involves NPL4 as the relevant target. Similarly, the observed hypersensitivity of BRCA1/2- deficient cancer cell models to CuET via NPL4 protein aggregation opens new avenues for further exploration in clinical scenarios associated with some DNA repair deficiencies.

Materials and methods

Cell lines

Human non-small cell lung carcinoma H1299 cells expressing a doxycycline (DOX)-inducible BRCA1 and BRCA2 shRNAs, U-2-OS cells expressing NPL4-GFP [33], human lung adenocarcinoma cells A549 (ATCC) and human chronic myelogenous leukemia K562 cells (ATCC) were cultured and maintained in DMEM medium (Lonza), supplemented with 10% fetal bovine serum (Thermo Fisher Scientific) and 1% penicillin/streptomycin (Sigma–Aldrich). H1299 expressing a DOX-inducible BRCA1 and BRCA2 shRNA were kindly provided [20]. For efficient BRCA1 and BRCA2 knockdown cells were cultivated in the presence of 2 µg/ml DOX for at least 3 days. Cell lines were tested for mycoplasma contamination and authenticated by CTR method.

Cell viability assays

H1299 and A549 cells were plated at a density 80,000–100,000 cells per well in six-well plates and in case of Olaparib treatment 20000 per well in 12-well plate. Next day cells were treated with compounds at indicated concentrations and left in culture for 5–7 days before analysing. On the day of analysing, growth medium was removed, cells were fixed in ice cold 70% ethanol and stained with 1% crystal violet in 96% ethanol and total growth area was calculated. Results are shown as mean values and standard deviations from at least three independent experiments.

K562 cell viability was analysed by XTT assay. Cells were plated at a density of 5000 per well in a 96-well plate. The next day, cells were treated as indicated. After 5 days, an XTT assay was performed according to the manufacturer's instructions (Applichem). XTT solution was added to the medium and incubated for 30–60 min, and then the dye intensity was measured at the 475 nm wavelength using a spectrometer (TECAN, Infinite M200PRO).

Immunoblotting

Equal amounts of cell lysates were separated by SDS-PAGE on NuPAGE™ 3–8% Tris-Acetate protein gels (Thermo Fisher Scientific) or hand-casted gels and then transferred onto nitrocellulose membrane. The membrane was blocked in Tris-buffered saline containing 5% milk in and 0.1% Tween 20 for 1 h at room temperature, and then incubated 1 h at room temperature with primary antibodies, followed by detection with secondary antibodies: Secondary antibodies were visualized by ELC detection reagent (Thermo Fisher Scientific).

Immunofluorescence

Cells were seeded on plastic inserts in 12-well dishes. Next day cells were treated with compounds at indicated concentrations and subsequently pre-extracted (0.1% Triton X 100 in PBS, for 2 min) and fixed with -20°C methanol for 15 min at room temperature, washed with PBS and permeabilized with 0.5% Triton X-100 in PBS for 5 min. After PBS washes, the cells on the plastic inserts were then immunostained with primary antibody for 120 min at room temperature, followed by a PBS washes and staining with fluorescently-conjugated secondary antibody for 60 min at room temperature. NPL4-GFP expressing cells were pre-extracted (0.2% Triton X 100 in PBS, for 2 min) and fixed with 4% formaldehyde for 15 min at room temperature, washed with PBS. Nuclei were visualized by DAPI staining at room temperature for 2 min. Dried plastic inserts with cells were mounted using Vectashield mounting medium (Vector Laboratories) and images were acquired using Zeiss Axioimager Z.1 platform.

Image quantification

Images were acquired using the Olympus IX81 fluorescence microscope and ScanR Acquisition software. The scans were quantified in automated image and data analysis software ScanR Analysis. The data were further analysed in the STATISTICA 13 software tool.

ALDEFLUOR assay

ALDH activity in cells were analysed by ALDEFLUOR assay (Stemcell) preformed according to manufacturer protocol. Briefly, cells were incubated with ALDH reagent in supplied buffer for 45 min at 37°C . After that, cells were centrifuged, resuspended in fresh assay buffer and kept on ice until measured by flow cytometry using BD FACSVerser (BD Biosciences), at least 10.000 events were acquired per sample. Collected data were processed by BD FACSSuite (BD Biosciences).

Measurement of CuET formation in vitro

To measure the formation of diethyldithiocarbamate-copper complex (CuET) in vitro, a complete cell culture medium (DMEM, 10% FBS) was incubated with $1\ \mu\text{M}$ DSF or $1\ \mu\text{M}$ DSF plus $1\ \mu\text{M}$ copper (ii) chloride, or DSF with BCDS ($20\ \mu\text{M}$). After 3 h of incubation in 37°C , the samples were vortexed and mixed with acetone in a ratio 1:4. The mixture was centrifuged $18\ 000\times g$ for 2 min at 4°C and immediately spinned for 30 min using small table centrifuge (Bio-San FVL-2400N) placed inside -80°C freezer. Supernatant was quickly transferred into glass HPLC vial and kept at -80°C not longer than 6 h. The CuET complex was analysed by HPLC-MS method described previously (Skrott et al. 2017). The quantification of CuET complex was calculated according to the calibration curve.

Cell fractionation for Triton X insoluble pellets

Cells were treated as indicated, washed in cold PBS and lysed in lysis buffer (50 mM Tris-HCl, pH 7.5, 150 mM NaCl, 2 mM MgCl_2 , 10% glycerol, 0.5% Triton-X100, protease inhibitor cocktail by Roche) for 2 min gently agitating at 4°C . Then, cells were scraped to eppendorf tubes and kept for another 10 min on ice with vortex steps. After that, the lysate was centrifuged at $20,000\times g$ for 10 min at 4°C . Insoluble fraction and supernatant were resuspended in LSB buffer.

Antibodies and chemicals

The following antibodies were used for immunoblotting: mouse monoclonal antibody against BRCA1 antibody (Santa Cruz, D-9, sc-6954), rabbit polyclonal antibody against BRCA2 (Bethyl, A300–005 A) antibody and mouse monoclonal antibody against β -actin (Santa Cruz, C4, sc-47778), lamin B (Santa Cruz, sc-6217), α -Tubulin (Santa Cruz, B-7, sc-5286), anti-ubiquitin lys48-specific (Merck Millipore, clone Apu2, 05–1307). For immunofluorescence were used following antibodies: mouse monoclonal antibody against NPL4 (Santa Cruz, D-1, sc-365796), AlexaFluor 488 goat anti-mouse (Invitrogen, A-11001). Chemicals used in this study were as follows: CuET (bis-diethyldithiocarbamate-copper complex, TCI chemicals), disulfiram (Sigma), copper chloride (Sigma), bortezomib (Velcade, Janssen-Cilag International N.V.), DEAB (Sigma), bathocuproinedisulfonic acid (Sigma), *S*-methyl-*N,N*-diethylthiocarbamate-sulfoxide (Santa Cruz).

Acknowledgements We thank Dr. M. Tarsounas (Oxford, UK) for the human H1299 cell lines with regulatable expression of shBRCA1 and shBRCA2. The study was supported by grants from: Grant agency of Czech Rep. GACR 17–25976 S, MEYS CR (LM2015062 Czech-BioImaging and DRO-61989592), Internal grant of University of

Palacky IGA_LF_2019_026, Cancer Research Czech Republic, Ministry of School, Education, Youth and Sports of the Czech Republic (EATRIS-CZ No. LM2015064 and ENOCN No. CZ.02.1.01/0.0/0.0/16_019/0000868), the Novo Nordisk Foundation (no. 16854), the Danish National Research Foundation (project CARD: no. DNRF125), the Danish Cancer Society (R204-A12617) the Swedish Research Council (VR-MH 2014-46602-117891-30), and the Swedish Cancer Society (no. 170176).

Compliance with ethical standards

Conflict of interest The authors declare that they have no conflict of interest.

Publisher's note: Springer Nature remains neutral with regard to jurisdictional claims in published maps and institutional affiliations.

References

- Marques DS, Sandrini JZ, Boyle RT, Marins LF, Trindade GS. Relationships between multidrug resistance (MDR) and stem cell markers in human chronic myeloid leukemia cell lines. *Leuk Res*. 2010;34:757–62.
- Battle E, Clevers H. Cancer stem cells revisited. *Nat Med*. 2017;23:1124–34.
- Tirino V, Desiderio V, Paino F, De Rosa A, Papaccio F, La Noce M, et al. Cancer stem cells in solid tumors: an overview and new approaches for their isolation and characterization. *FASEB J*. 2013;27:13–24.
- Koppaka V, Thompson DC, Chen Y, Ellermann M, Nicolaou KC, Juvonen RO, et al. Aldehyde dehydrogenase inhibitors: a comprehensive review of the pharmacology, mechanism of action, substrate specificity, and clinical application. *Pharm Rev*. 2012;64:520–39.
- Pors K, Moreb JS. Aldehyde dehydrogenases in cancer: an opportunity for biomarker and drug development? *Drug Disco Today*. 2014;19:1953–63.
- Marchitti SA, Brocker C, Stagos D, Vasiliou V. Non-P450 aldehyde oxidizing enzymes: the aldehyde dehydrogenase superfamily. *Expert Opin Drug Metab Toxicol*. 2008;4:697–720.
- Brooks PJ, Theruvathu JA. DNA adducts from acetaldehyde: implications for alcohol-related carcinogenesis. *Alcohol*. 2005;35:187–93.
- van den Hoogen C, van der Horst G, Cheung H, Buijs JT, Lippitt JM, Guzmán-Ramírez N, et al. High aldehyde dehydrogenase activity identifies tumor-initiating and metastasis-initiating cells in human prostate cancer. *Cancer Res*. 2010;70:5163–73.
- Charafe-Jauffret E, Ginestier C, Iovino F, Tarpin C, Diebel M, Esterni B, et al. Aldehyde dehydrogenase 1-positive cancer stem cells mediate metastasis and poor clinical outcome in inflammatory breast cancer. *Clin Cancer Res*. 2010;16:45–55.
- Ginestier C, Hur MH, Charafe-Jauffret E, Monville F, Dutcher J, Brown M, et al. ALDH1 is a marker of normal and malignant human mammary stem cells and a predictor of poor clinical outcome. *Cell Stem Cell*. 2007;1:555–67.
- Yip NC, Fombon IS, Liu P, Brown S, Kannappan V, Armesilla AL, et al. Disulfiram modulated ROS-MAPK and NFκB pathways and targeted breast cancer cells with cancer stem cell-like properties. *Br J Cancer*. 2011;104:1564–74.
- Allensworth JL, Evans MK, Bertucci F, Aldrich AJ, Festa RA, Finetti P, et al. Disulfiram (DSF) acts as a copper ionophore to induce copper-dependent oxidative stress and mediate anti-tumor efficacy in inflammatory breast cancer. *Mol Oncol*. 2015;9:1155–68.
- Liu X, Wang L, Cui W, Yuan X, Lin L, Cao Q, et al. Targeting ALDH1A1 by disulfiram/copper complex inhibits non-small cell lung cancer recurrence driven by ALDH-positive cancer stem cells. *Oncotarget*. 2016;7:58516–30.
- Liu P, Kumar IS, Brown S, Kannappan V, Tawari PE, Tang JZ, et al. Disulfiram targets cancer stem-like cells and reverses resistance and cross-resistance in acquired paclitaxel-resistant triple-negative breast cancer cells. *Br J Cancer*. 2013;109:1876–85.
- Liu P, Brown S, Goktug T, Channathodiyil P, Kannappan V, Hugnot J-P, et al. Cytotoxic effect of disulfiram/copper on human glioblastoma cell lines and ALDH-positive cancer-stem-like cells. *Br J Cancer*. 2012;107:1488–97.
- Liu P, Wang Z, Brown S, Kannappan V, Tawari PE, Jiang W, et al. Liposome encapsulated Disulfiram inhibits NFκB pathway and targets breast cancer stem cells in vitro and in vivo. *Oncotarget*. 2014;5:7471–85.
- Jin N, Zhu X, Cheng F, Zhang L. Disulfiram/copper targets stem cell-like ALDH(+) population of multiple myeloma by inhibition of ALDH1A1 and Hedgehog pathway. *J Cell Biochem*. 2018;119:6882–93.
- Choi SA, Choi JW, Wang K-C, Phi JH, Lee JY, Park KD, et al. Disulfiram modulates stemness and metabolism of brain tumor initiating cells in atypical teratoid/rhabdoid tumors. *Neuro Oncol*. 2015;17:810–21.
- MacDonagh L, Gallagher MF, Ffrench B, Gasch C, Breen E, Gray SG, et al. Targeting the cancer stem cell marker, aldehyde dehydrogenase 1, to circumvent cisplatin resistance in NSCLC. *Oncotarget*. 2017;8:72544–63.
- Tacconi EM, Lai X, Folio C, Porru M, Zonderland G, Badie S, et al. BRCA1 and BRCA2 tumor suppressors protect against endogenous acetaldehyde toxicity. *EMBO Mol Med*. 2017;9:1398–414.
- Raha D, Wilson TR, Peng J, Peterson D, Yue P, Evangelista M, et al. The cancer stem cell marker aldehyde dehydrogenase is required to maintain a drug-tolerant tumor cell subpopulation. *Cancer Res*. 2014;74:3579–90.
- Wu L, Meng F, Dong L, Block CJ, Mitchell AV, Wu J, et al. Disulfiram and BKM120 in combination with chemotherapy impede tumor progression and delay tumor recurrence in tumor initiating cell-rich TNBC. *Sci Rep*. 2019;9:236.
- Wang N-N, Wang L-H, Li Y, Fu S-Y, Xue X, Jia L-N, et al. Targeting ALDH2 with disulfiram/copper reverses the resistance of cancer cells to microtubule inhibitors. *Exp Cell Res*. 2018;362:72–82.
- Bista R, Lee DW, Pepper OB, Azorsa DO, Arcenci RJ, Aleem E. Disulfiram overcomes bortezomib and cytarabine resistance in Down-syndrome-associated acute myeloid leukemia cells. *J Exp Clin Cancer Res*. 2017;36:22.
- Lipsky JJ, Shen ML, Naylor S. In vivo inhibition of aldehyde dehydrogenase by disulfiram. *Chem Biol Inter*. 2001;130–132:93–102.
- Shen ML, Johnson KL, Mays DC, Lipsky JJ, Naylor S. Determination of in vivo adducts of disulfiram with mitochondrial aldehyde dehydrogenase. *Biochem Pharm*. 2001;61:537–45.
- Mays DC, Nelson AN, Fauq AH, Shriver ZH, Veverka KA, Naylor S, et al. S-Methyl N,N-diethylthiocarbamate sulfone, a potential metabolite of disulfiram and potent inhibitor of low Km mitochondrial aldehyde dehydrogenase. *Biochem Pharm*. 1995;49:693–700.
- Lam JP, Mays DC, Lipsky JJ. Inhibition of recombinant human mitochondrial and cytosolic aldehyde dehydrogenases by two candidates for the active metabolites of disulfiram †. *Biochemistry*. 1997;36:13748–54.
- Hart BW, Faiman MD. Bioactivation of S-methyl N,N-Diethylthiolcarbamate to S-methyl N,N-diethylthiolcarbamate sulfoxide. *Biochem Pharm*. 1993;46:2285–90.

30. Yourick JJ, Faiman MD. Disulfiram metabolism as a requirement for the inhibition of rat liver mitochondrial low Km aldehyde dehydrogenase. *Biochem Pharm.* 1991;42:1361–6.
31. Chen D, Cui QC, Yang H, Dou QP. Disulfiram, a clinically used anti-alcoholism drug and copper-binding agent, induces apoptotic cell death in breast cancer cultures and xenografts via inhibition of the proteasome activity. *Cancer Res.* 2006;66:10425–33.
32. Majera D, Skrott Z, Bouchal J, Bartkova J, Simkova D, Gachechiladze M, et al. Targeting genotoxic and proteotoxic stress-response pathways in human prostate cancer by clinically available PARP inhibitors, vorinostat and disulfiram. *Prostate.* 2019;79:352–62.
33. Skrott Z, Mistrik M, Andersen KK, Friis S, Majera D, Gursky J, et al. Alcohol-abuse drug disulfiram targets cancer via p97 segregase adaptor NPL4. *Nature.* 2017;552:194–9.
34. Farmer H, McCabe N, Lord CJ, Tutt ANJ, Johnson DA, Richardson TB, et al. Targeting the DNA repair defect in BRCA mutant cells as a therapeutic strategy. *Nature.* 2005;434:917–21.
35. Bryan N, Andrews KD, Loughran MJ, Rhodes NP, Hunt JA. Elucidating the contribution of the elemental composition of fetal calf serum to antigenic expression of primary human umbilical-vein endothelial cells in vitro. *Biosci Rep.* 2011;31:199–210.
36. Zhou L, Sheng D, Wang D, Ma W, Deng Q, Deng L, et al. Identification of cancer-type specific expression patterns for active aldehyde dehydrogenase (ALDH) isoforms in ALDEFLUOR assay. *Cell Biol Toxicol.* 2019;35:161–77.
37. Huddle BC, Grimley E, Buchman CD, Chtcherbinine M, Debnath B, Mehta P, et al. Structure-based optimization of a novel class of aldehyde dehydrogenase 1A (ALDH1A) subfamily-selective inhibitors as potential adjuncts to ovarian cancer chemotherapy. *J Med Chem.* 2018;61:8754–73.
38. Duan J-J, Cai J, Guo Y-F, Bian X-W, Yu S-C. ALDH1A3, a metabolic target for cancer diagnosis and therapy. *Int J Cancer.* 2016;139:965–75.
39. Lai C-L, Yao C-T, Chau G-Y, Yang L-F, Kuo T-Y, Chiang C-P, et al. Dominance of the inactive Asian variant over activity and protein contents of mitochondrial aldehyde dehydrogenase 2 in human liver. *Alcohol Clin Exp Res.* 2014;38:44–50.
40. Chang JS, Hsiao J-R, Chen C-H. ALDH2 polymorphism and alcohol-related cancers in Asians: a public health perspective. *J Biomed Sci.* 2017;24:19.
41. Suh JJ, Pettinati HM, Kampman KM, O'Brien CP. The status of disulfiram: a half of a century later. *J Clin Psychopharmacol.* 2006;26:290–302.
42. Chen W, Yang W, Chen P, Huang Y, Li F. Disulfiram copper nanoparticles prepared with a stabilized metal ion ligand complex method for treating drug-resistant prostate cancers. *ACS Appl Mater Interfaces.* 2018;10:41118–28.
43. Peng X, Pan Q, Zhang B, Wan S, Li S, Luo K, et al. Highly stable, coordinated polymeric nanoparticles loading copper(II) diethyldithiocarbamate for combinational chemo/chemodynamic therapy of cancer. *Biomacromolecules.* 2019;20:2372–83.